Conjugated Polymer Brushes (Poly(3-hexylthiophene) brushes): new electro- and photo-active molecular architectures

D I S S E R T A T I O N

zur Erlangung des akademischen Grades
Doktor rerum naturalium
(Dr. rer. nat.)

vorgelegt
am Fachbereich Chemie
der Fakultät Mathematik und Naturwissenschaften
der Technischen Universität Dresden

von

Natalya Khanduyeva

geboren am 8 September 1979 in Chita, Russland

Gutachter: Prof. Dr. M. Stamm
Prof. Dr. Th. Wolff
Prof. Dr. R. Jordan

Eingereicht am: 19.09.2008
Tag der Verteidigung: 16.01.2009

CONTENTS

Dedicated to my wonderful mother Larisa and my family,

and to my boyfriend Clemens

GENERAL INTRODUCTION

Motivation & actuality. A polymer brush is an array of macromolecular chains attached to a surface in sufficient proximity so that the solution dimensions (in a good solvent) of the chains are altered. Polymer brushes first gained attention in the 1950s when it was discovered that flocculation of dispersion could be prevented by grafting polymer molecules to colloidal particles. Since then, a great number of articles devoted to synthesis, characterization and applications of various kinds of polymer brushes was published and interest to this research area has continued to grow. Films composed of polymer chains that extend along a direction normal to the grafting surface can exhibit properties distinctly different from those of chains in solution. This makes polymer brushes an interesting field of research. Examples of interesting properties include (1) interfacial localization of terminal groups[1], (2) diffusion control[2], (3) regulation of steric repulsive forces[3], (4) control of phase-segregation in response to external stimuli[4], (5) wetting control[5], (6) control of protein and cell adsorption[6], (7) adsorption of molecules[7], (8) lubrication[8], and (9) adhesion[9]. To date, polymer brushes were grown on objects of different shape and size and applied for fabrication of stimuli-responsive surfaces[10], drug delivery systems, and stabilization of nanoparticles, etc.

Investigations in the field of polymer brushes were historically started from “simple” polymers such as polystyrene or polybutadiene; later on, more functional amphiphilic, charged, thermo- and photo-responsive polymers were involved into the brush-like configuration that allowed to significantly enrich properties of polymer brushes and to extend the areas of their application. We suggested that involvement of highly functional conjugated (or conductive) polymers (CPs) would be the next logical and promising step in the development of this class of polymer materials.

Conductive polymers and especially, poly(3-alkylthiophenes) (P3ATs), continue to attract considerable interest of researchers due to their exceptional electronic and photonic properties largely depending on mesoscale organization of CPs[11]. We presumed that a combination of these two attractive

[1] Netz, R.R; Schick, M., *Macromolecules,* **1998**, 31, 5105-5122.
[2] Kramer, E.J., *Isr. J. Chem.,* **1995**, 35, 49.
[3] Napper, D.H., *Polymeric Stabilization of Colloidal Dispersions*; Academic Press: New York, 1983.
[4] Fleer, G.; Cohen Stuart, M.A.; Scheujens, J.M.H.M.; Cosgrove, T.; Vincent, B., *Polymers at Interfaces*; Chapman and Hall: London, 1993.
[5] Zheng, Z.; Azzaroni, O.; Zhou, F.; Huck, W.T.S., *J. Am. Chem. Soc.,* 2006, 128, 7730 -7731.
[6] Senaratne, W.; Andruzzi, L.; Ober, C.K., *Biomacromolecules,* **2005**, 6, 2427-2448.
[7] Wirth, M.J.; Swinton, D.J., *J. Phys. Chem. B,* **2001**, 105, 7, 1472 -1477.
[8] Raviy, U.; Giasson, S.; Kampf, N.; Gohy, J.F.; Jerome, R.; Klein, J., *Nature,* **2003**, 425, 163-165.
[9] Retsos, H.; Senkovskyy, V.; Kiriy, A.; Stamm, M.; Feldstein, M.; Creton. C., *Adv. Mater.,* **2006**, 18, 2624-2628.
[10] Luzinov, I.; Minko, S.; Tsukruk, V., *Prog. Polym. Sci.,* **2004**, 29, 635-698.
[11] For ex.: Sirringhaus, H.; Brown, P.J.; Friend, R.H.; Nielsen, M.M.; Bechgaard, K.; Langeveld-Voss, B.M.W.; Spiering, A.J.H.; Janssen, R.A.J.; Meijer, E.W.; Herwig, P.; de Leeuw, D. M., *Nature,* **1999**, 401, 685-688.

issues of conjugated polymer and polymer brush might have a significant synergistic effect. For instance, brush-like architecture of CP films would have a beneficial effect on solar-cells performance, if CP chains will be grown directly from working electrodes thus forming optimized bulk heterojunctions[12]. On the other hand, immobilization of CPs onto a solid support without loss of their conformational freedom is a key step toward *regenerable* biological and chemical sensors[13]. Despite of obvious promises, little has been done in the field of CP brushes. This can be explained by the great difficulties encountered during the preparation of such brushes. It must be emphasized that in this work we were exclusively interested in *intrinsically soluble* conjugated polymers (such as poly(3-alkylthiophenes), having solubilizing groups), since only such systems meet the above-mentioned definition of polymer brushes and would be of interest for photovoltaic, sensors or other applications.

Outline of the thesis. *The first chapter* discusses the definition and the classification of polymer brushes and briefly reviews the main approaches for the preparation of polymer brushes. The chapter also considers the general types of conjugated polymers, main synthetic schemes to CPs, and the step- and chain-growth polymerization mechanisms. In the end of chapter presents the aim and outline of thesis. *The second chapter* describes experimental techniques most frequently used in this work (ellipsometry and cyclic voltammetry). *The third chapter* describes the basic principles, fabrication, and characterization of photovoltaic cells. *The fourth, fifth and sixth chapters* treat the experiments performed in the course of this work and discuss the results obtained. *The sixth chapter* includes the preparation of poly(3-alkylthiophenes), P3HT brushes from patterned surfaces. *The final seventh chapter* presents general conclusions and discusses the outlook of the work.

Results and novelty. A method for covalently grafting regioirregular poly(3-hexylthiophene) to substrates modified by macromolecular anchors was developed. To graft the *regioregular* poly(3,3"-dioctyl-[2,2';5',2"]terthiophene) (PDOTT), an electrochemical oxidative polycondensation of symmetrically substituted 3,3"-dioctyl-[2,2';5',2"]terthiophene (DOTT) was used. The modification of the supporting ITO electrode by a self-assembled monolayer of a compound having polymerizable head-groups with properly adjusted oxidative potential was found to be essential to achieve a covalent attachment of PDOTT chains. In collaboration with Prof. Leo group (TU Dresden), a feasible method

[12] Snaith, H.J.; Whiting, G.L.; Sun, B.; Greenham, N.C.; Huck, W.T.S.; Friend, R.H., *Nano Lett*., **2005**, 5, 1653-1757.

[13] (a) McQuade, D.T.; Pullen, A.E.; Swager, T.M., *Chem. Rev.,* **2000**, 100, 2537-2574. (b) Ho, H.A.; Dore, K.; Boissinot, M.; Bergeron, M.G.; Tanguay, R.M.; Boudreau, D.; Leclerc, M., *J. Am. Chem. Soc*., **2005**, 127, 12673-12676.

was developed for the production of semiconducting polymer brushes of grafted PDOTT for organic photovoltaic.

The thesis describes a new method to grow conductive polymer brushes of regioregular head-to-tail poly(3-alkylthiophenes) via surface initiated polycondensation of 2-bromo-5-chloromagnesio-3-alkylthiophene. Therefore a simple procedure for the preparation of the Ni(II) macroinitiator by the reaction of $Ni(tpp)_4$ with photo-cross-linked poly(4-bromostyrene) films was developed. Exposing the initiator layers to the monomer solution leads to selective chain-growth polycondensation of the monomer from the surface, resulting into P3AT brushes in a very economical way. In contrast to the P3AT films prepared by traditional solvent casting methods, our approach leads to mechanically robust CP films, stable against delamination. Furthermore, grafting of P3HT was performed from surface-immobilized poly(4-vinylpyridine)-*block*-poly(4-iodostyrene), P4VP-*b*-PS-I block copolymers that provided new possibilities for micro- and nano-patterning of conductive polymer brushes. Having in mind the high processability of poly(4-bromostyrene), PS-Br, poly(4-iodostyrene), PS-I, and their copolymers along with the possibility to apply various standard lithography methods (such as contact molding or photolithography) to such polymers, we believe that our approach represents a new dimension in fabrications of all-plastic devices.

Publications.

1. Khanduyeva, N.; Bocharova, V.; Kiriy, A.; Ulrich, O.; Mueller, M.; Stamm, M. "Grafting of Conductive Polymers from Poly(glycidyl methacrylate)-Based Macromolecular Anchoring Layer". *Polymeric Materials: Science & Engineering,* **2006,** *51,* 593-594.

2. Senkovskyy, V.; Khanduyeva, N.; Komber, H.; Oertel, U.; Stamm, M.; Kuckling, D.; Kiriy, A. "Conductive Polymer Brushes of Regioregular Head-to-Tail Poly(3-alkylthiophenes) via Catalyst-Transfer Surface-Initiated Polycondensation". *J. Am. Chem. Soc*., **2007**, *129*, 6626-6632.

3. Khanduyeva, N.; Senkovskyy, V.; Beryozkina, T.; Bocharova, V:, Simon, F.; Nitschke, M.; Stamm, M.; Rainer Grötzschel, Kiriy, A. "Grafting of Poly(3-hexylthiophene) from Poly(4-bromostyrene) Films by Kumada Catalyst-Transfer Polycondensation (KCTP): Revealing of the Composite Films Structure". *Macromolecules,* **2008**, *41*, 7383-7389.

4. Khanduyeva, N.; Senkovskyy, V.; Beryozkina, T.; Horecha, M.; Stamm, M.; Uhrich, C.; Riede, M.; Leo, K.; Kiriy, A. “Surface Engineering Using Kumada Catalyst-Transfer Polycondensation (KCTP): Preparation and Structuring of Poly(3-hexylthiophene)-Based Graft Copolymer Brushes”. *J. Am. Chem. Soc.,* **2009**, 31, 153–161.

CHAPTER 1

POLYMER BRUSHES AND CONJUGATED POLYMERS

In this chapter presents definitions and classifications of polymer brushes. It reviews the main approaches for the preparation of polymer brushes and describes general types of conjugated polymers, main synthetic schemes to CPs, and reviews main types polymerization mechanisms (i.e., the step-growth and chain-growth polymerization mechanisms). The aim and outline of this thesis are given in this chapter.

1.1 POLYMER BRUSHES: DEFINITIONS AND CLASSIFICATION

Polymer brushes refer to an assembly of polymer chains which are tethered by one end to a surface or an interface[14]. The tethering is sufficiently dense, such that the polymer chains are crowded and thus forced to stretch away from the surface or the interface to avoid overlapping, sometimes much farther than the typical unstretched size of a chain. These stretched configurations are found under equilibrium conditions; neither a confining geometry nor an external field is required. The situation in which polymer chains stretch along the direction normal to the grafting surface is quite different from the typical behavior of flexible polymer chains in solutions where chains adopt to a random-walk configuration. A series of discoveries show that the deformation of densely tethered chains affects many aspects of their behavior and results in many novel properties of polymer brushes[14].

Models of polymer brush architectures include polymer micelles, block copolymers at fluid–fluid interfaces, grafted polymers on a solid surface, adsorbed diblock copolymers, and graft copolymers at fluid–fluid interfaces as seen in Fig. 1.1.

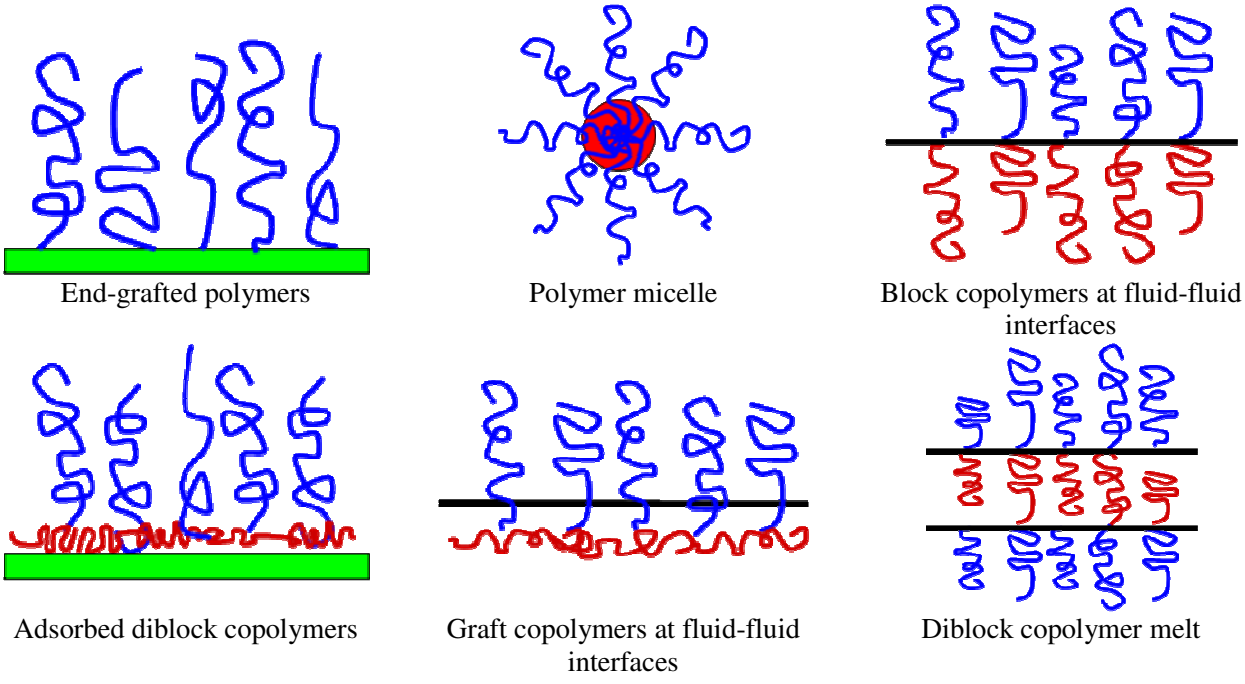

Figure 1.1. *Examples of polymer systems comprising polymer brushes.*

A common feature of various polymer brushes is that the polymer chains exhibit deformed configurations. Solvent can be either present or absent in polymer brushes. In the presence of a good solvent, the polymer chains try to avoid contact with each other to maximize contact with solvent

[14] Zhao, B.; Brittain, W.J., *Prog. Polym. Sci.,* **2000,** 25, 677-710.

molecules. Without solvent (melting conditions), polymer chains must stretch away from the interface to avoid overfilling incompressible space[14,15].

Polymer chains grafted on a surface show much richer conformations than free chains because of confinement of the chains near the surface. At low grafting density, the distance between grafting sites is larger than the size of the chains, and the grafted polymer chains do not overlap. If the polymer segments have an attractive interaction with the surface, the polymer chains exhibit a so called "pancake-like" conformation (see Fig. 1.2). In contrast, if the segment–surface interaction is non-attractive, a "mushroom" structure can be observed. At high-grafting density, as a consequence of the balance between segment–segment repulsion and elasticity of the chains, the grafted chains are stretched away from the surface to form brushes. The state of the surface-anchored polymer layer is determined by the grafting density, the structure of the chains, the solvent quality and the segment–surface interaction. If the chains are charged, the conformations are defined by electrostatic interactions. Accordingly, the ionic strength and pH of the surrounding medium have great influence on the formation of the brushes[16,17].

In terms of polymer chemical compositions, polymer brushes tethered on a solid substrate surface can be divided into homopolymer brushes, mixed homopolymer brushes, random copolymer brushes and block copolymer brushes. Homopolymer brushes refer to an assembly of tethered polymer chains consisting of one type of repeat unit. Mixed homopolymer brushes are composed of two or more types of homopolymer chains.

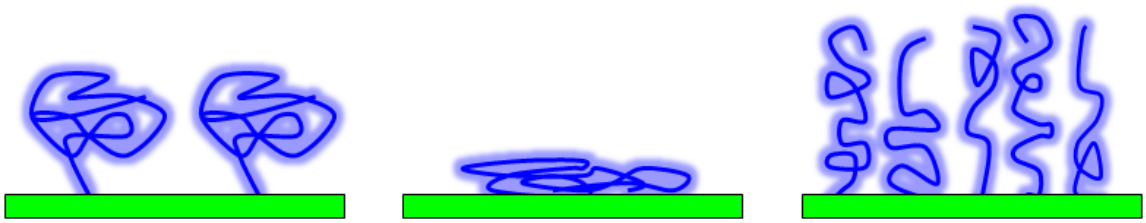

Figure 1.2. *Schematic depiction of the conformations of polymer molecules attached to a solid surface: mushroom, pancake, and brush conformation.*

Random copolymer brushes refer to an assembly of tethered polymer chains consisting of two different repeat units which are randomly distributed along the polymer chain. Block copolymer brushes refer to an assembly of tethered polymer chains consisting of two or more homopolymer chains covalently connected to each other at one end. Homopolymer brushes can be further divided into

[15] Minko, S., *Polym. Rev.*, **2006**, 46, 397–420.
[16] Liu, G.; Yan, L.; Chen, X.; Zhang, G., *Polymer*, **2006**, 47, 3157–3163.
[17] Rühe, J.; Knoll, W., *Polym. Rev.,* **2002**, 42, 91 – 138.

neutral polymer brushes and charged polymer brushes. They may also be classified in terms of rigidity of the polymer chain and would include flexible polymer brushes, semiflexible polymer brushes and liquid crystalline polymer brushes (Fig. 1.3)[14].

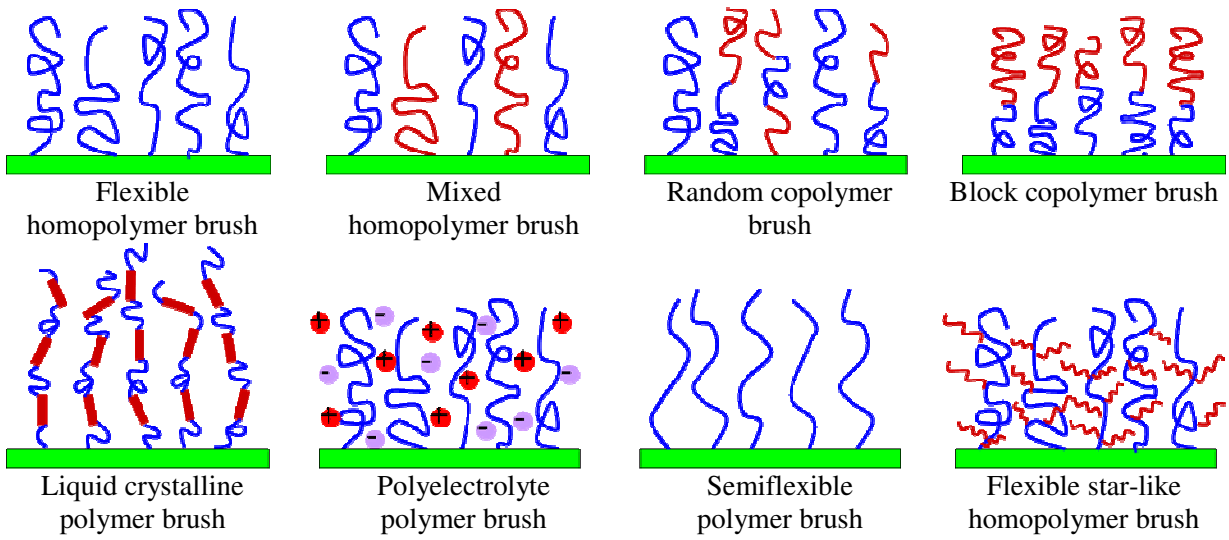

Figure 1.3. *Classification of polymer brushes.*

The most important parameters of polymer brushes are: the segment density profile of the surface-attached chains, the brush height (h) as a function of the graft density C (in mol per area) or A (in area per molecule), chain end-to-end distance $(r^2)^{1/2}$ and the molecular weight of the surface-attached chains. Within polymer brushes, the distance between grafting points d is smaller than the chain end-to-end distance. Polymer brushes can be introduced as thin films of end-grafted polymer molecules if the following conditions are satisfied: $h>(r^2)^{1/2}$, $d<(r^2)^{1/2}$.

A further important parameter is the solvent quality of the surrounding medium. The brush height (h) in solvent is larger than the chain end-to-end distance $(r^2)^{1/2}$ of the same non-grafted chains dissolved in the same solvent. The key idea behind the theoretical elucidations is that the free energy, F, of the chains is obtained from a balance between the interaction energy of two statistical segments $F_{int.}$ and the elastic free energy $F_{el.}$ of the chains[18].

$$F = F_{\text{int}} + F_{el} \qquad (1.1)$$

A first description of such a system has been attempted by Alexander[18] for monodisperse chains consisting of N segments, which are attached to a non-adsorbing surface with an average distance of the grafting anchor points (t_D) much smaller than the radius of gyration of the same unperturbed chains

[18] Alexander, S., *J. Phys*., **1977**, 38, 983–987.

not in contact with the surface. If both the interaction energy and the elastic energy are calculated and minimized with respect to the brush height, the following equation is obtained for brushes in a good solvent:

$$h \sim N\sigma^{1/3} \qquad (1.2)$$

This dependence of the brush height to the molecular weight of the polymer molecules is much stronger than that of the size of a polymer coil in solution where the size of the molecule, or more precisely the radius of gyration (R_g) scales according to $R_g \sim N^{1/2}$.

There are several theories describing the behavior of polymer brushes. A theory of polymer brushes has been developed by Alexander[18] and de Gennes[19] on the basis of a scaling argument in the athermal case (i.e., for a good solvent). Their treatment is based on a number of assumptions, most notably, that the free chain ends are confined to the top of the grafted layer, and that the vertical polymer concentration profile describes a step function[20]. Although the Alexander model is very simple, it predicts the experimentally observed scaling behavior accurately and allows an understanding of some of the most striking properties of polymer brushes, e.g. lubrication and wetting behavior. More sophisticated models are required to describe the segment density profile correctly or to allow for the presence of charges in the polymer molecule[21].

These assumptions have been relaxed in the self-consistent field theory[22], which predicts a parabolic concentration profile. Properties that are not particularly sensitive to the details of the profile, however, generally have the same functional dependence on the polymer chain length and grafting density in both theoretical approaches, with small differences in the numerical prefactors.

The mechanical properties of polymer brushes have been investigated by numerous authors on the basis of the Alexander and de Gennes approximation. Rabin and Alexander[23] themselves considered the vertical stretching of polymers in good solvents. Their approach was generalized to the poor solvent case by Halperin and Zhulina[24]. The behavior of brushes in good solvents under lateral shear has been studied extensively due to potential applications in lubrication of surfaces. Fredrickson *et al.*[25] have developed an expression for the free energy of a polymer brush as a function of deformation of its free surface. They have shown that the elastic properties of the grafted brush can be expressed in terms of an effective shear modulus, which depends on the square of the grafting density.

[19] de Gennes, P.G., *Macromolecules*, **1980,** 13, 1069-1075.
[20] Utz, M.; Begley, M.R., *J. of the Mechanics and Physics of Solids*, **2008,** 56, 801-814.
[21] Szleifer, I.; Carignano, M., *Ad. Chem. Phys*., **1996,** 94, 165-260.
[22] Milner, S.T.; Whitten, T.A., *J. Phys*., Paris, **1988**, 49, 1951.
[23] Rabin, Y.; Alexander, S., *Europhys. Lett*., **1990**, 13, 49-54.
[24] Halperin, A.; Zhulina, E.B., *Macromolecules*, **1991**, 24, 5393–5397.
[25] Fredrickson, G.H.; Ajdari, A.; Leibler, L.; Carton, J-P., *Macromolecules*, **1992**, 25, 2882–2889.

Zhang *et al.*[16] explored the mechanism of the formation of polymer brushes with quartz crystal microbalance and found a three-regime-kinetics of the grafting (Fig. 1.4). The first polymer chains form a random mushroom, then the chains rearrange themselves to eliminate the local overlapping and form an ordered mushroom. The conformation of the already grafted chains is changed so that the incoming chains can be grafted on the surface. In addition, the dissipation change also gives the information about the structure of the polymer layer formed by the grafted chains.

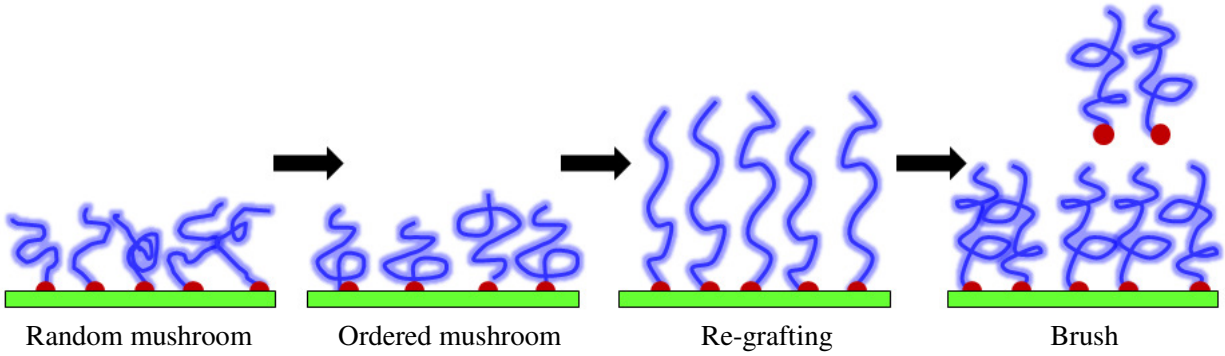

Figure 1.4. *The average grafting distance between polymer chains changes during the process of forming polymer brushes.*

1.1.1 SYNTHESIS OF POLYMER BRUSHES

Tethering of polymer chains onto a solid surface can be both a reversible or irreversible process depending on the nature of the bond (covalent, electrostatic interactions, hydrogen bonds, or the strong van der Waals interactions). Weak interactions however are less interesting. The elastic energy component accumulated in the polymer brush may destroy weak bonds due to stretching[25]. The synthetic strategies for the generation of polymer brushes can be classified into three main categories in respect to the driving force for brush formation[26]: phase separation (and compression), physisorption, and chemisorption. With *phase separation*, amphiphilic block copolymers consisting of a water-soluble block and a water insoluble block are spread at the air - water interface (Fig. 1.5a). The water-soluble block dissolves into the aqueous subphase, but is anchored to the air-water interface by the hydrophobic block leading to formation of a well-defined Langmuir monolayer. Upon compression of the monolayer, the distance between the anchor points of the polymer chains decreases and the hydrophilic block is stretched away from the surface into the aqueous subphase. Structurally well-defined layers are obtained when the hydrophobic block is in a molten state, which allows a rearrangement of the chains within the film upon compression. The obtained films can be

[26] Rühe, J.; Knoll, W., *Supramol. Polym.,* 2000, Marcel Dekker, New York, 565-613.

photochemically cross-linked and transferred to a solid substrate[27]. The situation is quite similar if lipopolymers are spread at the air-water interface (Fig. 1.5b)[28] instead of block copolymers. In both approaches, one important requirement for this synthetic strategy seems to be to avoid the loss of hydrophobic anchors to the subphase through dissolution and/or formation of micellar structures.

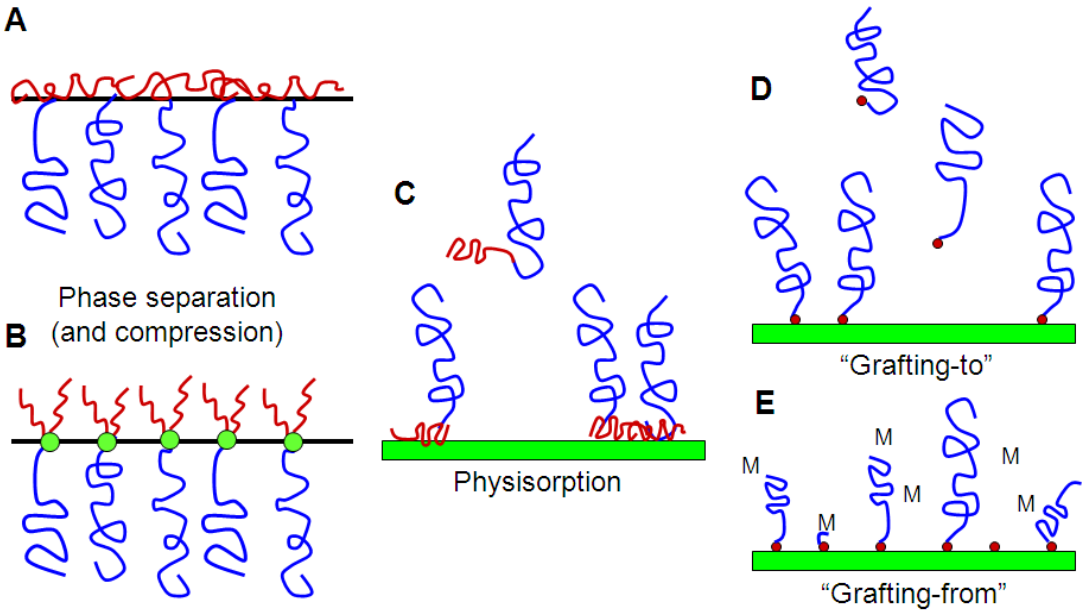

Figure 1.5. *Synthetic methods for the generation of polymer brushes.*

Physisorption on the other hand is a reversible process and is achieved by the self-assembly of polymeric surfactants or end-functionalized polymers on a solid surface (Fig. 1.5c). It is more suitable for block copolymers. Physisorption of block copolymers or graft copolymers occurs in the presence of selective solvents or selective surfaces, giving rise to selective solvation and selective adsorption, respectively. One block has strong interactions with the surface and acts as an "anchor" for the polymer chains; the other block has only weak interactions with the surface, but strong interactions with the solvent and oats in the solvent like a "buoy" or polymer brushes in the solution. The detailed polymer brush structure depends on the selectivities of these media and the nature of the copolymers, the architecture of copolymers, the length of each block and the interactions between blocks and surface. The surface grafting density and all other characteristic dimensions of the structure are controlled by thermodynamic equilibrium, but with possible kinetics[14].

[27] Gödel, W.A.; Luap, C.; Oeser, R.; Lang, P.; Braun, C.; Steitz, R., *Macromolecules,* **1999,** 32, 7599-7609.
[28] Naumann, C.A.; Brooks, C.F.; Fuller, G.G.; Knoll, W.; Frank, C.W., *Langmuir*, **1999,** 15, 7752-7761.

The preparation of polymer brushes by adsorption of block copolymer from a selective solvent (or on selective surface) is not difficult. However, polymer brushes exhibit thermal and solvolytic instability due to the weak interactions between the substrate and block copolymers[3]. The interactions result in most cases from van der Waals forces or hydrogen bonding. Desorption can occur upon exposure to other good solvents or the adsorbed polymers can be displaced by other polymers or other low molecular weight compounds. If these polymer ultrathin films are heated to high temperatures (e.g. above glass transition temperature or melting temperature), dewetting occurs and polymer films are no longer homogeneous due to formation of polymer droplets[29]. Also, it is not always easy to synthesize block copolymers, which are suitable for physisorption. Some of these drawbacks could be overcome by covalently tethering polymer chains to substrates. As a third option, polymer brushes can be obtained by *chemisorption*. Chemisorption is irreversible grafting which accomplished by chemical bonding. The method can be divided into a "grafting to" and a "grafting from" process.

The "grafting to" process is performed by attaching preformed polymer molecules to the substrate surface from a solution through addition or condensation reactions (Fig. 1.5d)[14,26]. While this method is very simple and straightforward, it has several limitations. On one hand, a fast and high yield surface reaction with a high number of chains covalently bound to the surface requires rather reactive anchor groups, which does not tolerate the coexistence of a large number of functional groups in the same molecule. For example, silane anchor groups prohibit the use of polymers containing amine or alcohol groups. A second problem is that for some applications, only rather thin films of typically 3-5 nm dry film thickness can be obtained by this method. As soon as the surface becomes significantly covered with attached chains, the polymer concentration at the interface becomes higher than the concentration of macromolecules in solution. Additional chains trying to reach the surface have to diffuse "uphill" against the concentration gradient, which becomes steeper with every additional attached chain. This diffusion barrier renders the immobilization of the chains at the surface more and more unfavorable. Due to the kinetic hindrance, further polymers are linked to the surface only at a very low rate.

Much higher graft densities can be obtained if the polymer chains are grown at the surface of the substrate *in situ,* which is called "grafting from". Initiator species are either generated or self-assembled at the surface of the substrate, followed by initiation of chain-growth from these surface-attached initiators *in situ,* e.g. by free radical chain polymerization (Fig. 1.5e). Surface polymerization can be started thermally either through a chemical process or photochemically. With the "grafting from"

[29] Zerushalmi-Royen, R.; Klein, J.; Fetters, L., *Science,* **1994**, 263, 793-795.

process, polymer monolayers have been obtained in the dry state with film thicknesses of more than 2000 nm. These extremely thick brushes are composed of polymer molecules with average molecular weights of several million g/mol attached at anchor points with distances between them of less than 3 nm. An interesting alternative to growing brushes by free radical processes is to use other chain-growth reactions: controlled radical polymerization, carbocationic polymerization, anionic polymerization, and ring opening metathesis polymerization. These allow obtaining surface-attached polymer chains with relatively narrow molecular weight distributions. It also facilitates comparison with the theoretical models developed for surface-attached polymer brushes, provided that the initiation is efficient enough to allow high graft densities and that the molecular weight of the surface-attached chains is high enough to allow such a discussion. Controlled polymerization approaches are expected to become even more interesting for the synthesis of surface-attached polymer brushes in the near future, as it seems to be possible that a large variety of functional brushes can also be obtained by these methods. Strenuous efforts are being made especially in the area of controlled radical polymerization to polymerize functionalized monomers to high molecular weight compounds with low polydispersity.

1.1.2 TYPES OF POLYMER BRUSHES

Polymer brushes can be divided into several types, depending on the kind of the polymer used for their preparation. The first type is *neutral polymer brushes,* which are flexible, non-conductive and have a low reactivity. Their morphology, surface chemical composition, and wettability can reversibly switch upon changes of the environment. Examples of neutral polymer brushes are polystyrene (PS), polymethacrylates (PMA), and polyvinylpyridine (PVP) brushes. The main characteristics of interest for neutral polymer brushes are the brush height and the polymer density profile, which can be well predicted from self-consistent calculations and simulations[30].

The next class of polymer brushes is *charged or polyelectrolyte polymer brushes*, which consist of polyelectrolytes carrying opposite electric charges. Charged polymers or polyelectrolytes are of practical importance since they are soluble in water. Counterion degrees of freedom determine the brush behavior in a decisive way and lead to a strong and non-linear swelling of the brush. They can be used for colloidal stabilization, control of adhesion, tuning of lubrication, selective adsorption of biological objects (DNA, proteins, etc.), or liquid-crystal displays. Examples of polyelectrolyte brushes are PSAs, PAAs, and PVPs.

[30] Naji, A.; Seidel, C.; Netz, R.R., *Adv. Polym. Sci.,* **2006**, 198, 149-183.

On the other hand, conductive polymers and especially, poly(3-alkylthiophenes) (P3ATs), continue to attract considerable interest of researchers due to their exceptional electronic and photonic properties largely depending on mesoscale organization of conjugated polymers (CPs)[12]. A surge of research has been performed on soluble conjugated polymers, due to their potential use as components in electronic applications, such as field effect transistors (FETs), light emitting diodes (LEDs), actuators, and solar cells. The development of these soluble conjugated polymers has led to significant improvements in their properties, including their high electrical conductivity (up to 2000 S/cm), high field effect mobility (~0.12 $cm^2/V \cdot s$) with excellent on/off ratios in FETs (10^7), high solid state photoluminescent and LED efficiencies (10% photons/electrons, external), and significant solar energy conversion efficiencies (4.2%)[31].

We suggested that a combination of these two attractive issues (polymer brush configuration and conductive polymer area) might have a significant synergistic effect. For instance, brush-like architecture of CP films would have a beneficial effect on solar-cells performance, if CP chains will be grown directly from working electrodes thus forming optimized bulk heterojunctions[12]. On the other hand, immobilization of CPs onto a solid support without loss of their conformational freedom is a key step toward *regenerable* biological and chemical sensors[13]. Despite of the obvious promises, little has been done in the field of CP brushes. This can be explained by great the difficulties which one meets during the preparation of such brushes. It must be emphasized that this work reports exclusively about *intrinsically soluble* conjugated polymers (such as P3HT, having solubilizing groups), since only such systems fall to the above mentioned definition of polymer brushes and thus would be of interest for photovoltaic, sensor or other applications.

1.2 MAIN SYNTHETIC WAYS TO PRODUCE THE CONJUGATED POLYMERS AND THEIR SUITABILITY IN THE PREPARATION OF POLYMER BRUSHES

This section briefly introduces the main synthetic routes to CPs and their suitability in preparation of polymer brushes. Conjugated polymers are macromolecules that possess alternating single and double bonds along the main chain. Some common conjugated polymers are polypyrrole (PPy), polythiophene (PT), polyacetylene (PA), polyphenylene (PPP), polyphenylenevinylene (PPV) and polyfluorene (PF).

[31] Skotheim, T.A.; Reynolds, J.R., *Conjugated polymers: processing and application*, 3rd ed., 2007, Publisher: by Taylor & Francis Group, LLC.

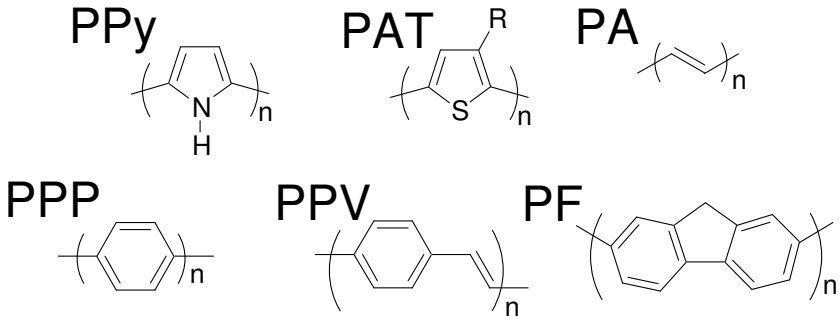

Conjugated polymers are classes of plastic materials with semiconducting characteristics. The polymers become conductive in a doped state, where a delocalized π-electron system exists along the molecular backbone. This system confers semiconducting properties to the polymer and gives it the ability to support positive and negative charge carriers along the polymer chains. The electronic and optical properties of π-conjugated polymers result from a limited number of states around the highest occupied and the lowest unoccupied levels. According to the band theory, the highest occupied band, originating from the HOMO of each monomer unit, is referred to as the valence band. The corresponding lowest unoccupied band originates from the LUMO and forms the conduction band. The evolution of bands in conjugated polymer during its formation by monomer addition is shown in Fig. 1.6.

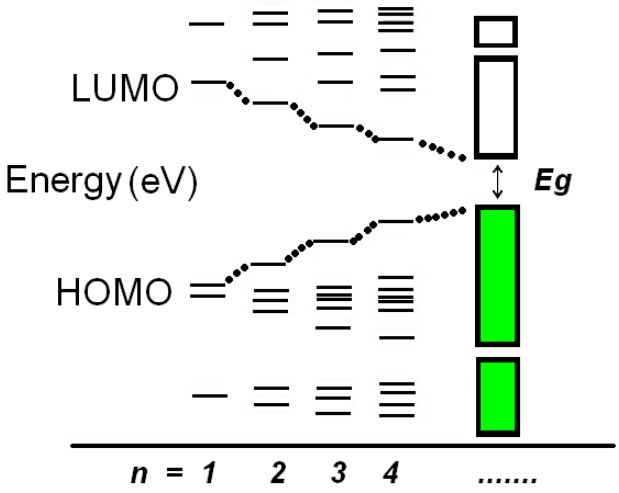

Figure 1.6. *Band formation during the polymerization of a conjugated monomer into a π-conjugated polymer, where* ***n*** *is the number of monomer units in the polymer chain.*

The longer the conjugation on the backbone, the smaller the resulting band gap (E_g). It was generally found that the band gap decreases with increasing conjugation length, approaching a finite value for infinite conjugation length. Torsion between the adjacent rings partially interrupts the conjugation and leads to an effective increase of the band gap.

Conjugated polymers in the non-doped and doped conducting state have a range of potential applications in the microelectronics industry. Conducting polymers are effective discharge layers as well as conducting resists in electron beam lithography. They also find applications in metallization (electrolytic and electro-less) of plated through-holes for printed circuit board technology, provide excellent electrostatic discharge protection for packages and housings of electronic equipment, excellent corrosion protection for metals, and may have applications in electromagnetic interference shielding and photovoltaic devices. Especially photovoltaic devices desire conductive polymers with a low band gap. There are several factors that influence the band gap of a conjugated polymer material, such as intra-chain charge transfer, bond-length alternation, aromaticity, substitutes effects, intermolecular interactions, and π-conjugation length[32,33]. Planarity along the aromatic backbone results in a low band gap due to a high degree of delocalization of π-electrons. Alternating single and double bonds along the polymer chain has a tendency to increase the band gap[34].

1.2.1 STEP-GROWTH CONDENSATION POLYMERIZATION

Step-growth polymerization is a polycondensation process in which condensation reactions between two functional groups A and B are used to build up polymers and low molecular products are extracted. The polymer is formed from monomer with difunctional molecules. Either "AB-type" monomers (with complementary functional groups in one molecule) or pairs of "AA-type" and "BB-type" monomers (with the same type of functionality in one molecule) may be used. Typically, hetero-chain polymers such as polyethers, polyesters, polyamides, polycarbonates, and polyurethanes are obtained via step-growth polycondensations or polyadditions. From the viewpoint of polymer brush synthesis, a number of problems encountered in step-growth polymerization arise. The required high degree of conversion of functional groups and the required exact stoichiometry of functional groups must be in balance. If conditions are not met, only poorly defined oligomers are typically obtained. This is why one has to ensure that the starting materials are pure, the stoichiometric ratio in the case of AA-type and BB-type monomers is exactly unity, and no side reactions consume functional groups. Another disadvantage of the step-growth polycondensations with regard to applications is the relatively broad molecular weight distribution of the products as a result of the statistical nature of the step-growth process. The typically observed polydispersity of PDI≈2 means in practice that even high

[32] Winder, C.; Sariciftci, N.S., *J. Mater. Chem.*, **2004,** 14, 1077-1088.
[33] Kitamura, C.; Tanaka, S.; Yamashita, Y., *Chem. Mater.*, **1996,** 8, 570-578.
[34] Bundgaard, E.; Krebs, F.C., *Sol. Energy Mater. Sol. Cells.*, **2007,** 91 954–985.

molecular weight polymers contain substantial amounts of oligomers. For this process it is difficult to synthesize condensation polymers having a controlled molecular weight with a narrow molecular weight distribution in a step-growth polymerization mechanism.

1.2.2 CHAIN-GROWTH ADDITION POLYMERIZATIONS

In chain-growth polymerizations, an active center, e.g. a radical, an anion, a cation etc. is generated in the initiation step. This active center adds monomers and grows into a polymer chain with an active chain end. This process is called chain propagation, and has the problem that there is always the possibility that the active center is quenched. Depending on whether a new chain is started during this process or not, the result is chain termination or chain transfer. The average molecular weight of the resulting polymers depends on the relative rates of chain propagation, chain transfer, and chain termination. Both termination and transfer are statistical processes. For this reason, the obtained polymers have a broad molecular weight distribution with a polydispersity index PDI≈2. As in the case of step-growth reactions, even high molecular weight products may contain considerable amounts of oligomers, which have a profound effect on materials properties. The main obstacle to obtaining high molecular weight materials is polymerization kinetics. The propagation reaction must be fast compared to termination and transfer.

In order to synthesize a polymer with controlled molecular weight and low polydispersity and escape problems such as diffusion limitation, inhomogeneity of the reaction mixtures, polymer precipitation, etc., the polymerization should start from an initiator unit and proceed in a chain-growth polymerization manner without disproportionation or termination. This is the case for so-called “living” chain polymerizations. If all polymer chains are started at about the same time, they grow at the same average rate, and never terminate until the reaction is quenched. The result is a narrow molecular weight distribution, with a polydispersity of typically PDI<1.1. The molecular weight of the obtained polymers can usually be adjusted by the stoichiometric ratio of the monomer and the initiator. As a result, while the polymers are still not monodisperse in molecular weight, the products are usually not contaminated with oligomers, which greatly improves most materials properties. These polymerization methods also have enabled polymers of various shapes, such as block and graft polymers as well as star polymers, making it possible to construct self-assembled supramolecular architectures with defined shapes and properties. However, living polymerization had been applicable only to additive polymerization of vinyl monomers and exothermic ring-opening polymerization of cyclic monomers, but not to polycondensation and polyaddition.

1.2.3 CHAIN-GROWTH CONDENSATION POLYMERIZATION

Yokozawa *et al.*[35] have, shown that even condensation polymerization can be realized in a *chain-growth* manner. In this process, selective activation of the polymer propagating termini suppresses the reaction of monomers between each other, such that the monomer reacts only with the initiator and the polymer end group. Fig. 1.7 shows this approach of chain-growth condensation polymerization, where a selective activation of polymer end groups has been implemented by using a change of substituent effects between the monomer functional groups.

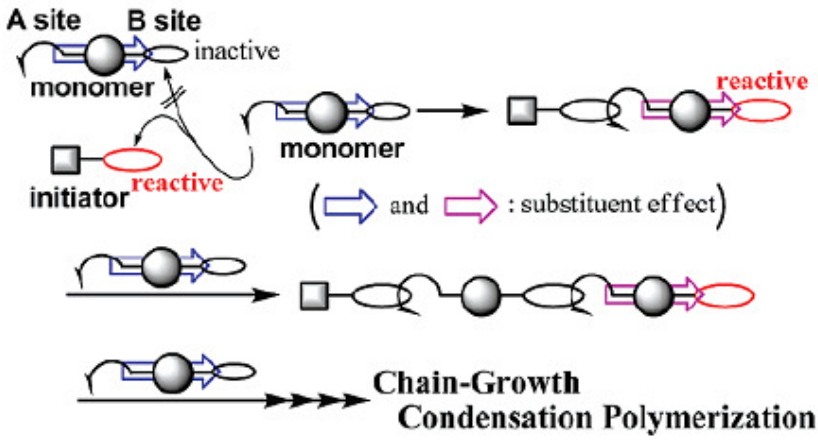

Figure 1.7. *Schematic illustration of chain-growth polycondensation of AB type monomers.*

In this monomer, the substituent effect of the A site diminishes the reactivity of the B site, suppressing undesired step-growth reactions between the monomers. When, the monomer reacts with an initiator having a reactive site, the substituent effect changes. If the substituent effect of the formed bond enhances the reactivity of the polymer end group, the next monomer would react selectively with the polymer propagating end. The chain-growth condensation polymerization differs significantly from living polymerization in terms of the reactivity of monomers: while living polymerization is generally conducted for monomers that are unable to polymerize without initiators, the monomers used in the chain-growth condensation polymerization can polymerize without initiators, resulting in undesired step-growth polymerization if the conditions are not appropriately controlled. Therefore, suppression of the reaction between monomers is one of the key points of successful chain-growth condensation polymerization.

[35] Yokoyama, A.; Yokozawa, T., *Macromolecules*, **2007**, 40, 4093-4101.

1.2.4 MAIN SYNTHETIC ROUTES TO PRODUCE THE CONJUGATED POLYMERS

Step-growth polycondensations. A majority of synthetic routes to CPs involve a step-growth condensation type of polymerization (polycondensation). Polymerization refers to a stepwise more or less statistical coupling of monomer molecules and the formation of oligomers in later stages via abstraction of small molecules (like water or salts), which proceeds via a step-growth mechanism. The main step-growth synthetic routes to CPs are:

1) Oxidative polycondensation is the simplest way to CPs. Monomers such as aniline, pyrrole and thiophene and their derivatives undergo oxidative polymerization by the interaction with various oxidative agents ($FeCl_3$, ammonium persulphate, etc.).

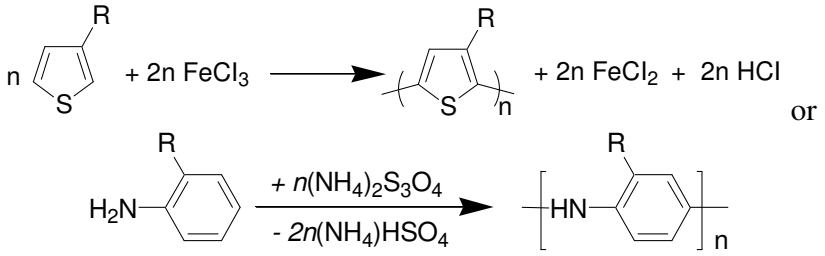

2) Electrochemical polycondensation represents another widely employed route for synthesis and immobilization of CPs. Direct *in situ* formation of a polymer film from a solution of monomers is induced electrochemically. Through electrochemical initiation, a monomer such as pyrrole, phenol or thiophene is oxidized to a polymerizable radical. Under suitable conditions, the polymer that is formed in the diffusion layer adheres firmly to the surface of the electrode. A common electrochemical technique that is employed in this process is cyclic voltammetry.

3) Wittig-Horner, Knoevenagel, polycondensation of aldehydes and amines into poly-Schiff bases:

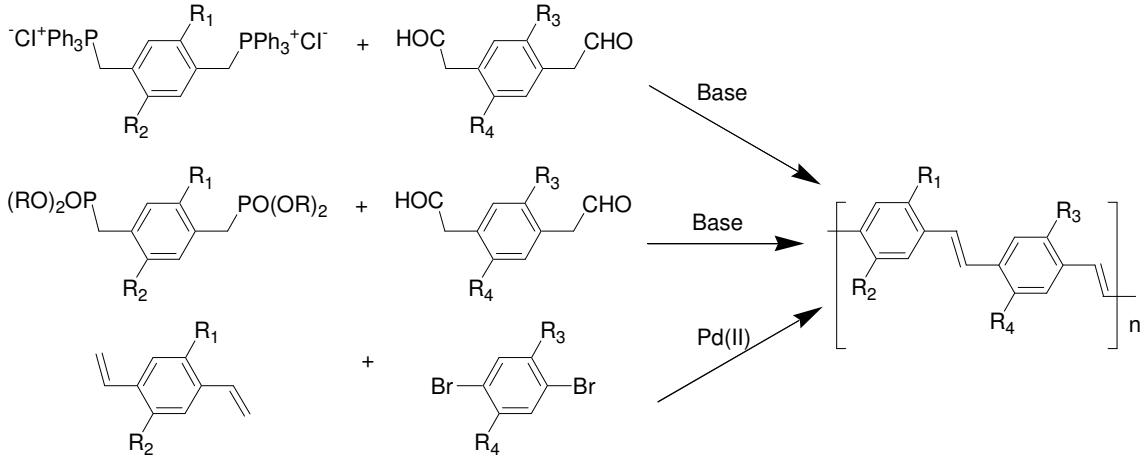

Wittig, Horner, and Heck routes to Poly(arylene vinylene)s.

4) Metal-catalyzed polycondensations are the most diverse and powerful tools for the preparation of well-defined CPs as well as random and alternative copolymers. The condensation reaction takes place via the coupling of electrophilic and nucleophilic functional groups A and B. Either "AB-type" monomers (with complementary functional groups in one molecule), or pairs of "AA-type" and "BB-type" monomers (with the same type of functionality in one molecule) may be used. The coupling, however, proceeds only in presence of catalysts (usually Ni and Pd) that activate just one or both function groups (usually the electrophilic component is activated). Depending on the exact nature of the functionality of A, B, and the catalyst used, the metal-catalyzed polycondensations can be categorized into Kumada, Stille, Suzuki-Miyaura, Heck and Sonogashira couplings:

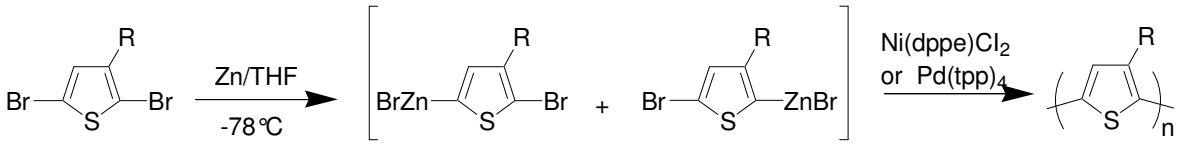

The Rieke method for the preparation of HT-PATs.

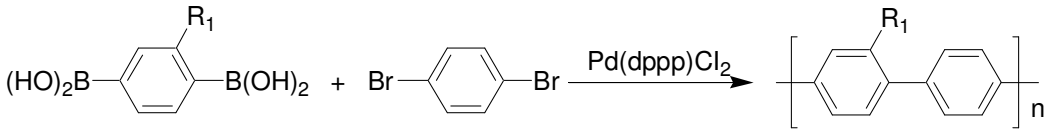

The Suzuki polymerization.

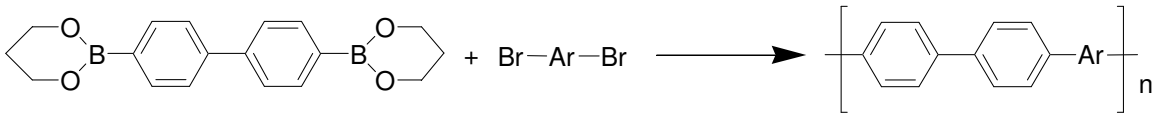

The Suzuki - Miyaura coupling.

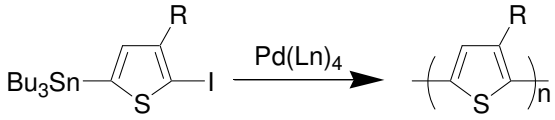

Synthesis of HT-PATs by Stille coupling reaction.

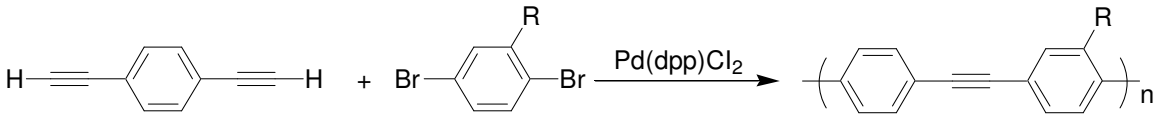

Sonogashira couplings.

Chain-growth approaches to CPs. Synthetic approaches to conductive polymers that involve chain-growth polycondensations are rare. One example is the polymerization of acetylenes. Due to the unique features of the acetylenes structure, which contains triple bonds, they are polymerized through addition polymerization of acetylenes.

Recently, Yokozawa[36] and Mcullough[37] have developed the polymerization of alkylthiophenes using a nickel-catalyzed cross-coupling reaction. The generally accepted mechanism of these reactions includes (1) oxidative addition of an organic halide with a metal-phosphine catalyst, (2) transmetallation between the catalyst complex and the reactive organometallic reagent (or disproportionate) to generate a diorganometallic complex, and (3) reductive elimination of the coupled product with regeneration of the metal-phosphine catalyst[38,39]. Numerous organometallic species such as organomagnesium, organozinc, organoboron, and organotin demonstrate sufficient efficiency to be used in cross-coupling reactions; further reports of regiospecific syntheses based on these types of monomers are appearing.

While the mechanism of metal-catalyzed cross-coupling reactions of small molecules is well understood, the exact mechanism as it applies to polymerizations has been reported only recently. As the nickel-catalyzed dehalogenative polymerization is formally a polycondensation reaction, it is generally believed to proceed through a step-growth mechanism. Recently, it has been proposed that the nickel-promoted cross-coupling polymerization proceeds through a chain-growth mechanism rather than the generally accepted step-growth mechanism. These new insights into the mechanism are particularly exciting because the chain-growth mechanism allows for very narrow molecular weight distributions and the defined molecular weights can be made for the first time. In addition, the methods have produced a quasi-living conductive polymer synthesis. A living system will lead to new regioregular PTs that have never been made before. Yokozawa provided evidence that the regioregular synthesis of poly(3-hexylthiophene) proceeds by chain-growth polymerization in the case of the chain-growth Grignard metathesis (GRIM) method. He has shown that the monomers are polymerized in a chain-growth polymerization manner, indicating that an initiator species existed from which polymerization was propagated. At the same time, another study by the McCullough group showed that the mechanism in question is chain-growth and the degree of polymerization of PATs increases with proceeding monomer conversion and can be predicted by the molar ratio of the monomer to the nickel initiator[36a]. This has been observed for two different monomers: 2-bromo-3-hexyl-5-chlorozincothiophene (obtained using the McCullough method) and 2-bromo-3-hexyl-5-

[36] a) Sheina, E.E.; Liu, J.; Iovu, M.C.; Laird, D.W.; McCullough, R.D., *Macromolecules,* **2004**, 37, 3526-3528. (b) Iovu, M. C.; Sheina, E.E.; Gil, R.R.; McCullough, R.D., *Macromolecules,* **2005**, 38, 8649-8656.

[37] (a)Yokoyama, A.; Miyakoshi, R.; Yokozawa, T., *Macromolecules,* **2004**, 37, 1169-1171. (b) Miyakoshi, R.; Yokoyama, A.; Yokozawa, T., *J. Am. Chem. Soc*., **2005**, 127, 17542-17547.

[38] Tamao, K.; Kodama, S.; Nakajima, I.; Kumada, M.; Minato, A.; Suzuki. K., Nickelphosphine complex-catalyzed grignard coupling—II. Tetrahedron, **1982,** 38, 3347–3354.

[39] Tamao, K.; Sumitani, K.; Kiso, Y.; Zembayashi, M.; Fujioka, A.; Kodama, S.I.; Nakajima, I.; Minato, A.; Kumada;. M., *Bull. Chem. Soc. Jpn*., **1976**, 49, 1958–1969.

bromomagnesiothiophene (obtained using the GRIM method)[36b,40]. Based on these experimental results, the McCullough group proposed a nickel-initiated cross-coupling polymerization system that is essentially living. This living system has produced PATs with low polydispersites and new block copolymers[41]. The data above allows two possible conclusions: the first is that the oxidative addition of the polymer chain occurs selectively. The oxidative addition of the monomer is kinetically slower, or thermodynamically less stable than the oxidative addition of the growing polymer chain, which is due to the decreased electron density of the thiophene ring on the polymer chain[42]. The second explanation would be the proposal by the McCullough group that the polymer chain and the metal catalyst exist as an associative pair via the formation of a π-complex, limiting polymerization to one end of the polymer chain.

The effect of the catalyst structure and reaction temperature on the regioregularity of PATs has also been investigated by Lucht[43]. Poly(3-octadecylthiophenes) (P3ODTs) were prepared using the GRIM method in the presence of palladium and nickel catalysts ($Ni(dppe)Cl_2$, $Pd(dppe)Cl_2$, $Ni(tpp)_4$, and $Pd(tpp)_4$). It was found that nickel catalysts provided P3ODTs with high regioregularity (>90% HT couplings), while palladium catalysts gave lower regioregularity. The effect of temperature on the regioregularity of P3ODT was also investigated. For all the catalysts studied, it was determined that the regioregularity of the polymer increased as the reaction temperature was increased.

Although a clear explanation of this effect was not presented, the authors suggest that polymerizations with nickel catalysts occur primarily through chain-growth reactions, whereas polymerizations with palladium catalysts have competing step-growth and chain-growth reactions. The temperature dependence of the regioregularity can be explained by the temperature dependence of the oxidative addition products and relative temperature independence of the transmetalation step of the catalytic cycle for the polymerization reaction. Both of which are critical factors for chain-growth polymerization. The ability to synthesize PATs with well-defined molecular weights and narrow PDIs is important in optimizing the electrical properties of conducting polymers.

[40] Iovu, M.C., Sheina, E.E.; McCullough. R.D., *Polym. Preprint,* **2005**, 46, 660–661.
[41] Iovu, M.C.; Jeffries-El, M.; Sheina, E.E.; Cooper, J.R.; McCullough, R.D., *Polymer,* **2005**, 46, 8582–8586.
[42] Yokozawa, T.; Shimura, H., *J. Polym. Sci., A,* **1999**, 37, 2607–2618.
[43] Mao, Y.; Wang, Y.; Lucht, B.L., *J. Polym. Sci., A,* **2004**, 42, 5538–5547.

1.2.5 APPLICABILITY OF THE SYNTHETIC ROUTES TO CONJUGATED POLYMERS FOR THE PREPARATION OF CONJUGATED POLYMER BRUCHES

There are two general approaches for the preparation of polymer brushes: "grafting-to" and "grafting-from" methods. The "grafting-to" approach assumes attachments of end-functionalized polymers to the surface and usually fails to produce sufficiently thick polymer brushes. Surface-initiated polymerization, or the "grafting-from" method, is recognized to be the most straightforward way to polymer brushes with adjustable thickness. However, the specific requirements for selective surface-initiated polymerizations (the polymer grows only from the surface and not in bulk solution) is that the polymerization process starts only after the activation of the reactive species (which in this case covalently bond to the surface) and has to involve the chain-growth mechanism. Thus the polymerization of olefins and some other addition polymerizations that fulfill the above requirements are widely employed in the "grafting-from" preparation of polymer brushes. However, as a literature review shows, a majority of synthetic approaches to CPs adopt the step-growth mechanism. In those cases, polymer chains propagate randomly through the coupling of monomers and/or earlier formed oligomeric fragments via the abstraction of small molecules. Even if an appropriate anchoring group (able to couple with the monomer) was immobilized on the surface, the process leads in the best case to a mixture of grafted chains and a large amount of unattached polymers. In practice this approach fails to produce CP brushes with reasonable grafting densities since polymerization products form faster in solutions, precipitate onto the surface and hinder the growth from the surface. Thus, step-growth polycondensations are hardly applicable for the synthesis of polymer brushes[44].

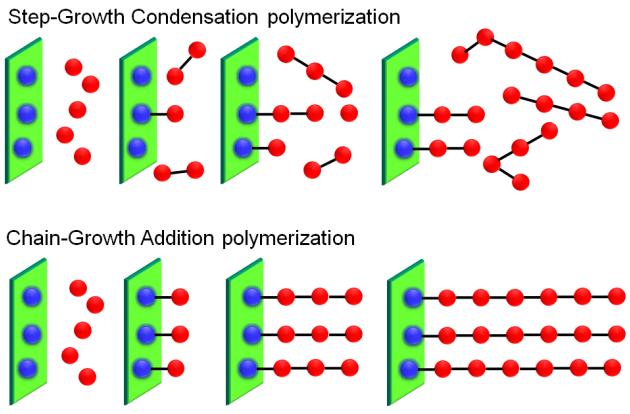

Figure 1.8. *Scheme of the preparation of conductive polymer brushes via step-growth and chain-growth polycondensation.*

[44] An attempt to prepare P3HT brush using the McCullough method was described in: Hagberg E.C.; Carter K.R., *Polym. Preprints*, **2005**, 46, 356-357.

On the other hand, the Kumada[45] catalyst transfer polycondensation discovered by Yokozawa[37] and Mcullough[36] seems to be the most viable opportunity to develop surface-initiated polycondensation to conductive polymer brushes. This direction constitutes an important part of this thesis.

1.3 AIM AND OUTLINE OF THESIS

The aim of the present work was to screen the main methods for the synthesis of conjugated polymers for their suitability in the preparation of conductive polymer brushes. The main focus was put on the grafting of intrinsically soluble substituted regioregular polyalkylthiophenes because of their excellent optoelectronic properties. The resulting polymer films were characterized and their optoelectrical properties studied.

Oxidative polycondensation is, perhaps, the oldest and the simplest way to conjugated polymers (CPs). This method was used for immobilization of intrinsically *insoluble* conductive polymers (such as unsubstituted polythiophenes, polyanilines, polypyrroles, etc.). However, examples of the grafting of *soluble* CPs using this method are much too scarce. We *a-priori* assumed that oxidative polycondensation is unlikely to be applicable for the realization of the scope since it is a typical step-growth process and because the polymerization in this case proceeds predominantly in bulk solution and not only at the surface. However, Collard *et al.* [46] have reported the chemical and electrochemical grafting of regioirregular poly(3-octylthiophene) from self-assembled monolayers (SAMs) of oligothiophene-substituted alkysilanes on glass. We therefore, tried to extend this approach for the grafting of P3ATs by the $FeCl_3$-mediated polycondensation of 3-alkylthiophenes using various anchoring compounds.

Electrochemical oxidative polycondensation potentially is a more promising way for selective grafting of CPs, since with this method the oxidation (and polymerization) proceeds in close vicinity to the electrode that in principle can promote selective grafting of the polymer to the electrode. Examples of immobilization of otherwise soluble CPs are limited, to the best of our knowledge, to just a couple of reports[46,47]. In our work we studied electro-grafting of 3,3"-dioctyl-[2,2';5',2"]terthiophene (DOTT) to indium-tin-oxide (ITO) coated electrodes modified with various SAMs.

Surface-initiated polymerization (or the "grafting-from" technique) is the most powerful approach for synthesis of polymer brushes with high and yet tunable thicknesses and grafting

[45] Tamao, K.; Sumitani, K.; Kumada, M., *J. Am. Chem. Soc*., **1972**, 94, 4374-4376.
[46] Inaoka, S.; Collard, D. M., *Langmuir,* **1999**, 15, 3752-3758.
[47] Zotti, G.; Zecchin, S.; Vercelli, B.; Berlin, A.; Grimoldi, S.; Groenendaal, L.; Bertoncello, R.; Natali, M., *Chem. Mater.,* **2005**, 17, 3681-3694.

densities[48]. This method, however, is applicable only for polymers which can be prepared through *chain-growth* polymerization (for example by addition polymerization of *olefins*[49] and *acetylenes,* ring-opening polymerization of epoxides, N-carboxyanhydrides of *amino acids*[50] or by ring-opening metathesis polymerization of olefines[51]). In that case the polymerization starts from the initiator and propagates via addition of monomers to the growing chain end on a one-by-one manner. The mechanism itself is easily adaptable to an initiation from surfaces or a realization of controlled (living) polymerization schemes. However, synthesis of a number of industrially important polymers, such as polyamides, polyesters, and also *conductive polymers*, involves *polycondensation reactions* that proceed through a *step-growth* mechanism[52]. In this case the synthesis involves a statistical coupling of monomers and/or earlier formed oligomers. In this case polymer chains propagate randomly by coupling monomers and/or earlier formed oligomeric fragments via the abstraction of small molecules. Hence, even if an appropriate anchoring group (able to couple with the monomer) was immobilized on the surface, the process in the best case leads to a mixture of grafted chains and a large amount of unattached polymers. In practice this approach fails to produce CP brushes with reasonable grafting densities since polymerization products form faster in solution, precipitate onto the surface and hinder the growth from the surface. Thus, step-growth polycondensations are hardly applicable for synthesis of polymer brushes[44].

A recent discovery of McCullough's[36] and Yokozawa's[37] groups is that the Ni-catalyzed Kumada-polycondensation of 2-bromo-5-chloromagnesio-3-alkylthiophene (**1a**) into regioregular P3ATs, does not involve the step-growth mechanism, as it was believed for decades, but instead follows the chain-growth scheme. The discovery attracted our attention as a viable opportunity to develop the surface-initiated polycondensation into conductive polymer brushes and other related polymer architectures. This idea constitutes the third, and the most important focus of the work. In particular, the aim of the work was put on the development of a method to prepare surface-immobilized initiators and development of surface initiated polycondensation process from the surface-grafted poly(4-bromostyrene) (PS-Br) and poly(4-vinylpyridine)-*block*-poly(4-iodostyrene) (P4VP-*b*-PS-I).

[48] In the case of non-conductive polymers relatively thin polymer brushes (5-15 nm) can be prepared by the grafting of end-functionalized polymers ("grafting-to" method).
[49] Matyjaszewski, K.; Davis, T., *Handbook of radical polymerization*, Publisher: Wiley-Inter science, 2002.
[50] Merrifield, R., *Science,* **1965**, 150, 178-185.
[51] Grubbs, R.H., *Handbook of Metathesis*, Wiley-VCH, Weinheim, 2003.
[52] Nalwa, H.S., *Handbook of Organic Conductive molecules and polymers*; J. Wiley & Sons: New York, 1996.

CHAPTER 2

EXPERIMENTAL TECHNIQUES USED

This chapter describes experimental techniques used in this work. In particular, ellipsometry was used to measure polymer film thicknesses in the dry and swollen state. The electro-polymerization and the electro-chemical measurements were performed using Cyclic Voltammetry. Further on, Rutherford Backscattering was used to determine the structure of the polymer films produced. Finally, the electrical characteristics of samples were measured using Atomic Force Microscopy. The last section describes other techniques applied for different investigations.

2.1 ELLIPSOMETRY

Null ellipsometry is a non-destructive optical method for determining the thickness and optical properties of thin films. It measures changes in the state of polarization of the light reflected off the film's surface. Ellipsometry methods for single or multi wavelength have also been adopted for the monitoring of film growth *in situ*, allowing precise control of a number adsorption and expansion processes[53].

Ellipsometry measures the change in polarization state of light reflected from the surface of a sample. The measured values are expressed as Ψ and Δ. These values are related to the ratio of Fresnel reflection coefficients, R_p and R_s for *p* and *s*-polarized light, respectively.

$$\tan(\Psi)e^{i\Delta} = \frac{R_p}{R_s} \qquad (2.1)$$

Because ellipsometry measures the ratio of two values, it can be highly accurate and very reproducible. Eq. 2.1 renders the ratio as a complex number, thus it containing "phase" information in Δ, which makes the measurement very sensitive. In Fig. 2.1, a linearly polarized input beam is converted to an elliptically polarized reflected beam. For any angle of incidence greater than 0° and less than 90°, *p*-polarized light and *s*-polarized will be reflected differently.

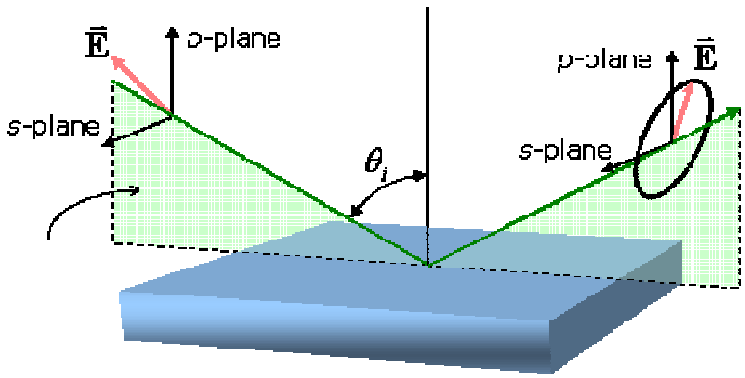

Figure 2.1. *Schematic of the geometry of an ellipsometry experiment.*

The coordinate system used to describe the ellipse of polarization is the *p*-*s* coordinate system. The *s*-direction is chosen to be perpendicular to the direction of propagation and parallel to the sample surface. The *p*-direction is taken to be perpendicular to the direction of propagation and contained in the plane of incidence.

[53] (a) Azzam, R. M. A.; Bashara, N. M., *Ellipsometry and Polarized Light*, 1987, Elsevier Science Pub Co.; (b)Tompkins, H. G.; Irene , E. A., *Handbook of Ellipsometry*, 2005, William Andrew Publishing, Norwich.

Optical constants. The optical constants define how light interacts with a material. The complex refractive index is a representation of the optical constants of a material, it is represented by:

$$\tilde{n} = n + ik \qquad (2.2)$$

The real part or index of refraction, n, defines the phase velocity of light in material:

$$v = \frac{c}{n} \qquad (2.3)$$

where *v* is the speed of light in the material and c is the speed of light in vacuum. The imaginary part or extinction coefficient, k, determines how fast the amplitude of the wave decreases. The extinction coefficient is directly related to the absorption of a material and is related to the absorption coefficient by:

$$\alpha = \frac{4\pi k}{\lambda} \qquad (2.4)$$

Were, α is the absorption coefficient and λ is the wavelength of light.

Liquid-state measurements. Instead of studying film growth after processing in air conditions, the null-ellipsometry provides a sensitive technique for the evaluation of thin film swelling and adsorption kinetics under appropriate conditions. Since most of the adsorption and surface takes place at the solid/liquid interfaces of water solvent, the ellipsometric measurements were adapted and optimized for experiments at aqueous/solid interfaces. Dealing with such matters, one can face difficulties related to independent estimation of thickness, d, and n. When the thickness of a layer is less than 10 nm (in dry state), a correlation between the thickness, d, and the refractive index of the layer, n exists. Thus the parameters cannot be independently determined with the necessary accuracy. "In situ" ellipsometric measurements were performed to examine the swelling behavior of the polymer brush in variable media quality. Fig. 2.2 gives a simplified view of the experiment.

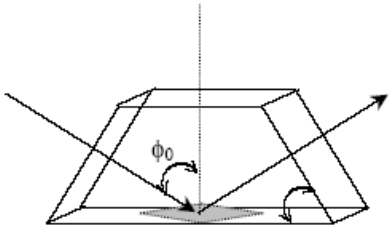

***Figure 2.2**. Ellipsometric setup for "in situ" experiments.*

For "in situ" studies of polymers at solid/liquid interface, one can use a cell with thin, stress free glass windows at a fixed angle. For a single, sharp, interface between two transparent media (water-polymer) Δ passes through an abrupt step between 0 and 180° at certain angle, called the Brewster

angle φ*Br*. Varying the wall-angles allows to remain closer to the Brewster angle of the system under investigation.

Ellipsometry, in dry state measurements. All the measurements were carried out using the null-ellipsometer in the polarizer-compensator-sample analyzer (Multiscope, Optrel Berlin) mode. As light source a He-Ne laser with λ=632.8 nm was applied at an angle of incident of 70°. A multilayer model for films covering or grafted on the silicon substrate has been used for the calculation the thickness of the polymer layers in air from the ellipsometric angles ψ and Δ. The refractive indexes used in the calculations were n=3.8850 for the silicon substrate, native silicon oxide layer SiO_2 n=1.459, n=1.525 for PGMA, n=1.63 for PS-Br, n=1.63 for P4VP-*b*-PS-Br(or I) and n=1.99 for P3HT.

"In situ" ellipsometric measurements were performed to examine the swelling behavior of the polymers. An ellipsometric cell with thin glass walls, fixed at a known angle (68°) from the sample plane, was used. The angle of incidence of the light was settled such that its path was normal to the window.

2.2 CYCLIC VOLTAMMETRY (CV)

Cyclic voltammetry (CV) is a type of potentiodynamic electrochemical measurement. In a cyclic voltammetry experiment, a voltage is applied to a working electrode in solution and the current flowing through the working electrode is plotted versus the applied voltage to give the cyclic voltammogram. Cyclic voltammetry can be used to study the electrochemical properties of species in solution as well as at the electrode/electrolyte interface.

In short, this method can be introduced as a reversal technique, which involves sweeping the electrode potential between two limits at a known sweep rate. At the beginning, the working electrode is held at some potential E_i, where no electrode reactions occur. During the measurement, the potential is swept linearly at a rate ν between two limiting potentials E_1 and E_2 (Fig. 2.3). Such that the potential at time *t* is:

$$\begin{aligned} 0 \prec t \prec \tau \quad & E(t) = E_i - vt \\ t \succ \tau \quad & E(t) = E_i - 2v\tau + vt \end{aligned} \qquad (2.5)$$

where τ is the time required for a scan in one direction. The same sweep rate is normally chosen for the forward and reverse sweep. Its typical value lies in the range from several mV/s to several V/s.

The corresponding current is recorded as a function of the varying potential. A theoretical cyclic voltammogram for a reversible system is shown in Fig. 2.3.

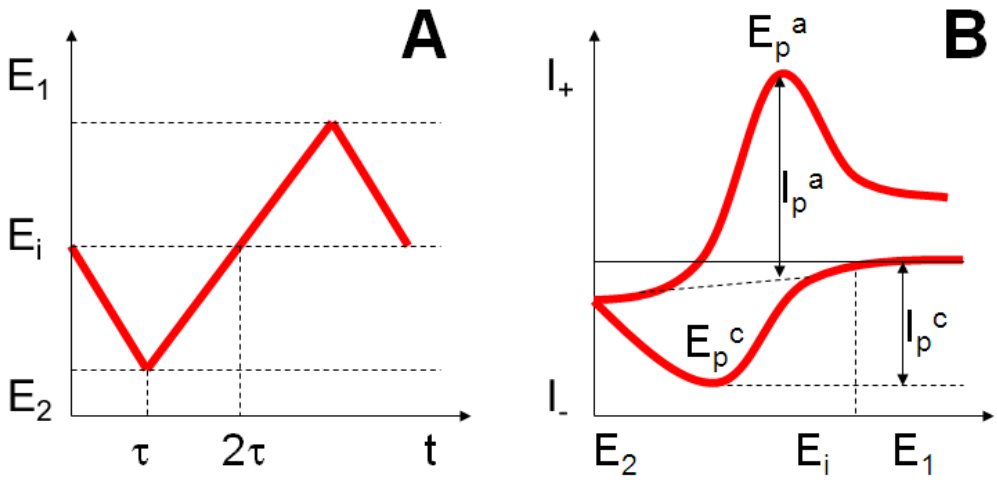

Figure 2.3. *Cyclic potential sweep voltammetry. a) Potential sweep during cyclic voltammetric measurement; E_i is initial value, E_1 and E_2 are two limiting values. b) A typical cyclic voltammogram of a reversible reaction; letters "a" and "c" are referred to anodic and cathodic process, E_p and I_p are potential and current peak.*

For the cathodic scan (applied potential is decreasing) the current has a negative sign, for the anodic scan (applied potential is increasing) the current has a positive sign. The reduction and oxidation peak potentials obtained by the CV measurements allow the estimation of the LUMO and HOMO levels of the investigated compounds.

2.2.1 REVERSIBLE REACTIONS

To obtain the exact form of the cyclic voltammogram it is necessary to solve Fick's second Law for O and R with the appropriate boundary conditions. Let's consider a reversible reduction of a species O.

$$O + ne^- \leftrightarrow R \qquad (2.6)$$

which takes place at a planar electrode and assume that a solution initially contains only O species. According to Fick's first Law, the current density is proportional to the concentration gradient of O at the electrode:

$$I = -nFD_O\left(\frac{\partial C_O}{\partial x}\right)_{x=0} \qquad (2.7)$$

where F is the Faraday constant, D_O is the diffusion coefficient of O, C_O is the concentration of O and x the distance from the electrode surface. This equation is valid if all other mechanisms of mass transport (such as migration and convection) can be neglected. In other words when the diffusion is the only mode of mass transport. Diluted and unstirred solutions at constant temperature can be taken as a good approximation[54].

If these conditions are fulfilled, the cyclic voltammogram is a result of the solution of Fick's second Law:

$$\frac{\partial C_O}{\partial t} = D_O\left(\frac{\partial^2 C_O}{\partial x^2}\right) \text{ and } \frac{\partial C_R}{\partial t} = D_R\left(\frac{\partial^2 C_R}{\partial x^2}\right) \qquad (2.8)$$

with the following boundary conditions:

$$\begin{aligned} &t = 0, x \geq 0 \quad C_O = C_O^{\infty} \text{ and } C_R = 0 && \text{a} \\ &t \geq 0, x \to \infty \quad C_O = C_O^{\infty} \text{ and } C_R = 0 && \text{b} \\ &t \succ 0, x = 0 \begin{cases} D_O\left(\frac{\partial C_O}{\partial x}\right) = -D_R\left(\frac{\partial C_R}{\partial x}\right) & \text{c} \\ \left(\frac{C_O}{C_R}\right)_{x=0} = \exp\left(\frac{nF}{RT}\left(E - E^0\right)\right) & \text{d} \end{cases} \end{aligned} \qquad (2.9)$$

where $E°$ is the equilibrium potential under standard conditions, C and D are concentration and diffusion coefficient of the species O and R, respectively, other parameters having their usual meaning (Eq. 2.7).

The first three conditions, Eq. 2.9(a-c), are quite general, whereas the last one, Eq. 2.9d, holds only for reversible reactions (reactions for which the electron transfer is so fast that for any change in electrode potential the Nernstian equilibrium is always maintained[55]. Details on how to solve this problem can be found in "Electrochemical Methods"[54]. The final result at 25 °C for the peak current is given by the following expression:

$$I_p = \left(2.69 \cdot 10^5\right) n^{3/2} A D_O^{1/2} \nu^{1/2} C_O^{\infty} \qquad (2.10)$$

Where, A is the electrode area. One can see that the peak current is proportional to the concentration of O species and to the square roots of sweep rate and the diffusion coefficient. Thus a simple test of the reversibility of the system can be made. If the system is reversible, then a plot of I_p as a function of $\nu^{1/2}$ should be linear and passes through the origin. In this case the diffusion coefficient can be estimated from the slope.

[54] Gosser, Jr., D.K., *Cyclic voltametry: simulation and analysis of reaction mechamisms*, 1993, New York.
[55] Southampton Electrochemistry Group, Instrumental Methods in Electrochemistry, Ellis Horwood Series in Physical Chemistry, 1990.

2.2.2 IRREVERSIBLE REACTIONS

The shape of the cyclic voltammogram can be altered if the electron transfer is very slow and surface equilibrium is not maintained. Such system is called irreversible. In this case the following expression for the peak current at 25 °C [54] holds:

$$I_p = \left(2.69 \cdot 10^5\right) \alpha^{1/2} n A D_O^{1/2} v^{1/2} C_O^{\infty} \qquad (2.11)$$

with α being the electron transfer coefficient.

For an irreversible system the peak current density is also proportional to the square root of the scan rate, but the peak potential shifts in the negative direction on 30/α mV for each decade increase in the scan rate. For both (reversible and irreversible) systems there are a number of additional criteria which should be satisfied. They are summarized in Tab. 2.1.

Table 2.1 *Diagnostic tests of reversibility and irreversibility of a system; letters "a" and "c" referred to anodic and cathodic process, $E_{p/2}$ is half peak potential, α is an electron transfer coefficient.*

Reversible process	**Irreversible process**
$I_p \sim \sqrt{v}$	N_O reverse peak
$\left\|I_p^A / I_p^C\right\| = 1$	$I_p^C \sim \sqrt{v}$
E_p independent of v	E_p^C shifts on $30/\alpha\, mV$ for each decade increase in v
$\left\|E_p - E_{p/2}\right\| = \left\|E_p^A - E_p^C\right\| = \ln 10 \frac{RT}{nF}$	$\left\|E_p - E_{p/2}\right\| = 48/\alpha\, mV$

The reversibility of a system can be strongly affected by the time scale of the experiment. It is possible that the system satisfies the reversible criteria at low sweep rates and becomes irreversible at higher sweep rates. It should be also mentioned, that sometimes a studied system can become even more complicated when several processes overlap. Then its analysis is not always straightforward.

Figure 2.4. *A typical three-electrode cell suitable for studies of materials includes a reference electrode, a counter electrode, and a working electrode.*

A typical cell design for a cyclic voltammetric experiment is shown in Fig. 2.4. It shows the three electrodes immersed in the solution in close proximity. At the outset of the experiment the cell contains the solvent, the electrolyte, one or more principal electroactive species, and possibly added reagents that will undergo reactions with the electrolytic products.

In cyclic voltammetry, mass transport of the reducible or oxidizable electroactive species occurs only by diffusion. Thus, in order to avoid migration currents and ensure conductivity, a 0.1 M solution of a ground or supporting electrolyte is added to the solution. Alkali metal and especially tetraalkylammonium salts have *proved* to be most effective. The latter can also be used in aprotic solvents and some, e.g. tetra-*n*-butylammonium hexafluorophosphate TBAPF6, tetra-*n*-butylammonium perchlorate TBACIO4, are characterized by extraordinarily high decomposition voltages. The concentrations of the electroactive substances normally lie between 10^{-3} and 10^{-5} M.

Besides the Faradaic current based on the heterogeneous charge transfer at the phase boundary, there exists also a capacitive current from the charging of the electrochemical double layer without charge transfer between electrode and electrolyte.

As it is impossible to monitor the absolute single electrode potentials, the working electrode (WE) potential *E* always refers to a nonpolarized reference electrode (RE), e.g. Ag/AgCl or the saturated calomel electrode (SCE). If the currents are low and the solvent-electrolyte system has a high conductivity, this type of two-electrode cell is sufficient for voltammetric measuring.

Before the experiment it is mandatory to remove dissolved oxygen, which would produce a cathodic signal that can interfere with observed current response. This is normally done by purging the solution with an inert gas such as N_2 or Ag.

2.3 RUTHERFORD BACKSCATTERING WITH HELIUM OR HEAVY IONS (RBS)

RBS is the most frequently used ion beam analysis method. It relies on the fact that the energy of an elastically backscattered particle depends on the mass of the target atom (kinematic factor) and on the depth at which the scattering took place (energy loss on the way to and from the point of interaction). This allows profiling the elemental composition of the sample close to the surface[56,57]. Combined optimization of the mass and depth resolution shows that a 4He beam with approximately 2MeV backscattered under an angle close to 180° is suitable for most problems. The detection of backscattered particles can be done with simple silicon surface barrier detectors. In principle all

[56] Döbeli, M., *Nucl. Instr. and Meth.* **2006**, 800–803.
[57] Chu, W.K.; Mayer, J.W.; Nicolet, M.A., *Backscattering Spectrometry*, 1978, Acad. Press.

elements from Be to U can be detected, though the sensitivity depends largely on the combination of elements and the sequence of layers in the target. RBS is best suited for the detection of heavy elements on light substrates. In such cases, sensitivities between 10 and 10^{-4} monolayers can be reached. The accessible depth for profiling is a couple of mm with a depth resolution of the order of 10 nm at the sample surface. With special detection systems monolayer depth resolution can be achieved. The analysis of the experimental spectra is facilitated by commercially available software. The accuracy of the results is of the order of 1%.

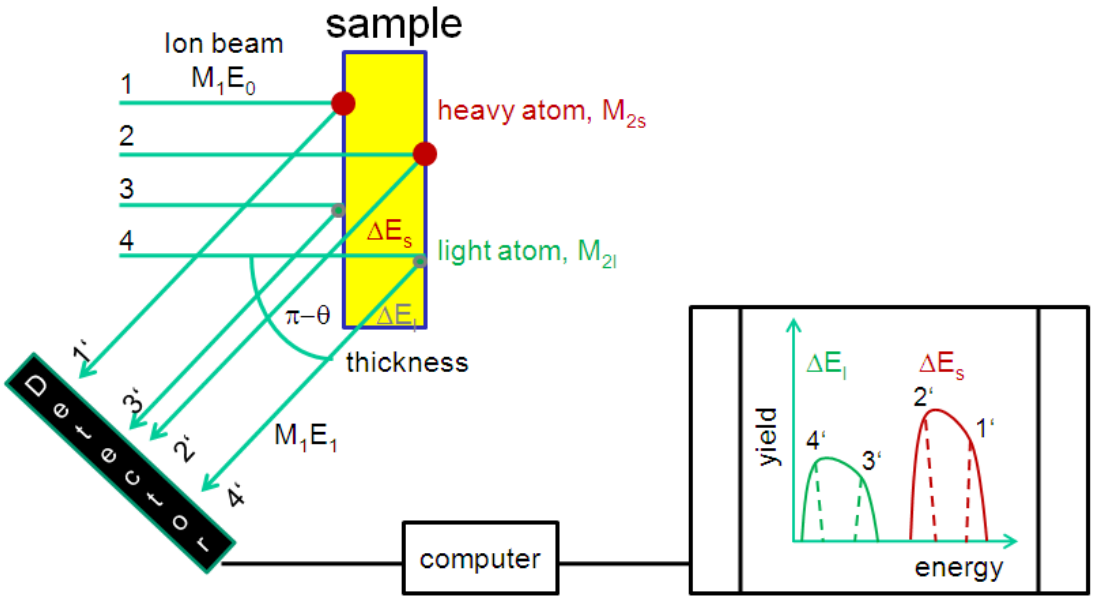

Figure 2.5. *Experimental setup for RBS.*

Target mass discrimination: The identification of a certain atomic mass in the target is made via the kinematic factor k:

$$k = \frac{E_1}{E_0} = \left[\frac{\left(M_2^2 - M_1^2 \cdot \sin^2\theta\right)^{\frac{1}{2}} + M_1 \cdot \cos\theta}{M_2 + M_1} \right]^2 \qquad (2.12)$$

Where, E_0 is the energy of the incident ion with mass M_1, E_1 the energy of the backscattered projectile, M_2 the mass of the target atom and q the scattering angle. Thus, the backscattered energy is equivalent to a mass scale (see Fig. 2.6 and 2.7).

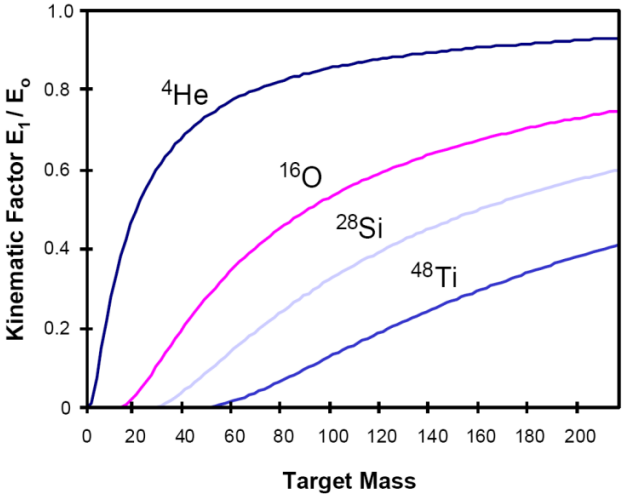

Figure 2.6. *Kinematic factor (at q=180°) as a function of target mass for a number of projectile types.*

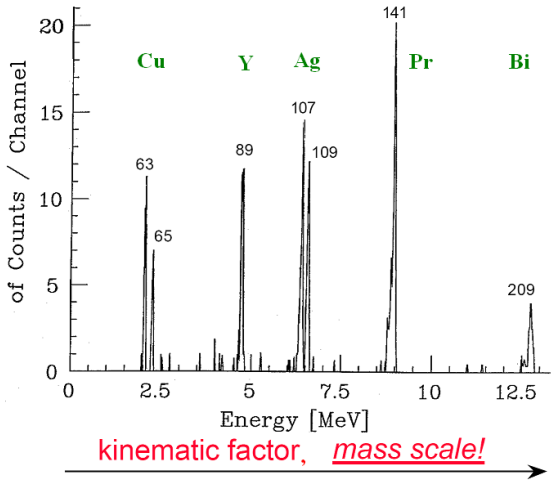

Figure 2.7. *RBS example demonstrating mass discrimination. Projectile: 25MeV ^{35}Cl; target: thin layers of Cu, Y, Ag, Pr, Bi. Isotopes of Cu and Ag are resolved.*

Depth scale. The signal from an atom at the sample surface will appear in the energy spectrum at a position $E_1=k\cdot E_0$. The signal from atoms of the same mass below the sample surface will be shifted by the amount of energy lost while the projectiles pass through the sample, both before (ΔE_{in}) and after a collision (ΔE_{out}).

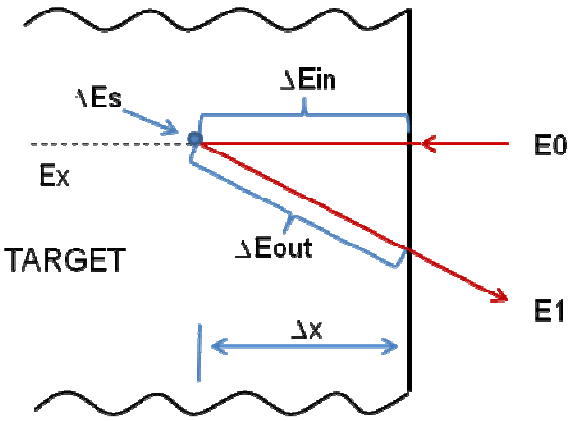

$$\Delta E_{in} = \left(\frac{dE}{dx}\right)_{in} \cdot \Delta x$$

$$\Delta E_s = (1-k)\cdot E_x \quad \text{(kinematic loss)}$$

$$\Delta E_{out} = \left(\frac{dE}{dx}\right)_{out} \cdot \frac{\Delta x}{\cos\theta}$$

Ex = energy before scattering

$$E_1 = E_0 - \Delta E_{in} - \Delta E_s - \Delta E_{out} \approx kE_0 - \underbrace{\left[\left(\frac{dE}{dx}\right)_{in} \cdot k + \left(\frac{dE}{dx}\right)_{out} \cdot \left(\frac{1}{\cos\theta}\right)\right]}_{S} \cdot x \qquad (2.13)$$

Detected energy

Figure 2.8. *Energy loss of ions gives rise to a depth scale.*

Close to the surface there exists a linear relation between the measured energy E_1 and the depth x at which the scattering took place (Fig. 2.8):

$$E_1(x) = kE_0 - S \cdot x$$

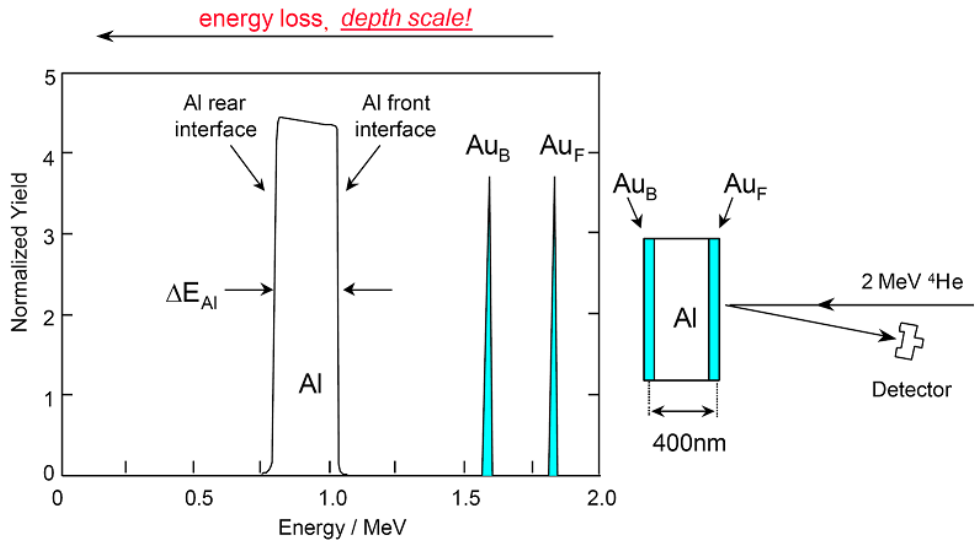

Figure 2.9. *Interpretation of the depth scale in RBS spectra.*

Thus, an RBS spectrum is an overlay of the depth profiles of all individual atomic species present in the target material (Fig. 2.9).

Cross section: If the projectile energy is chosen properly (above electronic screening, below Coulomb barrier) the scattering yield follows the well known Rutherford cross-section, which is basically inverse proportional to the projectile energy and proportional to the square of the atomic number of the target atom (Fig. 2.10).

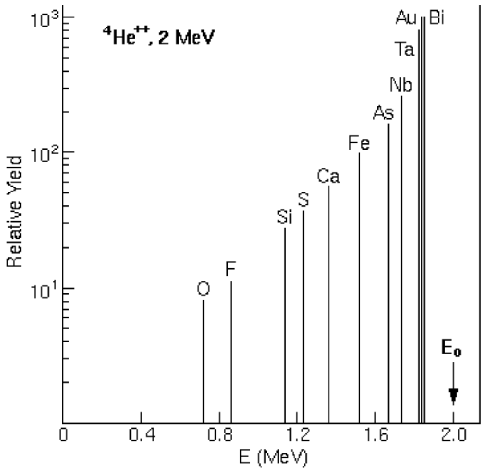

Figure 2.10. *Comparison of scattering yields as a function of the target atomic number.*

Rutherford Back Scattering studies at Forschungszentrum, Rossendorf, Dresden, Germany, using the 3MV Tandetron Accelerator that provided 1.7MeV He^+ ions.

2.4 ATOMIC FORCE MICROSCOPY (AFM) AND CONDUCTIVE ATOMIC FORCE MICROSCOPY (C-AFM)

AFM is a scanning technique which analyzes forces acting on a cantilever-like probe with a nanometer sharp tip at the end brought into the close vicinity of a sample surface. AFM measurements were performed with a Dimension 3100 (Digital Instruments, Inc., Santa Barbara) and CP (Park Scientific Instrument, Inc) atomic force microscopes in the tapping mode. The AFM probes of the spring constant of 1.5–3.7 N/m, the resonant frequency of 45–65 Hz and the tip radius of 10–20 nm were used. Processing (flattening, filtering) and analysis of AFM images (power spectral density (PSD) and fast Fourier transform (FFT) plots) were performed with the WSxM software (Nanotech Electronica).

CONDUCTIVITY MEASUREMENTS WITH CONDUCTIVE MODE ATOMIC FORCE MICROSCOPY (C-AFM)

Current mode Atomic Force Microscopy (C-AFM) is a current sensing technique for the local electrical characterization of samples. C-AFM can be used in either imaging or spectroscopy mode. C-AFM measures tip/sample currents through the samples. The geometry of the tip determines the lateral resolution, which is roughly equal to the end radius of the tip. With the tip at virtual ground, a selectable bias voltage is applied between the conductive tip and the sample (Fig. 2.11).

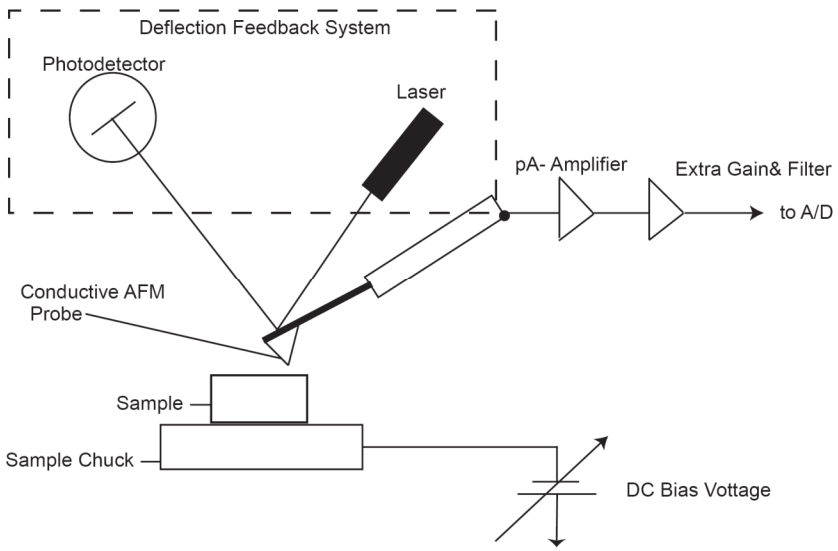

Figure 2.11. *Conductive mode AFM Block Diagram.*

While scanning in Contact Mode, a linear amplifier senses the current passing through the sample. By maintaining a constant force between tip and sample, simultaneous topographic and current images are generated, enabling the direct correlation of local topography with electrical properties. The tip/sample tunneling current depends on film thickness, possible leakage paths caused by defects, charge traps and the tip geometry.

In this work C-AFM measurements were carried out using a NanoScope IV-D3100 (Ditital Instruments, Santa Barbara) with conductive Pointprobe EFM N+ silicon tips coated with a Pt/Ir alloy (0.01-0.025 Ωcm) manufactured by Nanosensors (Wetzlar, Germany). The radius of the tip was 35 nm. Imaging has been performed at the resonance frequency of 190 kHz and an applied voltage of 1V. In both cases the conductive tip was grounded and the potential was applied to the ITO substrate. Both imaging and spectroscopy modes were used in this work to probe the electrical properties of the pristine and the doped PS-Br-*graft*-P3HT composite films.

2.5 OTHER INSTRUMENTATION

^{1}H and ^{13}C NMR spectroscopes . ^{1}H and ^{13}C NMR spectra were recorded on a Bruker DRX-500 spectrometer operating at 500.13 MHz for ^{1}H and at 125.23 MHz for ^{13}C using $CDCl_3$ as solvent. The spectra were referenced on the solvent peak ($\delta(^{1}H)$=7.26 ppm; $\delta(^{13}C)$=77.00 ppm). 2D spectra (COSY, TOCSY, tr-NOESY, HMQC, HMBC) were recorded using the standard pulse sequences of the Bruker software.

Ultraviolet–visible spectroscopy (UV-vis.). Ultraviolet–visible spectroscopy is a characterization technique which probes the electronic transitions of the molecule, as they absorb UV and/or visible light. UV-vis. measurements were carried out using a Perkin Elmer UV/vis. Spectrometer Lambda 800.

Gel Permission Chromatography (GPC). GPC measurements were carried out on a Knauer, Hewlett-Packard normal-temperature size exclusion chromatograph, equipped with refractive index detector and two column PL MIXED-C (Polymer Laboratories Ltd, UK), eluent - chloroform. Calibration was based on polystyrene standards obtained from Polymer Standards Service.

Matrix-assisted laser desorption/ionisation-time of flight (MALDI-TOF). The matrix-assisted laser desorption/ionisation-time of flight (MALDI-TOF) mass spectra were recorded on a Bruker Daltonics biflex IV mass-spectrometer. Experiments were conducted with an acceleration potential of 20kV in reflectron mode for collecting positive ions. Samples for measurements were prepared in

$CHCl_3$ by mixing 5µl of polymer solution with 50µl of matrix (dithranol) solution. A total of 1µl of this mixture was deposited on the plate, and after evaporation of the solvent the measurements were performed under high vacuum. To produce the final spectrum, mass spectra from 120 shots were accumulated. Polyethylenglycol (PEG) was used as external standard.

X-ray Photoelectron Spectroscopy (XPS). XPS spectra were carried out using an AXIS ULTRA (Kratos Analytical, England), X-Ray-source: Mono-Al $K\alpha_{1,2}$, the power of the x-ray source was chosen to be 300W at 20mA, the analyzer pass energy to be 160eV (survey spectra) and 20eV (high-resolved spectra), with charge compensation switched on.

Fourier Transform Infrared spectroscopy (FTIR). FTIR spectroscopy is a powerful technique for identifying functional groups and types of chemical bonds. Vibration energy levels of functional groups give rise to characteristic absorption spectra in the infrared region. In FTIR spectroscopy, there are three frequency regions which are attributed to different vibration modes: near (10000-4000 cm^{-1}), middle (4000-200 cm^{-1}) and far (200-10 cm^{-1}). Infrared spectra were recorded with a Bruker IFS 66v FTIR spectrometer in transmission mode.

CHAPTER 3

PHOTOVOLTAIC CELLS

This chapter presents the state-of-the-art of organic photovoltaic devices. It explains the basic principles of how sunlight is converted into electrical current, introduces the main characteristics that describe the process, and discusses different types of organic solar cells found in literature today.

3.1 INTRODUCTION TO ORGANIC PHOTOVOLTAIC DEVICES (OPV)

Organic photovoltaic devices (OPV) based on semiconductive polymers have intensively been investigated in the past decade. A comparison to the conventional, inorganic silicon-based photovoltaic (PV) shows the advantages of low cost, low thermal budget, solution processing, flexible substrates and a very high speed of processing. There are several factors that influence the efficiency of OPVs, which are: the structure of the polymer, the morphology of the film, the choice of electron acceptor, and the ratio between it and the polymer[58]. A polymer with a band gap below 2 eV, i.e. absorbing light with wavelengths longer than 620 nm, is defined as a polymer with a low band gap. A band gap is defined as the difference between the highest occupied molecular orbital (HOMO) and the lowest unoccupied molecular orbital (LUMO) in the polymer. A few examples of organic semiconductors used for solar cells are listed in Tab. 3.1.

Table 3.1. *The chemical structures of four different organic semiconductors used for organic solar cells.*

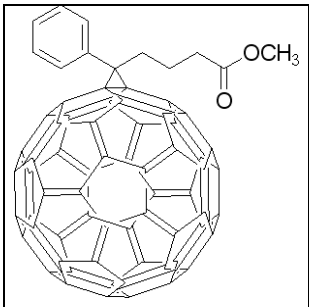	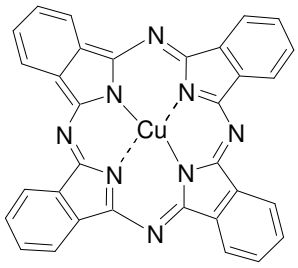	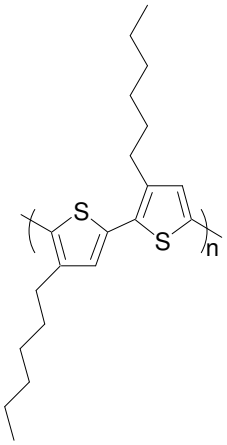	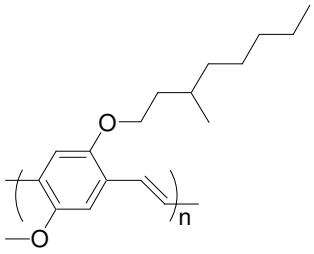
[6,6]-phenyl C_{61}-butyric acid methylester (C_{60} derivative/PCBM)	Copper phthalocyanine (CuPc)	Regioregular poly(3-hexylthiophene) (P3HT)	Poly[2-methoxy-5-(3',7'-dimethyloctyloxy)-p-phenylene vinylene] (OC_1C_{10}-PPV)

Most of the low band gap polymers described in literature is based on polythiophene or a copolymer as part of a fused ring system which can be achieved by modification of the electronic properties of existing polymer units. The poly(3-alkylthiophenes) (P3ATs) has a high absorption coefficient close to the maximum photon flux in the solar spectrum.

P3ATs are known in the field of organic electronics as a high-mobility material. A high mobility has been reported to be due to the well-ordered microstructure and alignment of polymer chains in the

[58] Hoppe, H.; Sariciftci, N.S., *J. Mater. Chem.*, **2006,** 16, 45-61.

charge-transport region at the interface of a gate insulator. In an ordered domain, a lamellar structure is formed by strong inter-chain coupling, showing quasi-two-dimensional characteristics, because of the π-π stacking of thiophene rings[59]. Since the solar cells active-layer thickness is a trade-off between enough light absorption and a decent charge-carrier extraction, the charge-carrier mobility is of considerable importance.

This chapter gives a brief introduction into photovoltaic and into the challenges that have to be accomplished on the route towards efficient organic solar cells.

3.2 BASICS OF PHOTOVOLTAIC DEVICES

The main processes observed in the inner working of photovoltaic device are: (1) light absorption, (2) exciton diffusion between two semiconductors, (3) charge transfer and (4) charge collection. The processes, which must occur inside the cells to generate electrical current, are shown in Fig. 3.1. Fig. 3.1 shows the first step of light absorption, the second step is exciton diffusion. A further is third step is exciton dissociation by charge transfer and the final step is charge collection at anode and cathode.

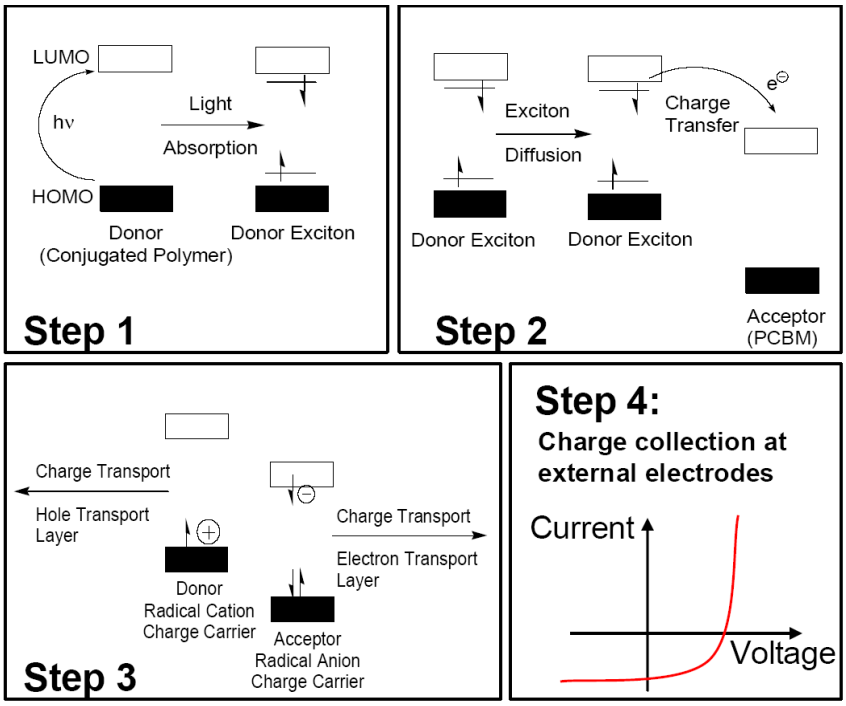

Figure 3.1. *The four main photovoltaic processes generating electrical current.*

[59] Ukai, S.; Marumoto, K.; Ito, H.; Kuroda, S., *Proc. Int. Symp. Super-Functionality Organic Devices IPAP,* Conf. Series 6,150-153.

Light Absorption. There two requirements to be met to absorb most wavelengths in the solar spectrum (process 1, Fig. 3.2a).

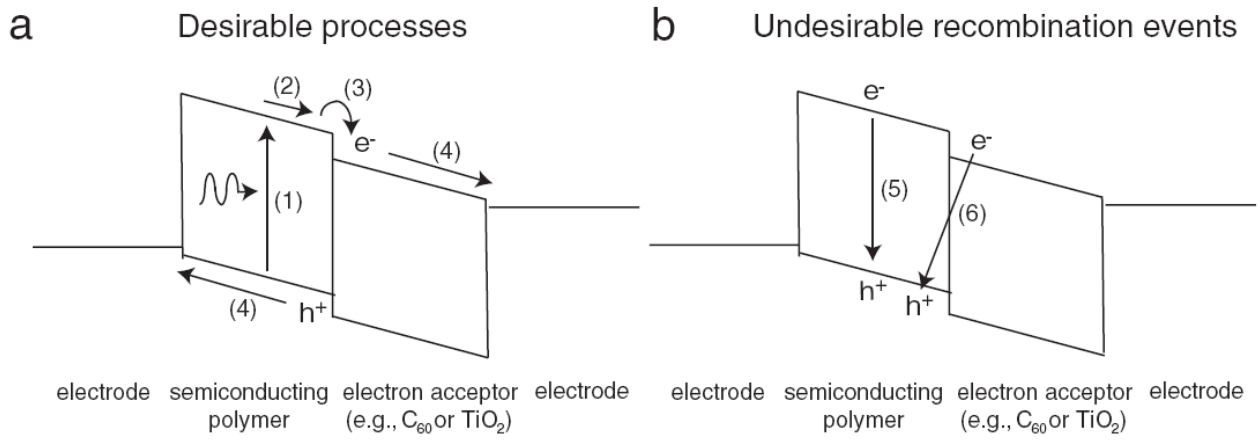

Figure 3.2. *Schematic energy diagram of the semiconductor and energy levels in a bulk heterojunction solar cell showing (a) the desirable and (b) the undesirable processes that can occur.*

The first is that the band gap must be small enough to enable the polymer to absorb most of the light in the solar spectrum. The ideal band gap is 1.5 eV according to theoretical calculations[60]. At this optimum, the largest amount of light can be absorbed and a voltage can be generated. The band gap size depends on the combination of semiconducting polymers and electron acceptors.

The second requirement is that the film must be thick enough to absorb most of the light. For most organic semiconductors, this means that films must be 150–300 nm thick, depending on how much of the film consists of a non-absorbing electron acceptor. The optimum film thickness will absorb much incident light without significant recombination loss.

Exciton diffusion. The exciton formed in the polymer must diffuse or travel by resonance energy transfer (process 2, Fig. 3.2a) to the interface with the other semiconductor and be split by an electron transfer before it recombines (process 5, Fig. 3.2b). The geminate recombination of electrons and holes in the polymer and the back electron transfer from the electron acceptor to the polymer can limit the performance of the cell. These are undesirable recombination processes which are shown in Fig. 3.2b.

Experiments have shown that an exciton can diffuse approximately 5–10 nm into most semiconducting polymers before it recombines. Therefore, no regions in the polymer should be farther than 5–10 nm from an interface. Templating or nanostructuring of the donor and acceptor phases to fabricate ordered bulk heterojunctions with controlled dimensions is an attractive approach to achieving

[60] Coakley, K.M.; McGehee, M.D., *Chem. Mater.,* **2004**, 16, 4533–4542.

full exciton harvesting[61]. Some small-molecule semiconductors have been shown to have larger exciton diffusion lengths[62].

Charge Transfer. The actual process of charge transfer (process 3, Fig. 3.2a) requires that the offset in LUMO levels of the donor and acceptor are sufficient to overcome the exciton-binding energy. The maximum voltage attainable from this type of bulk heterojunction solar cell is determined by the gap between the HOMO of the electron donor and the LUMO of the acceptor. The gap becomes smaller as the LUMO of electron acceptors is moved farther away from the LUMO of the polymer, which corresponds to a larger driving force for charge transfer. As can be seen from processes 1, 2 and 3, the design of an efficient organic solar cell involves optimization of the various energy levels to achieve an optimum level of extracted current with respectable voltage, as the power supplied by a solar cell is the product of current and voltage.

After forward electron transfer, the holes in the polymer and the electrons in the electron acceptor must reach the electrodes (process 4, Fig. 3.2a) before the electrons in the acceptor undergo back electron transfer to the polymer (process 6, Fig. 3.2b). This competition limits the efficiency of the cells. The problem can usually be mitigated by making cells that are only 100 nm thick so that the carriers do not have to travel very far. Unfortunately, most of the light is not absorbed by films this thin. If the films are thick enough to absorb most of the light, then only a small fraction of the carriers escape the device[63].

Charge collection is a characteristic of a photovoltaic device.

3.3 CHARACTERIZATION OF A PHOTOVOLTAIC DEVICE

Open-circuit voltage or V_{OC} is the difference in potential between the terminals of a cell; i.e. the voltage when the circuit is open (no-load condition). In the case of a solar cell or solar module, the open-circuit voltage is the maximum possible voltage across the cell or module, and appears when the cell is in sunlight and no current is flowing.

The open-circuit voltage, V_{OC}, can be describe also as the maximum voltage available from a solar cell, and this occurs at zero current. The open-circuit voltage corresponds to the amount of forward bias on the solar cell due to the bias of the solar cell junction with the light-generated current. The open-circuit voltage is shown on the *I-V* curve below (Fig. 3.3).

[61] Coakley, K.M.; McGehee. M.D., *Appl. Phys. Lett.*, **2003**, 83, 3380–3382.
[62] Peumans, P.; Yakimov, A.; Forrest S.R., *J. Appl. Phys.*, **2003**, 93, 3693–3723.
[63] Goh, C.; McGehee, M.D., *The bridge linking engineering and society*, **2005,** 35, 33-39.

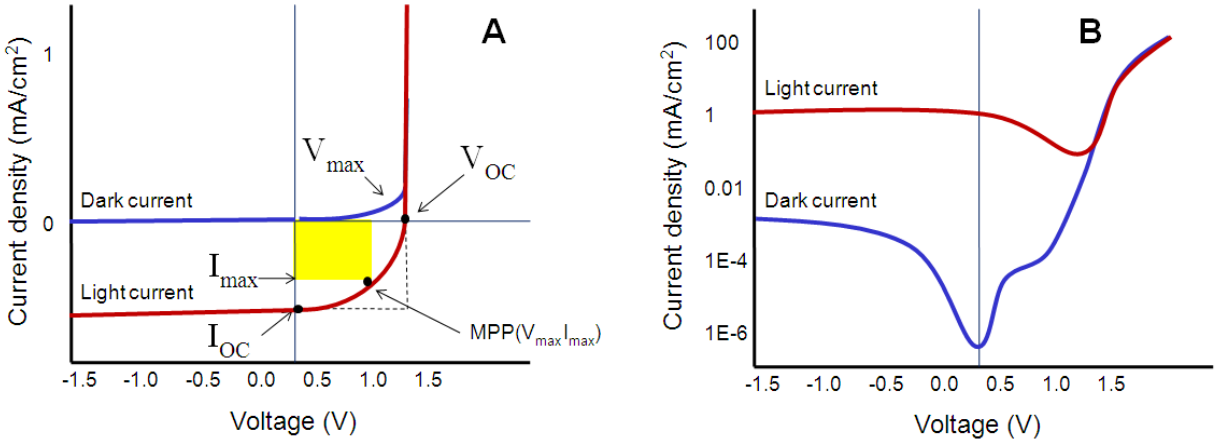

Figure 3.3. *(a) Linear and (b) logarithmic current-voltage (I-V) curves of a photovoltaic device. The short-circuit current I_{SC} corresponds to the ordinate while the open-circuit voltage V_{OC} is determined at the point where the I-V curve crosses the abscissa.*

Short-circuit current I_{SC}. Under short-circuit condition, an appliance is prevented from receiving charges, as the complete current flows through a zero-resistance path. There is no voltage change and thus no work is done even though a current is flowing. The short-circuit current (I_{SC}) is heavily dependent on the number of absorbed photons which originates from two different factors. First, I_{SC} shows a linear dependence on the incident light intensity as long as no saturation effects occur within the active layer. Second, the short-circuit current can be maximized by enlarging the absorption spectrum of the photoactive layer to harvest more photons within the sun spectrum. This can be accomplished by a careful design of the thickness of the distinct layers. Optical modeling of the organic solar cells revealed that the light distribution varies considerably throughout the whole photovoltaic devices[64]. Another option is to use low-band gap materials, which can also contribute to improved photon harvesting. The short-circuit current also depends on charge carrier mobility of the active layer where the photocurrent increases with temperature due to thermally active hopping transport[65,66]. Therefore, the synthesis of organic materials which are characterized by high charge carrier mobility and a low band gap are highly desired.

Fill factor (FF). The fill factor FF describes the quality of the solar cell and is determined by the fraction of photogenerated charge carriers that reach the electrodes when the built-in field is lowered toward the open-circuit voltage to the total number of photoexcitons generated. It serves as indicator for the degree to which $V_{max.}$ and $I_{max.}$ match V_{OC} and I_{SC}, respectively. The largest power output $P_{max.}$

[64] Hoppe, H.; Sariciftci, N.S., *J. Mater. Res.*, **2004**, 19, 1924-1945.
[65] Gregg, B.A., *J. Phys. Chem. B.*, **2003**, 107, 4688-4698.
[66] Brabec, C.J.; Shaheen, S.E.; Winder, C.; Sariciftci, N.S.; Denk, P., *Appl. Phys. Lett.*, **2002**, 80, 1288-1290.

is achieved at the point where the product of voltage $V_{max.}$ and current $I_{max.}$ is largest (Fig. 3.3). The fill factor is defined as the division of $P_{max.}$ by the product of V_{OC} and I_{SC} (Eq. 3.1).

$$FF = \frac{V_{\max} \cdot I_{\max}}{V_{OC} \cdot I_{SC}} = \frac{P_{\max}}{V_{OC} \cdot I_{SC}} \qquad (3.1)$$

In order to determine the power conversion efficiency η of a photovoltaic device, the maximum power $P_{max.}$ that can be extracted from the solar cell has to be compared to the incident radiation intensity (Eq. 3.2).

$$\eta = \frac{P_{out}}{P_{in}} = \frac{V_{\max} \cdot I_{\max}}{P_{in}} = \frac{V_{OC} \cdot I_{SC} \cdot FF}{P_{in}} \qquad (3.2)$$

In order to obtain a high fill factor FF, the shunt resistance of a photovoltaic device has to be very large in order to prevent leakage currents. This resistance is reflected in the horizontal part of the *I-V* curve at a negative applied bias. Another inherent resistance sums up all contributions of series resistances in the device. Among them are the transport through the contact, the interface transfer, and the bulk transport. For a good fill factor, this series resistance has to be very low, which then is reflected by a sharp rise in the forward current. For polymer fullerene solar cells, fill factors as high as 0.6 have been determined[67,68].

Quantum efficiency (QE) is a quantity defined for a photosensitive device such as photographic film or a charge coupled device (CCD) as the percentage of photons hitting the photoreactive surface that will produce an electron hole pair. It is an accurate measurement of the device's sensitivity. It is often measured over a range of different wavelengths to characterize a device's efficiency at each energy level. Photographic film typically has a QE of much less than 10%, while CCDs can have a QE of well over 90% at some wavelengths.

An experimentally accessible value is the external quantum efficiency (EQE) or incident photon to current efficiency (EQE) which is defined by the number of photogenerated charge carriers over the number of incident monochromatic photons (Eq. 3.3).

$$EQE = \frac{\text{Number of charges generated}}{\text{Number of incident photons}} = \frac{1240 \cdot I_{SC}}{\lambda \cdot P_{in}} \qquad (3.3)$$

EQE-values as high as 70% at the absorption maximum of the photoactive layer have been measured for polymer-fullerene solar cells[64], whereas the internal quantum efficiency IQE, defined as the number of photogenerated charge carriers over the number of monochromatic, absorbed photons

[67] Brabec, C.J.; Sariciftci, N.S.; Hummelen, J.C., *Adv. Funct. Mater.*, **2001**, 11, 15-25.
[68] Padinger, F.; Rittberger, R.S.; Sariciftci, N.S., *Adv. Funct. Mater.,* **2003**, 13, 85-88.

(Eq. 3.4) of these photovoltaic devices is close to unity. The IQE gives insight in the efficiency of the charge carrier generation, transport and collection process[69].

$$IQE = \frac{\text{Number of charges generated}}{\text{Number of photons absorbed}} \qquad (3.4)$$

3.4 TYPES OF HETEROJUNCTION PHOTOVOLTAIC DEVICES

The development history of the solar cell has seen four main types of devices: sandwich, bilayer, bulk heterojunction and penetrated brush systems of solar cells. The first, so called ***sandwitch solar cell,*** is the simplest organic photovoltaic made of a sandwich of thin films of organic semiconductors between two electrodes with different work functions (Fig. 3.4a). When such a diode is made, the electrons from the low-work-function metal flow to the high-work-function metal until the Fermi levels are equalized throughout the structure. When the organic semiconductor absorbs light, electrons are created in the conduction band, and holes (positive charge carriers) are created in the valence band. Thus, in principle, the built-in electric field can pull the photogenerated electrons to the low-work-function electrode and holes to the high-work-function electrode, thereby generating current and voltage (Fig. 3.4a). However, these cells have very low power-conversion efficiency (<0.1 percent) because the electric field is not strong enough to separate the bound excitons (i.e., the excited-state species formed in organic semiconductors described above).

The second type of organic ***bilayer solar cells*** is a heterojunction between donor and acceptor semiconductors, resembling a p-n junction in conventional solar cells (Fig. 3.4b). Such systems use two organic materials with offset electron affinities (lowest unoccupied molecular orbital, LUMO) or ionization potentials (highest occupied molecular orbital, HOMO). Here the electrons are transported in the acceptor material and the holes in the donor material to their respective electrodes. The efficiency of this type of device is limited by the exciton diffusion length, which is the distance over which excitons travel before undergoing recombination, which is approximately 5–10 nm in most organic semiconductors. It limits the active area of a solar cell as the polymer thickness should be thin and close enough to the interface, in order to not adsorb most of the solar radiation flux.

[69] Schilinsky, P.; Waldauf, C.; Brabec, C.J., *Appl. Phys. Lett.*, **2002**, 81, 3885-3887.

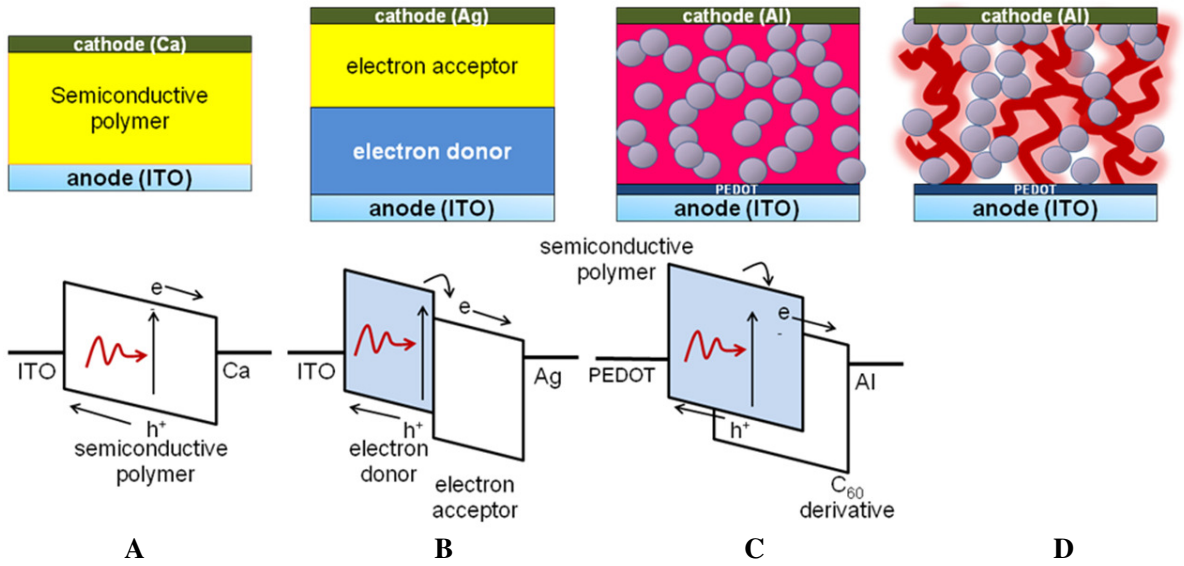

Figure 3.4. *The different structures of photovoltaic devices. A schematic energy-band diagram of (a) a single-layer semiconductor polymer solar cell, in which indium-tin oxide (ITO) serves as a transparent high-work-function electrode and calcium serves as the low-work-function electrode; (b) photoinduced electron transfer from the lowest unoccupied molecular orbital (LUMO) of an electron donor to the LUMO of an electron acceptor in a planar heterojunction cell; (c) a bulk heterojunction solar cell based on semiconducting polymer and C_{60} derivative, (d) a brush hererojunction solar cell based on semiconductive polymer and C_{60} derivative.*

The third type are the ***blend heterojunction devices*** Here, the fullerene derivatives are blended into the polymer matrix[70] (Fig. 3.4c). The fullerene (C_{60}) is a molecule that consists of 60 carbon atoms, arranged in 12 pentagons and 20 hexagons. Low solubility in organic solvents and the tendency of C_{60} to crystallize limit its use for high-concentration blends in bulk-heterojunction solar cells. Therefore, a series of soluble derivatives have been synthesized. One of these derivatives is a methanofullerene: [6-6]- phenyl C_{61}-butyric acid methyl ester, better known as PCBM. The PCBM acts as an electron acceptor inside the polymer. At concentrations in the range of 18–80 wt. percent, the polymer and the fullerene derivatives form a connected network to each electrode. The key to making efficient blend solar cells is to ensure that the two materials are intermixed very closely at a length scale less than the exciton diffusion length such that every exciton formed in the polymer can reach an interface with fullerenes to undergo charge transfer. In this case the film morphology enables charge-carrier transport in the two different phases to minimize recombination. The efficiency of the device depends on the film morphology, which is determined by the concentration of materials, film-casting solvents, annealing time, temperature, and other parameters. The best resulting efficiency of such solar cells of was recently reported to be 5 percent [71].

[70] Yu, G.; Gao, J.; Hummelen, J.C.; Wudl, F.; Heeger, A.J., *Science*, **1995**, 270, 1789–1791.
[71] Ma, W.; Yang, C.; Gong, X.; Lee, K.; Heeger, A.J., *Adv. Funct. Mater.*, **2005**, 15, 1617–1622.

The fourth type of solar cells is based on the brush architecture. The ability to infiltrate a polymer brush film with a second component is of central interest. The vertical alignment of polymer brushes makes them ideal candidates for incorporation as electroactive component within organic semiconductor devices, potentially improving transport properties and providing clear pathways for charge transport in the direction normal to the substrate (Fig. 3.4d). Polymer brush films can swell in a good solvent to many times their original thickness. This may generate sufficient free volume to accommodate a significant volume fraction of electron transporting material. However, since stretching the polymer brush is entropically unfavorable, a strong favorable interaction between the brush and the coating component is required to aid intercalation into the brush film.

The groups of Friend *et al.*[12] have first developed a ***solar cell based on the brush architecture.*** The polymer brush device shows a significantly enhanced performance, with an external quantum efficiency at 400 nm of approximately twice that of the blend device. The maximum external quantum efficiency of the brush device occurs where the polymer absorbs and is approximately 20%. The internal quantum efficiency (the fraction of collected electrons to absorbed photons) was calculated for the brush and blend devices by dividing the external quantum efficiency by the fraction of incident light absorbed in the active layer. This absorption was calculated taking full account of optical interference effects. The optical constants for the brush and spin-coated layers were determined by fitting a combination of reflection ellipsometry and transmission data. We found the brush device to be most efficient at converting absorbed photons to electrons where the nanocrystals absorb. Most significantly, the internal quantum efficiency is as high as 50%. This is considerably more than that of the blend device (20%); we therefore have a structure in the brush device, which is well-matched for charge collection.

CHAPTER 4

GRAFTING OF POLY(3-HEXYLTHIOPHENES) BY OXIDATIVE POLYCONDENSATION

Oxidation polymerization of 3HT is a simple method to produce P3HT polymers. An important advantage of the method is that the obtained polymers have a high molecular weight compared to other methods. This chapter demonstrates how the oxidation polymerization of 3-hexylthiophenes can be applied to the preparation of P3HT polymer brushes. For our work, we used direct oxidation of poly(3-hexylthiophenes) using $FeCl_3$ as oxidant/catalyst. By employing a two-step polymerization reaction, we were able to produce polymer films with tunable thicknesses up to 200 nm. Our hypothesis is that the creation of P3HT islands in the first polymerization step benefits an efficient growing of polymers in the second step.

4.1 OXIDATIVE POLYMERIZATION OF 3-ALKYLTHIOPHENES

The polymerization of 3-alkylthiophene in the presence of iron (III) chloride is a simple process. The resulting polymers are soluble in common organic solvents and their film can be formed by casting of the solution on a substrate. Thus, poly(3-alkylthiophenes) (P3ATs) and related polymers are commonly prepared using this method[72].

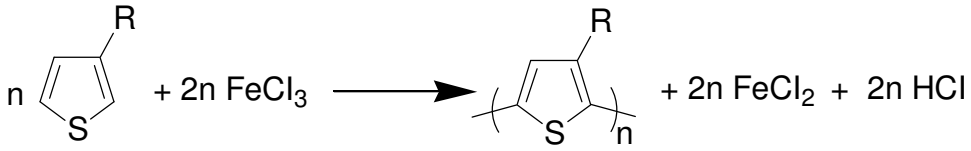

Niemi *et al.*[73] presented a detailed study on the mechanisms of the oxidation polymerization of alkylthiophenes with $FeCl_3$. They have investigated the mechanism of polymerization and found that only in the present of Fe (III) in the system can provide the desired polymer, and the $FeCl_3$ must be solid to be active as a polymerization oxidant for 3-alkylthiophenes (3AT). The soluble part of $FeCl_3$ seems to be inert. The solubility of $FeCl_3$ in chloroform and the consuming effect of evolved HCl gas explains the extra portion of $FeCl_3$ that is initially needed to get a high conversion in polymerization. The role of $FeCl_3$ in the polymerization synthesis is described and a feasible polymerization mechanism for 3ATs was developed on the basis of quantum chemical computations of thiophene derivatives. The polymerization is proposed to proceed through a radical mechanism rather than a radical cation mechanism, because the polymer produced by the former mechanism will have fewer regio-irregularities than the polymer produced by the latter mechanism (Scheme 4.1)[73].

The oxidation polymerization of 3HT with iron chloride is a heterogeneous process. The heterogeneous process is created by the solid and soluble state of the $FeCl_3$ component. The reaction does not begin until solid $FeCl_3$ is present. Thus, in a synthesis where $FeCl_3$ is dissolved completely in $CHCl_3$, no polymer is produced. As a consequence, the portion of $FeCl_3$ was chosen such that ~50% is solved by $CHCl_3$. The polymer yields are very low for the polymerization and a continuous flow of HCl gas is produced. The HCl consumes $FeCl_3$ (probably by complexation ($FeCl_4^-$)[74]), which removes the ~50% $FeCl_3$ not solved in $CHCl_3$. The $CHCl_3$ solvent is required to dissolve the P3AT formed in the polymerization process, which otherwise would precipitate on $FeCl_3$ and $FeCl_2$ and make washing of the polymer difficult.

[72] Kaeriyama, K., *Conductive polymer: synthesis and electrical properties*, 1997, 271-308.
[73] Niemi, V.M.; Knuuttila P.; Österholm, J.-E., *Polymer*, **1992**, 33, 1559-1562.
[74] Friedman, H.L., *J. Am. Chem. Soc.,* **1952**, 74, 5-10.

Scheme 4.1. *The mechanism of polymerization of the 3AT in the present of $FeCl_3$.*

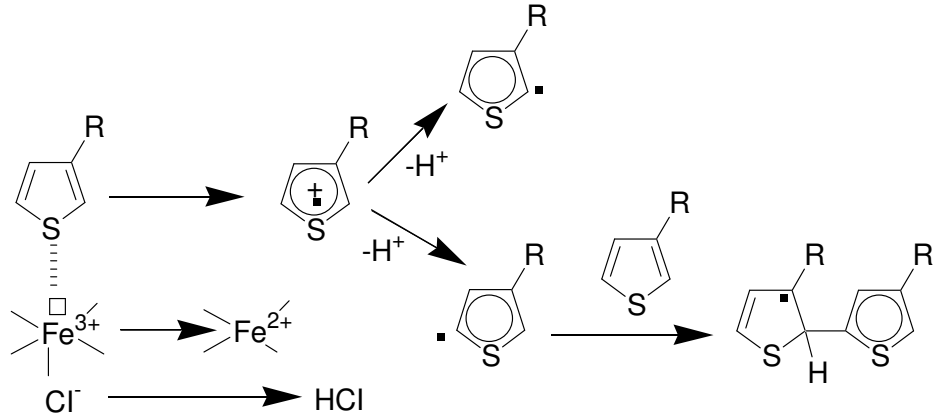

In solid $FeCl_3$, the iron(III) ions are mostly hidden within the crystal where they are chemically inert. Each chloride ion is coordinated to two iron(III) ions. The structure is slightly different at the surface of the crystal: in order for the total charge to be neutral there must be a deficiency of chloride ions, and some of the chloride ions are coordinated to only one iron (III) ion. Thus each iron (III) ion at the surface of the crystal has one unshared chloride ion and one free orbital. The active sites in polymerization are the iron(III) ions at the surface of the crystal, which have strong Lewis acid character because of one free orbital. The Lewis acid character also explains the highly hygroscopic nature of $FeCl_3$. In chloroform the soluble part of $FeCl_3$ is inert because it exists in dimeric form without free orbitals[75].

4.1.1 SURFACE-GRAFTING OF POLY(3-ALKYLTHIOPHENES)

Unsubstituted conductive polymers are insoluble in common solvents and they can be relatively easily immobilized *onto* surfaces by chemical or electrochemical oxidative polymerization of the corresponding monomers. Adhesion of such conjugated polymers (CPs) to the substrates can be modulated by modification of the surface properties. In contrast to unsubstituted polymers, anchoring of *intrinsically soluble* substituted CPs without affecting of their conformational freedom is a considerably more complicated task.

Some attempts to grow P3HT brushes from the acrylate matrix have been previously performed[44]. The film thickness was observed to increase only from 3 nm to 7 nm. The selectivity of this method proved to be limited with uncontrolled brush growth from surface with no added reactive functionality. Zhang *et al.*[76] have modified the Al_2O_3 or TiO_2 surface by 2-(3-

[75] Vertes, A.; Nagy-Czako, I.; Burger, K., *J. Phys. Chem.,* **1978**, 82, 1469-1473.
[76] Zhang, Y.; Wang, C.; Rothberg, L.; Ng, M.-K., *J. Mater. Chem.,* **2006**, 16, 3721-3725.

triethoxysilyl)propylthiophene initiators and a subsequent surface initiated polymerization through *in-situ* oxidation coupling of 3-hexylthiophene to fabricate regio-random P3HT that is covalently attached to the substrate surface. The thickness of the polymer walls was in the range from 10 to 30 nm.

Self-assembled monolayers (SAMs) of specially designed compounds were used as anchors for immobilization of CPs. SAM-forming anchors usually consist of a moiety for attachment to the substrate, polymerizable head-group for binding to conductive polymers, and a spacer between them to ensure self-assembly. Various thiophene and pyrrole derivatives having thiol-, siloxane-, or phosphonic- end groups were utilized for fabrication of SAMs on gold, silica or metal oxide surfaces (Al, Ti, or indium tin oxide (ITO) coated glass).

Collard *et al.*[46] have reported the preparation of SAMs of oligothiophene-substituted alkysilanes on glass surface followed by the chemical and electrochemical grafting of alkylthiophenes from SAM-modified surfaces. Although it was shown that chemically grafted poly(3-octylthiopene) displays reversible solvatochromism without dissolving the polymer, the detailed characterization of the film morphology and thickness was not reported. Although the approach utilized SAMs as anchoring layers as a powerful immobilization method, it lacks of universality, since each substrate type and each kind of polymer to be immobilized requires a certain design of the anchoring compound.

Luzinov *et al.*[10] proposed a novel macromolecular anchoring layer of poly(glycidylmethacrylate) (PGMA) for the preparation of non-conductive polymer brushes, as a viable and reasonable alternative to the traditional approach based on silane chemistry. They demonstrated that adsorption of PGMA onto Si-wafers and subsequent annealing results in smooth and robust thin films. The glycidyl methacrylate units serve as reactive sites for the attachment of carboxy-terminated polymers. The high adhesion of PGMA to Si-wafers and films robustness is assumed to be due to multiple bonding of epoxy groups to the hydrophilic substrate and the formation of highly cross-linked network films.

In the following paragraphs we report on the extension of this approach and demonstrate the utilization of PGMA as the macromolecular anchor for growing CP brushes on various surfaces: Si-wafer, glass, ITO modified glass, and various metals like Al, Ti and Au. Our method relies on the deposition of thin strongly adherent PGMA films, followed by a modification with properly functionalised polymerizable compounds and, finally, chemical growing of CPs. This convenient method has the advantage of the modular approach, allowing easy tuning of head-groups thus optimizing the polymerization process and the properties of resulting films of grafted CPs. To verify the applicability of the approach we were focused on $FeCl_3$-mediated oxidative coupling reaction which is among the simplest and most general polymerization techniques. 3-Hexylthiophene (3HT)

was used as a model monomer. Since 3HT possesses an *asymmetrical* structure, the polymerization leads to *regioirregular* P3HT consisting of a mixture of head-to-tail and head-to-head structural fragments. However, in principle, this method would be also suitable for the polymerization of various *symmetrically* substituted monomers and in these cases would lead to regioregular polymers with attractive optical and electrical properties.

4.2 RESULTS AND DISCUSSION

4.2.1 ANCHORING LAYERS

Spin-coating of PGMA solutions in chloroform or tetrahydrofuran (THF) leads to the formation of PGMA films with thicknesses of a few nanometers to a few tens of nanometers depending on the concentration of the solution used. The morphology of anchoring layers was studied with AFM. We found that PGMA coated from chloroform solution ($CHCl_3$) gave smoother films than the one formed from tetrahydrofuran (THF) solution. Fig. 4.1 shows the deposition of $CHCl_3$ results in smooth (RMS 0.2–1.0 nm) features-less films that were used in this work.

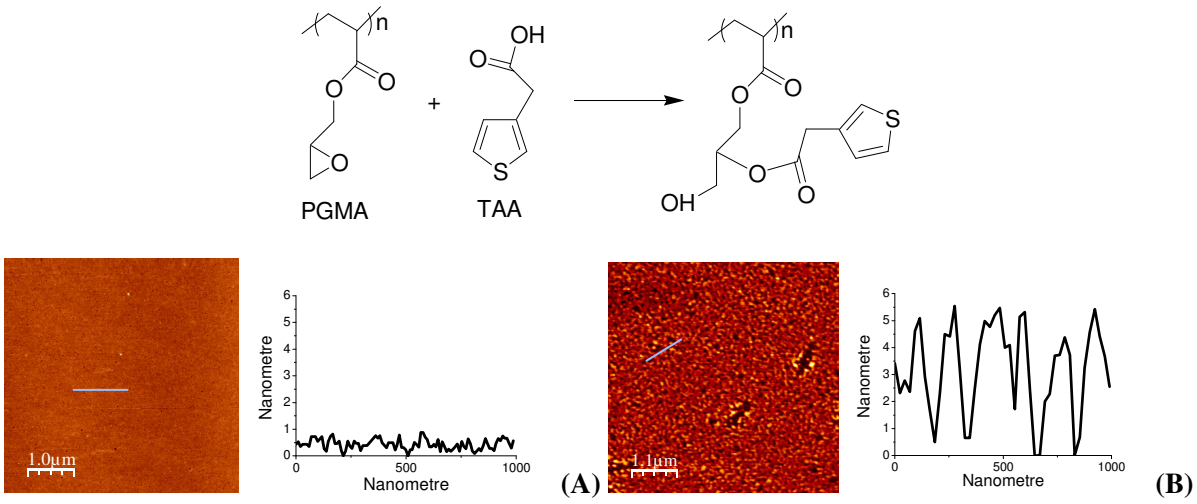

Figure 4.1. *AFM topography image and cross-sections of the 2 nm thick (as determined using ellipsometry) PGMA film on Si-wafer substrate. PGMA was deposited from (a) chloroform and (b) THF solutions.*

The presence of epoxy-groups in the PGMA structure provides the possibility of further modification of the layer with substances having carboxy- or amino-functions. To introduce polymerizable head-groups, commercially available thiophene-3-acetic acid (TAA) was deposited onto the PGMA layer and annealed in an inert atmosphere for 10 hours at 150 °C. The rest of unreacted

TAA was afterwards washed away by extensive rinsing in chloroform. During the annealing, TAA attaches to PGMA due to acid-induced cleavage of the epoxy-cycles.

In a series of control experiments we found that methyl ester of thiophene-3-acetic acid, with the structure similar to the structural fragment of TAA-modified PGMA, is practically inactive in $FeCl_3$ - mediated polymerization reaction, however can be easily copolymerised with 3HT. These experiments confirm the potential suitability of TAA-modified PGMA for the preparation of P3HT brushes.

Fig. 4.2 shows transformations of FTIR spectra of the 2 nm thick PGMA layer deposited onto a Si-prism upon modification with thiophene-3-acetic acid (TAA) followed by polymerization of 3HT. The spectra of the PGMA layer contains characteristic intense signals of carbonyl groups with a maximum of 1730 cm^{-1} and signals of moderate intensity at 2930-3030 cm^{-1} assigned to stretching of the aliphatic CH bonds.

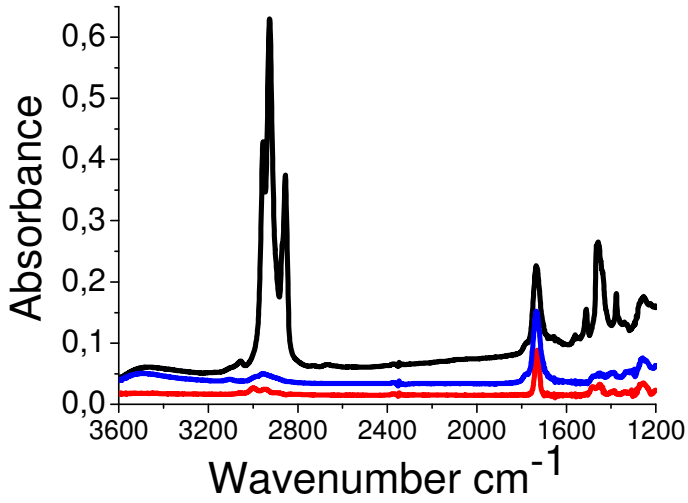

Figure 4.2. *FTIR-spectra of PGMA (red), PGMA-TAA (blue) and grafted P3HT film (black). P3HT film grown on the top of Si-prism modified with PGMA-TAA anchoring layer.*

The successful grafting of TAA is proven by the appearance of a signal at 3400 cm^{-1}, which is due to a stretching of the OH bonds, a signal at 3060 cm^{-1} of the CH-bonds of the thiophene ring and an increase in intensity and broadening of the carbonyl signal near 1740-1730cm^{-1}. Ellipsometrical thickness measurements revealed an approximate double of the initial thickness of PGMA layer upon the annealing with TAA. The thickness of the whole anchoring layer was measured to be 3-4 nm.

4.2.2 GRAFTING OF POLY(3-HEXYLTHIOPHENE) (P3HT)

General procedure preparing the *graft*-P3HT layer shows in Scheme 4.2. The grafting of P3HT was achieved by placing the respective PGMA-TAA-modified substrates in the reactor filled by a polymerization mixture consisting of 3HT monomers in dry chloroform and anhydrous $FeCl_3$. Polymerization was performed at room temperature in argon atmosphere. We found that the thicknesses of the resulting films measured by ellipsometry reached the value of 20-30 nm already after 30 minutes of reaction time and then no longer increases even upon prolonged stirring (up to 20 hours). The FTIR spectroscopy data is consistent with the assumption that the resulting deposit is P3HT (Fig. 4.2). The FTIR spectra show an intense signal at 2980 cm^{-1} originating from the stretching of the aliphatic CH bonds and a less intense signal at 3020 cm^{-1}, where aromatic CH-bonds are indicators of the formation of P3HT.

However, AFM-inspection of the resulting films reveals large morphological heterogeneity. As seen in Fig. 4.3, the films consist of randomly located bumps with a height of 100-200 nm, which occupies approximately 10–20% of the whole sample area and a number of smaller structures. Obviously, because of resolution limits of the size of the beam (in order of millimeters), ellipsometric measurements fail to resolve the surface heterogeneity and thus, the ellipsometrically determined value of 20–30 nm represents just the average thickness of the largely heterogeneous film.

Scheme 4.2. *Grafting of P3HT brush from anchoring layer using oxidation polymerization.*

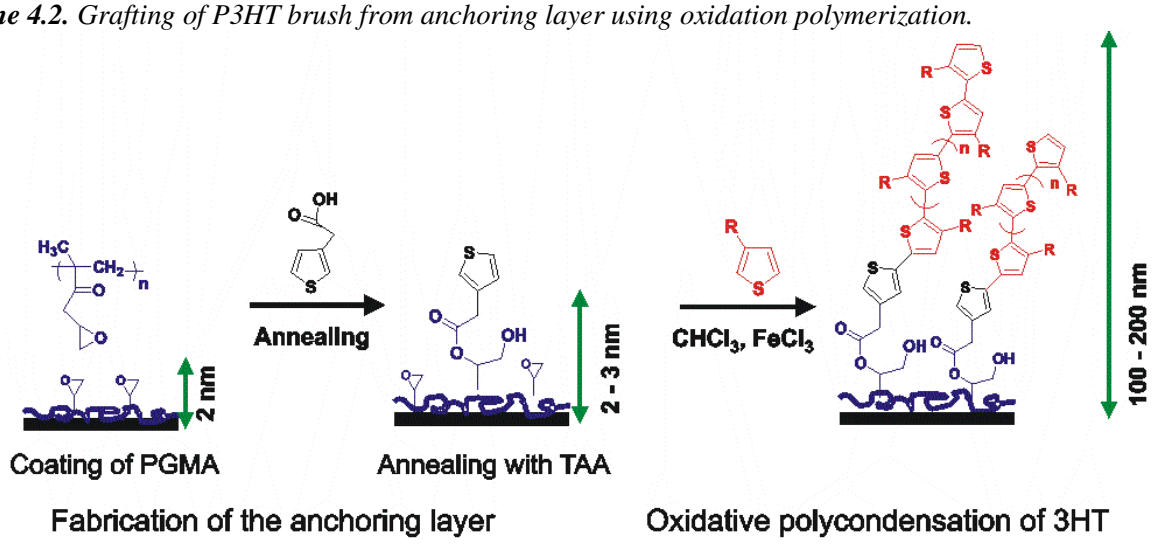

Collard *et al.*[46] previously used oligothiophene-based SAMs for the growing of strongly adherent poly(3-octylthiophene) films. Unfortunately, morphological studies were not presented in this paper

and it is therefore not clear, whether the observed heterogeneity of our P3HT films is an inherent feature of only PGMA-based technology or if it is also valid for other anchoring approaches.

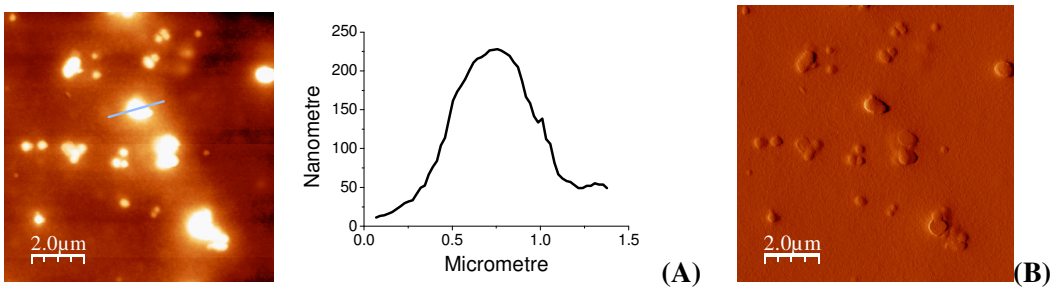

Figure 4.3. *(a) AFM topography image and cross-section and (b) AFM phase image of the 160 nm thick (as determined using ellipsometry) P3HT film grown from PGMA-TAA anchoring layer coated on top of the Si-wafer-supported.*

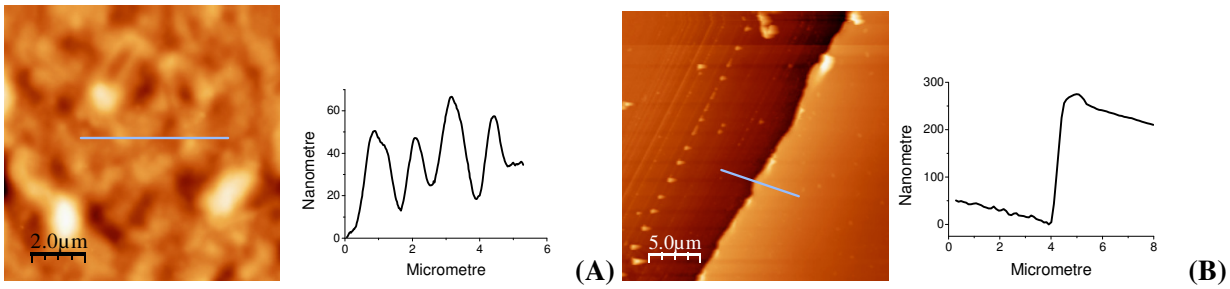

Figure 4.4. *(a) AFM topography image of P3HT film grown from PGMA-TAA anchoring layer coated on top of the Si-wafer-supported. The roughness of film is 20-40 nm; (b) AFM image of scratched area of this P3HT film. The thickness of film measured with AFM is 200 nm.*

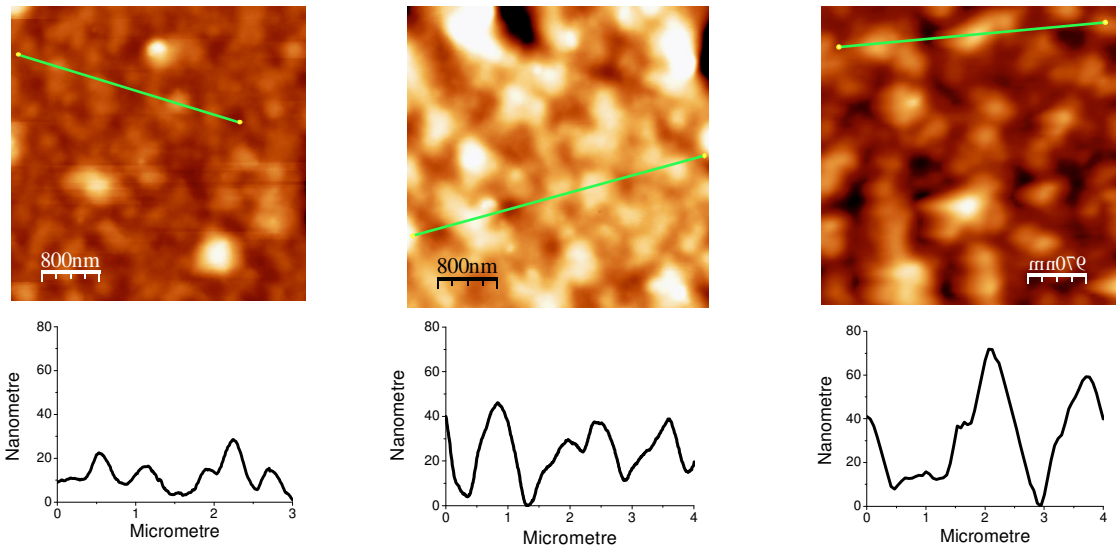

2 stage_1 hour
60 nm with ellipsometry

2 stage_2 hours
80 nm with ellipsometry

2 stage_3 hours
90-160 nm with ellipsometry

Figure 4.5. *AFM topography images and cross-sections of the P3HT films grown at different polymerization time.*

We found, however, that P3HT films prepared in the first polymerization step can be then used as anchoring layers for the second step of P3HT deposition. Surprisingly, in this case the grafting of P3HT occurs in a much more controllable way. The thickness of the resulting P3HT films can now be efficiently controlled in the range of 30 to 200 nm by varying the reaction time of the second polymerization step from a few minutes to several hours. AFM measurements revealed moderately smooth morphology in those cases with RMS roughness of 20-40 nm for the 200 nm thick P3HT film (see Fig. 4.4). In Fig. 4.5 presents the AFM images of P3HT films grown at different polymerization times. It shows that the increase of the polymerization time provides the increase of film thicknesses and film roughness.

Although the exact mechanism of the process still remains unclear, the observed results are consistent with the "nucleation-and-growth" mechanism frequently observed for heterogeneous reactions. It is reasonable to suggest that the polymerization of 3HT monomer at the surface leads to the P3HT brush to co-exists and compete with the polymerization in the bulk solution resulting in dissolved P3HT.

In consistence with the "nucleation-and-growth" mechanism, the polymerization starts from a slow process of the formation of "growing points". It was previously shown that $FeCl_3$ microcrystals serve as nucleating points that collect and oxidize monomers. Therefore, in the first polymerization step, the polymerization preferentially occurs in the bulk solution where $FeCl_3$ microcrystals are dispersed. An additional factor that lowers the rate of the "near-surface" polymerization is a diffusion barrier, which has to overcome monomer molecules approaching the surface. As a result, the first polymerization step results in the formation of some amount of P3HT islands (nuclei) on the surface and a large amount of unattached P3HT in solution. At the end of the first polymerization step the substrate is contaminated by insoluble polymerization products precipitated from solution. Washing of the samples and addition of a fresh portion of monomers and the oxidizer result in a fast growing of P3HT chains from already formed randomly located P3HT islands grown during the first polymerization step and this process can now efficiently compete with the polymerization in the bulk solution. Due to favored hydrophobic interactions P3HT islands grown during the first polymerization step accumulate the 3HT-monomer more efficiently than the PGMA-TAA anchoring layer, which results in a preferential growth of P3HT chains from these points or, at least, the surface-grafting can now compete with the polymerization in the bulk solution.

At the same time, such a nucleation-and-growth scheme suggests that the resulting P3HT deposit is not the "ideal" polymer brush of end-attached and perfectly C_2-C_5 connected chains, but rather

consists of highly branched structures with the involvement of C_4- hydrogen into polymerization on each branching step.

4.2.3 CHARACTERIZATION OF THE DEGRAFTED POLYMER

In order to investigate the chemical structure and molecular weight of the grafted P3HT a 15×15 cm^2 aluminum foil was used as support. After the polymerization, the Al foil was dissolved in HCl solution and P3HT was extracted using chloroform. That way, a sufficient amount of PHT was obtained to create a ^{1}H NMR spectrum (~6 mg). The main fraction of P3HT (~68%) was soluble in chloroform. The ^{1}H NMR spectra of soluble fraction confirm the formation of regioirregular P3HT (Fig. 4.6).

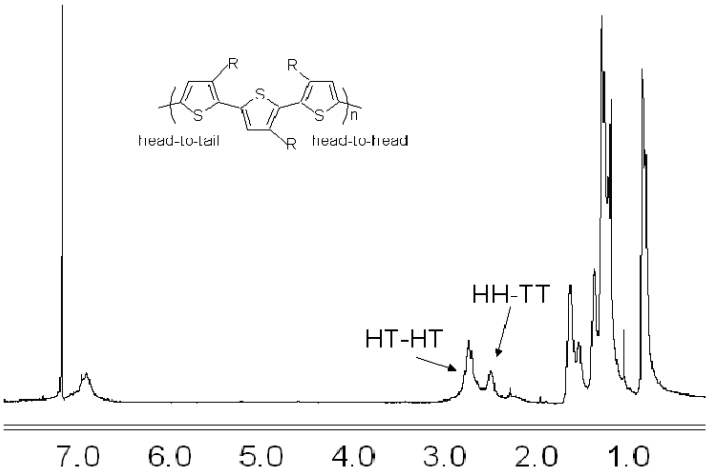

Figure 4.6. *^{1}H NMR spectra of P3HT degrafted from Al-foil.*

Although the main fraction of P3HT was soluble in chloroform, a significant amount of brown compound was insoluble even after full dissolution of the support. This insoluble fraction presumably represents high molecular weight and cross-linked P3HT. A gel permission chromatography (GPC) of the soluble fraction reveals Mn=12400 and Mw=52200, which corresponds to a weight average contour length of 28 nm and 118 nm, respectively. It must be noted that the thickness of the grafted P3HT film in the dry state in this experiment was 130 nm.

4.2.4 SOLVATOCHROMISM AND SWELLABILITY

P3HT grafted to glass slides displays solvatochromism similar to dissolved P3ATs. As shown in Fig. 4.7, the maximum absorbance of the P3HT film changes from 444 nm in chloroform, which is

"good" solvent, to 485 nm in methanol, a "bad" solvent, and to 490 nm in the dry state. The observed red shift in the UV-vis. spectra is due to a transition from a less conjugated (twisted) to a more conjugated (planar) conformation. This fact implies a certain conformational freedom of P3HT chains despite them being tethered to the substrate.

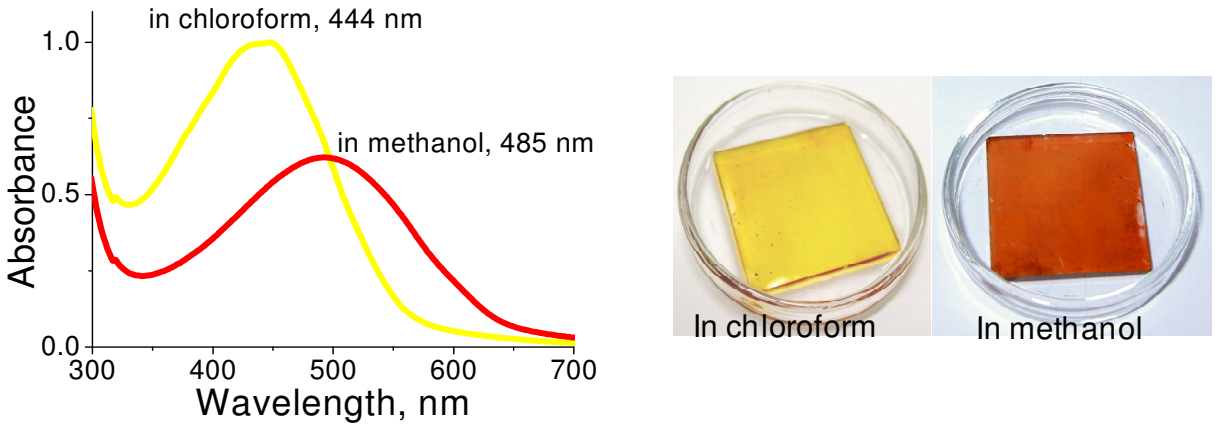

Figure 4.7. *UV-vis. absorption spectra and photographs of P3HT films grafted to a glass slide in chloroform and methanol solution.*

To investigate the swellability of P3HT layers grafted to Si-wafers, we measured their thicknesses in chloroform and compared them to their thickness in the dry state. As monitored by ellipsometry, the thickness of the given sample reversibly changes from 130 nm in the dry state to 370 nm in chloroform. This fact confirms the conformational freedom of the tethered P3HT chains, however, on the other hand, reflects that in the dry state the P3HT layer is still far from an ideal "brush regime" with perpendicularly oriented perfectly stretched chains for which further stretching upon the swelling in good solvents would be impossible.

4.2.5 ORIENTATION

The anisotropic properties of conductive polymers can be examined by polarized IR measurements (Fig. 4.8). The vibration modes are usually observed as very sharp bands in the IR region and their absorption intensity is sensitively enhanced or reduced along the specific polarization direction by polarized IR measurement. We do not observe dichroism in our spectra that reveal random orientation of P3HT chains.

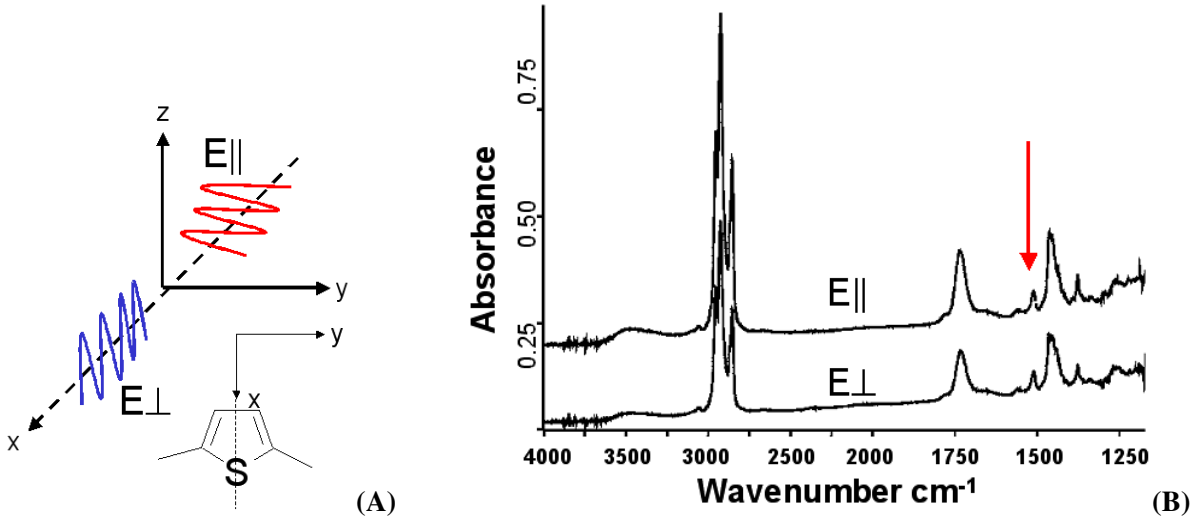

Figure 4.8. *(a) geometry of the polarized probe rays whose vibration plane is either on the x-y plane (E_{II}) or on the z-x plane ($E_{\perp}$). The inset shows a polythiophene segment lying on the x-y place whose symmetry axis (dotted line) coincides with the x axis.(b) IR dichroic spectra of the grafted P3HT film, anisotropy: (E_{II}) s-polarized spectrum, ($E_{\perp}$) p-polarized spectrum).*

4.2.6 ELECTRICAL MEASUREMENTS

To estimate the electrical conductivity we reoxidized the neutral polymer film chemically. The polymer brushes were prepared on the glass substrate and doped with solution of $FeCl_3$ (1M) in ethanol (or with iodine vapors in chamber) for 15 min. or 12 h. Then the lateral electrical conductivity using the two-point measurement setup was performed as shown in Scheme 4.2.

Scheme 4.2*. Principle of conductivity measurements. The sample under test is of bar shape with known cross sectional area. A current is passed through the sample in the direction of its longitudinal axis. The voltage drop is measured with two contacts, either point or blade type, at a known distance.*

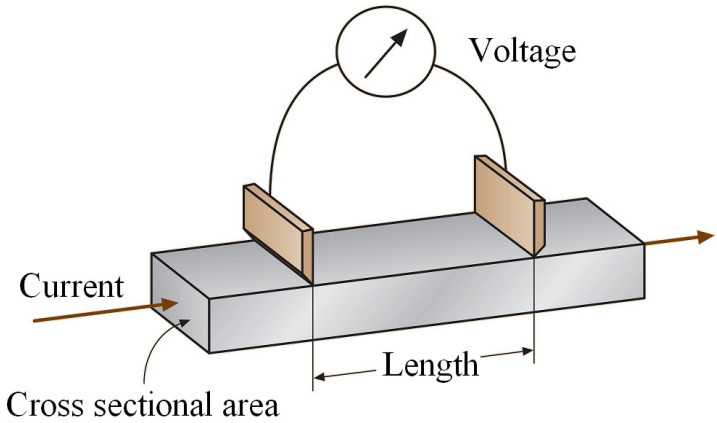

The determination of conductivity with direct current (*dc*) is made by measuring the resistance R and the dimension of the conductor (length *l*, width *w*, and thickness *d*). From these measurements, the conductivity is calculated:

$$\sigma = \frac{l}{w \cdot d \cdot R}$$

The resistance *R* is determinate by a voltage-current method. A current (*I*) of known value is fed into the sample and the voltage (*V*) is measured via point contacts. The resistance is then calculated according to Ohm's law: $R = V/I$.

The conductivity of the neutral polymer film by *dc* method was found to be 2.3×10^{-8} S/cm (Tab. 4.1). The conductivity of the sample increases with the increase of the doping time from 15 minutes to 12 hours. In the case of $FeCl_3$ doping of the sample, the conductivity increases from 0.49×10^{-5} S/cm to 0.67×10^{-2} S/cm. For the I_2-doped-P3HT film the conductivity was found to be 0.12×10^{-3} for 15 min. and 0.10×10^{-2} for 12 h. doping time. This is few orders of magnitude higher than the conductivity of the pristine P3HT films or dedoped P3HT films (rinsed with ammonia solution). The value of conductivity of $FeCl_3$-doped P3HT film is typical for poly(3-alkylthiophenes) film.

Table. 4.1. *The resistance and conductivities of the pristine P3HT film, $FeCl_3$-doped P3HT film and I_2-doped P3HT film in lateral direction (dc method).*

Thickness of P3HT film	Non-doped		Doped with $FeCl_3$			
			Doped during 15 min.		Doped during 12 h.	
	R, Ohm	σ, S/cm	R, Ohm	σ, S/cm	R, Ohm	σ, S/cm
170 nm	10^{12}	2.3×10^{-8}	4.8×10^{9}	0.49×10^{-5}	3.5×10^{6}	0.67×10^{-2}
			Doped with I_2			
			Doped during 15 min.		Doped during 12 h.	
			2.0×10^{8}	0.12×10^{-3}	2.2×10^{7}	0.10×10^{-2}

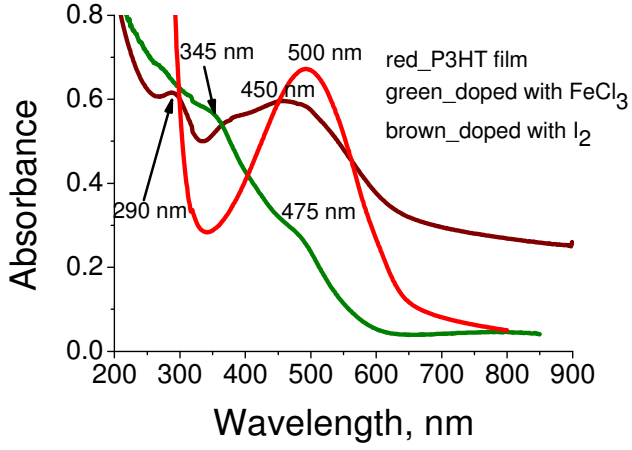

Figure 4.9. *UV-vis. spectra of P3HT film, $FeCl_3$-doped P3HT film and I_2-doped P3HT film.*

Fig. 4.9 shows the UV-vis. spectra of the pristine and doped P3HT films. As can be seen from Fig. 4.10 the absorption maximum of pristine P3HT in the film at $\lambda_{max.}$=500 nm changes to the two broad peaks with $\lambda_{max.}$ at 345 nm and 480 nm for the $FeCl_3$-doped P3HT film. After the doping with iodine the spectra shows small peaks at 290 nm and a broad peak at 450 nm. These changes in UV-vis. spectra is a consequence of π-π* transitions between the dopant molecules and the thiophene rings of the polymer backbone.

Having possible solar cell applications for the grafted P3HT in mind, an attempt to prepare a P3HT-fullerene derivative (PCBM) bulk heterojunction was undertaken. Since the P3HT layers are covalently attached to the substrate (and therefore could not be washed away), but still swellable, the PCBM solution in chloroform was spin coated on the P3HT film grafted onto the glass slide. The results allow to possible assumptions about possible structures of the resulting P3HT/PCBM film. The first assumption is that the resulting composite film is bilayered, with segregated PCBM atop the P3HT. The second assumption is that PCBM penetrated into the P3HT. This second structure would be preferable for solar cells due to better contact properties between the donor and acceptor components.

Fig. 4.10 shows the UV-vis. and fluorescence spectra of the P3HT film before and after treatment with PCBM solution. A drastic decrease of the fluorescence intensity in the later case reflects a near complete quenching that is most probably a result of PCBM intercalated into P3HT. Thus, the second assumption becomes more probable.

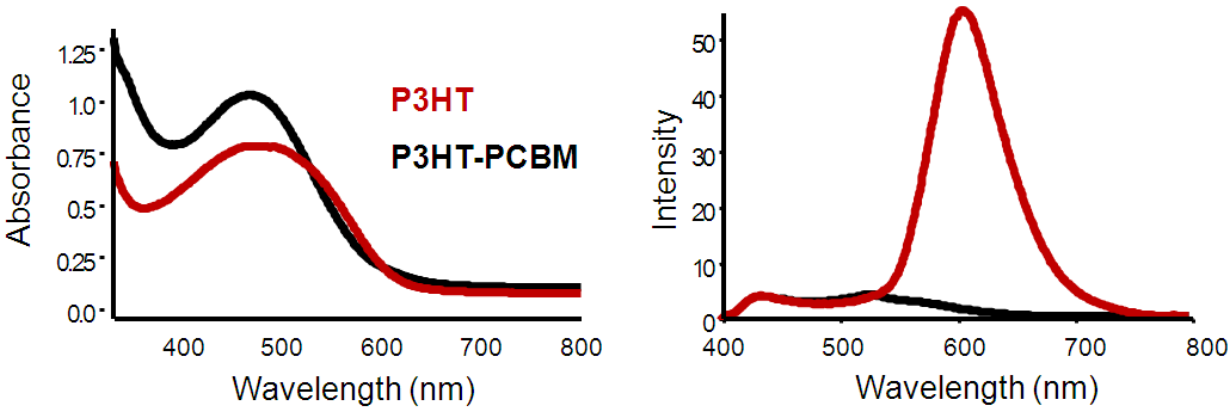

Figure 4.10. *UV-vis. and fluorescence spectra of the P3HT film (red line) and the same film after the treatment with PCBM solution (black line).*

Similar structures were also prepared on ITO glasses and tested for their photovoltaic response. Unfortunately, the solar cell performance was very weak, which can be explained by the irregular structure of the P3HT.

4.3 CONCLUSIONS

In this work, we have used oxidative $FeCl_3$-mediated polycondensation for the grafting of irregular P3ATs using various anchoring compounds. P3HT grafted to glass slides displays solvatochromism similar to dissolved P3ATs. The grafted P3HT film changes its color from yellow when placed in chloroform (a "good solvent" for P3HT), to red when placed in methanol (a "bad solvent"). The observed red shift in the UV-vis. spectra is due to a transition from a less conjugated (twisted) to a more conjugated (planar) conformation. This implies a certain conformational freedom of P3HT chains despite the fact that they are tethered to the substrate. The conductivity of P3HT film was found in order of 10^{-2} after doping with $FeCl_3$. The photovoltaic properties of the grafted P3HT were tested and found to be poor, most probably due to the irregular structure of P3HT.

4.4 EXPERIMENTAL PART

Chemicals. Ethanol, ammonium, hydrogen peroxide, tetrahydrofuran, chloroform, 3-hexylthiophene, thiophene-3-acetic acid (TAA), iron (III) chloride were obtained from Aldrich Chemical and used as received. Chloroform for polymerization was distilled under P_2O_5 in argon atmosphere and kept under argon atmosphere.

Si-wafers, Si-prisms (Wacker-Chemitronics) or the microscope glass slides (Menzel-Glaser) were cleaned as described in literatur[77,78]: with ethanol in an ultrasonic bath, then with a hot mixed solution of ammonium with hydrogen peroxide, and rinsed several times in Millipore water. The aluminum foil was cleaned with several solvents.

Poly(glycidyl methacrylate) PGMA. (Mw=70000 g/mol, PDI=1.7) was prepared by radical polymerization of glycidyl methacrylate in butanol-2 solution at 60 °C for 2 hours in argon atmosphere. AIBN (4,4-azobis(isobutyronitrile)) was used as an initiator.

Sample preparation. PGMA was deposited by spin-coating from chloroform (0.03mg/ml, 2000 rpm). Thiophene-3-acetic acid was afterward deposited by drop-casting (10gm/ml in chloroform) and the samples were annealed at 150 °C during 10 hours in argon atmosphere, then, extensively rinsed with chloroform. The respective PGMA-TAA-modified substrates were placed vertically in the reactor and the polymerization was carried out by stirring of the 5mg/ml solution of 3-hexylthiophene in dry chloroform with four equivalents of anhydrous $FeCl_3$ at room temperature in argon atmosphere during

[77] Tsukruk, V.V.; Luzinov, I.; Julthongpiput, D., *Langmuir,* **1999**, 15, 3029 –3032.
[78] Minko, S.; Müller, M.; Motornov, M.; Nitschke, M.; Grundke, K.; Stamm, M., *J. Am. Chem. Soc.,* **2003**, *125,* 3896.

20-60 minutes. In order to remove all unattached reaction products, the samples were then extensively rinsed with chloroform, ammonia solution (5% in water), HCl solution (5% in water), deionized water and finally with hot chloroform in ultrasonic bath.

In the experiments on aluminum foils, they were cleaned in ultrasonic bath with ethanol prior to use. PGMA was deposited on the Al-foils by dip-coating. Thiophene-3-acetic acid (TAA) was afterward deposited by drop-casting (10 gm/ml in chloroform) and the samples were annealed at 150 °C during 10 hours in argon atmosphere and then extensively rinsed with chloroform. Then, oxidation polymerization of 3HT was performed as describe above.

CHAPTER 5

GRAFTING FROM OF 3,3''-DIOCTYL-[2,2';5',2'']TERTHIOPHENE (DOTT) USING ELECTROCHEMICAL POLYCONDENSATION

3-Alkylthiophenes can be polymerized to the corresponding poly-3alkylthiophenes (P3ATs) using the electrochemical polymerization method. Electrochemical oxidative polycondensation would be the next promising way for selective grafting of the conjugated polymers (CPs). The polymers prepared by electrochemical route are not soluble, and the produced polymers remain on the electrode in doped state. After dedoping, the polymers become soluble in solvents. To achieve a covalent grafting of the polymers, the electrode must be modified with appropriate self-assembling monolayers (SAMs). The SAM forms a bridge layer between the electrode and the polymerizated monomers. In our work, we studied electro-grafting of symmetrical 3,3''-dioctyl-[2,2';5',2'']terthiophene (*DOTT) to indium-tin-oxide (ITO) electrodes covered with various SAMs.*

5.1 ELECTROCHEMICAL POLYCONDENSATION OF ALKYLTHIOPHENES

Electrochemical polycondensation represents a widely employed route for synthesis and immobilization of conjugated polymers (CPs). As the electrogenerated reactive species are mostly located in close vicinity to the electrodes, the undesired formation of ungrafted chains could be efficiently avoided. Direct *in situ* formation of a polymer film from a solution of monomers can be induced electrochemically. Through electrochemical initiation, a monomer such as pyrrole, phenol or thiophene is oxidized to a polymerizable radical. Under suitable conditions, the polymer that is formed in the diffusion layer adheres firmly to the surface of the electrode[79]. A common electrochemical technique that is used in this process is *cyclic voltammetry* (CV). This method is applicable to many electrode materials and many monomer compounds. The technique is often simple to carry out, requiring only basic electrochemical instrumentation. Furthermore, growth of polymer films can be controlled by stepping or cycling the electrode potential. The properties and the reproducibility of the surface polymer ultimately depend upon the nature of the polymerization solution, the electrode material and, to some extent, the cell geometry and attendant hydrodynamic conditions. Electrochemical synthesis has the advantage of producing the material on an electrode on which the analysis of the growing process is performed, as well as further experiments by electrochemical and/or spectroscopy techniques. Furthermore, the method allows easy control of the film thickness by deposition charge. A polymeric film is obtained by electrochemical polymerization. It is a very useful method for the preparation of polymers such as polythiophene, poly(3-methylthiophene) and poly(3-phenylthiophene) which are insoluble and infusible. When these polymer are obtained in the form of powder, we can not process them into a film or other useful forms.

Thiophene, bithiophene, terthiophene were galvanostatically polymerized in propylene carbonate using lithium perchlorate as electrolyte. The polymerization potential decreased in the order thiophene >bithiophene > terthiophene. The properties of the resulting film were depending on the polymerization potential. The high potential necessary for the polymerization of thiophene caused irreversible oxidation. On the other hand, the polymerization potential was low for bithiophene and terthiophene, such that high-quality films were obtained. The highest doping level and the best stability upon cyclic voltammetry (CV) were found for polyterthiophene. However, an electrochemical and spectroscopic analysis of these polymers showed that the conjugation length decreased from polythiophene to

[79] Sarac, A.S., *Electropolymerization, Encyclopedia of Polymer Science and Technology*, Copyright by John Wiley & Sons, Inc., **2004**, 9, 651-677.

polyterthiophene. Consequently a parallel decrease in electrical conductivity[80] occurred which is attributable to irregular interring bonding in polyterthiophene.

3-substituted thiophene can also be synthesized electrochemically. Poly(3-dodecylthiophene) with a conductivity of 67 S/cm was electrochemically prepared and the degree of polymerization was found to be 90 by vapor pressure osmometry[81,82]. Hotta improved the method of electrochemical polymerization of 3-alkylthiophene[83]. Polymerization was carried out under rigorous oxygen- and moisture-free conditions using a specifically designed electrochemical cell. This method increased the conductivity of poly(3-alkylthiophene) to 750 S/cm after doping with NOPF6. Poly(3-hexylthiophene) showed good solubility in various organic solvents and could be processed from a soluble in both neutral and doped state.

Although *intrinsically soluble* CPs can be also prepared electrochemically[84]. They remain insoluble only in doped state and dissolve completely in good solvents after dedoping. However, examples of covalent grafting using electrochemistry remain scarce. In general, for successful grafting, appropriate anchoring compounds strongly adherent to substrate and copolymerizable with the monomer must be immobilized on the electrode.

SAMs were widely investigated and found many applications[85]. The advantage of such structures is that they maintain their order on the surface. The good electron transfer behavior of SAMs also led to the development of new strategies for modification of the electrode surface aiming at the control of their electrochemical reactivity. Electrons can be transferred across a monolayer by a tunneling mechanism, which operates up to around 12 carbon atoms in the alkyl chain, affording electroactive properties to such monolayers[86]. The organic molecules used for this purpose consist of a thiophene head group and a phosphoric acid anchor group, which are connected via an alkyl chain. By dipping the passivated substrate into a solution of these specific molecules, covalent bondings are formed between the phosphoric acids group and the metal oxide in the passive layer. This way a highly oriented and densely packed monomolecular film can be built up, which is terminated to air by thiophene head groups[87]. Recently Zotti *et al.*[47] performed surface-initiated polymerization of different pyrrole- and thiophene-based monomers from self-assembled monolayers (SAMs) of carboxy-terminated

[80] Roncali, B.; Lemaire, M.; Garreau, R.; Garnier, F., *Synth. Metals*, **1987**, 18, 139-144.
[81] Sato, M.; Tanaka, S.; Kaeriyama, K., *J. Chem. Soc. Chem. Commun.,* **1986**, 773.
[82] Sato, M.; Tanaka, S.; Kaeriyama, K., *Synth. Metals,* **1987**, 18, 229-232.
[83] Hotta, S., *Synth. Metals,* **1987**, 22, 103-113.
[84] Dini, D.; Decker, F.; Zotti, G., *Electrochem. Sol. State. Lett.,* **1998**, 1, 217-219.
[85] Sullivan, J.T.; Harrison, K.E.; Mizzell, J.P.; Kilbey, S.M., *Langmuir,* **2000,** 16, 9797-9803.
[86] Michalitsch, R.; Kassmi, A.El.; Yassar, A.; Lang, P.; Garnier, F., *J. of Electroanal. Chem.*, **1998**, 447, 129-139.
[87] Harm, U.; Bürgler, R.; Fürbeth, W.; Mangold, K.-M., Jüttner, K., *Macromol. Symp.,* **2002**, 187, 65-76.

oligothiophenes. Since the corresponding polymers were soluble in the electrochemical medium, only the surface-coupled polymers remained on the modified indium tin oxide (ITO) electrodes.

5.2 SAMS ON THE ITO SURFACE

In this work I aimed to use the electrochemical polymerization method to covalently graft intrinsically soluble polythiophenes. To achieve regioregularity of the structure of the resulting polymer, *symmetrically* substituted terthiophene (3,3''-dioctyl-[2,2';5',2'']terthiophene (DOTT)) was used as monomer. Although ITO is not the best material for electrochemical investigations (e.g. compared to Pt), it was used in this study because of its optical transparency, which is important for photovoltaic applications. To achieve covalent grafting, various SAM-forming compounds with phosphoric acid anchoring groups and different hetero-aryl head groups were tested.

The SAM-forming compounds were synthesized by the group of Prof. Adler/Dr. Jähne (TU Dresden) and are displayed in the Tab. 5.1. The presence of phosphoric acid moiety in their structure provides bindings to various metal (Ti, Al, etc.) oxide surfaces, and in particular to ITO.

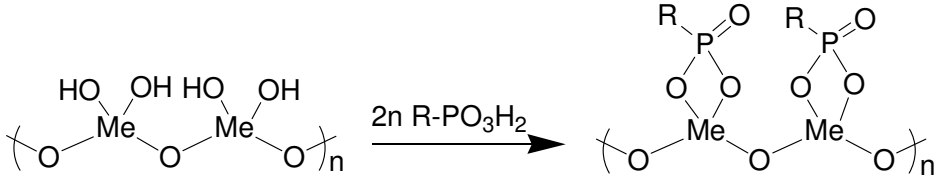

Table 5.1. *Oxidation potentials of SAMs attached to the ITO surface and oxidation potential of SAMs in solution. The oxidation potential was measured from the first voltammetric cycle in freshly prepared solutions in CH_3CN (0.1M TBAPF6, 0-2 V, scan rate=100mV/s).*

	SAM_1	SAM_2	SAM_3	SAM_4	SAM_5
	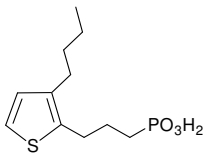	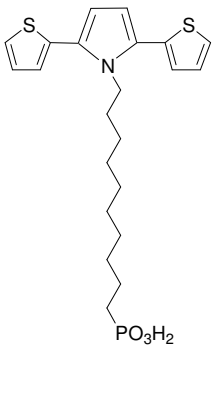	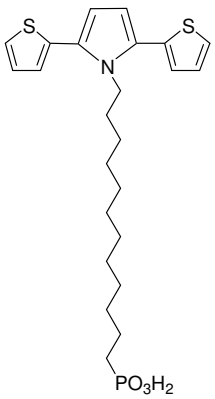	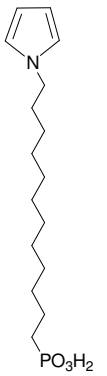	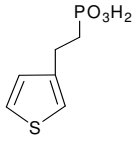
In solution	1.70 V	0.84 V	0.88 V	1.20 V	1.75 V
Onto ITO	1.45 V	0.95 V	0.80 V	1.10 V	1.60 V

The morphology of pristine ITO glass and ITO modified with SAM_3 was investigated using AFM (Fig. 5.1). The morphology of pristine ITO surface revealed by the AFM is shown in Fig. 5.1a. It was found that the deposition of SAM_3 (Tab. 5.1) increases its roughness from 1-2 nm for ITO to 2-3 nm for ITO-SAM_3 layer as can be seen in Fig. 5.1b.

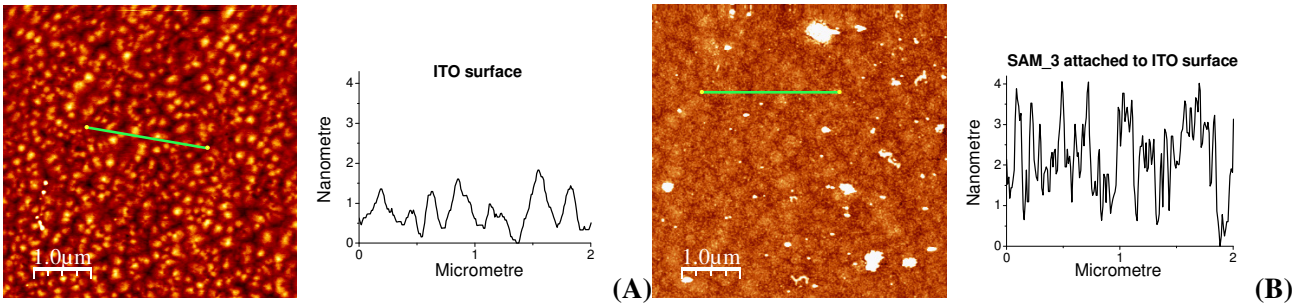

Figure 5.1. *AFM topography images and cross-sections of (a) the pristine ITO surface and (b) the ITO surface modified with SAM_3.*

5.2.1 ELECTROCHEMICAL PROPERTIES OF SAMS

The electrochemical properties of all SAMs were examined by cyclic voltammetry. The cyclic voltammograms for different SAMs are presented in Fig. 5.2.

It must be emphasized that the quality of cyclic voltammograms recorded using ITO as the working electrode was not as high as one can obtain using Pt wires. However, they allow determination of oxidative potentials for SAMs with sufficient accuracy. The red line shows the first voltammograms of the SAM-forming compound that were freely dissolved in CH_3CN. The blue lines correspond to voltammograms of the corresponding SAMs prepared *in-situ* from ethanol solutions, washed and afterwards placed into the electrochemical cell for the determination of the oxidative potential. Cyclic voltammograms in these later cases were recorded using CH_3CN without addition of the corresponding SAM-forming compounds. For the cyclic voltammograms recorded for freely dissolved SAMs (red lines) the current is higher than for the case of cycling of SAMs alone (blue lines) indicating the deposition of multilayers in the later case.

Oxidative potentials for all SAMs studied are given in Tab. 5.1. Lowest oxidation potentials have been found for SAM_2 and SAM_3 with head groups containing three aromatic-rings due to delocalization of electrons among the π–system. Interestingly, the oxidation potentials of the SAM_3 (0.88V) were found to be very close to the one found for the DOTT monomer (0.90V).

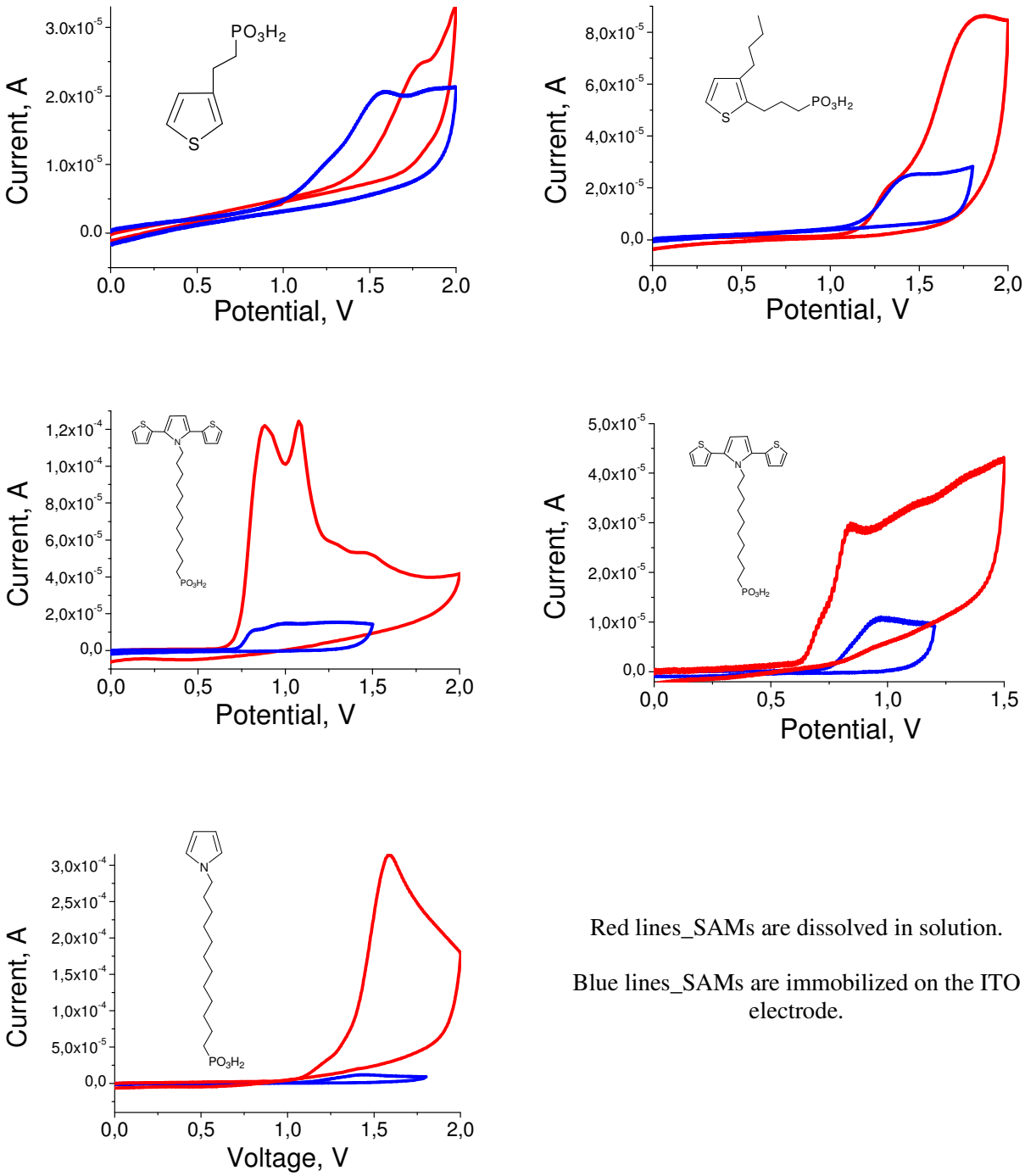

Red lines_SAMs are dissolved in solution.

Blue lines_SAMs are immobilized on the ITO electrode.

Figure 5.2. *Cyclic voltammograms of different SAMs.*

5.3 GRAFTING FROM OF 3,3''-DIOCTYL-[2,2';5',2'']TERTHIOPHENE (DOTT) USING CYCLIC VOLTAMMETRY

The electrochemical stability and the reversibility of the redox process of DOTT monomer was studied using cyclic voltammetry (Fig. 5.3). The potentials were measured against Ag/AgCI as reference electrode and each measurement was calibrated with a SCE redox system as internal standard. The HOMO and LUMO energy value of the compounds were determined from the first oxidation and the first reduction potentials (E_{ox1} and E_{red1}) respectively, by taking a value of -4.5eV as HOMO energy level for the Silver/silver chloride electrode. The 3,3''-dioctyl-[2,2';5',2'']terthiophene (DOTT) show irreversible reduction and reversible oxidation steps for the entire scanning rate in a region of 50mV/s to 100mV/s. The energy gap $Eg^{ele.}$ of DOTT was determined by difference between of HOMO and LUMO levels and is 2.08eV.

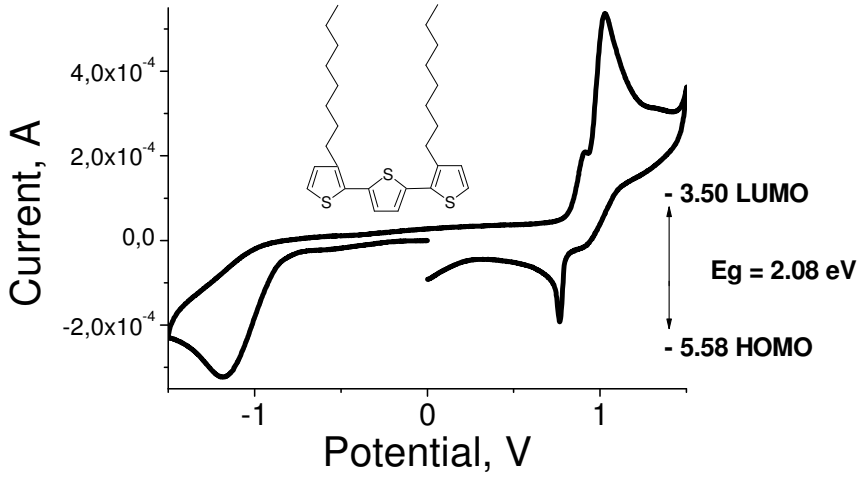

Figure 5.3. *Determination of the band gap of 3,3''-dioctyl-[2,2';5',2'']terthiophene from the first voltammetric cycle. It corresponds to the difference between the HOMO and the LUMO level.*

Electrochemical polymerization of DOTT was performed on ITO electrodes modified with different SAMs by repeatedly cycling between 0V and 1.6V at different rates and using different monomer concentrations. The CV shows quasi-reversible reduction and oxidation steps for the entire scanning rate in a region of 50mV/s to 200mV/s. As an example, the repeated cyclic voltammograms of monomers polymerized onto the ITO surface containing SAMs at the rate of 10mV/s are shown in Fig. 5.4. The first wave of oxidation of DOTT to a radical monocation occurs at an anodic potential of 1.2V. Upon reversing the direction of sweep from the first oxidation wave, a corresponding cathodic wave owing to the reduction of the oxidized polymer film is observed in the region from +1V to +0.75V. In the second subsequent anodic sweeps wave, we observe a new peaks, which is reversible as well. It

reveals the growth of the polymer film at a lower oxidation potential, where the peak potential (E_{pa}) occurs at ca. +0.8V and +0.96V. Thus, the cyclic voltammogram of DOTT has all the characteristics of an ECE reaction[88,89], i.e., a sequence of steps whereby an electron transfer event (E) is followed by a chemical reaction (C) and a subsequent electron transfer reaction (E). Since the film-forming reaction can be described as a cascade of ECE reactions, the general term E(CE)n, has been recently forwarded to describe the film-forming reactions[90].

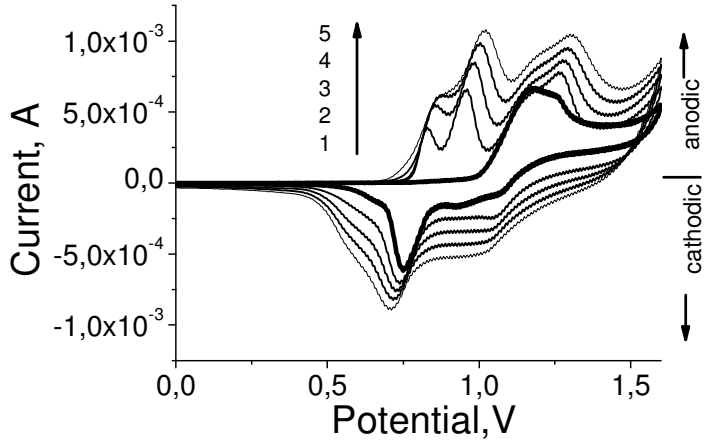

Figure 5.4. *Cyclic voltammogram of DOTT on the ITO surface modified with SAM_3.*

The electropolymerization reaction proceeds with an electrochemical stoichiometry of 2.2-2.3 Faraday/mol. The oxidation of the monomer requires 2 Faraday/mol, while the excess of charge (0.2-0.3 Faraday/mol) is proportional to the reversible oxidation (doping) of the polymer[89]. The mechanism of the electropolymerization of DOTT is very complicated. However, it is can be described on the model of electropolymerization of thiophene[91] (Scheme 5.1).

The initial step involves the oxidation of the thiophene monomer (R is thiophene) to its thiophene radical cation (R^{+*} is radical cation of thiophene) at the electrode surface (E). A rate of the electron transfer reaction is higher than the diffusion of R from the bulk solution to the electrode surface. Thus, at the anode, the concentration of monomer is low. Accordingly, at the applied voltage the molecules occur only in their oxidized state R^{+*} in the vicinity of the electrode surface. This insures a high concentration of R^{+*} at the electrode surface, which is continuously maintained by the steady state diffusion of R from the bulk. These conditions favor the radical cation dimerization process (C). The initial combination product of two radical cations is the dication of the dihydrodimer which

[88] Adams, R.N., Electrochemistry at solid electrodes. Marcel Dekker Inc., New York. 1969.
[89] Adams, R.N., *ACC. Chem. Res.,* **1969,** 2, 175.
[90] Waltman, R.J., Bargon, J., *Can. J. Chem.,***1986**, 64, 76-95.
[91] Entezaml, A.; Arsalanl, N., *Iran. J. Polymer Science & Technology*, **1992**, 1, 33-35.

subsequently deprotonates to produce the aromatic dimmer (C). The dimer is next oxidized, coupled, and deprotonated to produce the next higher homologue (E). The final step in the reaction to produce oxygenated material[90]. Thus, the electropolymerization reaction proceeds via an intermediate dihydro-oligomer dication, which then loses two protons to form the neutral oligomer.

Scheme 5.1. *Mechanism of the electropolymerization of thiophene.*

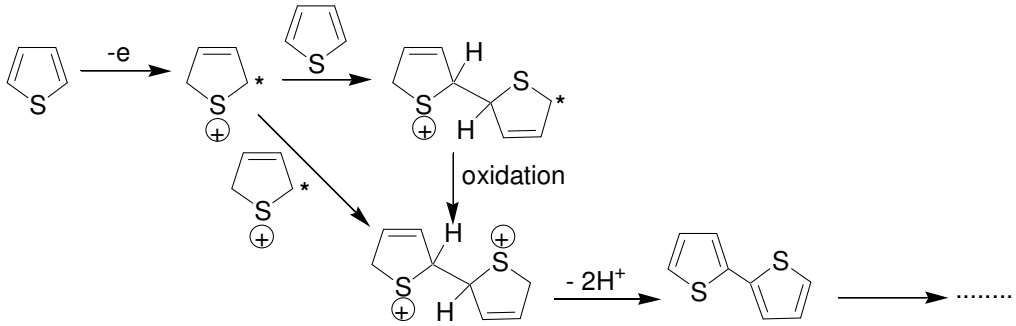

Important to note that these monomeric radical cations can undergo a variety of follow-up reactions depending upon their intrinsic stability. The first way, when R^{+*} is relatively stable, it can diffuse away from the electrode surface and undergo reactions to form low molecular weight soluble products. And second way, when R^{+*} is very unstable, it can rapidly undergo indiscriminate reactions with either the solvent or anions to form low molecular weight, and thus soluble, products equally well. The schematically formation of the PDOTT brush using electropolymerization depicted in Scheme 5.2.

Scheme 5.2. *Formation of the PDOTT brush using electropolymerization.*

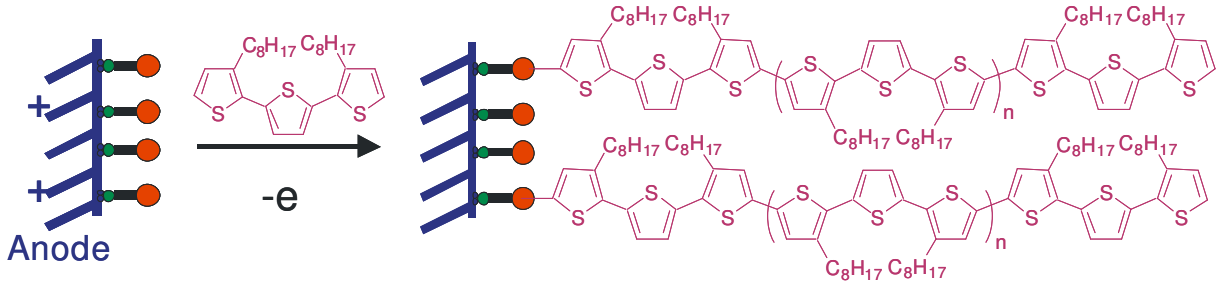

In such a reaction pathway of the monomer **R** (**R** is 3,3"-Dioctyl-[2,2';5',2"]terthiophene) electropolymerization, in which chain propagation is dependent on the presence of radical cation of DOTT ($\mathbf{R}^{+*}$) (as opposed to R), is defined as: (a) the cyclic voltammograms reveal an E(CE)n process, consistent with radical-cation coupling reactions; (b) in order to sustain film growth at the electrode surface the electrode potential (voltage) has to be maintained at the electrochemical oxidation potential

of **R**; (c) the film-forming reaction is surface localized, and no evidence of polymerization in the bulk of the solution has yet been observed (where for the concentrations the relation [**R**]>>>[$\mathbf{R}^{+*}$] holds)[89,92].

The grafted PDOTT film on an electrode surface, shows fast electrochromic switching behavior between red and dark green colors. The electrochromism is due to a reversible transition between undoped (red) and doped (dark green) states of the main polymer chain (Fig. 5.5).

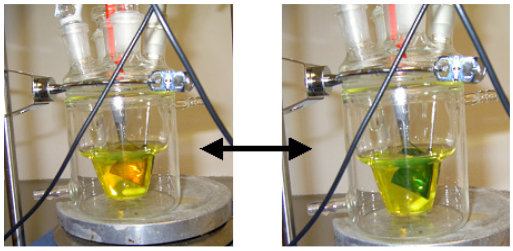

Reduction state (0V) Oxidation state (1.6V)

Figure 5.5. *Electrochromic process of PDOTT during the cyclic voltammetry.*

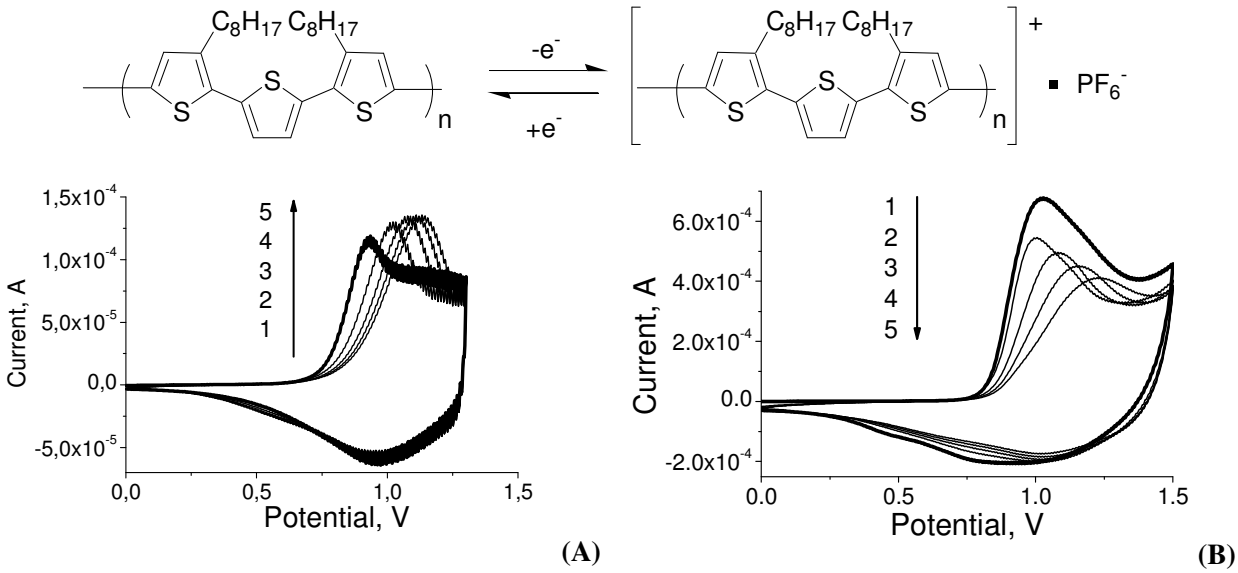

Figure 5.6. *Cyclic voltammograms with five repeated scans of PDOTT in CH_3CN at room temperature: (a) stability of the film and (b) dissolution of the film.*

The electrochemical properties and stability of the deposited PDOTT films were studied by cycling in a monomer-free electrolyte solutions in acetonitrile (Fig. 5.6). It was found that only those films that were prepared using SAM_3 were stable and remained on the electrodes (Fig. 5.6a). In all other cases, when the ITO was modified with other SAMs or left unmodified, the resulting PDOTT was readily and quantitatively removed (washed away) during this procedure (Fig 5.6b).

[92] Yano, J.; Yoshikawa, K-I.;Kitani, A., Anal. Sciences, **1997**, 13, 741-746.

For determination of the energy gap $E_g^{ele.}$ of PDOTT, a cyclic voltammetry of the grafted PDOTT film in the free monomer solution was performed (Fig. 5.7). The energy gap was calculated from the first voltammetric cycle as difference between of HOMO and LUMO levels. It was found to be 1.92eV.

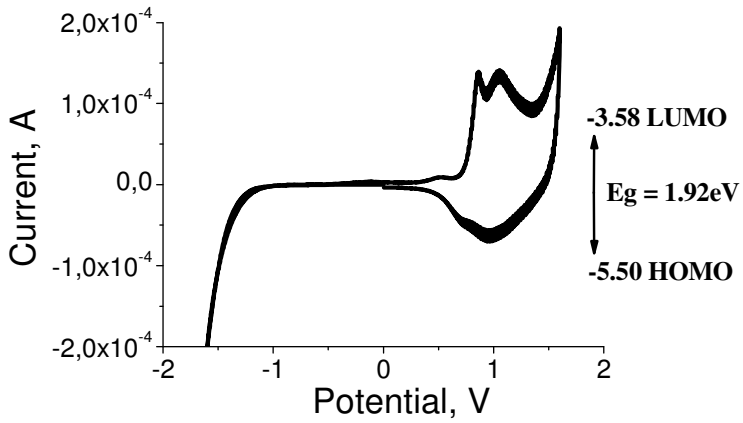

Figure 5.7. *Determination of the band gap of PDOTT from the first voltammetric cycle. It corresponds to the difference between the HOMO and the LUMO level.*

The energy gap between valence and conduction band of polymer is related to the lowest allowed energy of its monomer units and to the bandwidth resulting from the overlap between the monomer orbitals as shown in Fig. 5.8. The energy band gaps obtained from the band structure calculations for solids are analogous to Highest Occupied Molecular Orbital (HOMO) to Lowest Unoccupied Molecular Orbital (LUMO) energy differences in molecules.

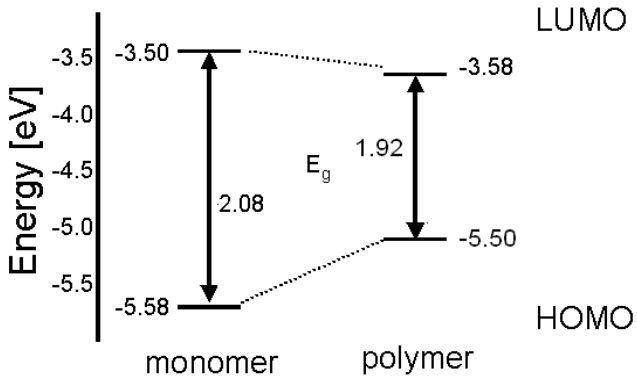

Figure 5.8. *HOMO and LUMO energy levels and band gaps, obtained from cyclic voltammogram measurements of DOTT and PDOTT.*

Tab. 5.2 presents the energy gap of PDOTT in comparing with different alkyl-substitutes terthiophenes. It was found that the energy gap of poly(3,3"-dioctyl-[2,2';5',2"]terthiophene) is close to the data of poly(3,3"-dihexyl-[2,2';5',2"]terthiophene).

Table 5.2. *HOMO and LUMO energy levels and band gaps, obtained using CV measurement of different polyterthiophenes.*

Polymer	HOMO	LUMO	$Eg^{elc.}$[eV]	$Eg^{op.}$[eV]
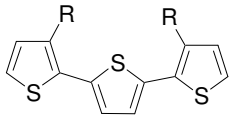 R = C_8H_{17}	- 5.50	- 3.58	1.92	1.99
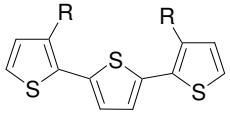 R = C_6H_{13} [93]	- 5.25	- 3.05	2.20	1.90
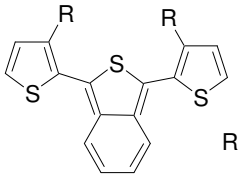 R = C_6H_{13} [94]	- 4.96	- 2.68	2.28	2.21

5.3.1 CHARACTERIZATIONS OF GRAFTED PDOTT FILM

The UV-absorption spectra show a broad and relatively blue-shifted peak as compared with the spectra of high molecular weight P3HT that further indicate low molecular weight and (or) poor ordering in PDOTT prepared by electropolymerization. The polymer synthesized on the ITO-SAM_3 shows solvatochromism: it becomes yellow in chloroform and turns red in methanol and in dry state as can be seen in Fig. 5.9.

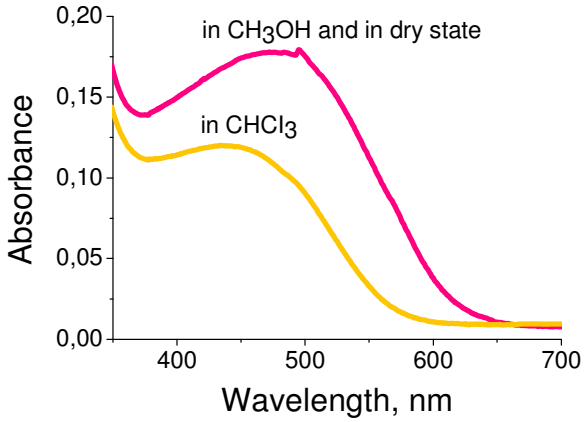

Figure 5.9. *UV-vis. spectra of PDOTT film using electropolymerization, in dry state and methanol (red) and in chloroform solution (yellow).*

[93] Koppe, M.; Scharber, M.; Brabec, C.; Duffy, W.; Heeney, M.; McCulloch, I., *Adv. Funct. Mater.,* **2007**, 17, 1371-1376.
[94] Kisselev, R.; Thelakkat, M., *Macromolecules,* **2004**, 37, 8951 -8958.

From this follows that polymers have the same conformation freedom despite of the fact that the chains are immobilized. The optical band gap of the polymer can be calculated from the curves and follows to be 1.99eV. In chloroform it is 2.17eV.

The morphology of the PDOTT films grown on ITO modified with SAM_3 was studied by AFM (Fig. 5.10). The films show quite rough, but homogeneous structures. Although some holes are clearly visible, they do not extend to the electrode surface. The thickness of the grafted layer measured with AFM was found to be 200 nm.

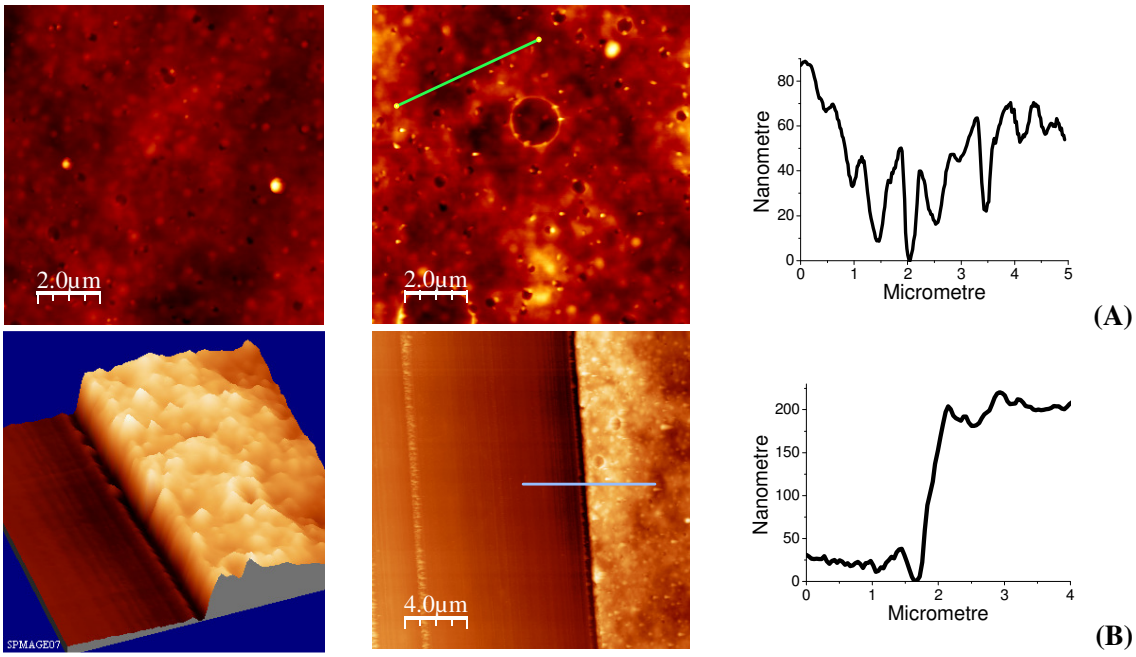

Figure 5.10. *(a) AFM topography images and cross-section of PDOTT film; (b) AFM images of the scratch area of PDOTT film and cross-section. The PDOTT film grown electrochemically on ITO surface modified with SAM_3. It shows the thickness of 200 nm.*

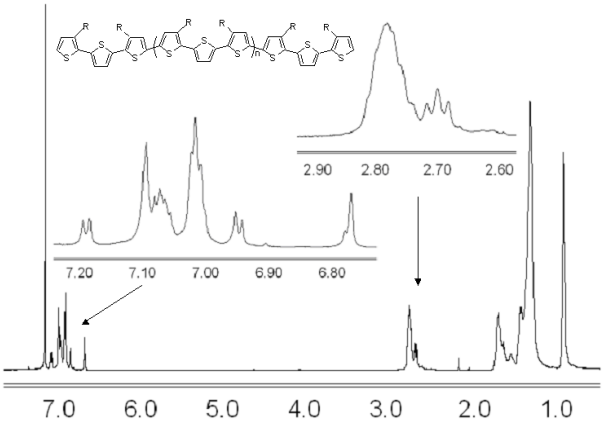

Figure 5.11. *^{1}H NMR spectra of PDOTT prepared by electropolymerization.*

The polymerization of PDOTT was performed on unmodified ITO glass and the resulting polymer was collected and investigated by ^{1}H NMR (Fig. 5.11). The signals at 2.60 and 2.79 ppm correspond to the methylene groups at the end-monomer units and internal monomer units of PDOTT, respectively. The integration of these signals at 2.60 and 2.79 ppm of methylene groups allow to find the polymerization degree. It was found to be around 3-6 terthiophene units, despite on the fact that the polymer was collected from quite thick film on ITO (1 mkm).

5.4 PHOTOVOLTAIC CHARACTERISTICS

The photovoltaic properties of these grafted poly(3,3''-dioctyl-[2,2';5',2'']terthiophene film on ITO-SAM_3 substrates were tested by Prof. K. Leo group (TU Dresden). The plastic solar cell device was prepared according to the following procedure: the ITO-coated glass substrate (thickness 150±10 nm, roughness is ≤1 nm) was firstly cleaned by ultrasonication in organic solvents and ammonium mixture, then dried in a nitrogen flow. Afterwards it was modified with SAM_3 (1-2 nm measured with AFM). Then the electropolymerization of DOTT was performed. The thickness was measured with an AFM study and found to be 150 nm. Before the photovoltaic measurements, the sample was stored in high vacuum (< 10^{-7} mbar) for 12 hours. A fullerene C_{60} (60 nm) was coated atop of the grafted PDOTT layer, using 1,2-dichlorbenzen as the solvent. The bathophenanthroline, Bphen (7 nm) layer as well as aluminum (70 nm) were deposited by thermal sublimation on the sample through shadow masks on the substrates. An operable solar cell was obtained.

Fig. 5.12 shows the current-voltage behavior of the grafted PDOTT-C_{60} solar cell under illumination with white light at an irradiation intensity of 108 mW/cm^2. The first measurement of the solar cell under illumination (red line) shows an open circuit voltage V_{OC} of 0.25V, a short circuit current I_{SC} of 3.26 mA/cm^2 and a fill factor FF of 35%. The short circuit current and FF are increased compared to sample PDOTT. Whereas the open circuit voltage decreased by 0.4V. A comparatively fast degradation of the solar cell is detectible. The characteristics of the solar cell in the dark shows very small currents with negative bias. This behavior points towards a complete coverage of the individual layers in the area of the solar cell.

The second detection shows of the *I-V*-characteristics under illumination (blue line) and the *I-V*-characteristics taken 10 minutes after recording the first characteristics (black line). A decrease in V_{OC}, FF and I_{SC} is detected, whereas the current at -0.5V remains almost constant. A possible explanation for the fast degradation of the solar cell might be impurities on the grafted PDOTT layer. These

impurities (such as H_2O) might be thermally and electrically activated leading to the observed fast degradation of the sample.

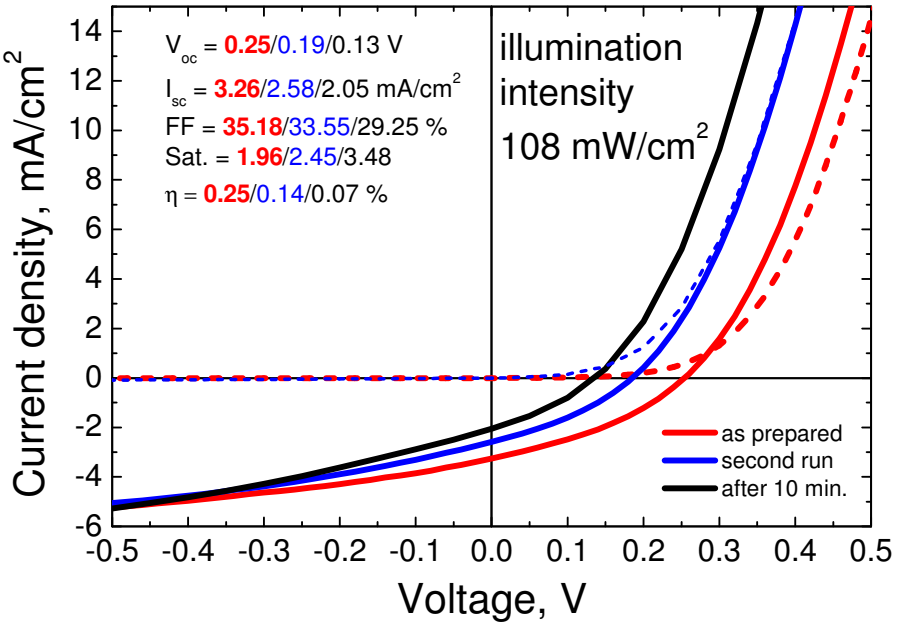

Figure 5.12. *The current density-voltage (I-V) characteristics of solar cell based on ITO/SAM_3/grafted PDOTT brush/C_{60} /Bphen/Al structure.*

One can clearly see in the current-voltage characteristics that the charge transport is severely inhibited and the devices are subject to rapid degradation. Problems in the charge transport most likely originate from the fact that the CP has an undesired morphology in grafted PDOTT:C_{60} blends. This can be explained by the grafted PDOTT having short polymer chains (≈ 3.5–6.7 nm) and that, despite that the thickness was found to be 150 nm, the film does not present as brush, but more likely a cross-linked layer.

5.5 CONCLUSIONS

Electrochemical grafting of 3,3"-dioctyl-[2,2';5',2"]terthiophene (DOTT) onto ITO glass modified with self-assembled monolayer (SAM) with aligned oxidative potentials of the monomer and the SAM was successful. The grafted PDOTT film display electrochromic and solvatochromic properties. The photovoltaic properties of these grafted poly(3,3"-dioctyl-[2,2';5',2"]terthiophene) films were tested by Prof. K. Leo group (TU Dresden). The beneficial self-ordering effects for grafted PDOTT in the donor-acceptor structures were not observed. The devices showed relatively poor photovoltaic response with best values at 0.25% (not corrected for spectral mismatch). The grafted polymers contribute to the

photocurrent, i.e. they are photovoltaic active. However, from the current-voltage characteristics it becomes clear that the charge transport is severely inhibited and that the devices are subject to rapid degradation. Problems in the charge transport most likely originate from the fact that the CP has an undesired morphology in grafted PDOTT:C_{60} blends.

5.6 EXPERIMENTAL PART

Chemicals. The ITO was washed in alcohol to remove all oil dust then cleaned by peroxide mixture (NH_4OH:H_2O_2:H_2O_1:1:4) at 80 °C during 1 hour. After rinsing in water several times, the ITO samples were dried by nitrogen and used immediately.

The SAMs were prepared in the lab of Prof. Adler and used without further purifications[95,96,97].

Acetonitrile, methanol, ethanol, tetrahydrofurane, acetic acid, 3-octylthiophene, tetra-*n*-butylammonium hexafluorophosphate (TBAPF6), N-bromsuccinimide (N-BS), N-iodsuccinimide (N-IS), bis(tetramethylethylborid)thiophene, 2,5-dibromthiophene, tetrakis(triphenylphosphine) palladium (0), [1,3-bis(diphenylphosphino)propane]dichloronickel (II), magnesium were obtained from Aldrich Chemical and used as received.

Bromination of 3-octylthiophene. N-BS (1.78 g, 10 mmol) was added at 0 °C to a stirred solution of 3-octylthiophene (1.96 g, 10 mmol in 30 ml mixture of chloroform and acetic acid (50/50 v/v)) and the mixture was stirred overnight at room temperature. Afterwards the reaction mixture was quenched with ice water and extracted with chloroform. The organic layer was washed successively with 6% aqueous KOH, water and dried over anhydrous $MgSO_4$. After filtration and evaporation, the residue was purified by chromatography column to give as a colorless oil of 2-brom,3-octylthiophene (2.75 g, 99% yield). ^{1}H NMR (500.13 MHz, $CHCl_3$), δ 7.17 (1 H), 6.69 (1 H), 2.58 (2 H), 1.61-1.55 (2 H), 1.32 (6 H).

The Iodization of 3-octylthiophene was synthesized as described above, only N-IS instead of N-BS was used.

3,3''-dioctyl-[2,2';5',2'']terthiophene (DOTT) via Suzuki coupling.

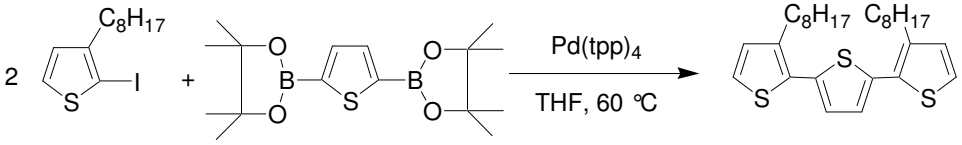

[95] Oberoi, S.; Jähne, E.; Adler, H.-J., *Macromol. Symp.,* **2007**, 254, 284-291.
[96] Steiner, G.; Sablinskas, V.; Savchuk, O.; Bariseviciute, R.; Jähne, E.; Adler, H.-J.; Salzer, R., *J. Molec. Struc.*, **2003**, 661, 429-435.
[97] Oberoi, S.; Jähne, E.; Adler, H.-J.; Varma, I.K., *Designed Monomer and Polymers*, **2008**, 1-14.

2,5-Bis(tetramethylethylborid)thiophene (1.30 g, 3.4 mmol), 2-iod, 3-octylthiophene (2.73 g, 8 mmol) and Pd-catalyst (0.48 g, 0.4 mmol) were dissolved in THF (30 ml) and sealed in a dry round-bottom reactor supplied with the refrigerator, then the solution was stirred for 15 min under argon atmosphere. Afterwards the reaction mixture was added to a solution of NaOH (0.12 g, 3 mmol) in 5 ml H_2O and stirred for 30 min at room temperature, then for 3 days at 70 °C. The reaction was quenched with water, extracted with chloroform, then, the organic layer was dried over anhydrous $MgSO_4$. After filtration and evaporation, the residue was purified by chromatography column to give 3,3''-dioctyl-[2,2';5',2'']terthiophene (1.77 g, 38% yield) as a yellow oil. Since this method gives a low yield of the product, another approach was predominantly used (see below).

3,3''-dioctyl-[2,2';5',2'']terthiophene (DOTT) via Kumada coupling.

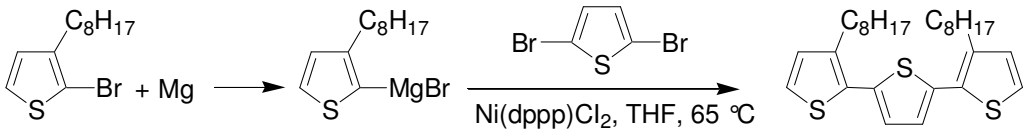

A thoroughly dried round-bottom flask was supplied with a refrigerator under argon atmosphere, Mg powder (1.01 g, 41 mmol) and I_2 was added and heated to form a violet cloud for the activation of the Mg powder. After that, 7 ml of dry THF in one portion and 2-brom, 3-octylthiophene (8.46 g, 30 mmol) in 26 ml of THF were added drop-wise during 30 min and stirred for 2 hours. The obtained Grignard reagent was added to a dry round-bottom flask with a refrigerator and containing 2,5-dibromthiophene (3.26 g, 13 mmol) and Ni-catalyst (0.13 g, 0.25 mmol) in 50 ml dry THF. The reaction was carried out during 2 days at 65 °C. The reaction mixture was quenched by water and extracted with chloroform; the organic solution was washed with diluted HCl, water and dried over $MgSO_4$. Then the solution was filtrated, evaporated and purified by column chromatography to release a yellow oil of 3,3''-dioctyl-[2,2';5',2'']terthiophene (6.88 g, 90% yield), ^{1}H NMR (500.13 MHz, $CHCI_3$), δ 7.21 (1 H), 7,09 (1 H), 6.91 (1 H), 2.79 (2 H), 1.61-1.55 (2 H), 1.32 (6 H).

Preparation of SAMs. The formation of SAM onto ITO surface was achieved by dipping the substrate into a 10^{-3} M solution of the respective SAM in ethanol for 24 hours under argon atmosphere. Solutions of SAMs are very sensible to light and oxygen. Therefore they must be used immediately after they were prepared or kept in dark in the refrigerator. Ungrafted molecules, were afterwards washed off with ethanol. After that the samples were transferred directly into the electrochemical cell.

Cyclic Voltammetry (CV). The electrochemical experiments were performed in a three-compartment cell by the using Autolab with potentiostat/galvanostat PGSTAT under computer control. The electrochemical process is performed in solution with a suitable potential window with a relatively high monomer concentration (0.1 mmol/L) and hexafluorophosphate salt as supporting electrolyte (0.1

mol/L) on inert electrode. The polymerization was performed at room temperature. For electrochemical polymerization of 3,3"-dioctyl-[2,2';5',2"]terthiophene (DOTT), the platinum sheet was used as the counter electrode and ITO with SAM layers as working electrode. All electrochemical solutions were deaerated by dry argon overpressure bubbling for 20 min. All potentials were referred to an Ag/AgCI electrode immersed directly in the solution. After polymerization, the ITO substrates were washed repeatedly with methanol and acetone to remove the electrolyte and monomer and with chloroform and THF to avoid unattached polymers.

CHAPTER 6

GRAFTING OF REGIOREGULAR HEAD-TO-TAIL POLY(3-HEXYLTHIOPHENE) BY KUMADA CATALYST-TRANSFER POLYCONDENSATION (KCTP)

This chapter describes a new method to grow conductive polymer brushes of regioregular head-to-tail poly(3-alkylthiophenes) (P3ATs) via Kumada Catalyst Transfer Polymerization (KCTP) of 2-bromo-5-chloromagnesio-3-alkylthiophene. Exposure of the initiator layers to monomer solutions leads to selective chain-growth polycondensation of the monomers from the surface, resulting into P3AT brushes in a very economical way. The grafting process was investigated in detail and the structure of the resulting composite films was elucidated using several methods. The obtained data suggests that the grafting process occurs not only at the poly(4-bromstyrene) (PS-Br)/polymerization solution interface, but also deeply inside the swollen PS-Br films, penetrable for the catalyst and for the monomer. We demonstrated in this chapter how surface structures of non-conductive block copolymers, such as poly(4-vinylpyrridine)-block-poly(4-iodstyrene) (P4VP-b-PS-I), can be converted into (semi)conductive P4VP-b-PS-graft-P3HT chains via surface-initiated polymerization of poly(3-hexylthiophene) (P3HT) from reactive surface-grafted block copolymers. We believe that the developed method for structured brushes of conductive polymers can be further exploited in the fabrication of novel stimuli-responsive materials to construct sensors or various opto-electronic devices.

6.1 DEVELOPMENT OF SITE-SPECIFIC CHAIN-GROWTH CATALYST-TRANSFER KUMADA POLYCONDENSATION (KCTP)

Recent publications of the groups of McCullough's[36] and Yokozawa's[37] described Ni-catalyzed chain-growth polycondensation of **1a** to regioregular HT P3HT, and attracted our attention as a viable opportunity to develop a surface-initiated polycondensation leading to CP brushes. It was shown that the first step of the mechanism involves the preparation of catalytic Ni(0) species from the catalyst precursor Ni(dppp)Cl_2 through the addition of two molecules of **1a** at their magnesium ends, yielding a symmetrical bis-organonickel *intermediate* ***1*** (Scheme 6.1)[36,37].

Scheme 6.1. *Mechanism of the chain-growth polycondensation of* ***1a*** *according to McCullough et al.*[36] *and Yokozawa et al.*[37].

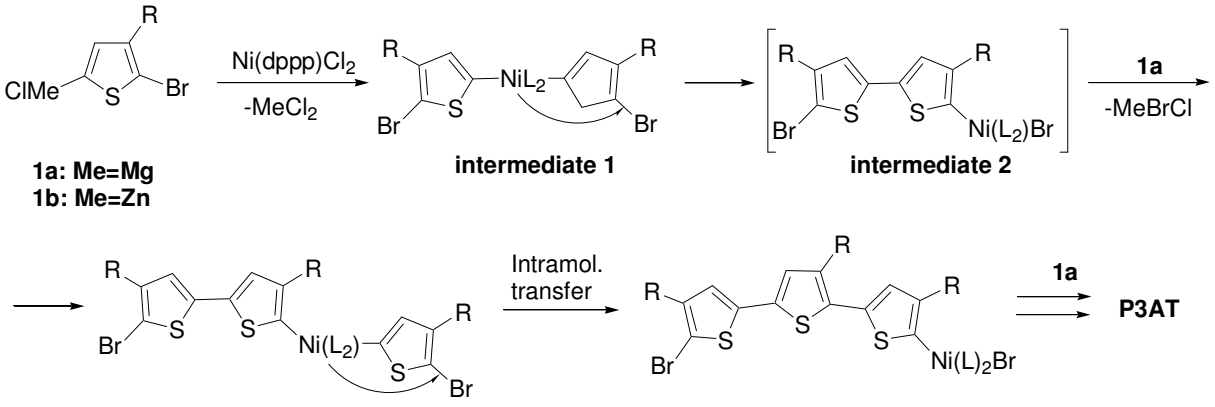

In the second stage, the reduced Ni(0)dppp migrates to the nearest end of the molecule by intramolecular insertion into the C-Br bond to form tail-to-tail bithiophene *intermediate* ***2*** terminated by the Ni-catalyst. The growth of the polymer chain occurs by addition of one monomer at a time at its magnesium-terminated end to Ni-Br bond of *intermediate* ***2*** followed by the *intramolecular* transfer of the Ni-catalyst into the terminal C-Br bond. An alternative *intermolecular* transfer of the Ni-catalysis into C-Br bond of the monomer **1a**, corresponding to the step-growth polycondensation mechanism, is less favored here because of the deactivating character of the electron-donating magnesium moiety in **1a**. Thus, the key peculiarity of the mechanism is that it involves a selective intramolecular insertion of the Ni-catalyst to the more reactive end group of the polymer. This results in a one-by-one successive addition of monomers to the growing point of the polymer chain, instead of the random coupling usual for polycondensation[98]. McCullough *et al*. demonstrated that this important feature of the mechanism gives access to various block copolymers, in which the first polymerized block is P3AT[36,99]. Our

[98] Kiso, Y.; Yamamoto, K.; Tamao, K.; Kumada, M., *J. Am. Chem. Soc.,* **1972**, 94, 4373-4374.
[99] Liu, J.; Sheina, E.; Kowalewski, T.; McCullough, R., *Angew. Chem., Int. Ed.,* **2002**, 41, 339-342.

ultimate aim is to develop a complimentary process – a procedure allowing one to grow P3AT selectively *from the initiator* and immobilized onto planar surfaces or any other objects.

In general, for the realization of surface initiated polymerization, a suitable initiator should be attached to the surface and the polymerization reaction has to involve a chain-growth mechanism. Since the synthetic procedure developed by McCullough[36] and Yokozawa[37] fulfills the crucial last requirement and can be realized in a "near leaving" manner, we first explored the possibility to employ a Ni(dppp)Cl_2 catalyst for the surface initiated polymerization of **1a**. The key step here is the synthesis of the Ni-based initiator, having an aryl moiety attached to the surface and a halide group reactive toward Grignard reagents. The direct coupling of Ni(0) complexes with arylhalides, as shown in the Scheme 6.1, would be one of the most straightforward and economical routes to the key organonickel initiator[100]. Unfortunately, Ni(dppp)$_2$, the Ni(0) analogous of Ni(dppp)Cl_2, is not sufficiently reactive with non-activated arylhalides[39]. We therefore switched our attention to the more reactive Ni(tpp)$_4$ complex, which smoothly reacts with various arylhalides and gives the desired adducts (tpp)$_2$Ni(Ar)Br (**2** or **3**)[101]. In this work, we utilized the easily available PS-Br for the preparation of the macroinitiator. To verify the applicability of the Ni(tpp)$_4$-based initiators for the surface initiated polycondensation, we investigated a polymerization using bromobenzene (Ph-Br) and *o*-bromotoluene (*o*-Tol-Br) as small-molecule models of PS-Br.

To replace the "classical" Ni(dppp)Cl_2 catalyst with the less-studied Ni(tpp)$_4$, we focused on studying the polycondensation mechanism, having in mind that only the chain-growth mechanism is desired for the synthesis of the polymer brushes. Another issue for investigation was the regioregularity of the Ni(tpp)$_4$-mediated polymerization products.

It was previously demonstrated that the degree of regioregularity of P3AT strongly depends on both metal and ligands of the catalytic complex. Rieke *et al.*[102] reported that the Ni(tpp)$_4$-catalyzed polycondensation of the mixture of **1b** (90%) and its regiomer 5-bromo-2-(bromozincio)-3-hexylthiophene **1b'** (10%) formed upon the treatment of 2,5-dibromo-3-alkylthiophene with activated Zn, which leads to P3HT with only 65% HT-regioregularity.

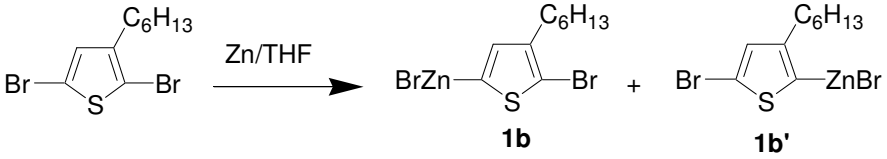

[100] Negishi, E.-I., *Acc. Chem. Res.,* **1982**, 15, 340-348.
[101] Hiday, M.; Kashiwagi, T.; Ikeuchi, T.; Uchida, Y., *J. Organomet. Chem.,* **1971**, 30, 279-282.
[102] Chen, T.-A.; Wu, X.; Rieke, R., *J. Am. Chem. Soc.,* **1995**, 117, 233-244.

In contrast, the Ni(dppp)Cl_2-mediated polymerization of the same monomer mixture resulted predominantly into HT P3AT. The high HT-regularity in the last case was a result of a selective consumption of only the major isomer **1b**.

It was, however, not clear whether the reduced regularity of the Ni(tpp)$_4$-polymerized products was a result of an equal coupling of both isomeric monomers present in the reaction mixture, or due to isomerization of the monomers during the coupling in a manner similar to the Pd(tpp)$_4$-catalyzed polycondensation. To distinguish between the mechanisms contributing to the decrease of the HT-regularity, the polycondensation was investigated for pure isomers **1a** and a mixture of isomeric monomers**.**

Scheme 6.2. *Mechanism of polycondensation of* ***1a*** *initiated by low molecular weight or macromolecular initiators.*

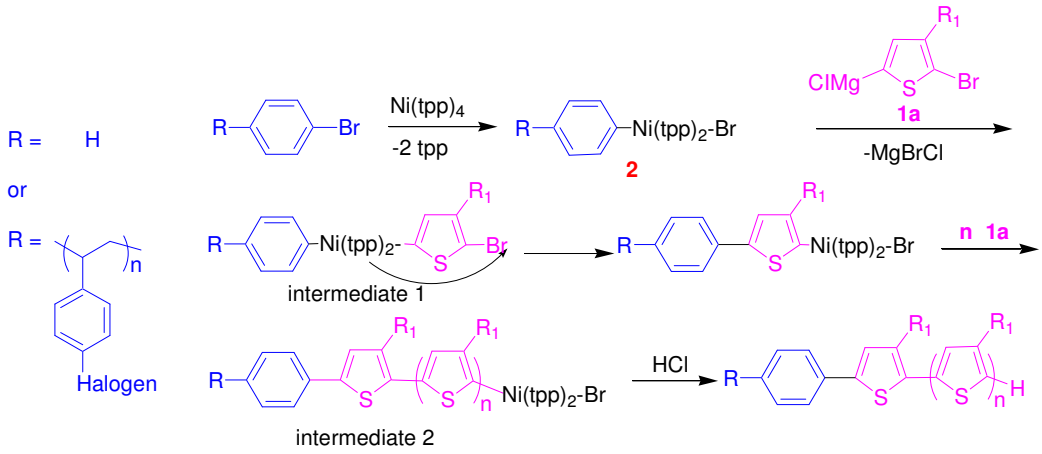

6.1.1 ROOM TEMPERATURE POLYCONDENSATION

Ni(tpp)$_4$ reacts with Ph-Br, yielding (tpp)$_2$Ni(Ph)Br (**2**) within a few hours at room temperature. The polymerization of **1a,** prepared from equimolar amounts of 2-bromo-3-hexyl-5-iodothiophene and *t*-BuMgCl, was performed at room temperature for 4 hours in the presence of 1.67 mol% of **2**. The reaction mixture was quenched with 5 M hydrochloric acid, as proposed by Yokozawa[37], and washed with methanol. P3HT was isolated with ≈70% yield (conversion of **1a**≈80%).

A detailed assignment and integration of all signals in the aromatic region of the ^{1}H NMR spectrum gives quantitative information about both the starting and end groups of the resulting P3HT products (see Fig. 6.1b).

Assuming that all P3HT chains are terminated by either hydrogen or bromine atoms, it was calculated that at least 55% of the P3HT molecules have a Ph starting group. Thus, a significant P3HT fraction (≈45%) does not contain a Ph-group. According to the MALDI-TOF, the content of the Ph-

initiated P3HT is higher. As shown in Fig. 6.1a, ≈80% P3HT is terminated by a Ph-group from one side and by either hydrogen or bromine atoms at the opposite terminus (67% of Ph/H and 13% of Ph/Br P3HT). The minor fraction of P3HT (≈20%), which falsified the NMR calculation, contains hydrogen atoms on both ends (H/H P3HT)[103]. The molecular weight of the resulting P3HT determined by GPC (M_n =4100 g/mol, M_w =8100 g/mol) is lower than what could be predicted for living polymerizations for the given feed ratio and monomer conversion rate (feed ratio **1a/2**=60/1, conversion of **1a**≈80%; $M_{n,\ living}$=8000 g/mol; DP_{step}=60×0.8=48). On the other hand, the measured value of M_n is much higher than expected for the step-growth polycondensation at ≈80% conversion of **1a** ($M_{n,\ step}$ =830 g/mol; DP_{step}=1/(1-0.8)=5).

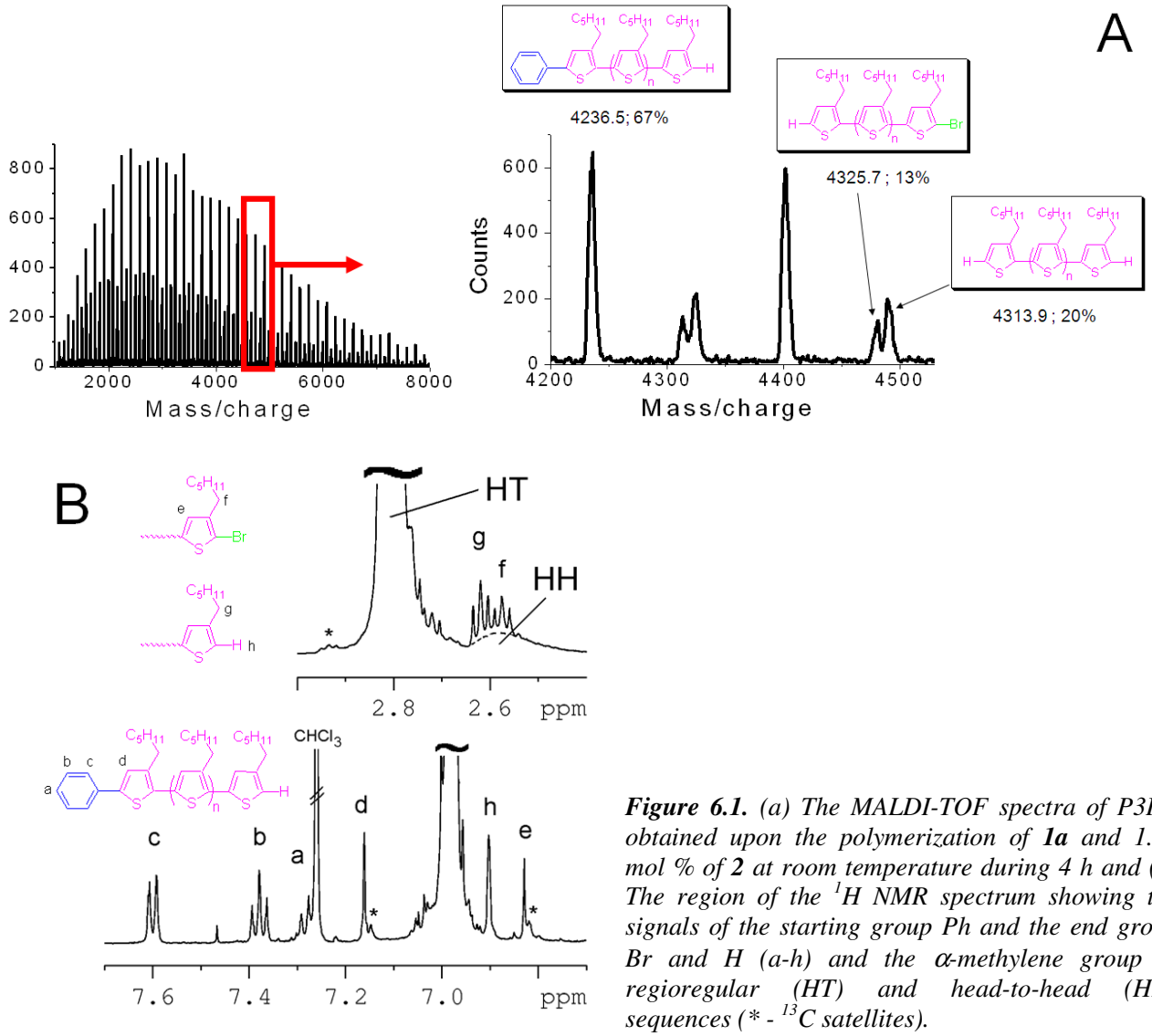

Figure 6.1. *(a) The MALDI-TOF spectra of P3HT obtained upon the polymerization of* ***1a*** *and 1.67 mol % of* ***2*** *at room temperature during 4 h and (b) The region of the ^1H NMR spectrum showing the signals of the starting group Ph and the end group Br and H (a-h) and the α-methylene group of regioregular (HT) and head-to-head (HH) sequences (* - ^{13}C satellites).*

[103] To further prove that the peaks with m/z=(166.28n+1+77) in the MALDI-TOF spectra indeed correspond to Ph/H P3HT, and not to Br/H P3HT with similar m/z values, we used also $(tpp)_2Ni(o\text{-}Tol)Br$, as the initiator instead of $(tpp)_2Ni(Ph)Br$. As expected, the main sets of peaks corresponding to Ar/H and Ar/Br P3HT were shifted on 15 Da.

The data allows the conclusion that the polycondensation starts from the initiator **2** and involves a chain-growth mechanism, giving predominantly Ph/H terminated P3HT upon hydrolysis of the C-Ni bond of the ***intermediate 2***. This reaction, however, is not as perfect as the "near living" Ni(dppp)Cl_2–catalyzed polymerization and a significant fraction of the growing chains terminates before the complete conversion of the monomer, resulting into Ph/Br terminated P3HT. The presence of a bromine group at the polymer end is an indicator of a chain transfer termination step. In this case, the Ni-catalyst undergo *inter*molecular transfer instead of *intra*molecular one, leaving the C-Br end bond intact. Obviously, H/H terminated P3HT is a result of a newly initiated polymerization, catalyzed by the "escaped" Ni-catalyst[104]. The MALDI-TOF spectrum confirms this assumption by showing that the portion of H/H terminated P3HT is maximal in the low molecular weight P3HT fraction (≈60% of H/H P3HT for M_n ≈1100 g/mol vs.≈15% for M_n ≈6000 g/mol). A relatively high polydispersity (PDI≈1.9) and a lower than expected molecular weight of resulting P3HT corroborated with the imperfect chain-growth polymerization. The number average molecular weight of the polymers can be predicted by the following formula:

$$DP_n = \frac{\Delta[M]_t}{[Ni-catalyst]}$$

6.1.2 LOW TEMPERATURE POLYCONDENSATION

Lowering the temperature from room temperature to 0 °C has a positive effect on the control of the polymerization process.

Fig. 6.2 presents the full 500 MHz ^{1}H NMR spectrum of a moderate molecular weight regioregular poly(3-hexylthiophene) (HT-P3HT). The main absorption signals of HT-P3HT are shown on Tab. 6.1.

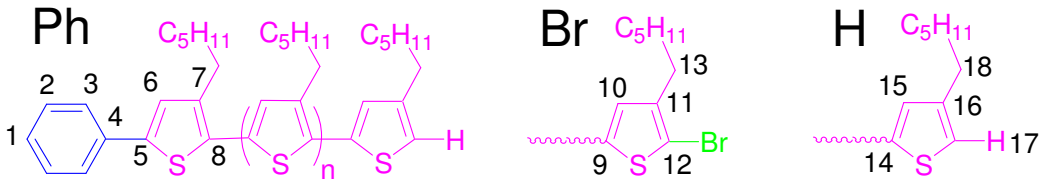

[104] The exact mechanism of the termination reaction remains unclear.

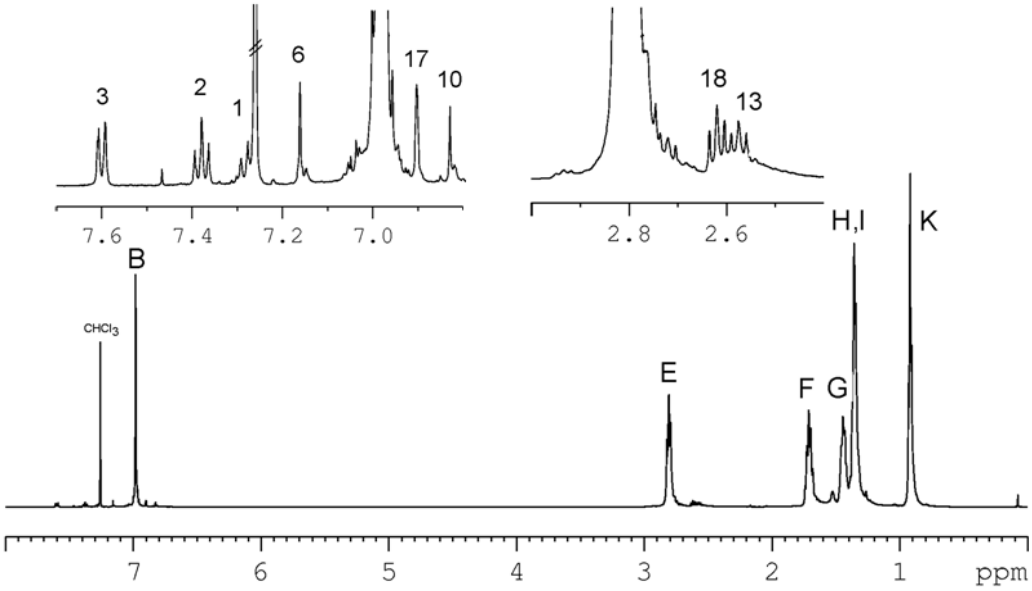

Figure 6.2. *^{1}H NMR spectrum of P3HT grown from bromobenzene initiators and activated with $Ni(tpp)_4$ inserts. The figure shows an enlarged end group signals region.*

Two small triplets at δ ~ 2.6 ppm of the same intensity for H/Br terminated HT-P3HT can be assigned to the methylene protons on the first carbon substituent (18 and 13) on the end units. Furthermore, the appearance of the two separate triplet signals at different resonance frequencies is due to different chemical environments around 18 and 13. The singlets at δ ~ 6.9 and 6.8 ppm correspond to the protons 17 and 10 or 15 of the structure shown in Tab. 6.1. When the H/Br terminated polymer is subject to a magnesium halogen exchange reaction and quenched with an acidic methanol/water mixture, a pristine H/H terminated HT-P3HT is formed. Consequently, the signal generated by the methylene protons 13 is shifted downwards with two groups (18 and 13) resonating at the same frequency. The doublet and triplet peaks at δ ~ 7.6 and 7.4 ppm, marked by 2 and 3 in Fig. 6.2 correspond to the protons in the benzene ring. The four singlets in the aromatic region can be clearly attributed to the protons on the 4-position on the thiophene ring, where each peak results from a different type of trimeric sequence of the HT-HT (δ=6.98), HT-HH (δ=7.00), TT-HT (δ=7.02), and TT-HH (δ=7.05) linked thiophene rings 10 and 15.

The regularity of P3HT is clearly demonstrated in the ^{13}C NMR spectrum (Fig. 6.3).

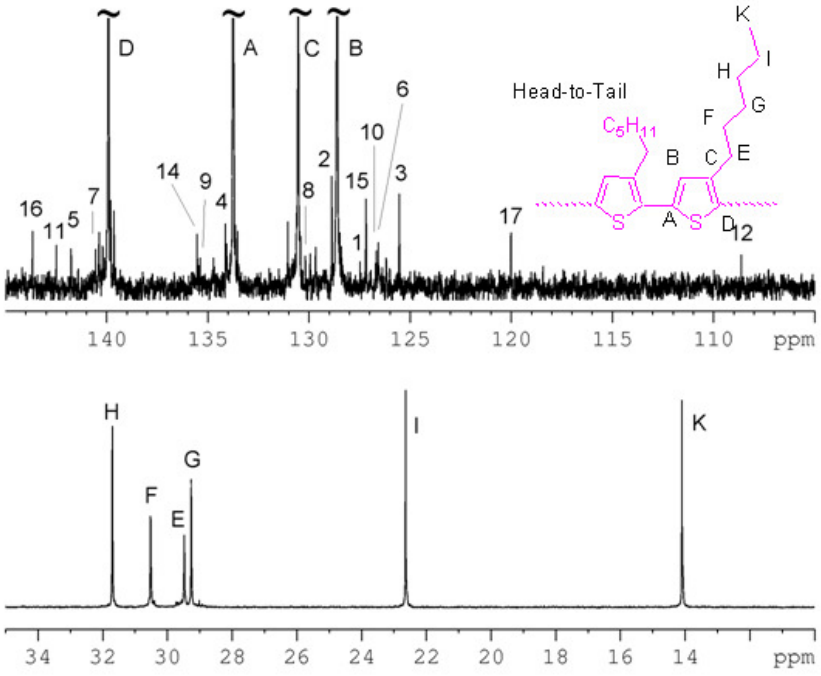

Figure 6.3. *^{13}C NMR spectrum of P3HT grown from a bromobenzene initiator activated with $Ni(tpp)_4$ (solvent: $CDCl_3$).*

Fig. 6.3 shows the full ^{13}C spectrum for our poly(3-hexylthiophene). The alkyl region only shows six absorptions corresponding to the hexyl side chain at 14.9, 23.6, 29.8, 30.3, 30.9, and 32.0 ppm marked as K, I, G, E, F, H.

Fig. 6.3 shows the expanded ^{13}C aromatic region for P3HT. The spectra for P3HT and the entire P3ATs series show only four predominant absorptions attributable to the carbons on one regiochemically defined thiophene ring. Absorptions at 128.5, 130.5, 134.0, and 140.0 are marked as B, C, A, D respectively. They represent the head-to-tail-coupled poly(3-hexylthiophene) structure.

Tab. 6.1 presents the integration values of the ^{1}H NMR (500 MHz) and ^{13}C NMR (125 MHz) spectra of HT-P3HT H/Br and HT-P3HT H/H terminated polymers.

Table 6.1. *Signal assignments for the ^{1}H and ^{13}C spectra of HT P3HT (solvent: $CDCl_3$).*

Ph	δ(^{13}C)	δ(^{1}H)	Br	δ(^{13}C)	δ(^{1}H)	H	δ(^{13}C)	δ(^{1}H)
1	127.5	7.27	9	135.4	-	14	135.5	-
2	128.9	7.38	10	126.6	6.83	15	127.2	6.97
3	125.5	7.60	11	142.5	-	16	143.7	-
4	134.1	-	12	108.6	-	17	120.0	6.90
5	141.75	-	13	29.4	2.58	18	30.5	2.62
6	126.2	7.16						
7	140.5	-						
8	130.2	-						

As it follows from the MALDI-TOF, GPC and NMR data, the molecular weight of the obtained polymer ($M_{n,MALDI}$ =3845 g/mol; PDI_{MALDI} =1.12; $M_{n,GPC}$ =5500 g/mol; PDI_{GPC}=1.44; DP_{NMR} =29; $M_{n,NMR}$ = 4900 g/mol) approaches the theoretical value, which can be predicted assuming a living polymerization mechanism for the given feed ratio ($M_{n,calc.}$ = 4656 g/mol).

According to the MALDI-TOF spectra, the reaction mixture obtained upon polymerization of **1a** in the presence of 3.56 mol % of **3** (feed ratio of 28/1, conversion of **1a** ≈95%) at 0 °C for 6 h contains only traces of P3HT terminated by hydrogen atoms from both sides (2% of H/H P3HT). The main product here is Ph-terminated P3HT (78% of Ph/H P3HT and 20% of Ph/Br P3HT, see Fig. 6.4b).

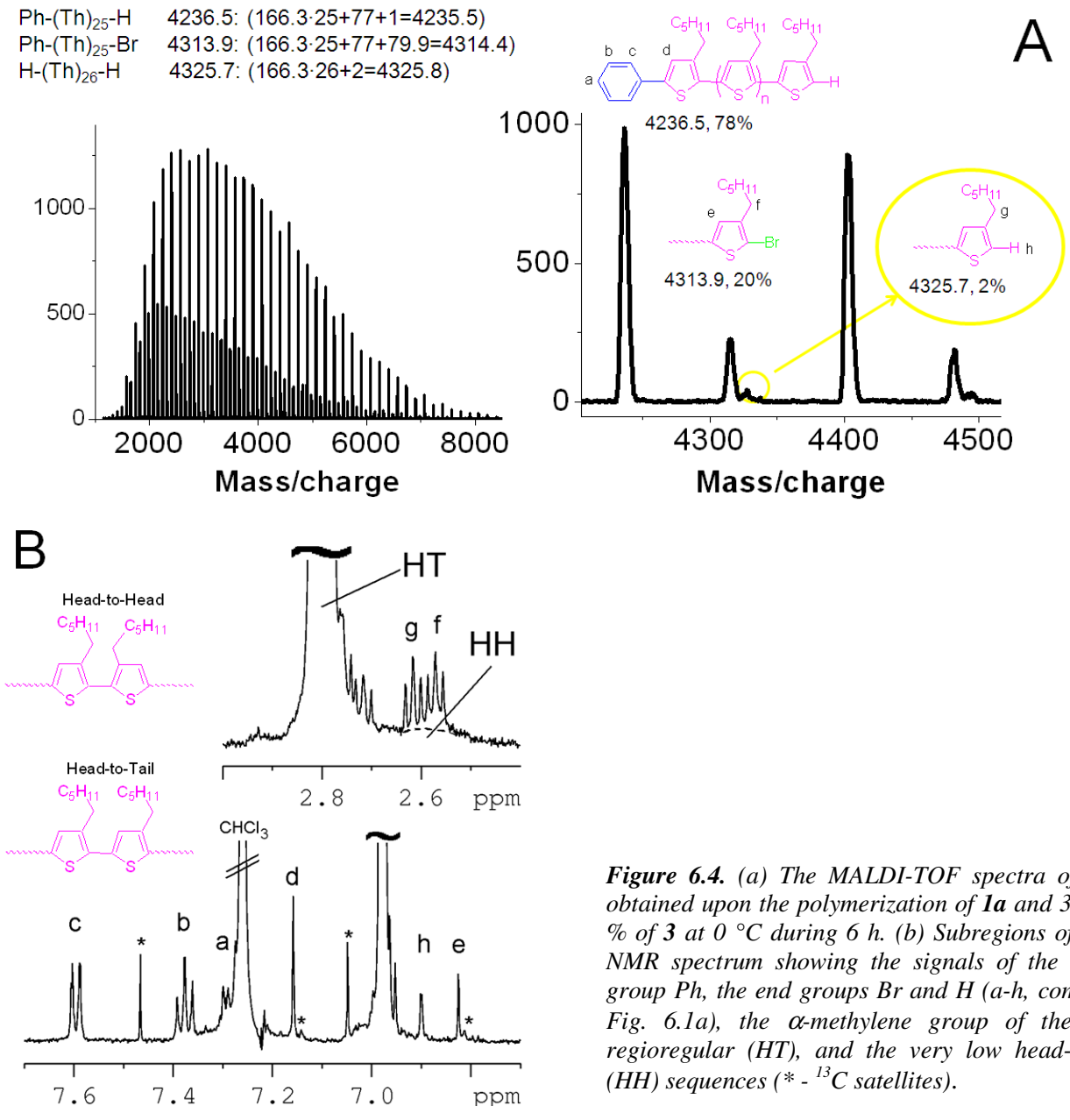

Figure 6.4. *(a) The MALDI-TOF spectra of P3HT obtained upon the polymerization of* ***1a*** *and 3.56 mol % of* ***3*** *at 0 °C during 6 h. (b) Subregions of the ^{1}H NMR spectrum showing the signals of the starting group Ph, the end groups Br and H (a-h, comp. also Fig. 6.1a), the α-methylene group of the major regioregular (HT), and the very low head-to-head (HH) sequences (* - ^{13}C satellites).*

A preliminary kinetic study performed for the polymerization of **1a** initiated by 1.11 mol % of bis(triphenylphosphine)ortho-tolylbromonickel(II), $(tpp)_2Ni(o\text{-}Tol)Br$, **(3)** (feed ratio of 90/1) at 0 °C confirms a chain-growth mechanism (Fig. 6.5). The determination of the monomer conversion rate for different stages of the polymerization was performed by a detailed analysis of the sampled fractions using ^1H NMR. The molecular weight of the P3HT fractions was evaluated by ^1H NMR and GPC. A slight deviation of the molecular weight vs. monomer conversion plot from the typical for living polymerization indicates the occurrence of termination reactions (Fig. 6.5b).

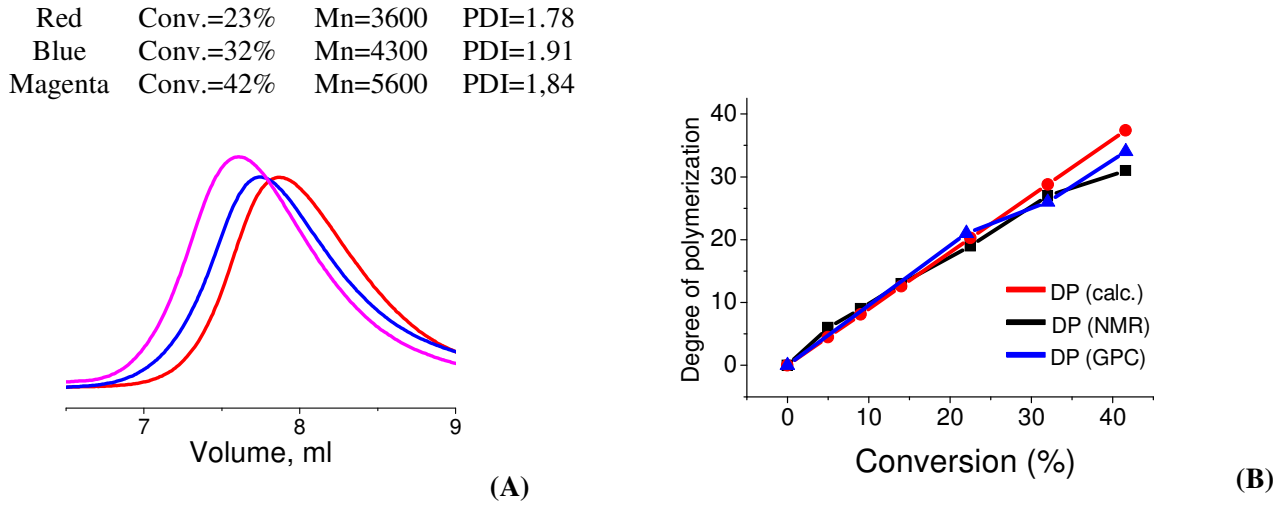

Figure 6.5. *(a) GPC traces for polymerization of* ***1a*** *in the presence of 1.11 mol % of* $(tpp)_2Ni(o\text{-}Tol)Br$ ***(3)*** *at 0 °C. (b) The dependence of DP on conversion for the same experiment: (red) – theoretical dependence for an ideal living polymerization for the giving feed ratio; (blue) – the dependence from GPC data; (black) – the dependence from* ^1H *NMR data.*

6.1.3 REGULARITY

To our surprise, a relatively high HT-regularity of 91-95% was found for the resulting P3HT obtained at room-temperature polycondensation of pure isomer **1a** initiated by **2** (Fig. 6.1). Furthermore, a decrease of the polymerization temperature to 0 °C results in an increase of the HT-regularity up to nearly 100% (Fig. 6.4). This result demonstrates that $Ni(tpp)_4$ and $Ni(dppp)Cl_2$-based catalysts behave similarly at low temperatures inducing polycondensation of the monomers without their isomerization. The difference, however, is in the reactivity of $Ni(tpp)_4$- and $Ni(dppp)Cl_2$-based intermediates. As demonstrated earlier, $Ni(dppp)Cl_2$ complexes differentiate the isomeric monomers **1a** and **1a',** selectively involving the isomer **1a** into the polymerization. In contrast, $Ni(tpp)_4$–based initiators are less selective and yield fully regular HT-P3HT only from pure **1a**. A $(tpp)_2Ni(o\text{-}Tol)Br$ mediated room temperature polycondensation of the mixture of isomers **1a** (75%) and **1a'** (25%),

obtained from dibromide-3-hexylthiophene, leads to P3HT with a HT-regularity of ≈70%. A decrease of the polymerization temperature to 0 °C, however, enhances the HT-regularity up to 85% due to a preferential consumption of the **1a** monomers.

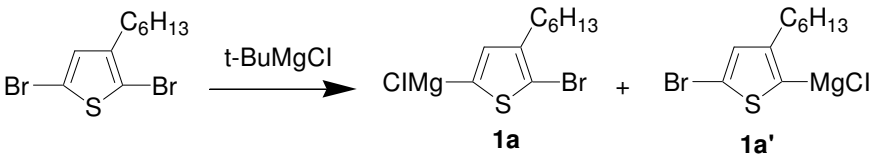

6.1.4 INITIATION BY (TPP)$_2$NI(PH)I CATALYST

In order to extend a range of aryl compounds that can be used for initiated polycondensation in the synthesis of P3HT, a (tpp)$_2$Ni(Ph)I **(4)** initiator was prepared from iodbenzene and Ni(tpp)$_4$. It was found that iodbenzene reacts much faster with Ni(tpp)$_4$ than bromobenzene, resulting into (tpp)$_2$Ni(Ph)I in one hour at room temperature. However, its reaction with the monomer **1a** proceeds slower than one induced by (tpp)$_2$Ni(Ph)Br **(3)** and the resulting P3HT is forming with lower yield. Fig. 6.6 compares polymerizations induced by (tpp)$_2$Ni(Ph)Br and (tpp)$_2$Ni(Ph)I. The MALDI spectrum shows that 95% of the polymer initiated by (tpp)$_2$Ni(Ph)I has a Ph-termination (see Appendix).

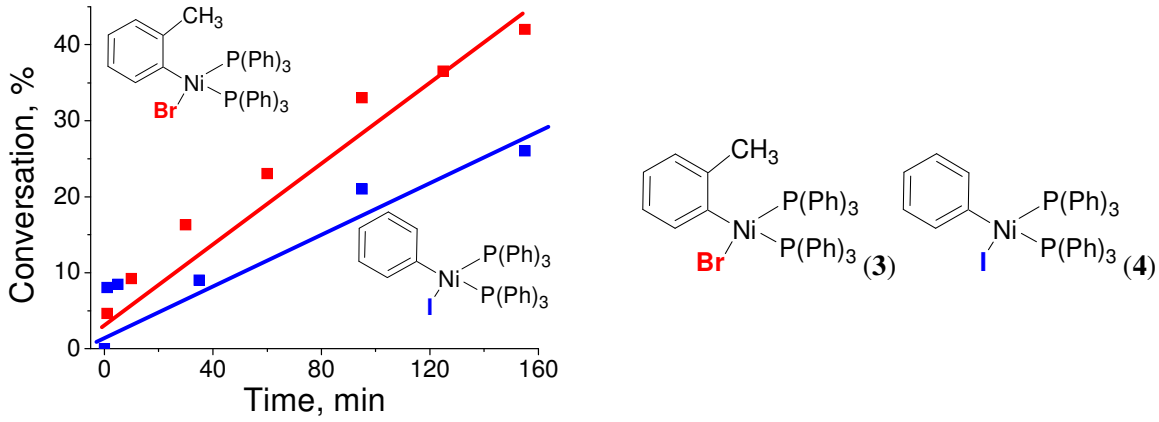

Figure 6.6. *Conversion vs. time plot for* ***1a*** *polymerization started from Ni-complex with Bromine-Toluene (**3**)(red) and from a Ni-complex with Iodide-Benzene (**4**) (blue).*

6.1.5 SYNTHESIS OF POLY(3-ALKYLTHIOPHENES) VIA A NI-INITIATOR CATALYST

An example, (tpp)$_2$Ni(*o*-Tol)Br-induced polymerization into poly(3-dodecylthiophene) was investigated. This polymerization was found to be relatively fast and very efficient, yielding almost 90% conversion of fully regioregular P3DT in 3 hours at 0 °C temperature. The molecular weight vs.

conversion plot (Fig. 6.7) shows an increase of molecular weight with conversion, which strongly supports the chain-growth polymerization mechanism. It is interesting to note that the polymerization into P3DT gives higher molar mass of the polymer and proceeds cleaner than the polymerization into P3HT as a result of higher solubility of the former polymer. The ^{1}H NMR spectrum of the resulting P3DT is given in the Appendix. GPC shows a narrow polydispersity index of ≈1.7.

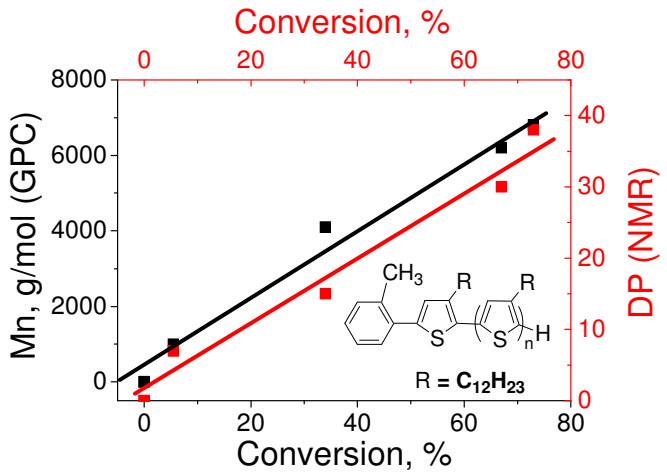

Figure 6.7. *Conversion of monomer concentration vs. Mn (GPC) and DP (^{1}H NMR) of P3DT.*

6.2 CONCLUSIONS-1

We can conclude that the Ni(tpp)$_4$-based initiators constitute a good compromise between reactivity and selectivity in the polycondensation reactions of thiophenes. Due to the high reactivity of Ni(tpp)$_4$, various Ni initiators can be prepared from easily available arylhalides. At the same time, the reduced selectivity of the Ni(tpp)$_4$-based intermediates resulting from enhanced mobility of its ligands can be efficiently compensated and undesired termination reactions can be suppressed by lowering the polymerization temperature and employing pure monomers. In that case, the polycondensation involves the chain-growth mechanism and leads to fully regioregular P3ATs. This is a good starting point to employ the process for the preparation of P3AT brushes.

6.3 POLY(3-HEXYLTHIOPHENE) (P3HT) BRUSHES

In the next step we explored the possibility to prepare P3HT brushes via surface-initiated polycondensation of **1a** from surface-immobilized macroinitiators. To enhance the adhesion of PS-Br to the substrate, 2 nm thick poly(glycidylmethacrylate) (PGMA) films were spin-coated onto freshly cleaned Si-wafers or glass slides and then annealed. PS-Br was deposited afterwards by spin-coating

the solution from $CHCl_3$. Finally, PS-Br layers were cross-linked by irradiation with UV-light, extensively rinsed with THF and dried. We found that a thickness of at least 30 nm of the PGMA/PS-Br anchoring layer is required to achieve stability under the polymerization conditions. The samples were placed into a round-bottomed flask under argon atmosphere, $Ni(tpp)_4$ solution was added and the samples were allowed to react overnight at room temperature. The samples were then extensively washed with THF to remove the excess of unreacted $Ni(tpp)_4$. Afterwards the solution of the monomer **1a** in dry THF was added and the samples were allowed to polymerize at 0 °C (Scheme 6.3).

Scheme 6.3. *The grafting of the P3HT brush from cross-linked PS-Br/PGMA anchoring layer.*

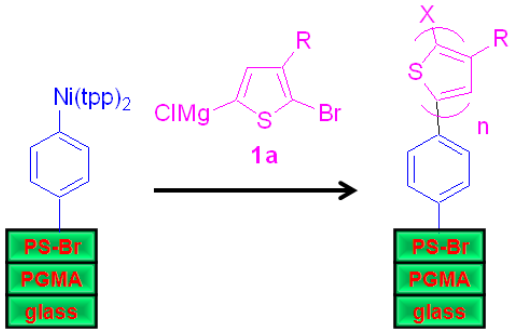

It is important to note that the polymerization proceeds selectively from the immobilized initiator and not in the bulk solution. The procedure results in smooth, uniform and strongly adherent P3HT films, which pass a peel-test with Scotch tape and remain intact upon extensive rinsing with various organic solvents in ultrasonic bath and Soxhlet apparatus. The thicknesses of the resulting P3HT brushes grown from 30-40 nm thick PGMA/PS-Br anchoring layers was typically between 40 nm to 90 nm depending on the polymerization conditions. The violet color of the P3HT films grown on the glass slide in a dry state is similar to the color of commercial HT P3HT deposited by spin coating (Fig. 6.8).

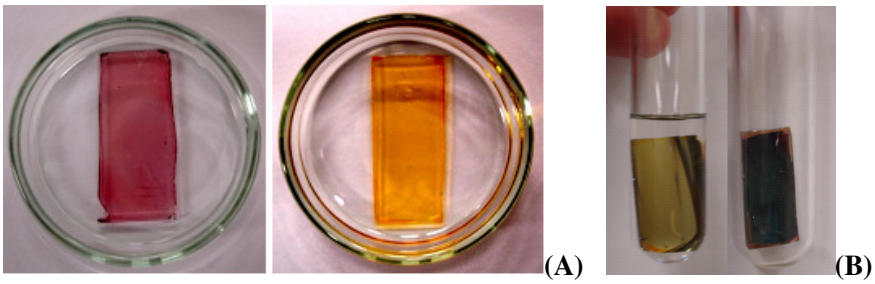

Figure 6.8. *Photographs of the 150 nm thick PS-Br-graft-P3HT brush film: (a) on top of glass slide in dry state (red) and in chloroform (yellow), (b) on top of Si-wafer in chloroform (yellow) and in dry state.*

This is an indication of regioregularity and high molecular weight of the grafted HT P3HT. The brushes grafted to glass slides display solvatochromism and thermochromism similar to the dissolved

P3ATs. P3HT brushes change their color from yellow being placed in chloroform, which is a "good solvent" for P3HT ($\lambda_{max.}$ =442 nm), to violet ($\lambda_{max.}$ =515 nm) in the dry state or in methanol (a "bad solvent") (see Fig. 6.8).

The observed red shift, the appearance of an absorbsion peak at $\lambda_{max.}$ = 504 nm, and the shoulders at λ = 550 nm and 600 nm in the UV-vis. spectrum are due to a transition from less conjugated (twisted) to more conjugated (planar) conformations. This is an usual phenomenon for regioregular HT P3ATs. The fluorescence was excited at the wavelength of maximum absorbance. Fluorescence was relatively strong and the fluorescence of the P3HT brush peaked at 630 nm (Fig. 6.9).

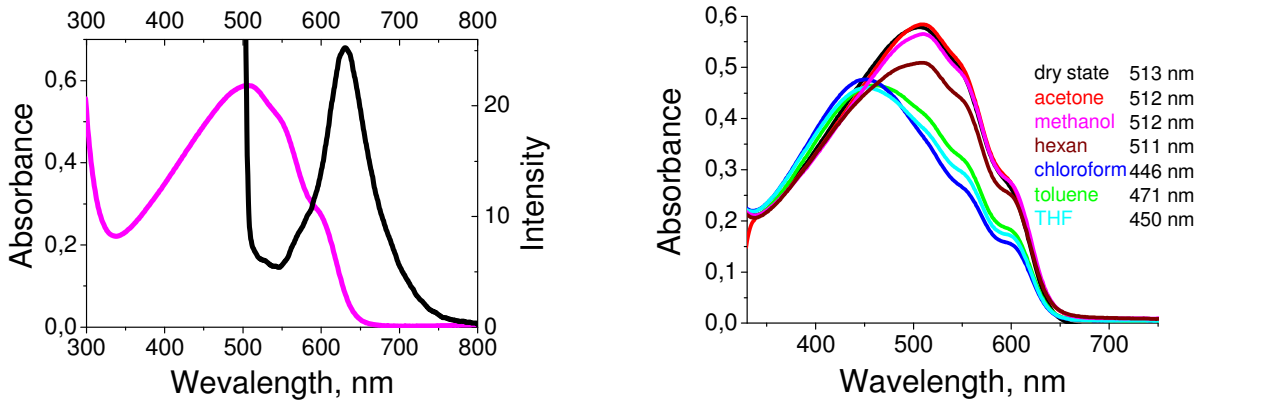

(A) **(B)**

Figure 6.9. *(a) Absorption and fluorescence intensity of the 150 nm thick PS-Br-graft-P3HT brush film and (b) absorption changes of the 150 nm thick PS-Br-graft-PHT brush film in different solvents.*

The UV-vis. spectra of the grafted HT P3HT recorded in different solvents reveal their solvatochromism that could in principle be used for the construction of regenerable sensors with immobilized active layers. It is also interesting to note, that although "good" solvents (THF, toluene and $CHCl_3$) derive an important blue shift of the $\lambda_{max.}$, some shoulders at 500-600 nm still remain. This reflects a significant aggregation and/or planarization of tethered P3HT chains that occur even in "good" solvents and might be due to decreased entropy of the grafted chains.

The swelling behavior of P3HT brushes was studied with the aid of AFM. Fig. 6.10 shows AFM images of the scratched area of the 65 nm P3HT brush grown from a 35 nm thick film of PGMA/PS-Br in both the dry state and in xylene vapors (a "good" solvent for P3HT and PS-Br). As the cross-sections show, the film thickness increases from 100 nm in the dry state to 160 nm in saturated xylene atmosphere.

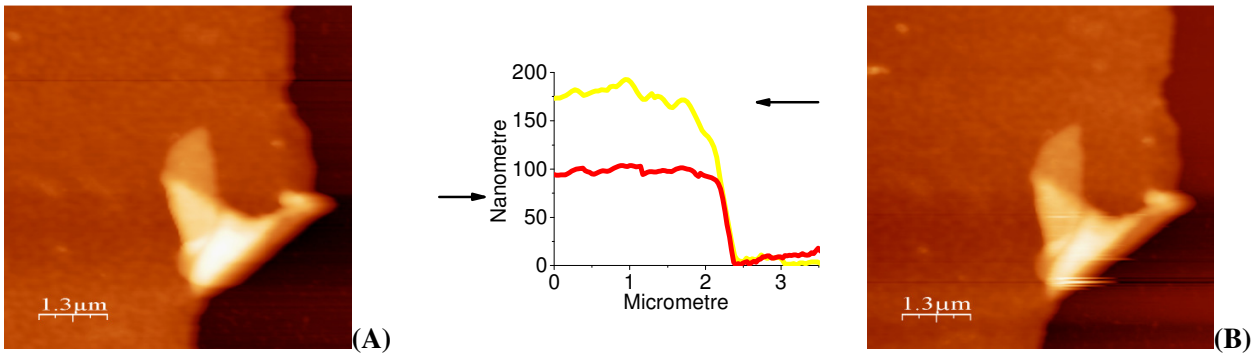

Figure 6.10. *AFM topography images and cross-sections of the scratched area of the 100 nm thick PS-Br-graft-P3HT brush film: (a) in dry state and (b) in xylene vapor.*

Fig. 6.11 shows the swelling process of P3HT brushes in xylene vapors versus time. The surface morphology of the film becomes more indistinct, indicating that the solvent enter deeply into the brush structure.

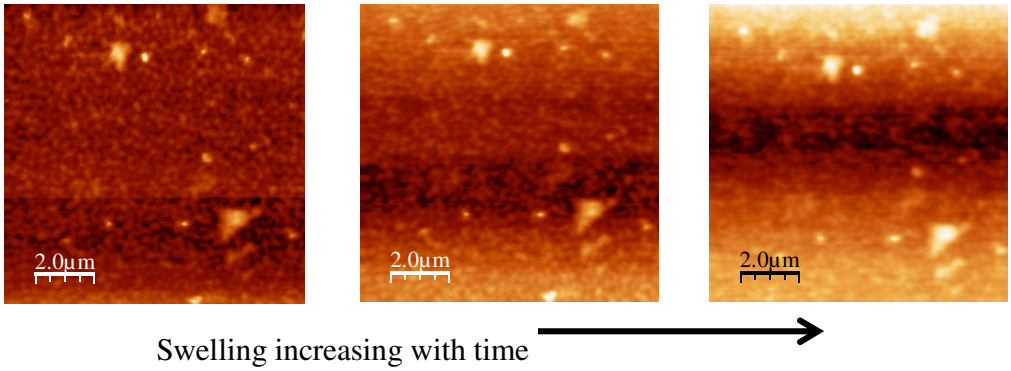

Figure 6.11. *AFM topography images of the 100 nm thick PS-Br-graft-P3HT brush film during the swelling process in xylene vapors.*

Similar swelling experiments were also performed for a film started from a 35 nm thick PGMA/PS-Br anchoring layer. This film swells in xylene to 40 nm (from 20 nm to 55 nm, AFM data not shown).

Assuming that the swellability of the anchoring PGMA/PS-Br layer inside the composite PGMA/PS-Br/P3HT film is about the same as for PGMA/PS-Br alone, the contribution of the P3HT component to the overall swelling of the PGMA/PS-Br/P3HT film is only 40 nm (60 nm–20 nm). This relatively low swellability of the P3HT brush (from 65 nm to 105 nm) can be explained by a relatively high rigidity of the polythiophene backbone or/and a high grafting density of the brush. From the thickness of the swollen brush (105 nm) and knowing the length of the thiophene monomer unit (0.38 nm) the DP of the grafted P3HT chains can be estimated to be at least 276.

Careful inspection of the P3HT brushes by tapping mode AFM revealed their lamellar morphology (Fig. 6.12), although the starting PGMA/PS-Br anchoring layers display a featureless morphology. Similar lamellae structures were previously observed for the films of regioregular HT P3HT prepared by a solvent casting method[105,106].

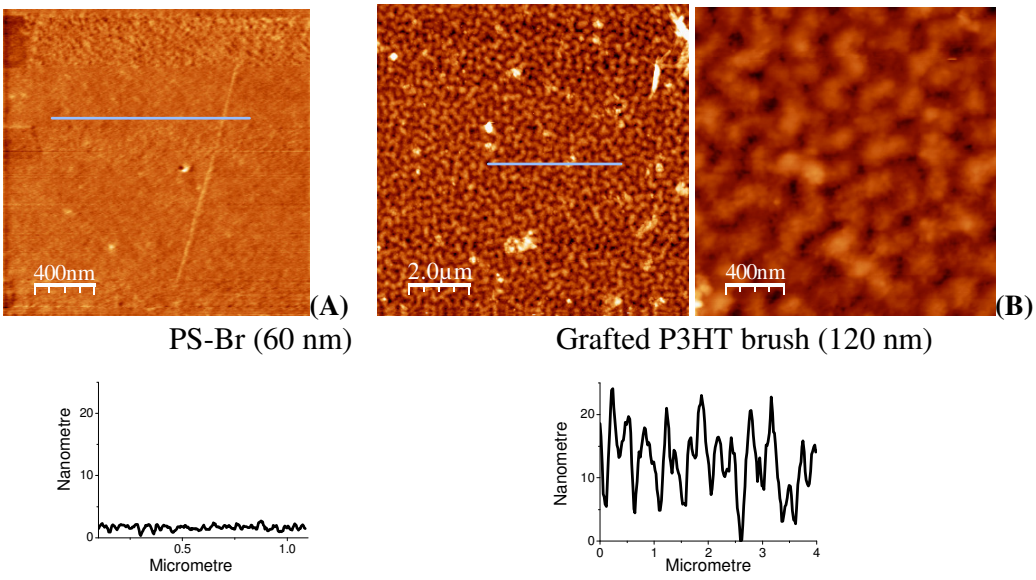

Figure 6.12. *AFM topography images and the cross-section of: (a) smooth cross-linked PS-Br layer on the top of coated PGMA layer onto Si-wafer and (b) grafted P3HT brush from cross-linked PS-Br layer.*

Previously, microphase separation was observed in *bicomponent* polymer brushes due to incompatibility of the polymers composing the brush, whereas monocomponent brushes usually displayed featureless morphologies[10]. The observed structuring of the *monocomponent* P3HT brushes found here might be explained by an amphiphilic nature of P3HT and by a strong tendency of polythiophenes to form rod-like semicrystalline aggregates due to π-staking interactions[105,106].

A series of polymer brushes grafted from cross-linked PS-Br layers were prepared with different alkyl substitutions in the thiophene ring. The UV-vis. spectra of the P3HT, P3OT and P3DT in the solid state show the vibrational structure with well-defined $\lambda_{max.}$ at 470 nm for P3DT and at 510 nm for the P3OT and P3HT brushes (Fig. 6.13). The AFM images of all P3ATs show a similar lamellar morphology (Fig. 6.14)[107].

[105] Kiriy, N.; Jähne, E.; Adler, H.–J.; Schneider, M.; Kiriy, A.; Gorodyska, G.; Minko, S., Jehnichen, D.; Simon, P.; Fokin, A. A.; Stamm, M., *Nano Lett.,* **2003**, 3, 707-712.

[106] Zhang, R.; Li, B.; Iovu, M. C.; Jeffries-El, M.; Sauve, G.; Cooper, J.; Jia, S.; Tristram-Nagle, S.; Smilgies, D.M.; Lambeth, D.N.; McCullough, R.D.; Kowalewski, T., *J. Am. Chem. Soc.,* **2006**, 128, 3480-3481.

[107] Segalman, R.A., *Materials Science and Engineering,* R 48, **2005**, 48, 191–226.

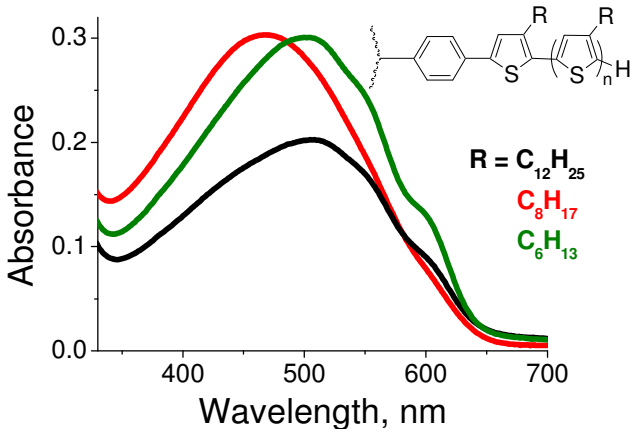

Figure 6.13. *UV-vis. spectra of the PS-Br-graft-P3DT brush film (black), PS-Br-graft-P3OT brush film (red) and PS-Br-graft-P3HT brush film (green) on glass substrate.*

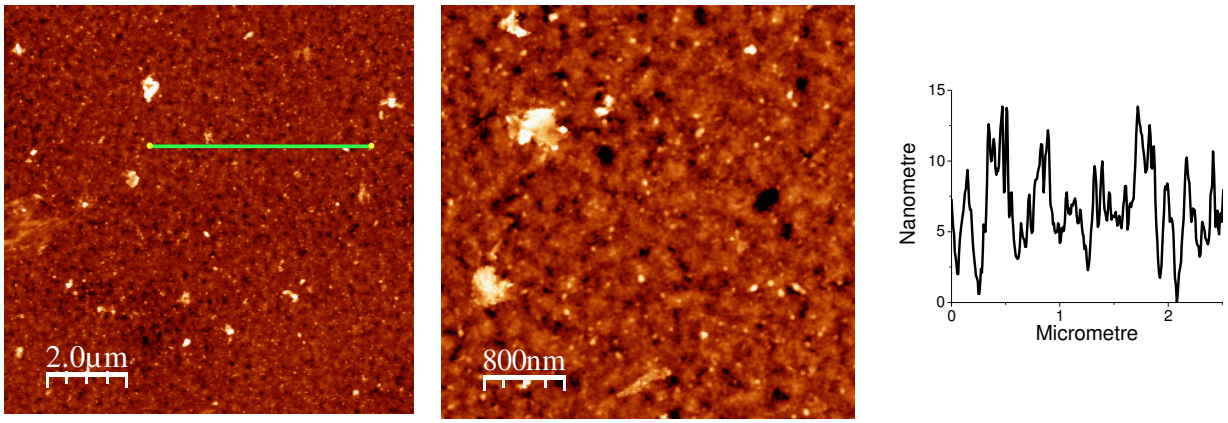

Figure 6.14. *AFM topography images and cross-section of P3ATs brushes.*

6.3.1 ELECTROCHEMICAL STUDY

Cyclic voltammetry is the simplest experimental tool to estimate the oxidative and reduction potentials and to calculate the values of the highest occupied molecular orbital (HOMO), the lowest unoccupied molecular orbital (LUMO) and the band gaps. The band gap of grafted P3HT was determined from the first voltammetric cycle in freshly prepared solutions in CH_3CN (0.1M TBAPF6, 0-2 V, scan rate=50mV/s). The cyclic voltammetry results shown in Fig. 6.15, with the HOMO and LUMO levels of the P3HT brush grafted from P4VP-*b*-PS-I copolymer layer coated onto an ITO surface, lead to an estimate of -5.46eV and -3.55eV, respectively. This corresponds to an electrochemical band gap of 1.91eV, which is similar to the optical band gap derived from the onset of optical absorption. Such a band gap is typical for poly(3-alkylthiophene)s[108].

[108] Pang, Y.; Li, X.; Ding, H.; Shi, G.; Jin, L., *Electrochem. Acta,* **2007**, 52, 6172–6177.

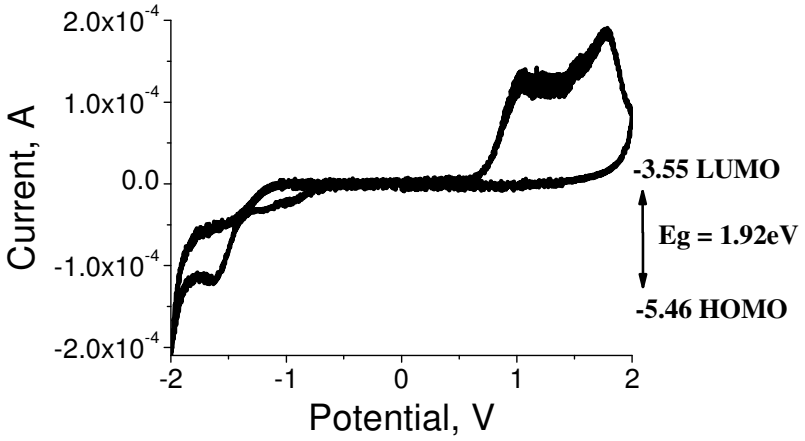

Figure 6.15. *The cycle voltammogram of the P3HT brush grafted from copolymer P4VP-b-PS-I coated on an ITO surface.*

The oxidation potential of the grafted P3HT brush was found to be 0.97V which is higher than the oxidation potential of the regioregular P3HT film with high molecular weight (0.55V) determined by Trznadel *et al.*[109].

6.4 ELECTRICAL MEASUREMENTS

The photo-cross-linked PS-Br films of different thicknesses deposited on flat glass substrates were used to grow PS-Br-*graft*-P3HT film for the electrical measurements according to the procedure described above. Two types of samples were used for electrical measurements. One type of samples was produced on top of glass substrates and used for electrical measurement in a lateral direction with in two point measurement setup (*dc* method). For comparison regioregular P3HT films of the same thicknesses were deposited by spin-coating and their conductivity in the lateral direction was also measured. The other type of samples was prepared on a top of ITO-glass substrates and used for electrical measurement in vertical direction with C-AFM. We a-priori expected that conductivities measured in lateral or vertical directions may result in different values.

6.4.1 REDOX DOPING OF P3HT FILMS WITH FECI3 AND IODINE VAPORS

Since the conjugated polymers in their pristine form do not contain intrinsic charge carriers, they must be provided extrinsically, e.g. by a charge-transfer process, generally called doping. For the

[109] Trznadel, M.; Chauver, O.; Lapkowski, M.; Pron, A., *Synth. Metals*, **1999**, 101, 358.

present investigation, doping of P3HT (a weak base) has been accomplished by using $FeCl_3$ or I_2 (a weak acid, oxidant) involving electron exchange (redox reaction) between the film and the oxidant (Schemes 6.4 and 6.5).

Scheme 6.4. *Schematic representation of cationic chains of P3HT brush – anionic dopant ($FeCl_4^-$) adduct.*

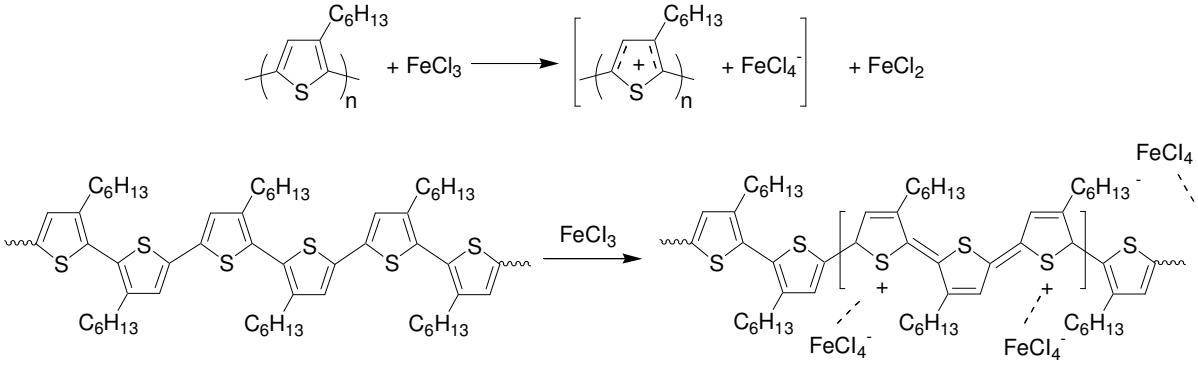

Scheme 6.5. *Schematic representation of cationic chains of P3HT brush – anionic dopant (I_5^-) adduct.*

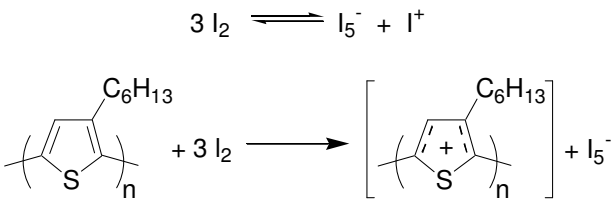

To dope the PS-Br-*graft*-P3HT films and the coated HT P3HT (see experimental part 6.10) films, the samples were dipped into 1M solution of $FeCl_3$ in ethanol for either 15 min. or 12 h. Then the samples were washed with ethanol and dried under nitrogen gas for several minutes and conductive measurements were performed. The doping with iodine was accomplished in the chamber containing iodine vapors for either 15 min. or 12 h. After the doping the conductivity was measured as described below.

The PS-Br-*graft*-P3HT films change their color from magenta to bright green or to greenish-black, if they were doped by $FeCl_3$ during 15 min. or 12 h., respectively (Fig. 6.16). Irrespective to the doping time (15 min. or 12 h.), the coated P3HT films change their color from dark magenta to black violet. The smoothness of the doped films remained intact. The same changes of color for PS-Br-*graft*-P3HT film in iodine vapor was observed. They color was changed from initial magenta of PS-Br-*graft*-P3HT film to dark brown in I_2-doped-PS-Br-*graft*-P3HT film (the photos does not presented). The color change indicates an electron transfer between the π-conjugated P3HT backbone and the dopant and reflects the formation of an organic (charged polymer)–inorganic (dopant ion) adduct. Doping with

I_2 results into change of the color to light-brown and dark-brown for the PS-Br-*graft*-P3HT and P3HT samples, respectively.

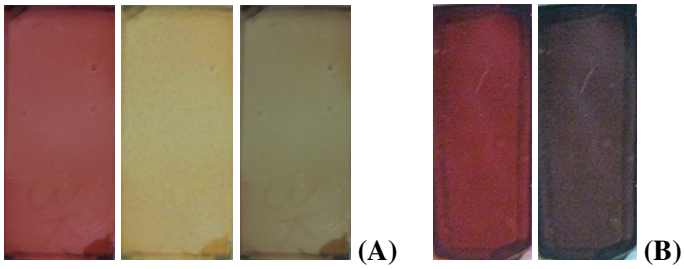

Figure 6.16. *(a) Photographs of the 120 nm thick PS-Br-graft-P3HT films on a glass slide in pristine (magenta) and $FeCl_3$-doped state (bright green (15 min.) and greenish-black(12 h.)). (b) coated HT P3HT film on to a glass slide in pristine (dark magenta) and $FeCl_3$-doped state (black violet).*

The chemical doping of the polymer lead to an important modification of the visible absorption spectrum. Fig. 6.17 shows the resulting UV-vis. spectra depicting the change in the π-π* transition. The intense sharp peaks of the pristine PS-Br-*graft*-P3HT and HT P3HT films at 510 nm were replaced by significantly broader peaks in the doped states, that is characteristic of free carries[110].

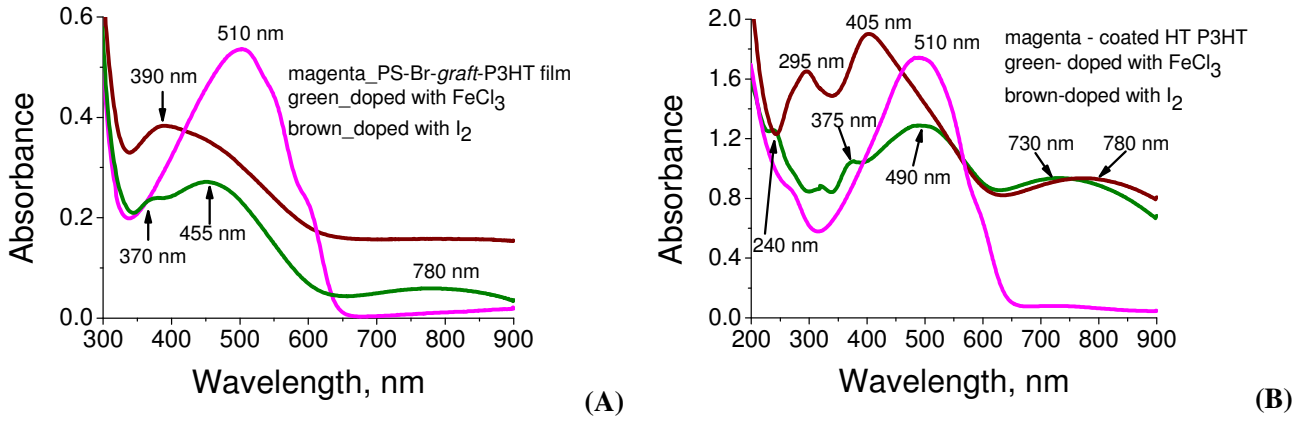

Figure 6.17. *UV-vis. spectra of the PS-Br-graft-P3HT (a) and of the coated HT P3HT (b films before and after doping.*

The small absorption at 370 nm for $FeCl_3$-doped-PS-Br-*graft*-P3HT films and the two peaks at 240 nm and 375 nm for $FeCl_3$-doped HT P3HT films , as well as broader peak in range 730-780 nm is a result of a thiophene - $FeCl_4^-$ ion band.[111] The appeared broad peak at 390 nm for I_2-doped HT-P3HT film and the two small peak at 295 nm and 405 nm and broader peak at 780 nm are all indicated the formation of thiophene - I_5^- ion complex. The intensity of absorption of the grafted P3HT and the

[110] Tourillon, G.; Garnier, F., *J. Phys. Chem.*, **1983**, 87, 2289-2292.
[111] Sandberg, M.; Tanaka, S.; Kaeriyama, K., *Synth. Metals,* **1993**, 57, 3587-3590.

coated P3HT films becomes low due to the formation of the organic–inorganic adduct (Schemes 6.4 and 6.5).

Fig. 6.18 shows the UV-vis. and fluorescence spectra of the PS-Br-*graft*-P3HT films with different thicknesses before and after $FeCl_3$-doping for 12 h. The absorption intensity depends on the thickness of grafted P3HT layer in the PS-Br-*graft*-P3HT films and it gradually decreases as the thickness decreases from 200 nm to 50 nm.

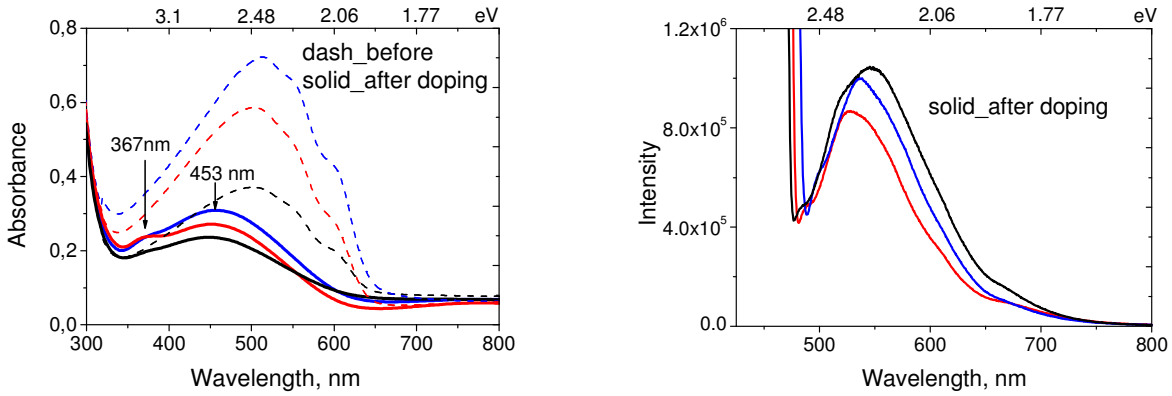

(A) **(B)**

Figure 6.18. *(a) UV-vis. absorption and (b) fluorescence spectra of PS-Br-graft-P3HT films with different thicknesses before and after $FeCl_3$-doping: black lines - 50 nm thick, red lines – 160 nm , blue lines – 200 nm PS-Br-graft-P3HT films.*

6.4.2 MEASUREMENTS IN LATERAL DIRECTION

The measurements in lateral direction were performed as shown in Scheme 6.6.

Scheme 6.6*. Scheme of dc conductivity measurements in lateral direction .*

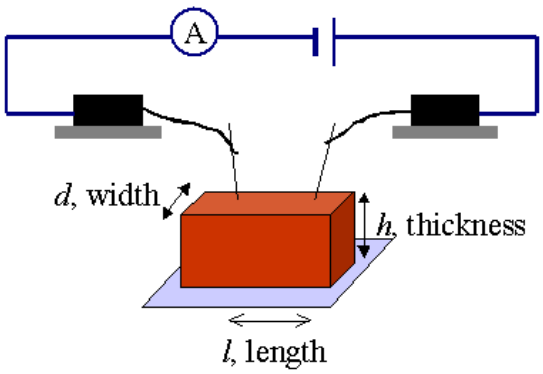

d (width) = 1 cm
h (thickness) = nm
l (length) = 0.4 cm
S (area) = $d \times h$ = cm^2

$$\sigma = \frac{l}{S \cdot R}$$

Tab. 6.2 shows the variation of direct current (*dc)* conductivity of the PS-Br-*graft*-P3HT films with different thicknesses and different time of doping process at room temperature. The resistance of

pristine films was in the order of 10^{12} Ohm, which corresponds to a conductivity in the order of 10^{-8} S/cm. After doping with $FeCl_3$ for 15 min. or 12 h., the resistance dropped to a 10^8 Ohm or 10^7 Ohm, which correspond to the conductivity in the order of 10^{-4} and 10^{-3} S/cm, respectively. Such values are typical for poly(3-alkylthiophenes) film[112,113].

Table 6.2. *The resistance and conductivity of the pristine PS-Br-graft-P3HT film, $FeCl_3$-doped PS-Br-graft-P3HT film and I_2-doped PS-Br-graft-P3HT film in lateral direction.*

Thickness of PS-Br-*graft*-P3HT	Non-doped		Doped with $FeCl_3$			
			15 min.		12 h.	
	R, Ohm	σ, S/cm	R, Ohm	σ, S/cm	R, Ohm	σ, S/cm
50 nm	10^{12}	8.0×10^{-8}	47×10^{8}	0.17×10^{-4}	24×10^{7}	0.33×10^{-3}
160 nm	10^{12}	2.5×10^{-8}	4.0×10^{8}	0.62×10^{-4}	3.9×10^{7}	0.64×10^{-3}
200 nm	10^{12}	2.0×10^{-8}	3.2×10^{8}	0.60×10^{-4}	1.6×10^{7}	1.56×10^{-3}
			Doped with I_2			
160 nm	10^{12}	2.5×10^{-8}	15 min.		12 h.	
			3.75×10^{8}	0.66×10^{-4}	2.96×10^{7}	0.84×10^{-3}

The PS-Br-*graft*-P3HT films doped with iodine vapors for 15 min. or 12 h. show essentially the same conductivity (10^{-3}-10^{-4} S/cm) as the conductivity of the $FeCl_3$-doped samples (Tab. 6.2).

The electrical measurements for the pristine and doped 200 nm thick HT P3HT films deposited on the top of glass substrates were performed for comparison. After the doping of the HT P3HT films, a drastic decrease in its solubility in $CHCl_3$ occurred. The resistance was found to be 2×10^6 Ohm that corresponds to the conductivity of 0.01 S/cm (Tab. 6.3).

Table. 6.3. *The resistance and conductivity of the pristine and doped HT-P3HT films.*

Thickness of coated film	Non-doped		Doped with $FeCl_3$ (12 h.)	
	R, Ohm	σ, S/cm	R, Ohm	σ, S/cm
200 nm	10^{12}	$\times10^{-8}$	2×10^{6}	0.01
			Doped with I_2 (12 h.)	
			1.3×10^{5}	0.15

As a conclusion, it was found that the conductivity of PS-Br-*graft*-P3HT films is greater for the samples doped longer (12 h. vs. 15 min.). The maximum conductivity of ~1.5×10^{-3} S/cm is obtained for the PS-Br-*graft*-P3HT sample with thickness of 200 nm after 12 h. of doping. The conductivity of the coated HT P3HT films is one order of magnitude higher than the conductivity of the PS-Br-*graft*-P3HT

[112] Singh, R.K.; Kumar, J.; Singh, R.; Kant, R.; Rastogi, R.C.; Chand, S.; Kumar, V., *New J. Phys.*, **2006**, 8, 112.
[113] Kumar, J.; Singh, R.K.; Chand, S.; Kumar, V.; Rastogi, R.C.; Singh, R., *J. Phys. D: Appl. Phys.*, **2006**, 39, 196–202.

films. It can be explained by the existence of the isolating PS-Br layer in the structure of the PS-Br-*graft*-P3HT films. The absorption of films dramatically changes after the doping.

6.4.3 CONDUCTIVITY MEASUREMENTS IN VERTICAL DIRECTION

It was shown above that the PS-Br-*graft*-P3HT films display rather good lateral direct current (*dc*) conductivity in their doped state (~1.5×10^{-3} S/cm). To probe the local vertical conductivity of the films, we have performed C-AFM measurements in tapping and contact mode.

In tapping mode of C-AFM, a conductive tip is scanned across the sample surface using a fixed tip-sample interaction force as a feedback parameter to generate a sample topography. Simultaneously, a voltage is applied across tip and sample to generate a map of the corresponding electrical current response[114,115]. The Pt/Ir alloy coated tip was used in C-AFM.

Furthermore, C-AFM was used for current-voltage characteristic in contact mode. The information made available by electrical current imaging gives insights into the characteristics of the thin film. Of particular interest are the structures of conducting and non-conducting regions. The 160 nm thick PS-Br-*graft*-P3HT film on the ITO coated glass was grown for the C-AFM measurements from 60 nm thick photo-cross-linked PS-Br according to the procedure described above.

Fig. 6.19a displays a typical height image of the 160 nm PS-Br-*graft*-P3HT film under 2.6V bias. The morphology of the P3HT brush surface has been measured with a RMS of the surface roughness to be of 20 nm. The corresponding current image (Fig. 6.19b) at 2.6 V shows patches of conductivity (white spaces) surrounded by low-conductive regions (dark spaces) with a RMS of current inhomogeneity of 6 pA.

The *I-V* characteristics of the sample was performed in C-AFM using the contact mode. Conductive atomic force microscope (C-AFM) was used to study the current on a conductive polymer sample with optimal loading force[116,117]. The optimal loading force was found to be of 16.25 nN (spring constant of cantilever is 0.2N/m for contact mode), as described in the Appendix. The load force was maintained to avoid damage to the tip and the sample, and to produce the optimal current-voltage characteristic. During the measurement, the electrical current sensed by the C-AFM is monitored while performing a standard force displacement ramping cycle.

[114] Wu, C.-C.; Chang, S.-S., *J. Phys. Chem. B,* **2005**, 109, 825-832.
[115] Li, J.K.; Zou, S.; Rider, D.A.; Manners, I.; Walker, G.C., *Adv. Mater.* **2008**, 9999, 1–5.
[116] Rong, W.; Pelling, A.E.; Ryan, A.; Gimzewski, J.K.; Friedlander, S.K., *Nano Lett.,* **2004**, 4, 11, 2287-2292.
[117] Manual description about Conductive AFM.

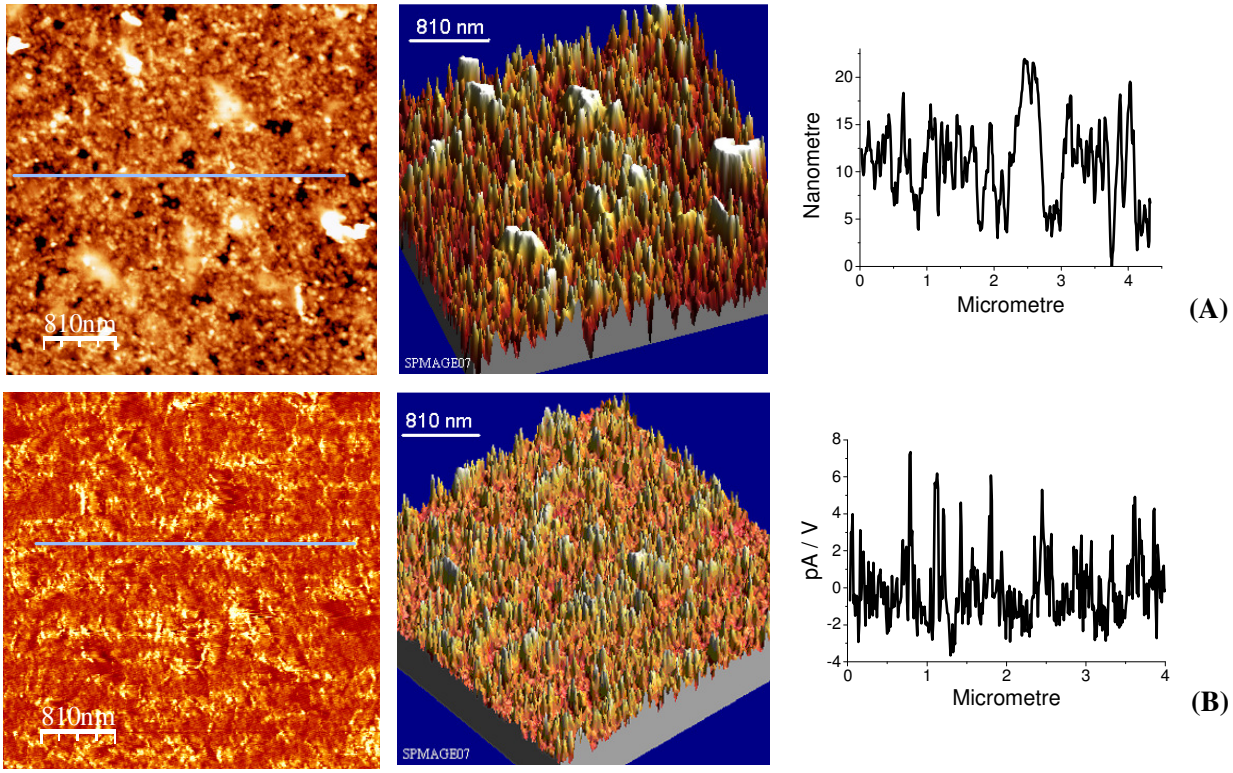

Figure 6.19. *4× 4 μm (a) topography of height and (b) C-AFM current images of the 160 nm thick of PS-Br-graft-P3HT film grown from cross-linked 60 nm thick PS-Br film deposited on an ITO glass surface. The applied voltage was 2.6V.*

The C-AFM measurements were performed for the pristine film and for the $FeCl_3$-doped films. The doping of sample was done in solution of $FeCl_3$ (1M) for 15 min. The electrical characteristic of the pristine and the doped films were investigated by recording the tip current (*I*) as a function of the bias voltage (*V*). To obtain the vertical *I-V* characteristics of the PS-Br-*graft*-P3HT film, the C-AFM measurements were performed in contact mode with a preset pressure between the tip and the sample. The current was continuously measured as a function of voltage (*V*), which was scanned from 1V to 7V for the pristine films, and from 0V to 5V for the doped films. The measurements were performed several times for at least 7 different points for each of the sample investigated to obtain representative data. The results are shown in Fig. 6.20.

The *I-V* curves for the PS-Br-*graft*-P3HT films exhibit semiconductive characteristics[108,109,118]. I conclude that the current at voltage from 1V to 5V is predominantly determined by the tip-polymer junction conductivity and polymer properties, while in the range from 5V to 7V the current follows the thin film conductivity. The sample resistance was thus derived by linear interpolation from the *I-V*-

[118] Xu, B.Q.; Li,X.L.; Xiao, X.Y.; Sakaguchi, H.; Tao, N.J., *Nano Lett.,* **2005**,5, 1491-1495.

curve from 5V to 7V. The changes of resistance observed after $FeCl_3$-doping of the sample are presented in Fig. 6.20b.

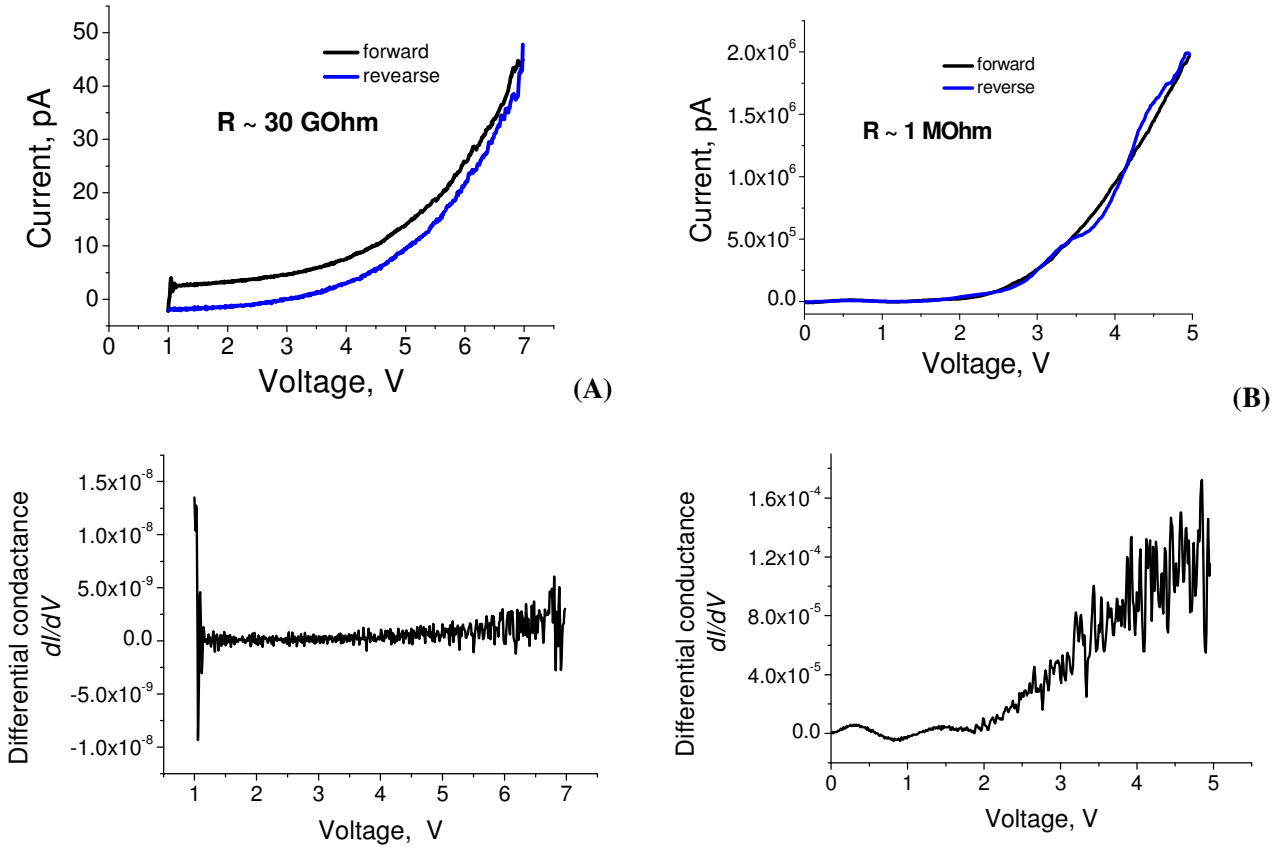

Figure 6.20. *Representative I-V characteristics collected by C-AFM for 160 nm thick PS-Br-graft-P3HT film atop an ITO coated glass substrate (a) before) and (b) after doping with $FeCl_3$. The spectra were recorded while ramping the bias from the start voltage (1V) to the end voltage (7V) forward, and then back for the film, and from the start voltage 0V to the end voltage 5V for the doped film and then back. The lower plots show the dependence of differential conductance vs. voltage.*

Fig. 6.20a shows a relatively high resistance *R* (~30 GOhm) of the 160 nm thick PS-Br-*graft*-P3HT film atop the ITO coated glass substrate as the bias voltage ramped from 1V to 7V. However, Fig. 6.20b shows that the *R* value drops five orders of magnitude after the doping (*R*~1 MOhm, with $FeCl_3$ dopant) over the range of bias voltage from 0V to 5V. These results clearly can be seen in the lower graphics showing the dependence of the differential conductance on voltage for the pristine film and the doped films. The spectra show an exponential dependence of the current from the applied bias voltage. Fig. 6.20 also shows that the conductivity of the PS-Br-*graft*-P3HT film is very low; consequently, no current flow was detected at bias voltages smaller than 5V. Doping of the PS-Br-*graft*-P3HT film with $FeCl_3$, leads to a higher conductivity. The *I-V* curve of the doped film exhibits semiconductor-like characteristic. The conductivity, σ, was roughly estimated by modeling the contact

between tip and the sample area (*S*) by the size of the tip ($S=\pi R^2$, where R is radius of the tip ~35 nm). The sample resistance was estimated from the inverse slope of the *I-V* curve. Where the *I-V* curve was not linear, the slope of the curve was estimated using a linear fit to the curve. Thus, the resistances of the film in the pristine and in the doped states were found to be of the order of 10^{10} and 10^{6}, respectively. The corresponding conductivities were found to be ~10^{-5} and ~10^{-1}-10^{-2} S/cm, which is higher than to the lateral conductivities found for these samples (the table of results present in Appendix (Tab. 1-2)).

Measurements of the conductivity of the freshly cleaned ITO glass and of the photo-cross-linked 60 nm thick photo cross-linked PS-Br film reference samples were performed for comparison (Fig. 6.21). As expected for a good conductor, the ITO-coated glass displays an Ohmic *I-V* characteristic with a large current response when voltage was applied. It shows the lowest resistance (*R*) among the samples (Fig. 6.21a). In contrast, the PS-Br film demonstrated an insulator characteristic. The current response of the PS-Br curve was flat and remained at zero over the entire voltage range (Fig. 6.21b).

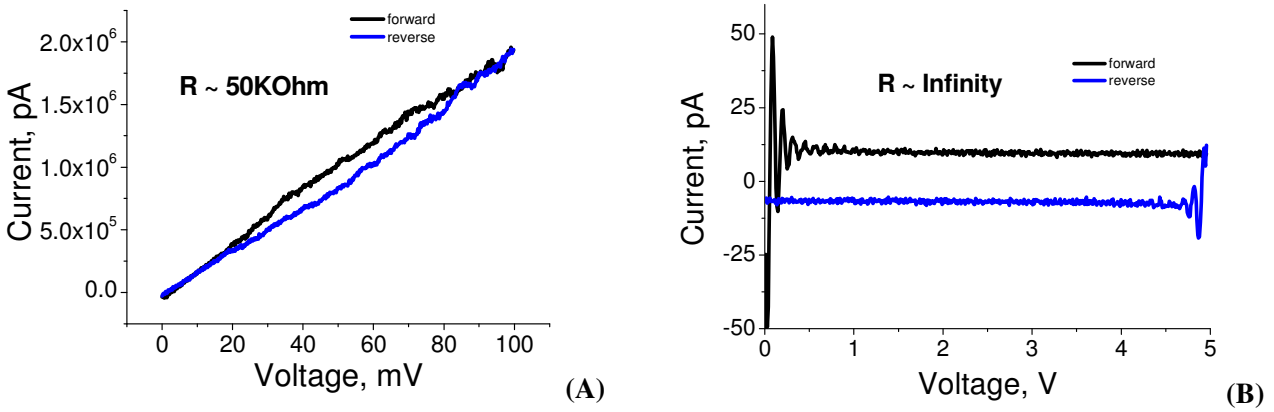

Figure 6.21. *I-V dependence of ITO substrate and 60 nm thick PS-Br film coated atop the ITO substrate as reference sample measured by C-AFM. The spectra were recorded while ramping the bias from the start voltage (0V) to the end voltage: (a) 100mV for the ITO and (b) 5V for PS-Br film, first forward, then back.*

For comparison the electrical measurements on pristine and doped HT P3HT-coated films on the top of ITO glass were also done (the results present in Appendix (Tab. 3-4)). The resistance of the pristine HT P3HT film have the same value as PS-Br-*graft*-P3HT film with order of 10^{10} and conductivity of 10^{-5} S/cm. However, after the $FeCl_3$ doping , the resistance increases significantly to the value of 10^5 Ohm that corresponds to conductivity of ~1-10^{-1} S/cm. As it was for the conductivity in the lateral direction, the conductivity of coated HT P3HT films in their doped state is high than the conductivity of the doped PS-Br-*graft*-P3HT films.

In conclusion, we have shown that C-AFM is a useful tool to measure the current-voltage characteristics of conducting polymer films. The current flowing through Pt/Ir coated tip/polymer

film/ITO substrates was analyzed. The resulting *I-V* curve of doped PS-Br-*graft*-P3HT film showed semiconducting characteristic. The conductivity of the doped films was found to be one order of magnitude higher than the conductivity measured in their lateral direction. The conductivity of the coated HT P3HT films after the doping is higher than the conductivity of the PS-Br-*graft*-P3HT films, that is a consequence of the isolating PS-Br layer. These results further confirm that the procedure developed for the P3HT grafting converts the insulating PS-Br film into a semiconductive PS-Br-*graft*-P3HT. Furthermore, the fact that the films are conductive in a direction perpendicular to the surface confirms the assumption that the grafting of P3HT occurs inside the PS-Br matrix. Tab. 6.4 summarizes the results of conductive measurements in-planar and in perpendicular directions.

Table 6.4. *In-plane and perpendicular electrical conductivity measurements of grafted P3HT from cross-linked PS-Br layer for in pristine and $FeCl_3$-doped state.*

P3HT brush	In-plane (*dc*)		In perpendicular (C-AFM)	
	R, Ohm	σ, S/cm	R, Ohm	σ, S/cm
Non-doped	$\sim 10^{12}$	$\sim 10^{-8}$	$\sim 10^{10}$	10^{-5}
Doped with $FeCl_3$	$\sim 10^{7}$	$\sim 10^{-3}$	$\sim 10^{6}$-10^{8}	$\sim 10^{-1}$-10^{-3}

6.5 DETERMINATION OF THE STRUCTURE OF P3HT GROWN FROM CROSS-LINKED PS-BR FILMS

A series of PS-Br films with variable thicknesses from 1 to 200 nm were spin-coated onto Si-wafers, and covered by 2 nm thick PGMA adhesive layer. The PS-Br films were cross-linked upon a brief irradiation with UV-light to ensure their insolubility, while keeping them swellable in solvents "good" for PS-Br. The samples were activated with a $Ni(tpp)_4$ catalyst, and the surface initiated polycondensation of **1a** was performed according to Scheme 6.2. Results of the ellipsometric thickness measurements for the starting PS-Br and resulting composite PS-Br-*graft*-P3HT films are given in Tab. 6.5 and plotted in the Fig. 6.22.

The data refers to identical polymerization conditions (polycondensation time, *t*=10 h, T=0 °C, [1a]=15 mmol/L) and corresponds to the maximal reachable thickness in each case. However, in most experiments, the films continue to grow substantially for only 3 hours and further increasing the reaction time does not change their thickness significantly.

Table 6.5. *Thicknesses of the photo-cross-linked PS-Br* and grafted P3HT layers** as measured by ellipsometry.*

Entry	1	5	3	4	5	6	7
PS-Br (dry), $h_{PS\text{-}Br}$, nm*	1.7	19	33	37	47	84	115
PS-Br (swollen), $h^*_{PS\text{-}Br}$, nm	9	40	187	137	144	227	393
Swelling ratio, $h^*_{(PS\text{-}Br)}/h_{(PS\text{-}Br)}$	5.7	2.1	5.7	3.7	3	2.7	3.4
P3HT (dry), h_{P3HT}, nm **	5	48	77	79	70	101	150
Grafting coefficient, $h_{P3HT}/h_{PS\text{-}Br}$	2.9	2.5	2.3	2.1	1.5	1.2	1.3
PS-Br-*graft*-P3HT (swollen), nm***	17	98	171	173	288	267	518

**All samples contain 2 nm thick PGMA layer under the PS-Br layer.*
***These values refer to an increase of the thickness of the parent PS-Br film after polymerization of P3HT; for example, the overall thickness of the sample Entry 7 is equal to 2 nm (PGMA)+115 nm (PS-Br)+150 nm (P3HT)=267 nm.*
**** These values refer to the overall thickness of the swollen PS-Br-graft-P3HT films.*

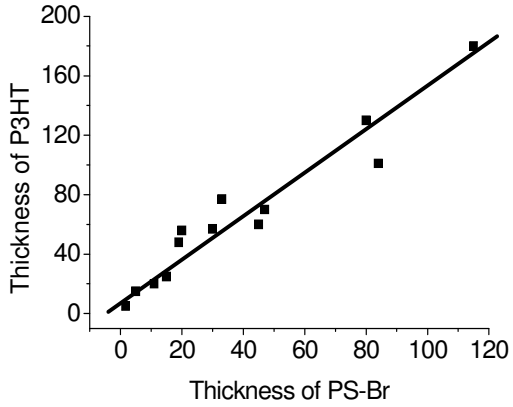

Figure 6.22. *Dependence of the thickness of the P3HT layers on the thickness of the PS-Br layers.*

As seen in Fig. 6.22, the thickness of the grafted P3HT layers increases with the thickening of the PS-Br layers. Thus, the polymerization from the PS-Br monolayer (1.7 nm) results into a grafting of only 5 nm of P3HT, whereas the 115 nm thick PS-Br layer was transformed into 265 nm thick composite film that corresponds to 150 nm of the grafted P3HT[119]. Furthermore, no saturation in this dependence (Fig. 6.22) was found up to a PS-Br film thickness of 115 nm. Thicker PS-Br films were no more stable under the preparative conditions[120] that would allow further monitoring of this thickness dependence.

These results imply that the polycondensation proceeds not only from the topmost layer of the initiating PS-Br film, as in "classical" surface initiated polymerizations into polymer brushes[121] (Fig.

[119] In all cases, "the thickness of the grafted P3HT" means an increase of film thickness after the polymerization of P3HT; thus, a PS-Br film with initial thickness of 115 nm becomes 115+150=265 nm-thick, as deduced by ellipsometry.
[120] They detached from Si-support during the rinsing step resulting into PS-Br-*graft*-P3HT free-standing films.
[121] Surface-initiated polymerizations of polyolefines usually do not require thick layers of initiators; living surface-initiated polymerizations shows linear dependence of the thickness of the grafted polymer layers on the polymerization time.

6.23a), but that also the inner layers of the initiating films contribute to the grafting process, as shown in Fig. 6.23b.

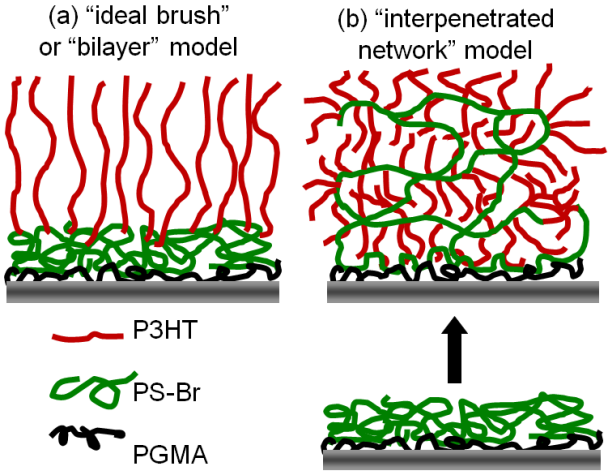

Figure 6.23. *Schematic representation of two possible structures for the P3HT film grafted from photo-cross-linked PS-Br film: (a) "ideal brush" or "bilayer" model, (b) "interpenetrated network".*

The fact that only quite thin P3HT layers are obtainable from the monolayer of the initiator, independent of the polymerization time, points to an important termination processes that limits the kinetic chain length (DP_{kin}). According to this assumption, the thickness of the composite PS-Br-*graft*-P3HT films does not correlate directly with the contour length of the P3HT grafts (which must be very large for thick PS-Br-*graft*-P3HT films). Instead, the composite films, whatever their thickness, contain rather short P3HT grafts that emanate not only from the topmost PS-Br chains, but also grow from strands located deeply inside the PS-Br matrix.

The lowest limit of the contour length of the P3HT grafts can be estimated from the results of the polycondensation from the PS-Br monolayer (DP_{kin} =5 nm/0.38 nm=13). Assuming that P3HT grafts are tilted or somewhat coiled, the real DP_{kin} might be somewhat higher. Unfortunately, a precise determination of the polymerization degree of P3HT grafts is a challenging task because of the impossibility to selectively detach P3HT chains grown from PS-Br.

6.5.1 UV-VIS. SPECTRA

A crude estimation of the molecular weight of P3HT can be made from UV-vis. spectra. It is known that an increase of the polymerization degree (DP) of regioregular head-to-tail P3HT results into a gradual red-shift in the adsorption spectra[122], especially in "bad" solvent and in solid state. To the

[122] Trznadel, M.; Pron, A.; Zagorska, M.; Chrzaszcz, R.; Pielichowski, J., *Macromolecules,* **1998**, 31, 5051-5058.

calibrate UV-vis. absorption versus DP, we synthesized several Ph-terminated P3HT samples of different DPs using $(tpp)_2Ni(Ph)Br$ as initiator, and according to the previously reported method. We found that an increase of the DP from 10 to 30[123], results in a red-shift of the main absorption band from λ_{max} =445 nm to 518 nm. Unfortunately, no significant changes in the UV-vis. spectra of P3HTs are observable when the DP exceeds 30 (e.g. the spectra of 30-mer and 100-mer are very similar). This limits the applicability of this method[124].

We have also found that most of the PS-Br-*graft*-P3HT films obtained by polycondensation from PS-Br films of different thicknesses have a similar UV-vis. spectrum and an absorption intensity roughly proportional to their thickness (Fig. 6.24). Most of the films are violet with the UV-vis. spectrum fitting any DPs equal to or higher than 30 ($\lambda_{max.}$=515 nm; shoulders at λ=550 nm and 610 nm). It must be noted that even if we keep the thickness of the PS-Br supporting layers and the other polymerization parameters constant, due to unintended variations of the reaction conditions, some of the PS-Br-*graft*-P3HT samples still have slightly blue-shifted UV-vis. spectra that correspond to DP~20 ($\lambda_{max.}$ =500 nm and less pronounced red-shifted shoulders. Importantly, the samples with the blue-shifted adsorption and "violet" one have nearly the same thickness (if they are grown from the PS-Br films of the same thickness).

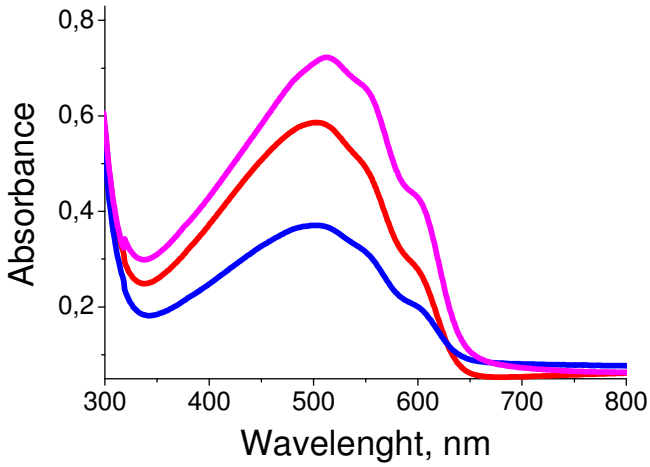

Figure 6.24. *UV-vis. spectra of three PS-Br-graft-P3HT films prepared in identical conditions demonstrate unintended variations of the growing process which result into different DP of P3HT. The P3HT films were grafted from 20 nm (blue), 40 nm (red) and 60 nm (magenta) of PS-Br layer.*

Thus we suggested that the DPs of the P3HT grafts even for the most "violet" samples could not be much larger than 25-30. Such values are consistent with the kinetic chain length determined

[123] DP was determined by ^{1}H NMR.

[124] Senkovskyy, V.; Khanduyeva, N.; Komber, H.; Oertel, U.; Stamm, M.; Kuckling, D.; Kiriy, A., *J. Am. Chem. Soc.*, **2007**, 129, 6626-6632.

previously for the "bulk solution" polycondensation of **1a** mediated by the model $(tpp)_2Ni(Ph)Br$ initiator under the same reaction conditions, as in the grafting experiments.

6.5.2 SWELLABILITY

Grafting of P3HT inside the cross-linked PS-Br films is only possible if the PS-Br networks are swellable enough to allow the immobilization of Ni-catalyst and a penetration of the monomer. Tab. 6.4 depicts the swelling behavior for a set of PS-Br films of variable thickness, before and after the polymerization of P3HT. All PS-Br films, independent of their thickness, are swellable in good solvents (THF, toluene) with a swelling degree (the ratio between "wet" and "dry" thicknesses) varying from 5 to 2. In all cases, the PS-Br-*graft*-P3HT composite films swell to higher thicknesses than the parent PS-Br films. This might be attributed to increased excluded volume interactions inside the networks during the grafting of P3HT. More importantly, the obtained data suggests that the grafting of P3HT takes place not only in the upper PS-Br layers, but also deeply inside the swollen cross-linked PS-Br matrix and even the internal PS-Br layers are accessible for the polymerization reagents and thus participate in the grafting process[125]. However, the fact that the grafting coefficient ($h_{P3HT}/h_{PS\text{-}Br}$, the ratio between the thicknesses of the grafted P3HT and the parent PS-Br) decreases with increasing PS-Br film thickness implies that the contribution of the internal PS-Br layers is smaller than the contribution of the top PS-Br layer. This suggests a diffusion-controlled process. Although such a grafting mechanism has to derive a certain gradient in the film composition within the upper layers enriched by P3HT, the structure of the resulting PS-Br-*graft*-P3HT composite films is closer to the "interpenetrated network" (Fig. 6.23b) than to the "bilayer" ("brush") model (Fig. 6.23a). From the grafting coefficient ($h_{P3HT}/h_{PS\text{-}Br}$), density (ρ) of PS-Br and P3HT and DP of the P3HT grafts, one can estimate a grafting density for the P3HT grafts along the PS-Br chain. The calculations show that for $h_{P3HT}/h_{PS\text{-}Br}$=2.5, $\rho_{PS\text{-}Br}$=1.6 g/cm^3, ρ_{P3HT}=1.33 g/cm^3 [126], and DP=25, each 11th monomer unit of PS-Br contains the P3HT graft that corresponds to the mean distance between two adjacent P3HT grafts to be ~3.0 nm (for the fully stretched PS-Br backbone)[127].

[125] For example, comparing entries **5** and **6** in Tab. 3 and assuming the polymerization conditions in these two experiments to be identical, we can estimate the contribution of deepest layers of the PS-Br of the sample **6** into the grafting process. Since the 84 nm thick PS-Br film grafts 101 nm of P3HT (entry **5**), whereas the 115 nm thick sample **6** gives 150 nm thick P3HT film, the contribution of the additional 31 nm thick PS-Br in the sample **6** (115 nm 84nm) is responsible for the grafting of additional 39 nm of P3HT.

[126] Erwin, M.M.; McBride, J.; Kadavanich, A.V.; Rosenthal, S.J., *Thin Solid Films,* **2002**, 409, 198–205.

[127] $DP_{P3HT}\times\rho_{PS\text{-}Br}\times m_{P3HT}/[m_{PS\text{-}Br}\times(h_{P3HT}/h_{PS\text{-}I})\times\rho_{P3HT}]$=25×1.6×166/(184×2.5×1.33)=10.85.

6.5.3 XPS STUDY OF THE PS-BR-*GRAFT*-P3HT COMPOSITE FILMS

To directly investigate the structure and composition of the films, XPS and RBS measurements were undertaken. XPS reveals that 40 nm thick cross-linked PS-Br film indeed contains C and Br as major atomic components.

The [C]/[Br] ratio is less than the theoretical value (22.7 vs. 8), mostly because of contamination of the surface with carbon and oxygen-reach compounds (Tab. 6.6)[128]. As expected, an activation of the PS-Br film with Ni-catalyst introduces Ni and P. From the atomic ratio [Br]/[Ni] (6.1) we estimate that ~16% of all Br reacts with the catalyst. The amount of P is reduced by a factor of 2.5 that might be either due to deviation of the complex structure from the $(tpp)_2Ni(Ar)Br$ stoichometry, or due to a presence of some insoluble ligand-free Ni formed due to a decomposition of the Ni complexes. Incorporation of the Ni-catalyst is also confirmed by ellipsometry – the treatment of the 40 nm thick PS-Br films with $Ni(tpp)_4$ in the Ar glove-box followed by a washing of the excess of $Ni(tpp)_4$ with dry toluene results into 61 nm thick film. A rather significant amount of S ([C]/[S] ratio of 21.4) and no Ni and P was found in the sample after the grafting of P3HT (the overall thickness increases from 40 to 130 nm). An important conclusion is that the high content of Br ([S]/[Br]=4.9) could not be explained by the P3HT termination, even if all P3HT chains would be terminated by Br atoms (the observed [Br]/[S]=1/5 ratio corresponds to DP=5 and the contour length of 0.38 nm×5=1.9 nm, which is much less than the penetration depth of X-rays in this experiment, i.e. of 8 nm). Thus, the high content of Br reflects that a significant amount of PS-Br is still remaining even in the top layer of the PS-Br-*graft*-P3HT composite film.

To reveal the PS-Br-*graft*-P3HT film composition in deeper layers than the penetration depth of X-rays, the samples were etched with Ar plasma. To diminish the sample damage, the etching was performed in relatively mild conditions with a rate of 0.6 nm/min. After the removal of the upper 20 nm of the 130 nm thick composite film (40 nm of PS-Br+90 nm of P3HT) with Ar plasma, the XPS measurements were conducted. They revealed a lower oxygen content compared to the sample before the etching. We found an increase of S content compared to the sample before the etching. Even more important was that the content of Br atoms also increased substantially, proving that the bromine is not only present in the P3HT chain terminations, but could also be found in PS-Br present here.

[128] 10.7% of O is found in PS-Br sample. We cannot rule out the possibility of oxidation of PS-Br during UV-cross-linking, however, this would not explain the major part of the oxygen found, since even the sample after P3HT polymerization contains 9% of O.

Table 6.6. *Elemental compositions of polymer surfaces after different transformation steps of the grafting process (samples 1-3) and after the Ar-plasma etchings (samples 4 and 5), as derived from the XPS spectra.*

	Atomic concentration %						Atomic ratio		
	C 1s	O 1s	P 2p	Ni 2p3/2	Br 3d	S 2p	[C]:[Br]	[C]:[S]	others
① PS-Br	84.9[a)]	10.93	0.43	–[a]	3.74	–[a)]	22.7	–	–
② S(Br)/Ni(tpp)$_2$	81.27	11.23	0.66	0.82	5.02	–	16.19	–	[P]:[Ni]: 0.80 [Br]:[Ni]: 6.1
③ PS-Br/P3HT	86.23	8.91	–	–	0.82	4.03	105.16	21.40	[S]:[Br]: 4.91
④ PS-Br/P3HT etched "mild"	89.36	5.13	–	–	0.88	4.63	101.54	19.30	[S]:[Br]: 5.26
⑤ PS-Br/P3HT etched "hard	33.13	66.02	–	–	0.85	–	38.98	–	–

Thus, these experiments further confirm the validity of the "interpenetrating" model and decline the "bilayer" (or "brush") structure (Fig. 6.23). Unfortunately, attempts to etch the composite films deeper without significant damage to their surface composition by prolonged exposure to Ar plasma have failed: neither S nor Br was found by XPS in such extensively etched samples without with the appearance of O, F, Na and clear signs of polymer degradation.

6.5.4 RBS STUDY OF THE PS-BR-*GRAFT*-P3HT COMPOSITE FILMS

RBS is ideally suited to obtain elemental depth profiles of heavy elements (such as S, and Br) in a matrix of lighter elements (such as C) with a resolution up to 10 nm[129]. As such, the "intermixed" and "bilayer" models for the structure of the PS-Br-*graft*-P3HT composite films can be clearly distinguished with this technique. According to the "intermixed" model, S and Br are distributed more or less homogeneously within the film, whereas the "bilayer" model assumes depth segregation of S and Br with S located atop of Br.

A 140 nm thick PS-Br-*graft*-P3HT composite film similar to one used in XPS experiments was prepared by grafting of P3HT from 50 nm thick cross-linked PS-Br layer. Its RBS spectrum is shown in Fig. 6.25a and 6.25b. The horizontal scale shows the kinetic energy of the backscattered helium ions. Different species can be readily identified by their position along abscissa and are indicated on the plot.

The sulfur and bromine peaks confirm the presence of P3HT and PS-Br, respectively. The signals arising from carbon and hydrogen in the polymer and the Si substrate occur both at lower energy and are ignored in the further analysis. An incorrect C/H ratio has practically no influence on the Br/C and the S/C atomic ratios. The layer thickness measured by RBS was found to be 2800×10×15 Atom/cm^2. Concentrations of S of 7% and of Br of 4.5% in the brush model were estimated by comparison of the

[129] Lee, W.P.; Gundabala, V.R.; Akpa, B.S.; Johns, M.L.; Jeynes, C.; Routh A.F., *Langmuir,* **2006**, 22, 5314-5320.

signal intensities and standard *k*-factor analysis. The quite intense Br signal suggests that not all bromine atoms in the PS-Br layer are consumed during the grafting process. This correlates with XPS data showing that only ~16% of Br atoms react with $Ni(tpp)_4$. The thick distribution of the components S and Br proved that the P3HT and PS-Br components are *intermixed* in this sample. Fig. 6.25b presents the SIMNRA simulation for the same PS-Br-*graft*-P3HT, but assuming a "bilayer" model. Clearly, the RBS spectra could not be fitted satisfactorily by this model.

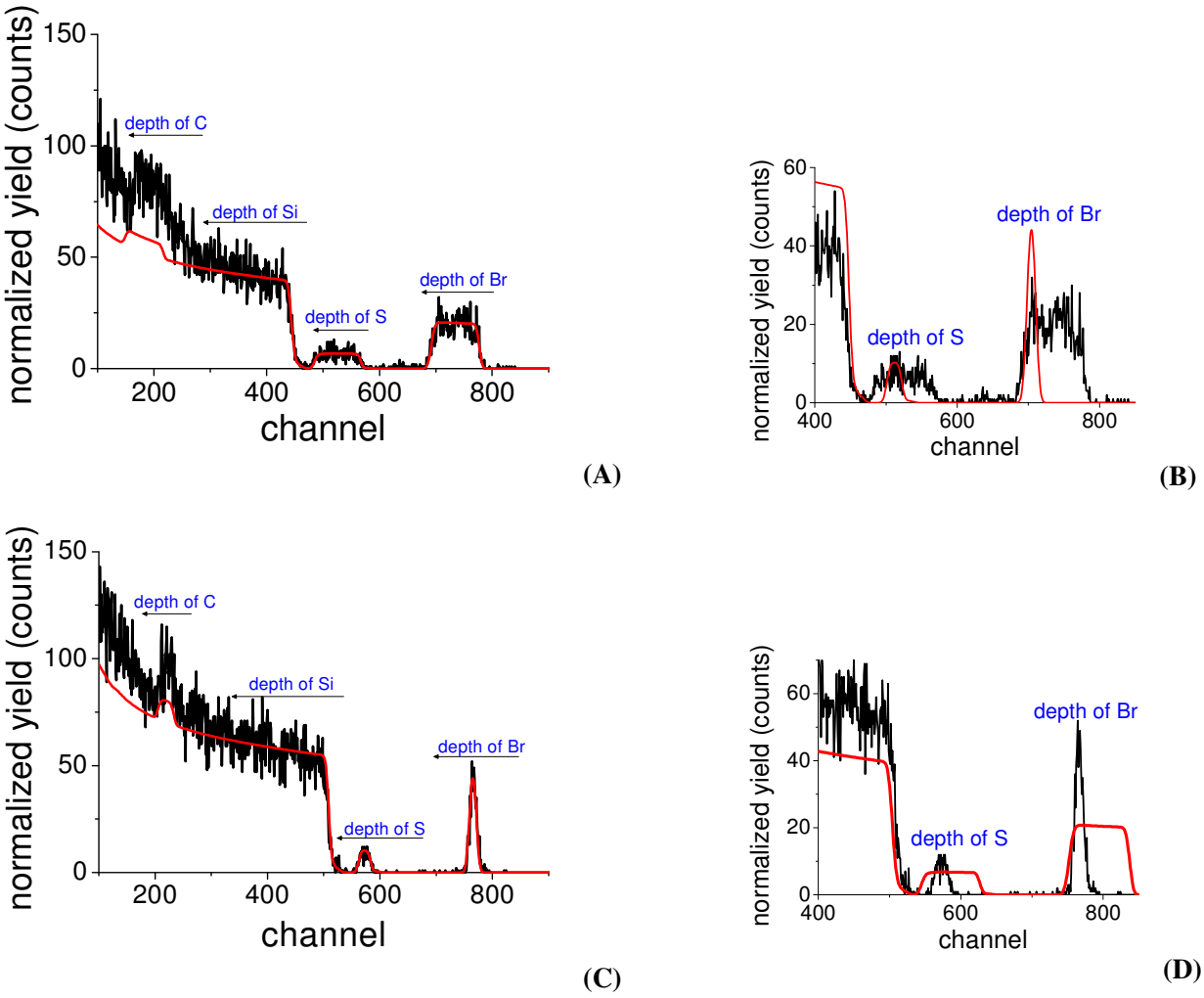

Figure 6.25. *RBS spectra (black line) and SIMNRA simulations (red line) of the PS-Br-graft-P3HT sample (a and b). The "bilayer" sample with P3HT film spin-coated atop of the cross-linked PS-Br film is shown for reference (c and d). SIMNRA simulations were performed for both samples assuming either "intermixed" or "bilayer" structures. The best fit was achieved for the PS-Br-graft-P3HT sample by the "intermixed" model and for the reference "bilayer" sample by the "bilayer" model.*

For comparison, the RBS measurements and simulations were performed for the reference sample with the pre-defined bilayer structure (Fig. 6.25c and 6.25d). To this end, 2 nm PGMA and 50

nm of PS-Br were deposited by spin-coating and cross-linked by UV-irradiation during 1 minute. Afterwards, 90 nm of regioregular HT P3HT was spin coated atop. A best fit of the RBS measurements is obtained here using a "bilayer" model. The amounts of each component in the "bilayer" model are: on the top layer, a concentration of S of 7% and of Br of 0.2% of the coated P3HT. On the bottom, the Br makes up 8% of the PS-Br. The thickness of the top layer is 830×10×15 atoms/cm^2 and the thickness of the bottom layer is 420×10×15 atoms/cm^2. As expected, no signal of sulfur was found in the bottom layer, confirming the validity of the method.

6.6 CONCLUSIONS-2

Only a marginal grafting of P3HT is observed if the surface initiated Kumada catalyst transfer polymerization (KCTP) is performed from thin PS-Br layers because of significant chain termination processes. However, much thicker P3HT films (up to 150 nm) can be grafted from thick (100 nm), highly swellable PS-Br films. A detailed investigation of the grafting process and a direct study of the structure of the resulting composite PS-Br-*graft*-P3HT films by ellipsometry, XPS, and RBS techniques allow to conclude that the grafting proceeds not only from the topmost layer of PS-Br film, but also takes place deeply inside the PS-Br matrix (Fig. 6.23b). The process results into a kind of interpenetrated network, in which relatively short (~10 nm) P3HT grafts emanate from long and cross-linked PS-Br chains. The films show good stability against delamination, high electrical conductivity in the doped state, and a high swellability that might be exploited for construction of fully "plastic" electronic devices and sensors.

6.7 GRAFTING OF THE P3HT FROM PATTERNED SURFACES

Conventional electronics are fabricated using photolithography, a technique that uses a polymer photoresist chosen for both its sensitivity to irradiation and dissolution characteristics, and not for its electronic properties. This requires that either the photolithographic method is modified, or alternative strategies for the deposition of conjugated materials in a spatially controlled fashion are developed.

A variety of techniques are available for patterning π-conjugated polymers[130]. A critical feature in this emerging technology is device fabrication and the reproducible deposition of active material. The technique of choice depends on the material under consideration, the substrate, and the intended

[130] Holdcroft, S., *Adv. Mater.,* **2001**, 13, 1753-1765.

application or objective. For instance, if the goal is to pattern materials for electrochromic devices that require rapid redox switching, then conjugated polymers patterned by electro-deposition on SAM-modified electrodes provide a conjugated material that is optimized for electrochemical switching. On the other hand, if the goal is to prepare a limited number of channels of conjugated material between specific locations in order to study physico-chemical characteristics of polymer wires, then scanning probe deposition techniques might prove useful. It is unreasonable to assume, however, that these latter two techniques will prove useful in the preparation of mass-produced devices such as FETs[131] and LEDs[132]. High-performance organic semiconducting devices will require materials that are free from both structural defects and impurities. Device patterning will likely require the use of preformed and pre-characterized polymers.

Block copolymers constitute an attractive option for surface-engineering because of their ability to form a variety of nanoscale ordered phase-separated structures. However, block copolymers containing conjugated blocks are less abundant compared to their non-conjugated counterparts and their phase-behavior is not always predictable. Herein, we demonstrate how surface structures of non-conductive block copolymers can be converted into (semi)conductive ones via surface-initiated polymerization of P3HT from reactive surface-grafted block copolymers.

In this work was used poly(4-vinylpyridine)-*block*-poly(4-iod-sterene) P4VP-*b*-PS-I as reactive block copolymer. We describe two approaches for the fabrication of patterned surfaces: the top-down and bottom-up. Top-down techniques in general correspond to the traditional methods of the semiconductor industry, in which pattern transfer from block copolymers is used to pattern an underlying substrate. The bottom-up techniques let the active components directly self-assemble.

6.7.1 GRAFTING OF P3HT BRUSHES FROM BLOCK COPOLYMER PATTERNS

Block copolymer thin films can be obtained from two dimensional patterns with very high regularity. Patterning from block copolymers has been subject of investigation, as it provides access to a length scale not possible with traditional lithographic techniques. The focus has therefore been on the patterning of microelectronic components on a length scale inaccessible by optical lithography.

Postpolymerization modification of polymers has proven to be a general route to materials that might otherwise be difficult or impossible to produce using direct polymerization routes. In contrast to

[131] Briseno, A.L.; Roberts, M.; Ling, M.-M.; Moon, H.; Nemanick, E.J.; Bao, Z., *J. Am. Chem. Soc.,* **2006**, 128, 3880-3881.
[132] Li, Z.L.; Yang, S.C.; Meng, H.F.; Chen, Y.S.; Yang, Y.Z.; Liu, C.H. Horng, S.F.; Hsu, C.S.; Chen, L.C.; Hu, J.P.; Lee, R.H., *Appl. Phys. Lett.*, **2004**, 84, 18, 3558-3560.

its halogenated counterparts, styrene can be easily be polymerized by means of various controlled polymerization techniques (including the anionic polymerization). As a result, polystyrene-based block copolymers are one of the most readily available classes of well defined polymer materials. It was found earlier that bromine or iodine atoms can be introduced into *para*-position of the aromatic ring by direct halogenation of the polystyrene homopolymer. We found that these procedures work well also for the halogenation of P4VP-*b*-PS block copolymers, if PS is a major block[133]. For example, the iodination of $P4VP_{25}$-*b*-PS_{350} and $P4VP_{75}$-*b*-PS_{313} into $P4VP_{25}$-*b*-$PS(I)_{350}$ and $P4VP_{75}$-*b*-$PS(I)_{313}$, respectively, proceeds selectively into the PS-block and nearly completely (more than 95 % by ^{1}H NMR, Fig. 6.26).

The ^{1}H NMR-spectroscopy shows the change of the aromatic area due to addition of an iodine atom to the benzene group.

Although both P4VP-*b*-PS-Br and P4VP-*b*-PS-I can be used for further grafting of P3HT, the immobilization of the Ni-catalyst proceeds much faster with PS-I. Therefore only iodinated block copolymers were used in the present work.

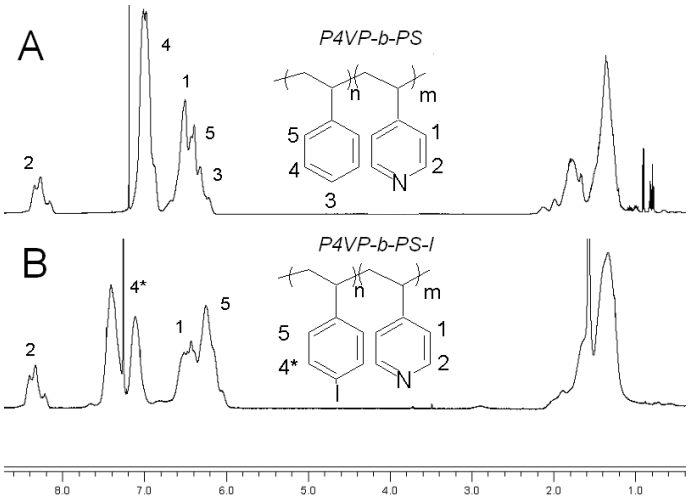

Figure 6.26. *^{1}H NMR-spectra of the block copolymers (a) P4VP-b-PS and (b) P4VP-b-PS-I.*

The copolymer was dissolved in toluene, which is a selective solvent for polyiodbenzene and "bad" for poly(4-vinylpyridine) components. A very strong, quasi-irreversible binding of polyvinyl homopolymers to various substrates was previously described by Luzinov *et al.*[134]. The interaction on an individual pyridyl group with the surface is not strong and can be described in terms of

[133] However, poor solubility of the P4VP block in the protonated state causes difficulties upon the iodination of P4VP-*b*-PS with a high P4VP content (more than 50%) and thus for halogenation of such polymers, another solvent must be found.
[134] Malynych, S.; Luzinov, I.; Chumanov, G., *J. Phys. Chem. B.* **2002**, *106*, 1280-1285.

phisiosorption, however, the fact that one polymer molecule simultaneously interacts with the surface through many pyridyl groups provides an entropic advantage for the quasi-irreversible adsorption of this molecule to the surface, even in the presence of strong solvents. We exploited this binding activity to graft highly asymmetric $P4VP_{25}$-*b*-$PS(I)_{350}$ and less asymmetric $P4VP_{75}$-*b*-$PS(I)_{313}$ block copolymers to Si-wafers and glass-slides. In contrast to polymer brushes formed upon adsorption of asymmetric block copolymers by hydrophobic interactions, $P4VP_{25}$-*b*-$PS(I)_{350}$ grafted films were found to be stable in various solvents even in ultrasonic bath conditions[135,136]. The thicknesses of the grafted $P4VP_{25}$-*b*-$PS(I)_{350}$ films, which were $h_{P4VP\text{-}b\text{-}PSI}$ ~8 nm, is typical for polymer monolayers obtained by the "grafting-to" approach. The volume fraction of the P4VP block lets infer that the thickness of the anchoring P4VP layer is ~0.5 nm. A thickness of the $PS(I)_{350}$ block of 7.5 nm corresponds to the distance between adjacent chains, D~2.9 nm and a grafting density of $\sigma=1/D^2$~0.11 chains/nm^2. Assuming that the radii of gyration, R_g, for $PS(I)_{350}$ in toluene are the same as for PS_{350}, a reduced tethered density of $\Sigma = \sigma \cdot \pi \cdot R_g^2$~12.4 can be found. The values of Σ and σ show that the grafted $P4VP_{25}$-*b*-$PS(I)_{350}$ is in a "true brush" regime, however close to the "mushroom-to-brush" transition. The $P4VP_{25}$-*b*-$PS(I)_{350}$ brushes show a good swellability in good solvents; for example, the thickness of the $P4VP_{25}$-*b*-$PS(I)_{350}$ brush in THF was found to be 15 nm, as determined by *in-situ* ellipsometry.

It is well-known that well-defined block copolymers provide an interesting option in nanopatterning. $P4VP_{25}$-*b*-$PS(I)_{350}$ does not form micelles in for PS-I selective solvents, since the P4VP block is too small. Therefore, less asymmetric $P4VP_{75}$-*b*-$PS(I)_{313}$ was used for nanostructuring. The micellar dispersion of $P4VP_{75}$-*b*-$PS(I)_{313}$ in toluene was spin-coated onto Si-wafers and the samples were annealed at 150 °C in inert atmosphere. At this temperature, PS-I constituting the shell of the micelles does not melt and act as nanoreactors, in which molten P4VP is grafted to the surface. As a result, the $P4VP_{75}$-*b*-$PS(I)_{313}$ monolayer preserves the characteristic quasi-regular arrangement of the micelles even after extensive rinsing with solvents good for both blocks (like THF and chloroform). The structural characterization of the films was conducted using AFM measurements (Fig. 6.27).

[135] The radius of gyration corresponding to free PS coils of molecular weight 40 000 and 35 000 are estimated to be 6.4 and 5.9 nm, respectively, from $R_g=0.117\ Mw^{0.595}$ for PS in toluene. (a) Higo, Y.; Ueno, N.; Noda, I., *Polym. J.,* **1983**, 15, 367. (b) Kent, M.S.; Lee, L.-T.; Farnoux, B.; Rondelezt, F., *Macromolecules,* **1992**, 25, 6240-6247.

[136] $\rho_{PS\text{-}I}=2\ g/cm^3$; $M_{nPS(I)350}=81312\ g/mol$; $V_{PS(I)350}=M_{nPS(I)350}/(\rho_{PS\text{-}I}\times N_A)=67\ nm^3$, $D^2=V_{PS(I)350}/h=67/7.5=8.9$.

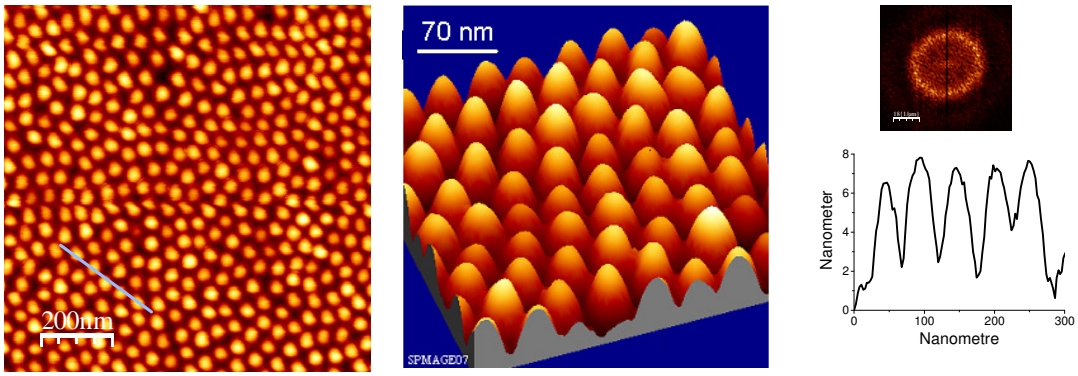

Figure 6.27. *AFM topography images and cross-section of a P4VP$_{75}$-b-PS(I)$_{313}$ copolymer.*

Fig. 6.27 shows the "eggs box" structure, with distance between centers of the micelles of 40 nm and a height of ~6 nm. In general, when a block copolymer is deposited on a substrate, one block preferentially wets an interface to minimize interfacial and surface energy. As a result, the lamellae and cylinders are induced to align with their planes (or axes) parallel to the surface due to a preferential interaction of one block with the surface. This orientation tends to propagate throughout the thickness of the film.

Scheme 6.7. *The scheme of "grafting from" of the P3HT brush grown from P4VP-b-PS-I layer.*

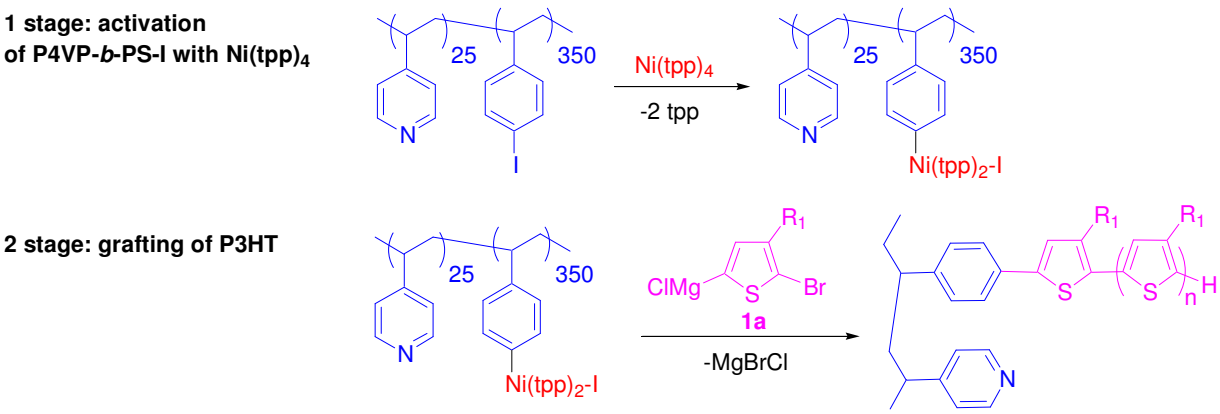

The next step is the grafting of conductive polymer to form the conductive polymer brushes (Scheme 6.7). The activation of 8 nm thick P4VP$_{25}$-*b*-PS(I)$_{350}$ brushes with Ni(tpp)$_4$ catalyst and a subsequent placement of the activated brushes into the monomer solution leads to selective polycondensation of the monomer from the surface.

The maximally reachable thickness of the composite P4VP-*b*-PS-I-*graft*-P3HT film lies between 30 and 50 nm. The schematic representation of surface structures of P4VP-*b*-PS-I copolymer and the resulting P4VP-*b*-PS-I-*graft*-P3HT are depicted in Fig. 6.28.

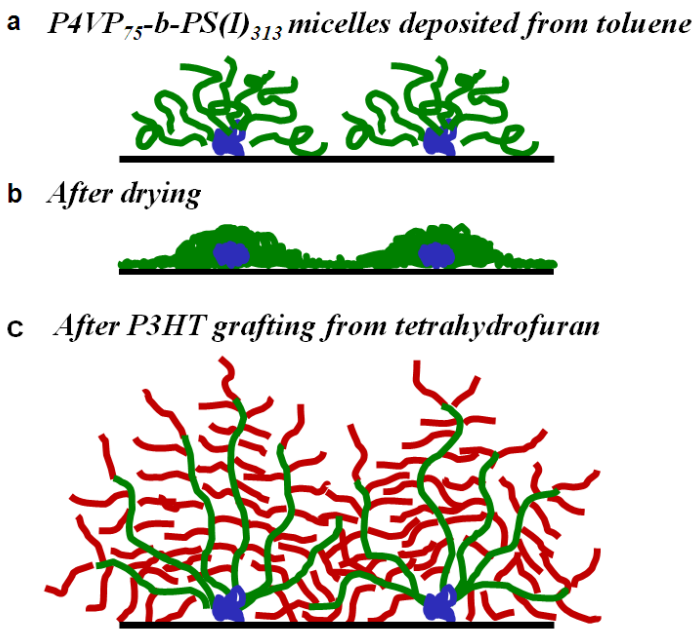

Figure 6.28. *(a) deposition of P4VP-b-PS-I from toluene, (b) morphology of P4VP-b-PS-I in dry state and (c) schematic representation of P4VP-b-PS-I-graft-P3HT brushes from tetryhydrofuran.*

To precisely monitor the grafting process over time, we prepared a series of 8 nm thick $P4VP_{25}$-*b*-$PS(I)_{350}$ brush sample on Si-wafers and glass slides, activated it with $Ni(tpp)_4$ catalyst and exposed the sample to the monomer solution for different time periods, ranging from 10 to 900 minutes[137]. We found that the films continue to grow substantially within 3 hours, then a further increase of the reaction time only moderately increases their thickness. The results of the ellipsometric thickness measurements for the resulting composite P4VP-*b*-PS-I-*graft*-P3HT films polymerized at different times steps at 0 °C are given in Tab. 6.7 and plotted in Fig. 6.29.

Table 6.7. *Results of thickness measurements, UV-vis. and calculated DP of P4VP-b-PS-I-graft-P3HT.*

Thickness	T, min	UV-max	Calc. DP
6 nm	10	420 nm	<5
11 nm	30	420 nm	<10
16 nm	50	445 nm	10
22 nm	110	485 nm	19
35 nm	Overnight	505 nm	25

[137] A precise monitoring of the evolution of the film thickness during the grafting for the given sample was not possible since the setup for in-situ ellipsometric measurements is not compatible with the rather demanding polymerization conditions (air- and water-sensitivity, low temperature). The reaction course, therefore, was monitored for a series of samples with the grafting process terminated after the respective time periods.

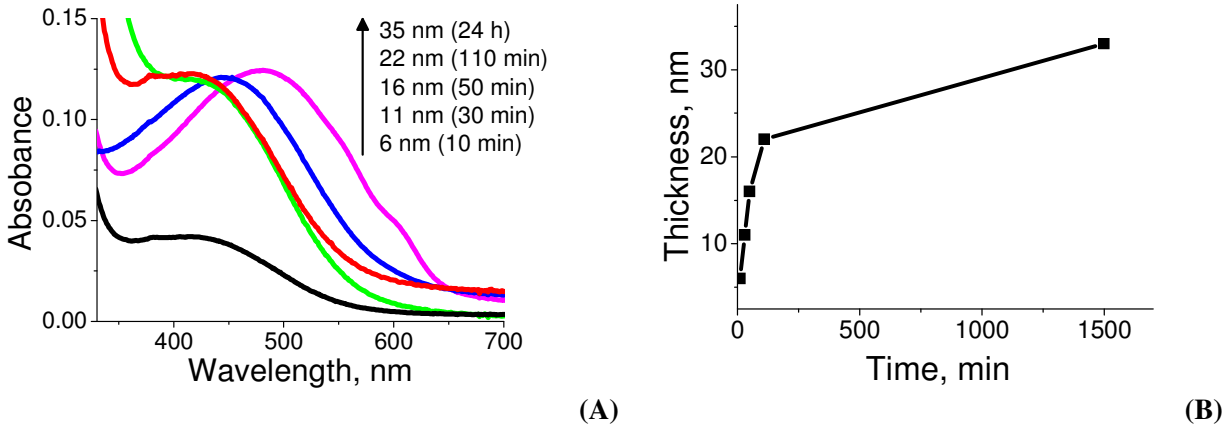

Figure 6.29. *(a) UV-vis. spectra and (b) thickness dependence of the grafted P3HT brush from the P4VP-b-PS-I copolymer (2 nm) at the time of polymerization.*

The UV-vis. spectra of the grafted P3HT show that an increase of grafting time results in a gradual increase of the absorption intensity and depicts the red-shift of $\lambda_{max.}$ from 420 nm to 505 nm. This corresponds to a DP evolution from <5 to ~25. The later value is consistent with the kinetic chain length determined previously for the "bulk solution" polycondensation of **1a** mediated by the model $(tpp)_2Ni(Ph)Br$ initiator under the same reaction conditions, as in the "grafting-from" experiments. It is interesting to note that the DPs of the P3HT grafts grown at different polymerization time show nearly linear dependence on the thickness of the P4VP-*b*-PS-I-*graft*-P3HT. This suggests that the number of polymerization sites remain constant (fast initiating and slow chain propagation).

Unfortunately, the verification of the postulated structure for the resulting film (see Fig. 6.28) is a challenging tasks, as due to the impossibility to selectively detach the P3HT chains grown from PS-I, a precise determination of the grafting density of P3HT along the PS-I backbone and the polymerization degree (DP) of the P3HT grafts are difficult. However, a crude estimation of the molecular weight of the P3HT grafts can be acquired from the UV-vis. spectra. It is known that an increase of the DP of regioregular head-to-tail P3HT results into a gradual red-shift in the adsorption spectra, especially in "bad" solvent and in a solid state. To calibrate UV-vis. absorption versus DP, we synthesized several P3HT samples of different DPs according to a previously proposed method (Fig. 6.30). It was found, that an increase of the DP from 10 to 30 results in a red-shift of the main absorption band from $\lambda_{max.}$ = 445 nm to 518 nm.

From the DP_{P3HT} and the observed film thickening upon the grafting of P3HT, the mean distance between the P3HT grafts along the PS-I backbone (k) can be estimated as follows; assuming that each PS-I monomer unit derives a P3HT graft (with a maximal possible grafting density and a distance between the grafts of k=0.25 nm), the observed increase of film thickness from 7.5 nm to 38.5 nm upon

the grafting corresponds to $DP_{P3HT\text{-}imaginary}$~3.8 [138]. As in reality, the DP_{P3HT} for 39 nm thick film is equal to ~25, P3HT, the grafts grow on average from every eighth PS-I monomer unit (25/3.8~6.58), which corresponds to a k~1.6 nm.

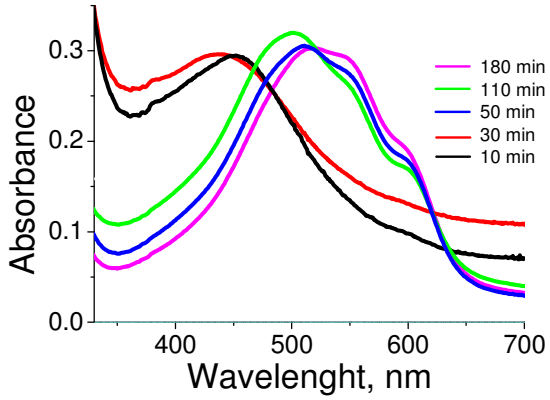

Color	T, min	UV-max	DP_{NMR}
Black	10	445 nm	10
Red	30	452 nm	15
Blue	50	504 nm	22
Green	110	511 nm	28
Magenta	180	518 nm	35

Figure 6.30. *UV-vis. spectra and table of different DP of the P3HT films coated onto glass support covered by PGMA.*

Compared to combed brushes of non-conductive polymers with polymer grafts propagating from each monomer unit of the main chain reported by Matyjaszewski *et al.*[139], the grafting density observed in our work is much lower. Nevertheless, even such a grafting density provides significant stretching of the main chain of the grafted comb-like polymer, as demonstrated below. Fig. 6.31 presents the schematic structure of P4VP-*b*-PS-I-*graft*-P3HT brushes in swelled state.

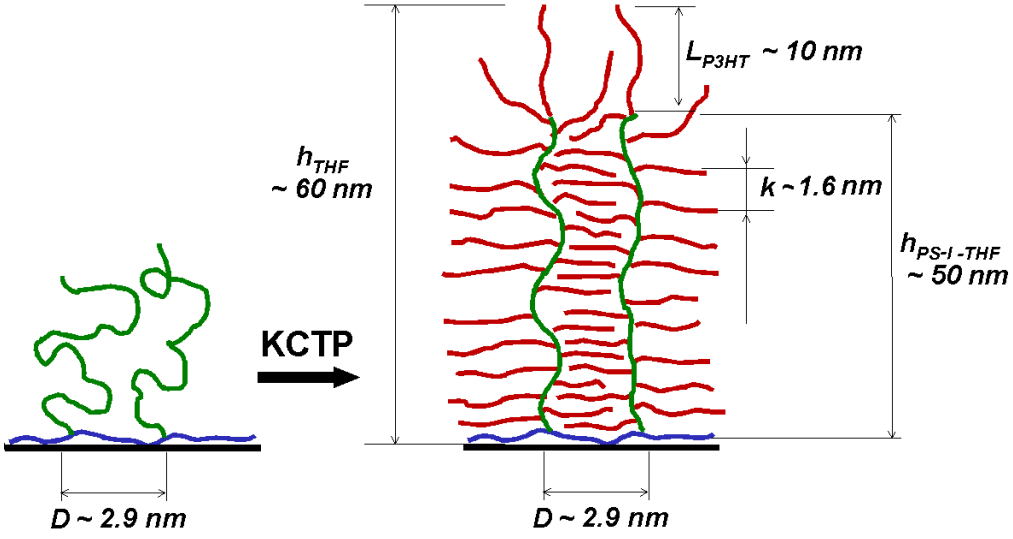

Figure 6.31. *Schematic of grafted P3HT brushes from coated P4VP-b-PS-I copolymer onto surface in swelled state.*

[138] $m_{PS\text{-}I} \times \rho_{P3HT} \times (h_{PS\text{-}I\text{-}graft\text{-}P3HT} - h_{PS\text{-}I}) / m_{P3HT} \times \rho_{PS\text{-}I} \times h_{PS\text{-}I}$ =231×1.33×(38.5-7.5)/166×2.0×7.5 ~3.8.
[139] Börner, H.G.; Beers, K.; Matyjaszewski, K., *Macromolecules,* **2001**, 34, 4375 –4383.

Table 6.8. *Thicknesses in the dry and swollen states, $\lambda_{max.}$, and estimated DPs for the P4VP-b-PS-I-graft-P3HT composite films and the parent P4VP-b-PS-I brush.*

Entry	*T*, min	λ_{max}, nm	Calculated *DP* of P3HT grafts	h_{dry}, nm	h_{THF}, nm
1	0	-	-	6	15
2	10	400	<5	12	26
3	30	420	~5	17	31
4	50	445	10	22	37
5	110	485	19	28	45
6	200	487	20	32	50
7	900	505	25	39	60

The swelling behavior of the P4VP-*b*-PS-I-*graft*-P3HT was studied by *in situ* ellipsometry and compared with the behavior of the parent P4VP-*b*-PS-I brushes (Tab. 6.8). We found that the P4VP-*b*-PS-I-*graft*-P3HT composite films swell to even higher thicknesses than the parent P4VP-*b*-PS-I brushes. This might be attributed to increased excluded volume interactions of the comb-like polymer (Tab. 6.8). At the same time, the swelling capability (the ratio between the thicknesses in the dry and the swollen states) is gradually decreased. For example, P4VP-*b*-PS-I brushes with a dry thickness of 8 nm, swell in THF up to 15 nm, whereas the P4VP-*b*-PS-I-*graft*-P3HT films with a dry thickness of 39 nm swell in THF up to 60 nm. It is interesting to estimate the stretching degree of the tethered PS-I backbone in the dry and in the swollen states after the grafting of P3HT. The size of the PS-I coil ($h_{PS\text{-}I\text{-}THF}$ and $h_{PS\text{-}I\text{-}dry}$, for the swollen and the dry state, respectively) can be evaluated by subtracting the thickness of the anchoring P4VP layer (which is negligibly small, since P4VP is grafted to the surface on many points) and the contour length of the P3HT graft (L_{P3HT} ~10 nm for D_{P3HT}=25, Fig. 6.31) from the overall film thickness (h_{THF} or h_{dry}). Thus, the $h_{PS\text{-}I\text{-}THF}$ for the swollen P4VP-*b*-PS-I-*graft*-P3HT film is equal to 60–10=50 nm, which is not much less than the PS-I length in a fully stretched conformation (350×0.25=87.5 nm). In the dry state, the contribution of the P3HT grafts to the overall thickness is somewhat lower due to possible tilting and/or coiling of the P3HT chains and is roughly equal to the thickness of the P3HT brushes obtainable from the PS-I monolayers (~6 nm). Thus, $h_{PS\text{-}I\text{-}dry}$ can be estimated to be at the level of 39-6=33 nm. In both the dry and the swollen states, the PS-I backbone in P4VP-*b*-PS-I-*graft*-P3HT is much more stretched than it is in the starting P4VP-*b*-PS-I (7.5 nm and 14.5 nm for the dry and swollen states, respectively). Thus, grafting from the polymer brushes leads to an increase of the side-chain bulkiness and is an efficient way to increase of the stretching degree of the tethered polymer chains at constant grafting density.

The morphology of grafted P3HT brushes was studied using AFM measurements and the result is shown in Fig. 6.32. Although the grafting of P3HT destroys the initial order, the particular morphology of the film is preserved.

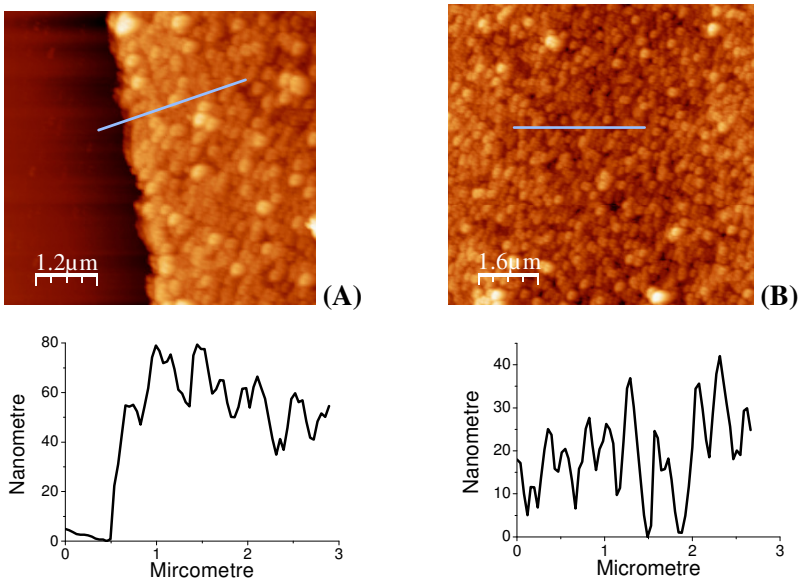

***Figure 6.32**. AFM images and cross-section of the P4VP-b-PS-I-graft-P3HT composite films: a) scratched area and (b) topography image.*

Fig. 6.33a shows the surface of coated $P4VP_{25}$-*b*-$PS(I)_{350}$. It is quite smooth with a roughness of 2 nm. Due to a low amount of poly-4vinylpirridine, we did not observe any signs for nanophase separation. The morphology of the *$P4VP_{25}$-b-$PS(I)_{350}$-graft-P3HT* brush grown from $P4VP_{25}$-*b*-$PS(I)_{350}$ is given in Fig. 6.33b.

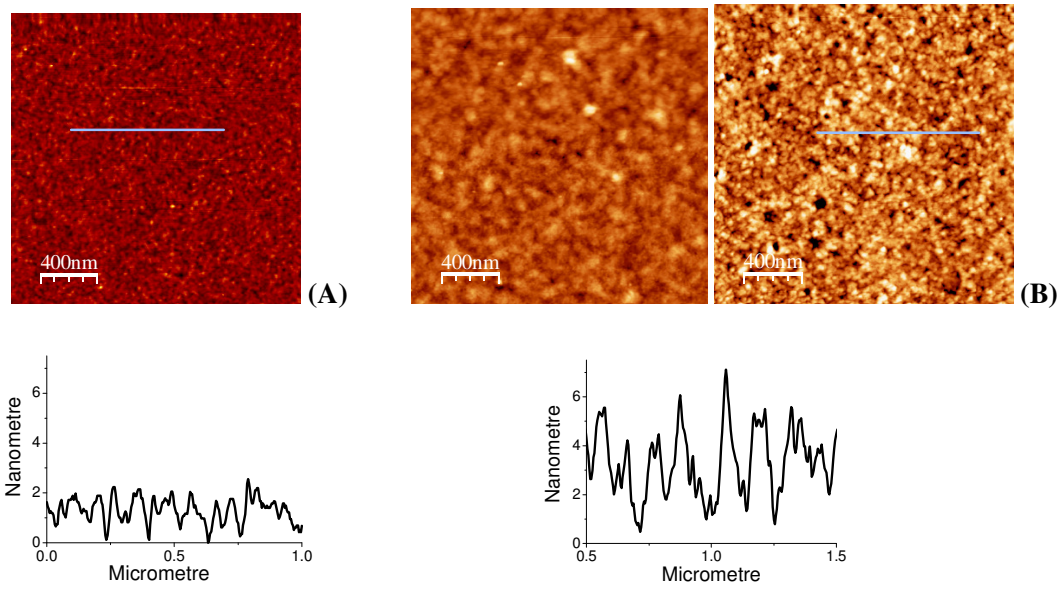

***Figure 6.33.** AFM topography images and cross-section: (a) $P4VP_{25}$-b-$PS(I)_{350}$ and (b) $P4VP_{25}$-b-$PS(I)_{350}$-graft-P3HT composite films.*

6.7.2 COMBINATION OF TOP DOWN AND BOTTOM-UP PATTERN FABRICATION FOR P3HT BRUSHES

The micro- and nano-scale patterning of the P3HT brushes is an important step for exploitation towards opto-electronic devices and sensors. A specific and strong adsorptivity of the P4VP block to polar metallic and metal oxide surfaces was used in this work to pattern $P4VP_{25}$-*b*-$PS(I)_{350}$. In principle, various kinds of lithography ranging from conventional photolithography and inject-printing, to micro-contact printing, micro-imprinting and dip-pen lithography can be applied for the site-specific deposition of the reactive block copolymer. As an example, in this work we used a variant of colloidal lithography, which arranges sub-micron hydrogel particles on Si-wafers by deep coating and usage of as a mask.

Fig. 6.34 presents a scheme of the patterning procedure. First, hydrogel particles were arranged on the Si-wafer by dispersion in water. The size of the particles was adjusted using oxygen plasma to have a width in the range of 1 μm to 700 nm. The residual surface was then covered with octadecyltrichlorsilane to form a hydrophobic environment.

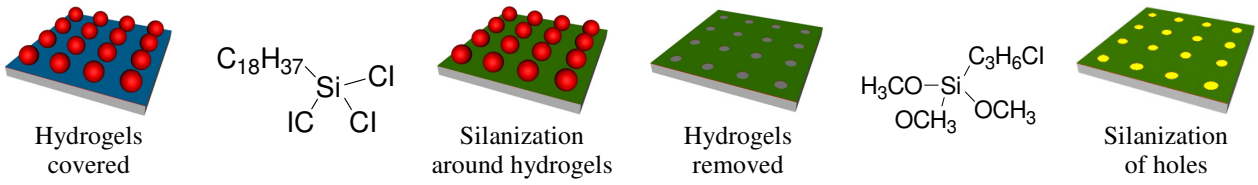

Figure 6.34. *Schematic representation of the patterning: deposition of the hydrogel particles and treatment by the oxygen plasma; silanization with octadecyltrichlorsilane around the particles, removing of the particles in ultrasonic bath; and silanization of the holes with 3-chloropropyltrimethoxysilane.*

The particles were removed through an ultrasonic bath, and the appearing holes were silanizated with 3-chloropropyltrimethoxysilane in the gas phase. Afterwards, the solution of P4VP-*b*-PS-I copolymers was spin-coated and a chemical bonding between the chloride of the silane and the nitrogen of the copolymer was established by annealing overnight at 150 ^{0}C in a vacuum. The subsequent treatment of the samples with Ni-catalyst and a monomer solution **1a** resulted into a selective grafting of P3HT from the patterned $P4VP_{25}$-*b*-$PS(I)_{350}$ disks, which follows from an increase of their thickness by up to 30 nm (Fig. 6.35c).

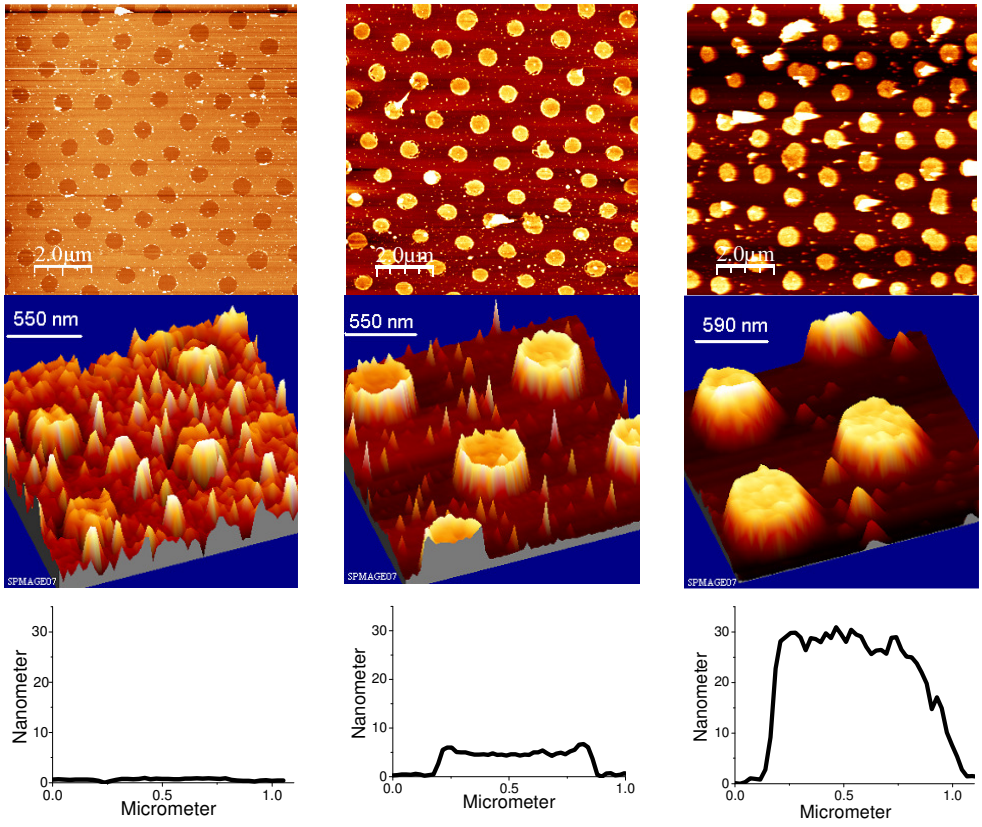

(A) Silanization of holes **(B)** Coated P4VP-*b*-PS-I copolymer **(C)** "Grafting from" P3HT brush

Figure 6.35*. The AFM topography images and the cross-sections of all production steps of the P3HT brushes from the patterned surfaces.*

6.8 CONCLUSIONS-3

P4VP-*b*-PS-I block copolymers obtained by iodination of readily available P4VP-*b*-PS block copolymers strongly adsorb to various polar substrates including Si-wafers, glasses and metal oxide surfaces due to polarity of the P4VP block forming polymer brushes with the tethered PS-I that are moderately stretched in toluene and THF. Kumada catalyst transfer polycondensation from the P4VP-*b*-PS-I brushes. A pre-activation with a $Ni(tpp)_4$ catalyst results in planar brushes of a comb-like polymer with relatively short (~10 nm) P3HT grafts emanating from the surface-tethered PS-I chains. Grafting of the P3HT leads to significant stretching of the PS-I backbone as a result of increased excluded volume interaction. The specific adsorptivity of the P4VP block to polar surfaces was used in this work to pattern $P4VP_{25}$-*b*-$PS(I)_{350}$ brushes. The microscopically structured $P4VP_{25}$-*b*-$PS(I)_{350}$ brush was converted into a patterned P4VP-*b*-PS-I-*graft*-P3HT brush. We demonstrated that functional block copolymers are an attractive option for nanostructuring polymer brushes. $P4VP_{75}$-*b*-$PS(I)_{313}$ micelles obtained in a block solvent selective for PS-I block form an ordered hexagonal array on Si-

wafers. The high glass transition point of PS-I (200 °C) prevents the diffusion of the P4VP anchoring block over the whole surface and therefore the order is preserved even after the grafting procedure at 150 °C. An interesting point is that the $P4VP_{75}$-*b*-$PS(I)_{313}$ monolayer preserves the characteristic quasi-regular arrangement of the micelles even after the extensive rinsing with various solvents. Although the grafting of P3HT from the nanopatterned $P4VP_{75}$-*b*-$PS(I)_{313}$ brush destroys the initial order, the particular morphology of the resulting film is preserved (Fig. 6.32). We believe that the developed method for structured brushes of conductive polymers can be further exploited as novel stimuli-responsive materials for the construction of sensors or in various opto-electronic devices.

6.9 PHOTOVOLTAIC CHARACTERISTICS

We assume that a polymer brush film containing a great level of order at the molecular level can display a significantly higher characteristic of charge mobility compared to a spin-coated film of the same polymer (see chapter 3).

6.9.1 DEVICE PREPARATION

The two solar-cell devices were prepared on glass substrates coated with indium tin oxide (ITO). The thickness of the ITO layer was 150±10 nm, with a roughness is ≤1 nm[140]. Two types of solar cells were prepared as can be seen in Fig. 6.36. For the first, P4VP-*b*-PS-I was directly coated atop the ITO substrate. Afterwards the sample was annealed at 150 °C, and washed with several solvents. The obtained thickness was 8 nm. Then the polymerization of the 3HT was conducted.

The second type of solar cell, a hole transport layer of PEDOT:PSS (80 nm) was spin-coated on the ITO structure. It was then treated by an ethanol solution of $FeCl_3$ overnight to cross-link the PSS, and washed with ethanol and water. Treating the sample with $FeCl_3$ improved the adhesion of the PEDOT:PSS film to the ITO surface such that it became highly insoluble in solvents[141,142]. Afterwards the P4VP-*b*-PS-I copolymer was spin-coated atop the PEDOT:PSS layer, annealed at 150 °C and washed with several solvents. The obtained thickness was 8 nm. Then the polymerization of 3HT was performed. The thickness of the grafted P3HT brushes in both types of solar cells was measured with AFM and found to be 35 nm.

[140] ITO substrates were ordered from company "Thin Film Devices Inc." 1180N Tustin Ave, Anaheim, CA 92807.
[141] Ghosh, J.R.; Rasmusson, O.; Inganäs., *Adv. Mat.*, **1998,** 10, 1097-1099.
[142] Vazquez, M.; Danielsson, P.; Bobacka, J.;. Lewenstam, A; Ivaska, A., *Sensors and Actuators, B,* **2004,** 97, 182-189.

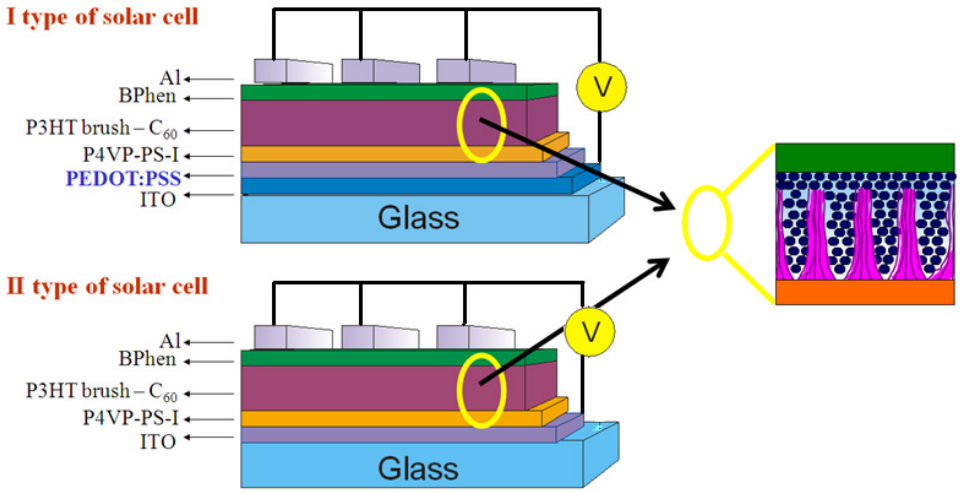

Figure 6.36. *Two types of solar sell were prepared.*

Before the deposition of additional layers, the samples were stored in high vacuum (<10^{-7} mbar) for 12 hours. A 42 nm layer of fullerene C_{60}, a 8 nm thick layer of 4,7-diphenyl-1,10-phenanthroline (bathophenanthroline, or BPhen) and a 80 nm aluminum layer (Al) were deposited on the sample through shadow masks on the substrates. The underlying ITO layer was structured in such a way that four solar cells with an area of 6.0 mm^2 could be prepared on each sample.

6.9.2 PHOTOVOLTAIC CHARACTERISTICS OF DEVICES

The photovoltaic characteristics were investigated at TU Dresden in group of K. Leo. The current density–voltage characteristics of the first device under illumination and in the dark are shown in Fig. 6.37. Under illumination, excitons are formed by absorption of photons in the photoactive materials P3HT and fullerene C_{60}. The exiton can diffuse to the interface of P3HT and fullerene C_{60} materials. The excitons[143] are dissociated into an electron on the acceptor (C_{60}) and a hole on the donor (P3HT). The free charge carriers are now driven by the electrical field and diffuse to the contacts. Thereby, a short circuit photocurrent is generated. It was found that under illumination, the short circuit current density (I_{sc}) is 0.12 mA/cm^2. The open-circuit voltage (V_{oc}) and the fill factor (FF) are 0.37V and 21.36% respectively. The resulting power conversion efficiency (η) was calculated to be 0.008%[144].

When a negative voltage (–1V) was applied, a small current density can be observed as seen in Fig. 6.37 (black line). The device shows a comparatively good blocking behavior in the dark.

[143] An exciton is a bound state of an electron and an imaginary particle called an electron hole in an insulator or semiconductor, and such is a Coulomb-correlated electron-hole pair.

[144] $\eta=(V_{oc}\times I_{sc}\times FF)/P_{in}$ =(0.12 mA/cm^2×0.37 V×21.36%)/111 mW/cm^2 =0.008 %.

Irradiating the device with simulated sunlight (AM 1.5, 111 mW/cm^2), produces the current at –1V that by a factor of 6.47[145] lager than the current at 0V. This points towards field assisted exciton separation and field dependent recombination of photo generated charge carriers (see chapter 3).

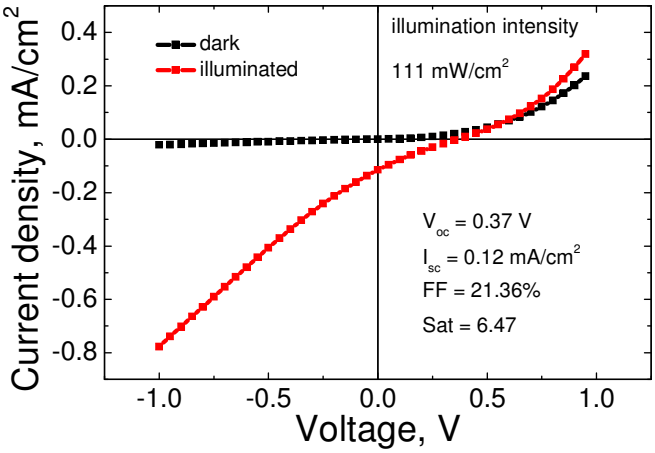

Figure 6.37. *The current density–voltage (I-V) characteristics of solar cells based on ITO/P4VP-b-PS-I-graft-P3HT brush/C_{60}/BPhen/Al structure.*

The external quantum efficiency is defined as the fraction of photogenerated electrons at the contact and the number of incoming photon. It therefore depends on both the absorption of light and the collection of charges. Fig. 6.38a shows the results of the IPCE (Incident Proton to Controlled Electron efficiency) measurements for the solar cell based on P4VP-*b*-PS-I-*graft*-P3HT brush with fullerene C_{60}.

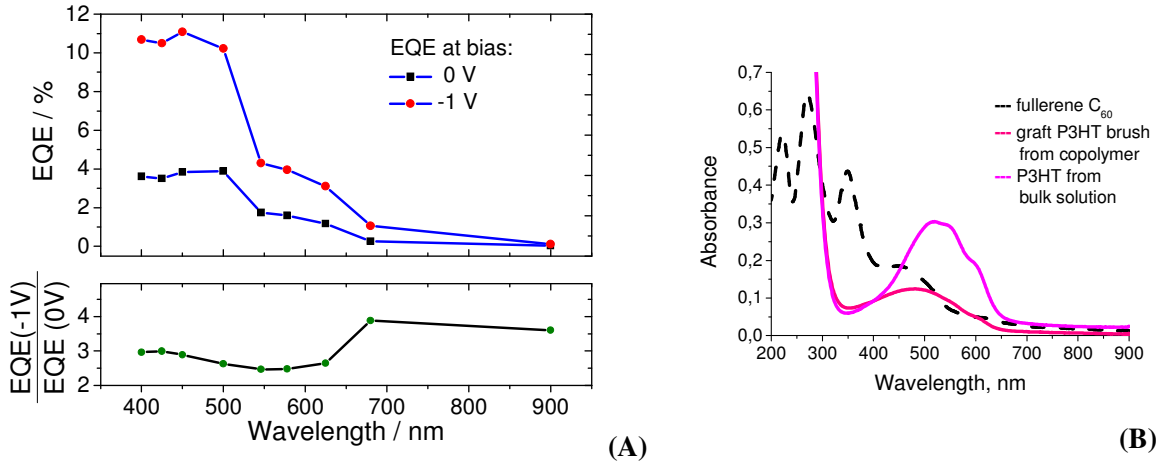

Figure 6.38. *Photocurrent spectral response (EQE, external quantum efficiency) of solar cells based on ITO/P4VP-b-PS-I-graft-P3HT brush/C_{60}/BPhen/Al structure. The graph shows: (a) the external quantum efficiency at a bias of 0V and –1V, while the lower graph shows their ratio, (b) the absorbance of a deposited fullerene C_{60} (20 nm) thin film, graft-P3HT brush from P4VP-b-PS-I copolymer and coated HT-P3HT.*

[145] Saturation *(Sat.)*=$I_{(at\ -1V)}/I_{(at\ 0\ V)}$=*-0.77/-0.12=6.47.*

Fig. 6.38b shows the absorption of fullerene C_{60} thin film with a thickness of 20 nm and absorption of HT-P3HT and graft-P3HT brush from P4VP-PS-I copolymer. The external quantum efficiency (EQE) of the device with the P3HT brush architecture was measured at a bias of 0V (under short current) and wavelength of 450 nm, and is 3.8%. The shoulder at 580 nm shows an EQE of 1.5%. The external quantum efficiency at a bias of –1V has an EQE are 11.09% at 450 nm and 4% at 580 nm.

The lower graph (Fig. 6.38a) shows the ratio of the EQE at –1V and at 0V bias. The EQE at zero bias shows a maximum at around 480 nm and shoulder at 600 nm. The EQE shows similar features compared to the absorbance of the C_{60} thin film. The EQE at bias of –1V is higher by a factor of about 3 (upper graph) than at bias of 0V, but does not show any significant different features in the spectrum.

The results measured for the second type of solar cell based on ITO/PEDOT:PSS/ P4VP-*b*-PS-I-*graft*-P3HT brush/C_{60}/BPhen/Al structure is presented in Fig. 6.39. The device shows a short-circuit current density (I_{SC}) of 0.83 mA/cm^2, V_{OC} of 0.22 V, and a calculated filling factor (FF) of 24. The dark characteristic shows a nearly linear behavior. The inset shows the same sample in a broader voltage range (from -2V to 2V). Here, a diode-like *I-V*-characteristic is observed. The comparatively high gradient in the dark characteristic points towards a low parallel resistance. Power conversion efficiencies of 0.04%[146] were achieved under the illumination of simulated sunlight (AM 1.5, 108 mW/cm^2).

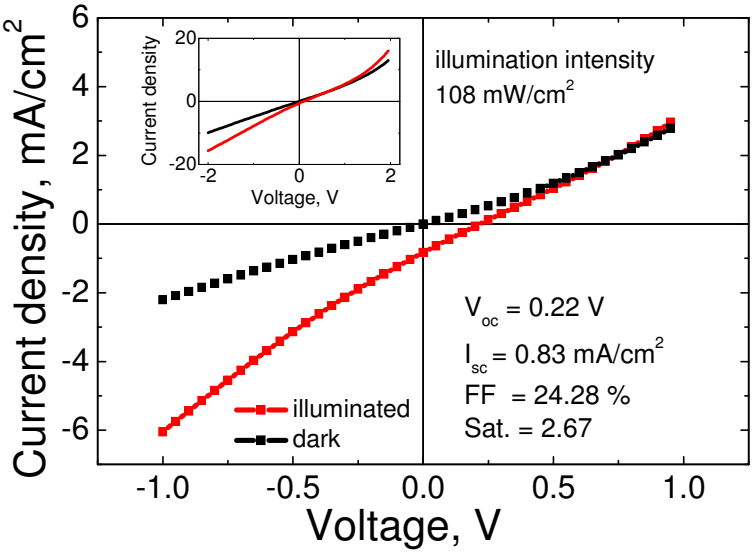

Figure 6.39. *The current density–voltage (I-V) characteristics of solar cells based on ITO/PEDOT:PSS/P4VP-b-PS-I-graft-P3HT brush/C_{60}/BPhen/Al structure.*

[146] $\eta=(V_{oc}\times I_{sc}\times FF)/P_{in}=(0.83\ mA/cm^2\times 0.22\ V\times 24\%)/108\ mW/cm^2=0.04\ \%$. Saturation $(Sat.)=I_{(at\ -1V)}/I_{(at\ 0\ V)}=-6.16/-2.30=2.67$.

Fig. 6.40 presents the external quantum efficiency of the second type of the solar cell device based on the ITO/PEDOT:PSS/P4VP-*b*-PS-I-*graft*-P3HT brush/C_{60}/BPhen/Al structure. The external quantum efficiency measured at an applied voltage of 0V shows a maximum at 425 nm of 20% and a local maximum of 10% at 550 nm. The same feature appears in the external quantum efficiency measured at an applied voltage of –1V and was found to be 75% at 425 nm and 40% at 550 nm.

The lower graph shows the ratio of EQE at a bias of –1V and 0V. The EQE shows maximum at around 430 nm and 550 nm, and a shoulder at 600 nm. The shape of the spectrum is not changed significantly when a voltage of –1V is applied. This values of ration EQE (-1V) and EQE (0V) increase by a factor of 3.3

Comparing the EQE of Fig. 6.40 with the absorption of C_{60} in Fig. 6.38b, the maximum at 550 nm is missing. It is means that the photocurrent in not entirely caused by the absorption of C_{60}, but can be related to the absorption of P3HT absorbed at 550-600 nm which as can be seen in Fig. 6.38b.

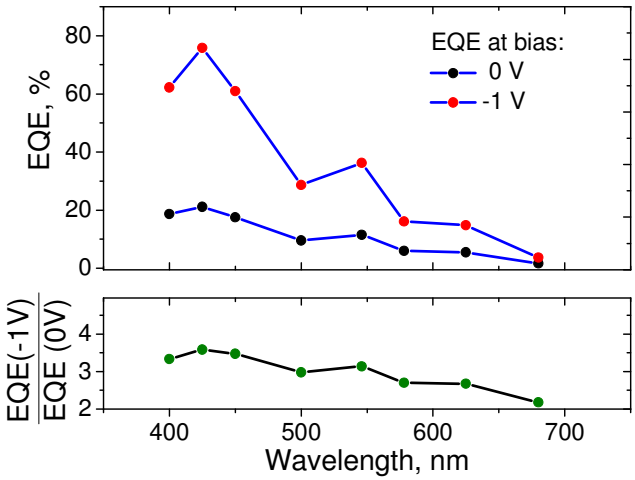

Figure 6.40. *Photocurrent spectral response (EQE, external quantum efficiency) of solar cells based on ITO/PEDOT:PSS/P4VP-b-PS-I-graft-P3HT brush/C_{60}/BPhen/Al structure.*

In conclusion, it was demonstrated that the polymer brush layers are suited for use in electronic devices such as photovoltaic. We shown that polymer brush layer can be use as a hole-accepting component for a hybrid photovoltaic device. Unfortunately, we did not observe such a high charge collection efficiency with our polymer brush layer as reported in literature for spin-coated P3HT layers[147]. The main problem is the structure of the solar cell based on grafted P3HT brush from P4VP-*b*-PS-I copolymer. The P4VP-*b*-PS-I-*graft*-P3HT brushes display poor photovoltaic properties due to

[147] For ex.: a) the power efficiency of the device with P3HT:PCBM is 2.19% (I_{SC} = 6.69 mA/cm^2; V_{OC} = 0.61 V; FF = 53.14 %). Shrotriya, V.; Li, G.; Yao, Y.; Moriarty, T.; Emery, K.; Yang, Y., Adv. Funct. Mater. 2006, 16, 2016–2023. (b) the power efficiency of the device of P3HT:PCBM is 3.5% as reported by Sariciftci (ref. 68).

their penetrated network structure, which seems improper for charge-separation. The main drawbacks are first the existence of an at least 0.5 nm thick insulating P4VP layer. Second, the orientation of the P3HT graft chains parallel to the interface as predicted in Fig. 6.31. The third is that a low molecular weight of P3HT graft chains can limit the charge carrier mobility.

The second type of solar cell which has an additional hole-transport PEDOT:PSS layer shows a better power efficiency (η) and higher external quantum efficiencies (EQE) compared to the first type of solar cells.

Despite all those problems, the polymer structures developed herein are attractive materials for the manufacturing of regenerable sensors in which surface-tethered conjugated polymers with conformation-dependent properties will act as transducers converting (bio)chemical signals into optical ones. Our preliminary investigations demonstrate that the surface-initiated KCTP could be extended to other, more functional kinds of monomers (i.e., 2-bromo-5-chloromagnesio-3-bromohexylthiophene).

6.10 EXPERIMENTAL PART

Materials. *tert*-butylmagnesium chloride (2.0 M solution in THF), tetrakis(triphenylphosphin)-nickel(0), 4-bromostyrene, octadecyltrichlorsilane, 3-chloropropyltrimethoxysilane, poly-N-isopropylacrylamide (PNiPAM), methylenbisacrylamide (MBA), hydroxyethylmethacrylate (HEMA), acrylamide (AA), *N*-bromosuccinimide, *N*-iodosuccinimide, acethylacetic acid, bromobenzene, iodobenzene, *o*-bromotoluene, nitrobenzene, iod, iodic acid, hexane, methanol, ethanol, toluene and dry tetrahydrofuran (stabilizer-free, anhydrous) were purchased from Aldrich and used as received without further purification. Poly(glycidyl methacrylate) (M_n=65000 g/mol, PDI=2.05) was purchased from Polymer Source Inc. Poly(4-bromostyrene) (M_n=51000 g/mol, PDI=2.05) was obtained via radical polymerization of 4-bromostyrene[148]. Two samples of poly(4-vinylpyridine)-*block*-polystyrene (P4VP-*b*-PS) were purchased from Polymer Source Inc.: sample-I, further designated as $P4VP_{25}$-*b*-PS_{350}, M_{nP4VP}=2700 g/mol, M_{nPS}=36700 g/mol, PDI=1.08; sample-II, further designated as $P4VP_{75}$-*b*-PS_{313}, M_{nP4VP}=8000 g/mol, M_{nPS} =32900 g/mol, PDI=1.06. 2-Bromo-3-hexyl-5-iodothiophene and 2-bromo-5-chloromagnesio-3-hexylthiophene (**1a**) were prepared as previously described[36,37,93].

Preparation of 2-bromo-3-hexylthiophene. 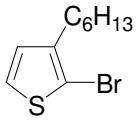

[148] Yoshida, E.J., *Polym. Sci., A,* **1996**, 34, 2937.

N-Bromosuccinimide (5.29 g, 29.7 mmol) was added to a stirred solution of 3-hexylthiophene (5.00 g, 29.7 mmol) in a mixed solution of $CHCl_3$ (15 ml) and acethylacetic acid (15 ml) at 0 ºC. The mixture was stirred at 0 ºC overnight. After addition of water, the mixture was extracted with $CHCl_3$. The organic layer was washed successively with 10% aqueous NaOH, and water, and dried over anhydrous $MgSO_4$. After filtration, the solvent and 2-bromo-3-hexylthiophen were removed by evaporation under reduced pressure. Then the monomer was purified by silica gel column chromatography (eluent: hexane) to release the uncolored liquid. ^{1}H NMR (500 MHz, $CDCl_3$): δ 7.17 (d, *J*=5.4 Hz, 1H), 6.79 (d, *J*=5.4 Hz, 1H), 2.55 (t, *J*=7.6 Hz, 2H), 1.57 (quint, *J*=7.4 Hz, 2H), 1.31 (m, 6H), 0.88 (t, *J*=6.7 Hz, 3H).

Preparation of 2-bromo-3-hexyl-5-iodothiophen.

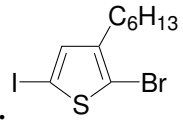

N-Bromosuccinimide (2.76 g, 12.5 mmol) was added to a stirred solution of 2-bromo-3-hexylthiophene (2.53 g, 10.2 mmol) in a mixed solution of the $CHCl_3$ (15 ml) and acetylacetic acid (15 ml) at 0 ºC. The mixture was stirred at room temperature overnight. Then 10% aqueous NaOH was added, and the mixture was extracted using chloroform. The organic layer was washed with water and dried over anhydrous $MgSO_4$. After filtration, the solvent and 2-bromo-3-hexyl-5-iodothiophen were removed by evaporation under reduced pressure. The residue was purified by silica gel column chromatography (eluent: hexane) to give a product of pale yellow oil (7.35 g, 97%). ^{1}H NMR (500 MHz, $CDCl_3$): δ 6.95 (s, 1H), 2.51 (t, *J*=7.7 Hz, 2H), 1.53 (quint, *J*=7.4 Hz, 2H), 1.29 (m, 6H), 0.88 (t, *J*=6.6 Hz, 3H).

Preparation of 2-bromo-3-hexyl-5-bromomagnezium-thiophene (1a).

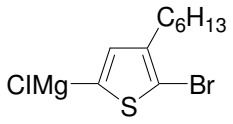

All glass apparatus were dried prior to use. The reagents were combined into a reaction flask and the withdrawal of a small aliquot of the reaction mixture for analysis was carried out via a syringe from the three-way stopcock with a stream of nitrogen. A round-bottomed flask equipped with a three-way stopcock was heated under reduced pressure, then, cooled to room temperature under argon atmosphere. 2-Bromo-3-hexyl-5-iodothiophene (559 mg, 1.50 mmol) was placed in the flask, and the atmosphere in the flask was replaced with argon. Dry THF (20 ml) was added to the flask via a syringe, and the mixture was stirred at 0 ºC. *t*-BuMgCl (2.0 M solution in THF, 0.825 ml, 1.6 mmol) was added via a syringe, and the mixture was stirred at 0 ºC for 1 h.

The preparation of 2-bromo-3-octylthiophene, 2-bromo-3-dodecylthiophene, 2-bromo-3-octyl-5-iodothiophen, 2-bromo-3-dodecyl-5-iodothiophen has been the same as shown before.

Preparation of the low molecular weight initiator (2)[149].

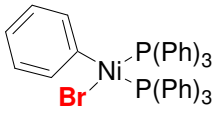

To a solution of $Ni(tpp)_4$ (222 mg, 0.2 mmol) in dry toluene (3.5 ml, glove-box, argon atmosphere) bromobenzene (0.1 ml, 0.95 mmol) was added at room temperature. The homogeneous mixture was stirred for 15 min and was then allowed to stand unperturbed overnight. The original deep red color of the reaction mixture gradually changed to brownish-yellow following the precipitation of **2** in form of brownish-yellow crystals, which were separated by filtration, washed with dry hexane and dried in vacuum. Yield: 0.07 g, 47%.

Preparation of the low molecular weight initiator (3).

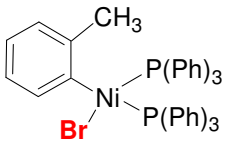

To a stirred mixture of $Ni(tpp)_4$ (470 mg, 0.47 mmol) and dry toluene (7.5 ml, glove-box, argon atmosphere) was added *o*-bromotoluene (0.29 ml, 1.90 mmol) was added at room temperature. After stirring the solution for 10–20 min., the homogeneous solution obtained was allowed to stand undisturbed for overnight. The original deep red color of the reaction mixture gradually changed to brownish-yellow together with the precipitation of **3** in form of brownish-yellow crystals, which were separated by filtration, washed with dry hexane and dried in vacuum. Yield: 0.12 g, 40%.

Preparation of the low molecular weight initiator (4).

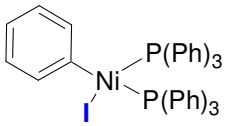

4 was prepared as brown solid according to the protocol above for (**3**) from $Ni(tpp)_4$ (470 mg, 0.45 mmol), iodobenzene (0.59 ml, 0.53 mmol), and toluene (10 ml), it formed Yield: 0.15g, 50%.

Iodination of P4VP-*b*-PS. In a 25 ml one-necked round-bottomed flask equipped with a magnetic stir bar and reflux condenser 0.56 g of $P4VP_{25}$-*b*-PS_{350} or 0.65 g of $P4VP_{75}$-*b*-PS_{313} (0.005 mol of styrene monomer units) was dissolved in 15 ml of nitrobenzene and then 0.51 g (0.002 mol) iodine, 0.19 g (0.001 mol) iodic acid and 1 ml ~66% solution of H_2SO_4 was added and the mixture was heated at 90 °C for 35 hours. Afterwards, the mixture was poured into 200 ml of methanol and white precipitate was collected by filtration, washed with 10 ml of 10% $NaHSO_3$ solution, copious amounts

[149] Hidai, M.; Kashiwagi, T.; Ikeuchi, T.; Uchida, Y., *J. Organometal. Chem.,* **1971,** 30, 279-282.

of water, methanol and finally dried in vacuum at 60 °C giving ~1.0 g (>80%) of pale yellow solid of iodinated products designated as $P4VP_{25}$-*b*-$PS(I)_{350}$ and $P4VP_{75}$-*b*-$PS(I)_{313}$[150].

LOW TEMPERATURE POLYMERIZATION

2-Bromo-3-hexyl-5-iodothiophene (373 mg, 1 mmol) was placed in a round-bottomed flask equipped with a magnet stirrer bar, and the atmosphere was replaced with argon. Dry THF (20 ml) was added via a syringe, and the mixture was cooled to 0 °C. Afterwards, *tret*-butylmagnesium chloride (2.0 M solution in THF, 0.50 ml, 1.0 mmol) was added via a syringe, and the mixture was stirred at 0 °C for 1 h. A solution of **3** in toluene (26.4 mg in 1 ml, 3.56 mol %) was added via a syringe at 0 °C and then the mixture was stirred for 6 h at 0 °C. The reaction mixture was quenched by 5 M hydrochloric acid and the products were extracted with $CHCl_3$. The organic layer was washed with water, dried over anhydrous $MgSO_4$ and concentrated under reduced pressure. Finally, MeOH was added to the residue, the insoluble material was washed with MeOH and collected by filtration under vacuum to give pure P3HT as a purple solid (122 mg, 74%).

KINETIC STUDY

2-Bromo-3-hexyl-5-iodothiophene (559 mg, 1.5 mmol) and naphthalene (11 mg, 0.08 mmol) as an internal standard were placed in a round-bottomed flask equipped with a magnet stirrer bar, and the atmosphere was replaced with argon. Dry THF (20 ml) was added via a syringe, and the mixture was cooled to 0 °C. Afterwards, *tret*-butylmagnesium chloride (0.825 M solution in THF, 1.0 ml, 1.65 mmol) was added via a syringe, and the mixture was stirred at 0 °C for 1 h. Afterwards the first portion of the reaction mixture (1 ml) was sampled, quenched with 5 M HCl, extracted with $CHCl_3$, dried over anhydrous $MgSO_4$, and concentrated under reduced pressure. The analysis of this fraction by ^1H NMR gave the information about the conversion of 2-bromo-3-hexyl-5-iodothiophene into the monomer **1a**, which was near complete in our experiment. Then a solution of bis(triphenylphosphine)ortho-tolylbromonickel(II) prepared from $Ni(tpp)_4$ and *o*-bromotoluene in toluene (12.5 mg in 4 ml, 0.0165 mmol, 1.11 mol %) was added via a syringe at 0 °C and the mixture was stirred at 0 °C. To follow the reaction course we sampled additional 7 portions of the reaction mixture (1 ml) on 1st, 10th, 30th, 60th,

[150] Braun, D., *Macromol. Chem.,* **1959**, 30, 85-95.

95th, 125th, 155th minutes of the reaction. Each sample was immediately quenched with 5 M HCl, extracted with $CHCl_3$, dried over anhydrous $MgSO_4$, and concentrated under reduced pressure.

The analysis of these fractions by ^1H NMR allowed a precise measure of the monomer conversion by integrating and comparing the signals at 7.18 ppm assigned to hydrolyzed monomer and the signals around 6.90–7.05 corresponding to P3HT. Afterwards, the same seven fractions were repeatedly washed with MeOH, and insoluble P3HT was collected by filtration under vacuum. An analysis of the ^1H NMR spectra of the purified fractions allowed estimating the molecular weight by integration and comparison of the peaks at 6.82-6.90 and 2.55-2.65 ppm, corresponding to the aromatic and aliphatic protons of the last monomer unit of the polymer with the peaks at 6.98 and 2.75-2.85 ppm corresponding to all other (internal) repeat units of the polymer. A valuable information was also obtained from the analysis of the peaks corresponding to the starting aromatic group of the polymer (especially at 2.49 ppm, s, 3H corresponding to methyl of the starting *o*-tolyl moiety). The highest conversion achieved in this experiment (reaction time is 155 minutes) was only 43%. At this conversion, the polymer precipitated and polymerization was terminated. However, in other polymerization experiments conversions up to 100% at DP=30 were achieved even at 0 °C without precipitation of the products, using lower feed ratio.

GRAFTING OF P3HT

Highly polished Si-wafers (Wacker-Chemitronics) or glass slides (Menzel-Glaser) were first cleaned in an ultrasonic bath three times for 5 min with dichloromethane, placed in cleaning solution (prepared from NH_4OH and H_2O_2) for 1 h, and finally rinsed several times with Millipore water (18 MQxcm).

Poly(glycidyl methacrylate) (PGMA) layers of the same 2 nm thickness (ellipsometry data) were used in all experiments as adhesion promoter between PS-Br and Si-substrates. It was deposited by spin-coating from chloroform (0.03 mg/ml, 2000 rpm) and the samples were annealed at 150 °C during 10 hours in argon atmosphere. PS-Br layers with variable thicknesses from 1 to 200 nm were spin-coated onto PGMA from $CHCl_3$ and cross-linked upon a brief irradiation (from 5 to 200 seconds, depending on the PS-Br thickness) with UV-light to achieve their insolubility, while keeping the films still swellable in “good” solvents for PS-Br. The samples were extensively rinsed with THF, dried and placed into a round-bottomed flask equipped with a septum, and the atmosphere was replaced with argon. Afterward, a solution of $Ni(tpp)_4$ in dry toluene (0.05 weight %, 10 ml) was added to the flack via a syringe, and the samples were allowed to react overnight at room temperature. The samples were

then repeatedly washed in the glove-box with dry and deoxygenated THF to remove the excess of unreacted $Ni(tpp)_4$. Therefore, the reaction mixture was removed by the syringe and the new portion of THF was added to the flask to fully cover the samples, stirred for a few minutes and then removed. Finally, the 15 mmol/L solution of the monomer **1a** in dry THF was added and the samples were allowed to polymerize at 0 °C for 10 h to achieve a maximal thickness of the grafted P3HT. Whatever the thickness of the initiating layer, the resulting composite films were very robust against delamination upon extensive rinsing with various organic solvents in an ultrasonic bath and a Soxhlet apparatus. This unambiguously proves the covalent grafting of P3HT[151].

COATING OF HT P3HT FILMS ON TO GLASS OR ITO SUPFACES

Regioregular HT P3HT was prepared via KCTP at low temperature polymerization. The molecular weights of HT P3HT are M_w=7600 and M_n=6000 with a polydispersity (PD) index (M_w/M_n) of 1.26. The concentration of polymer solution is 0.4 mg/ml (2 mg of polymer was dissolved in 5 ml of chloroform). The polymer solution was coated on to the glass or to the ITO-glass surface. The thickness of coated HT P3HT film was measured with AFM and found to be 200 nm.

GRAFTING OF P3HT FROM PATTERNED SUPFACES

Unstructured films. To prepare homogeneous films, $P4VP_{25}$-*b*-$PS(I)_{350}$ was deposited by spin-coating from chloroform (1 mg/ml, 2000 rpm) onto Si-wafers or glass slides and the samples were annealed at 150 °C during 10 hours in argon atmosphere. An excess of $P4VP_{25}$-*b*-$PS(I)_{350}$ was washed away by chloroform. The typical thickness for the grafted $P4VP_{25}$-*b*-$PS(I)_{350}$ films is 8 nm. Although the grafting is provided by physiosorption of the P4VP block, the films were found to be fairly stable. AFM reveals smooth feature-less surface with RMS~0.3 nm.

Prior to the grafting of P3HT, the samples were extensively rinsed with THF, dried and placed into the round-bottomed flask equipped with a septum, and the atmosphere was replaced with argon. Afterwards, a solution of $Ni(tpp)_4$ in dry toluene (0.05 weight %, 10 ml) was added to the flask via a syringe, the samples were allowed to react overnight at room temperature. The samples were then

[151] Several control experiments revealed that all preparation steps during the grafting of P3HT are essential. For example, when the catalyst-immobilization-step was omitted and, instead, the catalyst $Ni(dppp)Cl_2$ or $Ni(tpp)_4$ was added into the bulk solution of the monomer **1a**, no grafting of P3HT was observed and only unattached P3HT was isolated. The same result (no grafting) was observed when the -Br group of the anchoring PS-Br was converted into -MgCl one (by a prolonged reaction with *t*-BuMgCl solution), and afterwards the polycondensation of **1a** was performed in the presence of either $Ni(dppp)Cl_2$ or $Ni(tpp)_4$.

repeatedly washed in the glove-box with dry and deoxygenated THF to remove the excess of unreacted $Ni(tpp)_4$. For this, the reaction mixture was removed by the syringe and a new portion of THF was added to the flask to fully cover the samples, stirred for a few minutes and then removed. Finally, the 15 mmol/L solution of the monomer **1a** in dry THF was added and the samples were allowed to polymerize at 0 °C for 10 h to achieve a maximal thickness of grafted P3HT. The resulting composite films are very robust against delamination, even upon extensive rinsing with various organic solvents in an ultrasonic bath and a Soxhlet apparatus.

Microstructured films. $P4VP_{25}$-*b*-$PS(I)_{350}$ microstructures were prepared by a variant of colloidal lithography. Hydrogel particles were prepared by precipitation-polymerization of PNIPAM and MBA cross-linker and used as a mask. The particles were arranged on Si-wafers by deep coating. Afterwards, the samples were treated by octadecyltrichlorsilane (0.4% solution in toluene) to hydrophobize the surface between the particle. In the next step, the particles were removed by ultrasonocation at 50-60 °C in the acetone/water mixture for 15 minutes and then dried. When the particles were successfully removed by ultrasonic bath, the appearing holes were silanizated with 3-chloropropyltrimethoxysilane from the gas phase. Then the chloroform solution of $P4VP_{25}$-*b*-$PS(I)_{350}$ was spin-coated and the nitrogen of the copolymer was reached with 3-chloropropyltrimethoxysilane by annealing at 130 °C in vacuum overnight. Each step of the micropatterning was monitored by ellipsometry and AFM.

Nanostructured films. To prepare a micellar dispersion, $P4VP_{75}$-*b*-$PS(I)_{313}$ was dissolved in hot toluene (1 g/L) and allowed to equilibrate at room temperature at least for one week. Afterwards, the micelles were arranged by spin-coating (2000 rpm) and the samples were annealed at 150 °C during 10 hours in argon atmosphere. The samples were extensively rinsed with chloroform and further investigated. AFM revealed quasi-periodic nanostructures with a height of undulations of ~6 nm and a mean distance between centers of the micelles of ~45 nm. P3HT was grafted as described in a previous section.

DRY STATE ELLIPSOMETRY THICKNESS MEASUREMENTS

The thickness of the polymer layers in the dry state was measured by an SE400 ellipsometer (SENTECH Instruments GmbH, Germany) with a 632.8 nm laser at a 70° incident angle. A multilayer model has been used for the calculation of the thickness of the multi-component polymer films from the ellipsometric angles ψ and Δ. Initially, the thickness of the native SiO_2 layer was calculated at the refractive indices n=3.858 and n=1.4598 for the Si-wafer and the SiO_2 layer, respectively. The thickness of the PGMA layer was evaluated using the two-layer model Si/SiO_2/PGMA with n=1.525

for PGMA. The thickness of the PS-Br layer was evaluated using the three-layer model Si/SiO_2/PGMA/PS-Br with n=1.63 for PS-Br. Since there was no option for the incorporation of a fourth layer in the program package, the thickness of the grafted P3HT layer was evaluated using the three-layer model, Si/SiO_2/(PGMA+PS-Br)/P3HT with n=1.99 for P3HT. In this model we considered PGMA+PS-Br as a single layer with the n value averaged according to the relative contribution of the PGMA and the PS-Br components. In most cases, PS-Br was a major component and therefore n was close to 1.63. The measurements were averaged for at least 10 points per sample.

The thickness of the P4VP-*b*-PS-I layer was evaluated using the two-layer model Si/SiO_2/ P4VP-*b*-PS-I with n=1.6 for P4VP-*b*-PS-I. The thickness of the grafted P3HT layer was evaluated using the three-layer model, Si/SiO_2/P4VP-*b*-PS-I/P3HT with n=1.99 for P3HT. The measurements were averaged for at least 10 points for each sample.

SWELLABILITY EXPERIMENTS

In order to examine the swelling behavior of the polymer layers in THF and toluene, the measurements were carried out using a null-ellipsometer in a polarizer-compensator-sample analyzer (Multiscope, Optrel Berlin) mode. As light source, a He-Ne laser with λ=632.8 nm was applied, and the angle of incidence was set to 70°. An ellipsometric cell with thin glass walls, fixed at a known angle (68°) from the sample plane, was used[152]. The angle of incidence of the light was set such that its path was normal to the window. The bilayer model (silicon/silicon oxide/swollen polymer film) was used to calculate the thickness of the swollen layer from the ellipsometric angles[153]. As the films displayed in the swollen state a rather large thickness (few hundreds of nm), their refractive index could be determined simultaneously with their thickness.

XPS MEASUREMENTS

The XPS spectra were recorded on an AXIS ULTRA (Kratos Analytical, England) spectrometer using a mono-Al $K\alpha_{1,2}$ X-Ray source operating at 300 W and 20 mA power. Five samples that allow monitoring of all chemical transformations were prepared on PGMA-modified Si-wafers: 1) 40 nm thick PS-Br; 2) 40 nm thick PS-Br, activated with $Ni(tpp)_4$; 3) 40 nm thick PS-Br, activated with $Ni(tpp)_4$ followed by the grafting of 90 nm of P3HT; 4) the sample analogous to 3) followed by Ar-

[152] Houbenov, N.; Minko, S.; Stamm, M., *Macromolecules,* **2003**, 36, 5897-5901.
[153] Azzam, R.M.A.; Bashara, N.M., Ellipsometry and Polarized Light, North Holland, Amsterdam, 1999.

plasma etching of 20 nm in "mild" conditions (see below); 5) the sample analogous to 3), but 30 nm was etched under "hard" conditions.

ARGON PLASMA ETCHING

The argon plasma etching was carried out in a computer-controlled MicroSys apparatus by Roth&Rau (Wüstenbrand, Germany)[154]. A 2.46 GHz microwave plasma (pressure 5×10^{-3} mbar, effective power 100W, sample placed on a grounded holder 200 mm away from the excitation volume of the plasma source) and a 13.56MHz radio frequency plasma (pressure 1×10^{-2} mbar, effective power 100W, sample placed on the driven electrode) were used. In the case of the radio frequency plasma, significant self bias voltages[155] lead to ion energies of several 100eV ,which result in a more intense etching effect compared to the mild conditions of the microwave discharge.

RUTHERFORD BACKSCATTERING SPECTROSCOPY (RBS) MEASUREMENTS

RBS measures the energy of particles elastically scattered from the atoms at or near the target sample surface[156]. It thereby can determine the mass of the scattering centers (the atomic nuclei) from the kinematics (using conservation of momentum), and it determines the depth of the scattering centers in the target from the electronic (inelastic) energy loss. The RBS measurements were performed at Rossendorf-Dresden Forschungszentrum (Germany) using the 3MV Tandetron Accelerator using 1.7MeV He^+ ions with a detector angle of 170°. Usually, the ion beam analysis of polymer layers is challenging, since those materials tend to decompose under the analyzing beam even when they are deposited at backings of good thermal conductivity[157]. Therefore low current densities of <1 nA/mm^2 were used to minimize deterioration of the polymers by the beam. In order to monitor any changes in the layers during the measurement, their spectra were obtained in a sequence of exposures, each taken with a fluency as low as 0.1μC. After each run the beam was shut off and the data were examined and stored separately. When we observed any significant change in the spectra, the last two spectra were discarded and the former ones were summed up to improve the statistics. Then, a fresh spot was

[154] Nitschke, M.; König, U.; Lappan, U.; Minko, S.; Simon, F.; Zschoche, S.; Werner, C., *J. Appl. Polym. Sci.,* **2007**, 103, 100-109.
[155] Köhler, K.; Coburn, J.W.; Horne, D.E.; Kay, E.; Keller, J.H., *J. App. Phys*., **1985**, 57, 59.
[156] (a) Chu, W.K.; Mayer, J.W.; Nicolet, M.A., In Backscattering Spectrometry; Academic Press: NewYork, 1978.; (b) Tesmer, J.R., Nastasi, M., Eds., In Handbook of Modern Ion Beam Analysis; Materials Research Society: Pittsburgh, 1995.
[157] Duggan, J.L.; Morgan, I.L.; Musket, R.G.; Felter, T.E., *Nucl. Instr. Meth. in Phys. Res. B*, **2004,** 379, 219.

brought to the beam position. The program SIMNRA[158] was used to calculate the depth profiles of sulphur and bromine atoms by fitting the simulated spectra to the RBS data.

[158] Mayer, M., SIMNRA, a Simulation Program for the Analysis of NRA, RBS and ERDA, Proceedings of the 15th International Conference on the Application of Accelerators in Research and Industry, J. L. Duggan and I.L. Morgan (eds.), American Institute of Physics Conference Proceedings, 1999, 475, 541.

CHAPTER 7

GENERAL CONCLUSIONS AND OUTLOOK

For the first time, a synthesis of conductive polymer brushes on solid substrates using "grafting-from" method was performed. Regioregular poly(3-alkylthiophenes), P3ATs were in the center of attention. Due to their excellent electrical and optical properties, they are among the most promising conductive polymers for commercial applications. Our new method for their synthesis allows precise control over the nanoscale organization of the conductive polymers, which is strongly desired for accurate construction of organic electronic devices. It is believed that polymer brush architectures can contribute to improvement of the self-assembly properties of conductive polymers. This will greatly improve the adhesion of the polymer layers to the substrate, thus allowing to build more stable devices.

In the course of this work, several approaches for the preparation of polythiophene-based brushes were tested. The most important, from my opinion, finding of this work is that regioregular head-to-tail poly-3-alkylthiophenes – benchmark materials for organic electronics - can be now selectively grafted from appropriately-terminated surfaces to produce polymer brushes of otherwise soluble polymers - the architecture earlier accessible only in the case of non-conductive polymers. In particular, we developed a new method to grow P3ATs via Kumada Catalyst Transfer Polymerization (KCTP) of 2-bromo-5-chloromagnesio-3-alkylthiophene. Exposure of the initiator layers to monomer solutions leads to selective chain-growth polycondensation of the monomers from the surface, resulting into P3AT brushes in a very economical way.

The grafting process was investigated in detail and the structure of the resulting composite film was elucidated using ellipsometry, X-ray Photoelectron Spectroscopy (XPS), Rutherford backscattering spectroscopy (RBS), and Conductive atomic force microscopy (C-AFM). The obtained data suggests that the grafting process occurs not only at the poly(4-bromostyrene), PS-Br/polymerization solution interface, but also deeply inside the swollen PS-Br film, which is penetrable for the catalyst and the monomer. The process results in an interpenetrated PS-Br/P3HT network, in which relatively short poly(3-hexylthiophene), P3HT grafts emanate from long, cross-linked PS-Br chains. We demonstrated how surface structures of non-conductive block copolymers, such as poly(4-vinylpyrridine)-block-poly(4-iodstyrene) (P4VP-b-PS-I), can be converted into (semi)conductive P4VP-b-PS-graft-P3HT chains via surface-initiated polymerization of poly(3-hexylthiophene) (P3HT) from reactive surface-grafted block copolymers. The composite films we prepared show good stability against delamination, solvatochromism, high lateral electrical conductivity in the doped state, and high swellability. All those properties benefit the construction of fully "plastic" electronic devices and sensors.

Nevertheless, it is still a challenging task to synthesize regioregular P3HT brushes of high molecular weight and high grafting density from monolayers of anchoring compounds attached directly to conductive electrodes. These properties will make the polymer brushes attractive for the production of properly ordered semiconducting layers for solar cells. Thus, it is strongly desired to continue developing more efficient catalytic systems that will provide a higher kinetic chain length for polythiophene grafts.

Another method investigated during our work was to covalently graft P3HT to substrates modified by macromolecular anchors using oxidative polymerization of 3-hexylthiophene (3HT) with $FeCl_3$. P3HT layers with variable thicknesses from 30 nm up to 200 nm were produced using two steps of polymerization reaction. However, the P3HT obtained by oxidative polymerization had always an irregular structure, which was a result of the starting monomer being asymmetric, which is undesired for electronic applications.

The third method for the production of conductive polymer brushes was to graft *regioregular* poly(3,3''-Dioctyl-[2,2';5',2'']terthiophene) (PDOTT) by electrochemical oxidative polycondensation of symmetrically substituted 3,3''-Dioctyl-[2,2';5',2'']terthiophene (DOTT). A modification of the supporting ITO electrode by the self-assembled monolayers (SAMs) of compounds having polymerizable head-groups with properly adjusted oxidative potentials was found to be essential to achieve a covalent attachment of PDOTT chains. The polymer films produced show solvatochromism and electrochromism, as well as the previous two methods. Nevertheless, the PDOTT film does not present as brush, but more likely a cross-linked layer.

On the other hand, the polymer structures developed in my thesis would be attractive materials for manufacturing of regenerable sensors in which surface-tethered conjugated polymers with conformation-dependent properties will act as transducers converting (bio)chemical signals into optical ones. Preliminary investigations demonstrate that the surface-initiated polycondensation could be extended onto other, more functional kinds of monomers (i.e., 2-bromo-5-chloromagnesio-3-bromohexylthiophene) leading to surface-tethered poly[3-(6-bromohexyl)thiophene], P3BrHT, easily convertable onto a variety of conjugated polyelectrolytes. Postpolymerization modifications of P3BrHT is a route to highly water-swellable conjugated polyelectrolyte brushes. We believe that utilization of surface-immobilized patterned conjugated polymers for bio-sensing would have technological advantages compared to sensors used dissolved conductive polymers.

APPENDIX

MALDI-TOF.

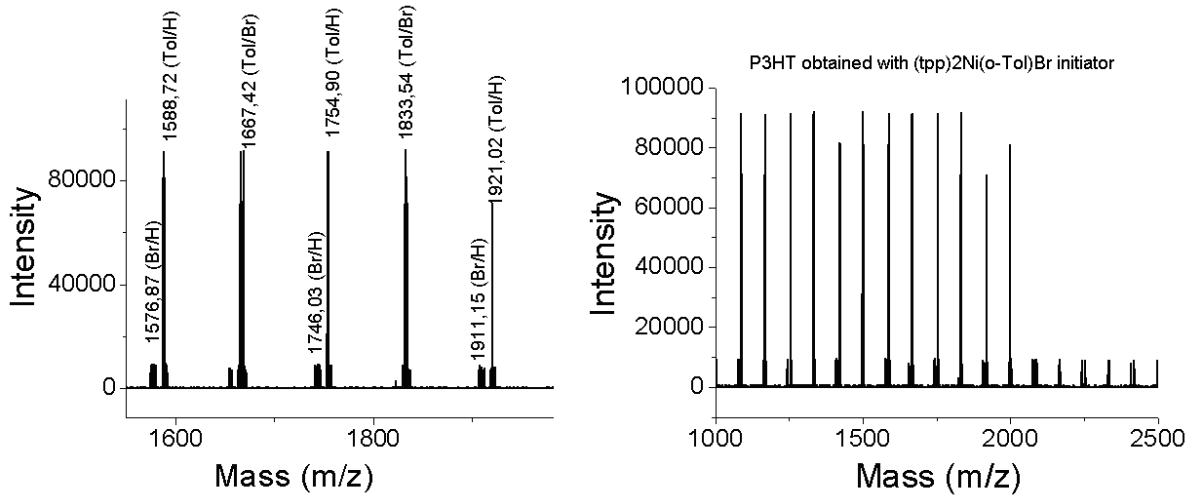

Figure 1. *MALDI-TOF mass spectra of P3HT obtained with* ***1a*** *and 1.65 mol % of $(tpp)_2Ni(o\text{-}Tol)Br$ at 0 °C for 3 hours (conversion of* ***1a****=42%, M_n=5600, M_w/M_n=1.84). The MALDI-TOF spectra of P3HT shows three types of end groups (Ph/H; Ph/Br; Br/H).*

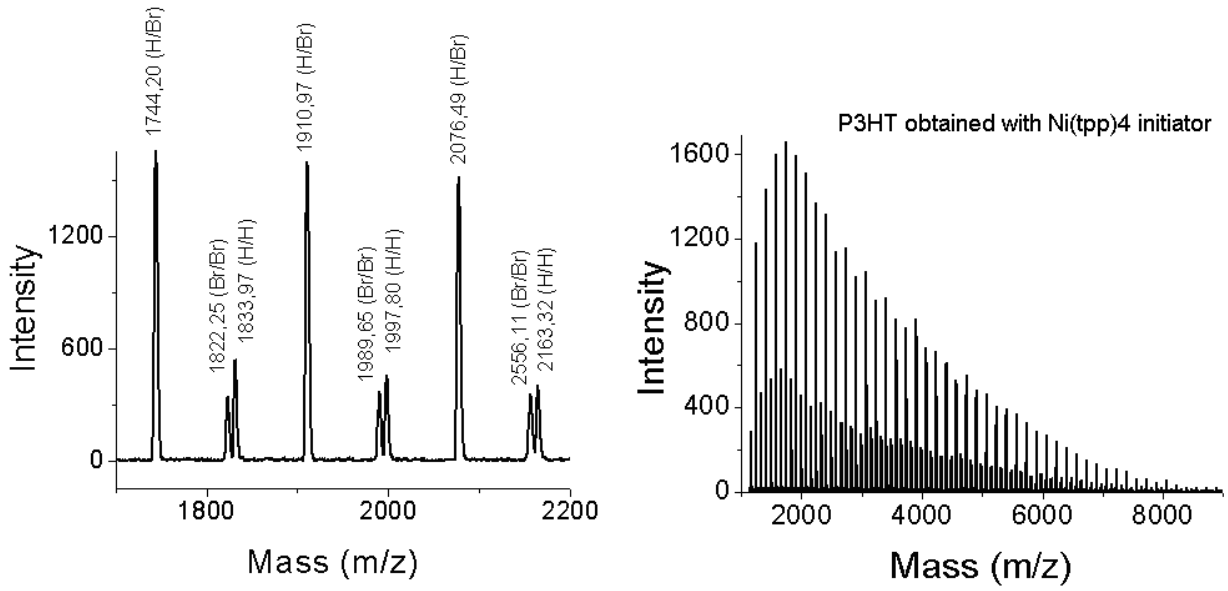

Figure 2. *MALDI-TOF mass spectra of P3HT obtained with* ***1a*** *and 1.65 mol % of $Ni(tpp)_4$ at 0 °C for 3 hours (conversion of* ***1a****=27.5%, M_n=5800, M_w/M_n=2.36). The MALDI-TOF spectra of P3HT show three types of end groups (H/H; Br/Br; Br/H).*

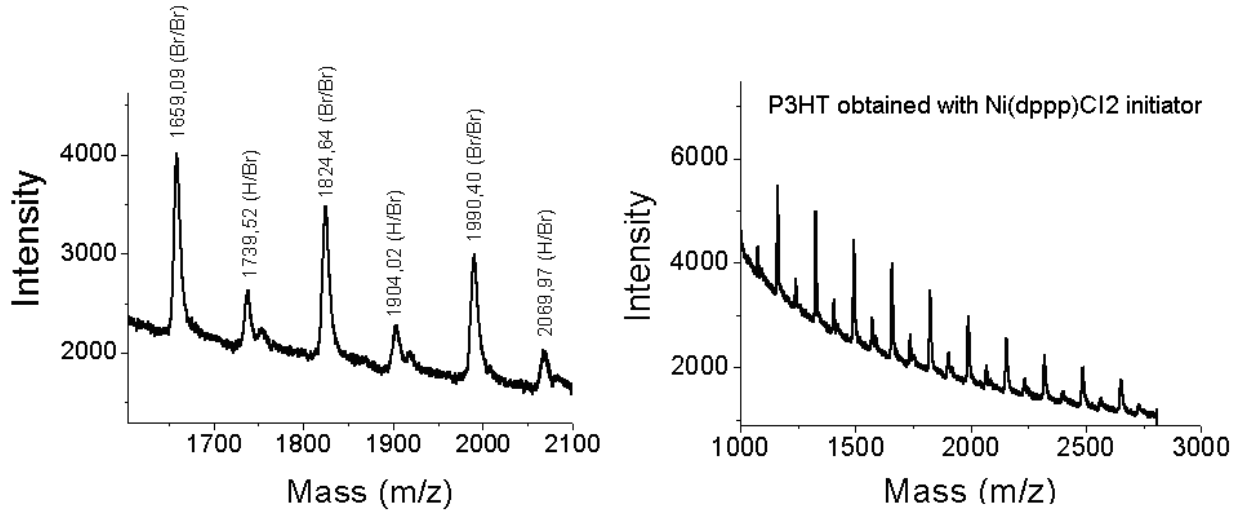

Figure 3. *MALDI-TOF mass spectra of P3HT obtained with* ***1a*** *and 1.65 mol % of Ni(dppp)CI_2 at 0 °C for 3 hours (conversion of* ***1a****=42.2%, M_n=6400, M_w/M_n=1.55). The MALDI-TOF spectra of P3HT show two types of end groups (Br/Br; Br/H).*

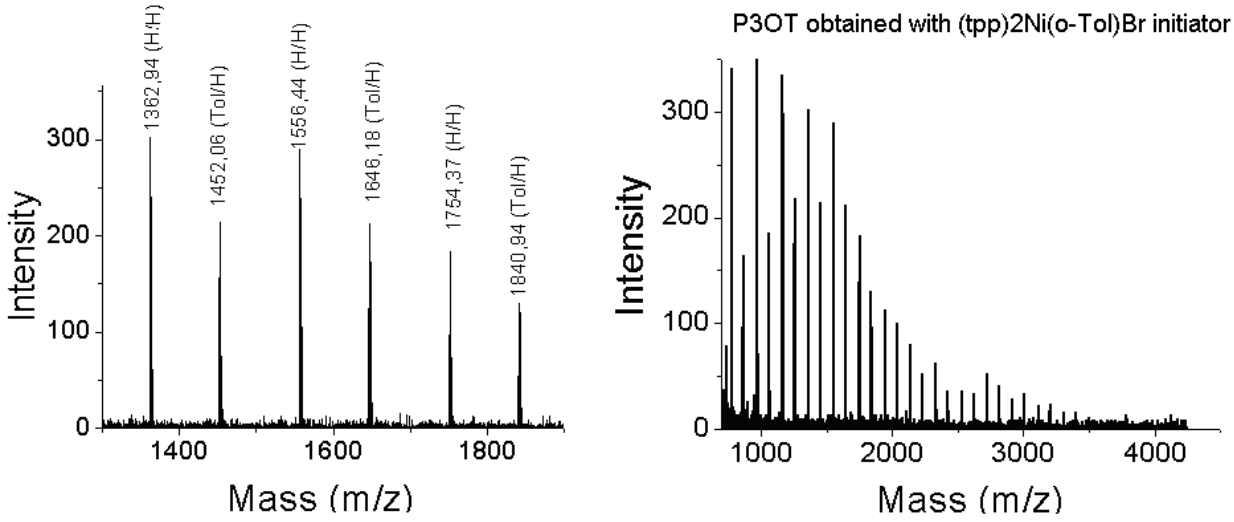

Figure 4. *MALDI-TOF mass spectra of P3OT obtained with* ***2-bromo-3-octyl-5-bromomagnezium-thiophene*** *and 1.65 mol % of $(tpp)_2$Ni(o-Tol)Br at 0 °C for 3 hours (conversion of monomer=87%, M_n=6000, M_w/M_n=1.71). The MALDI-TOF spectra of P3HT show two types of end groups (Ph/H; H/H).*

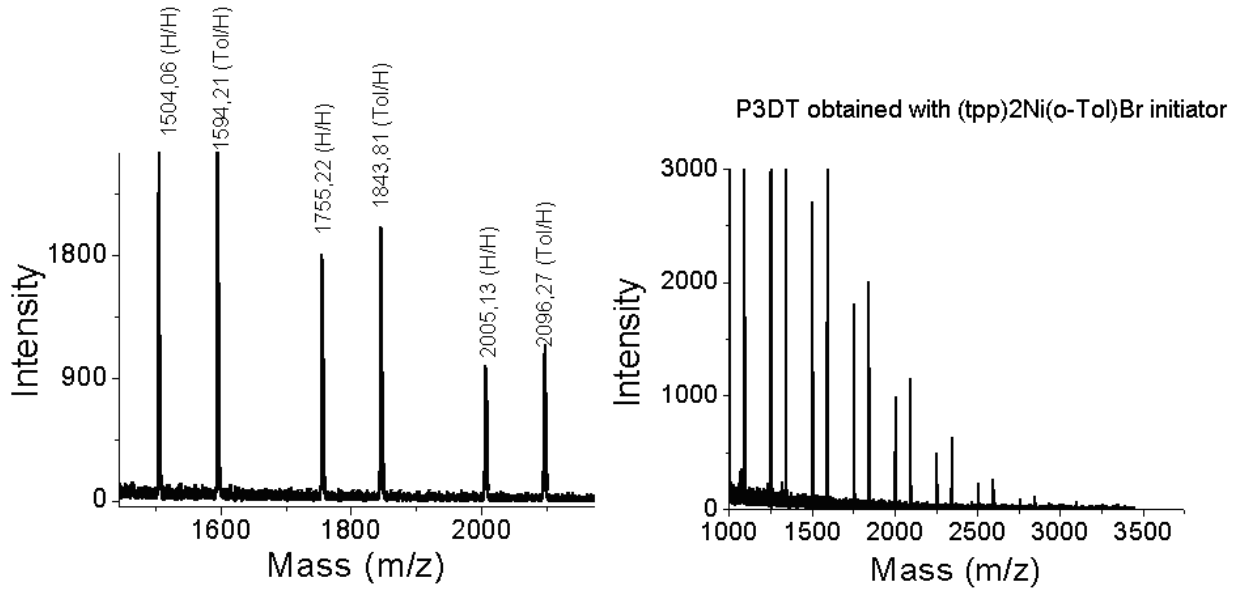

Figure 5. *MALDI-TOF mass spectra of P3DT obtained with* ***2-bromo-3-dodecyl-5-bromomagnezium-thiophene*** *and 1.65 mol % of $(tpp)_2Ni(o\text{-}Tol)Br$ at 0 °C for 3 hours (conversion of monomer=67%, M_n=6800, M_w/M_n=1.80). The MALDI-TOF spectra of P3HT show two types of end groups (Ph/H; H/H).*

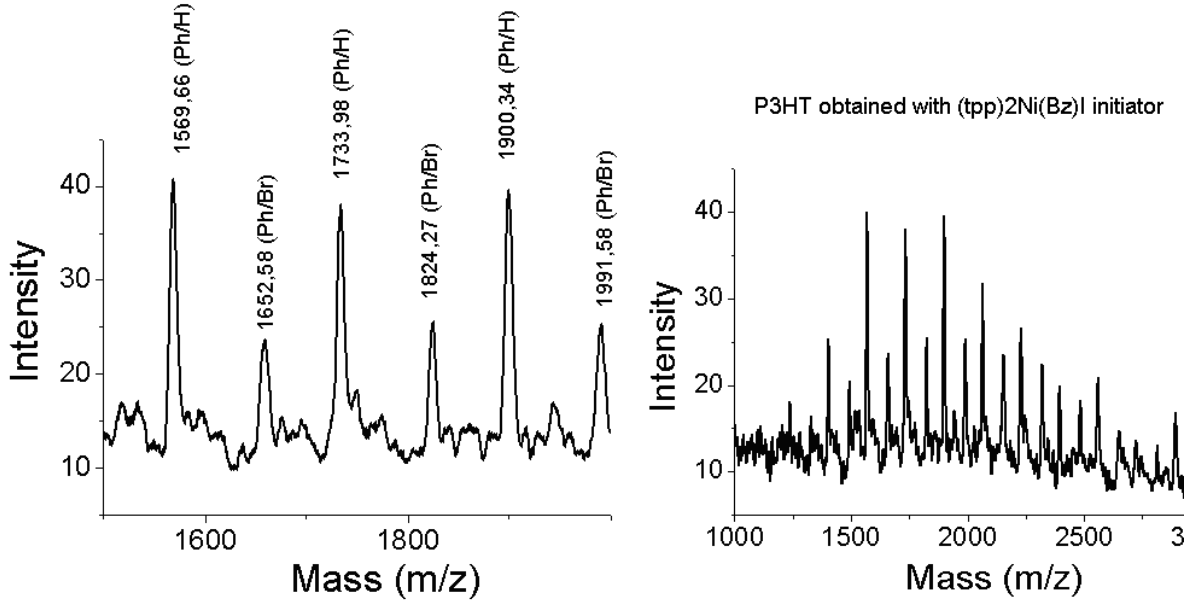

Figure 6. *MALDI-TOF mass spectra of P3HT obtained with* ***1a*** *and 2.09 mol % of $(tpp)_2Ni(Bz)I$ at 0 °C for 3 hours (conversion of* ***1a****=26%). The MALDI-TOF spectra of P3HT show two types of end groups (Ph/H; Ph/Br).*

^{1}H NMR-Spectra of samples.

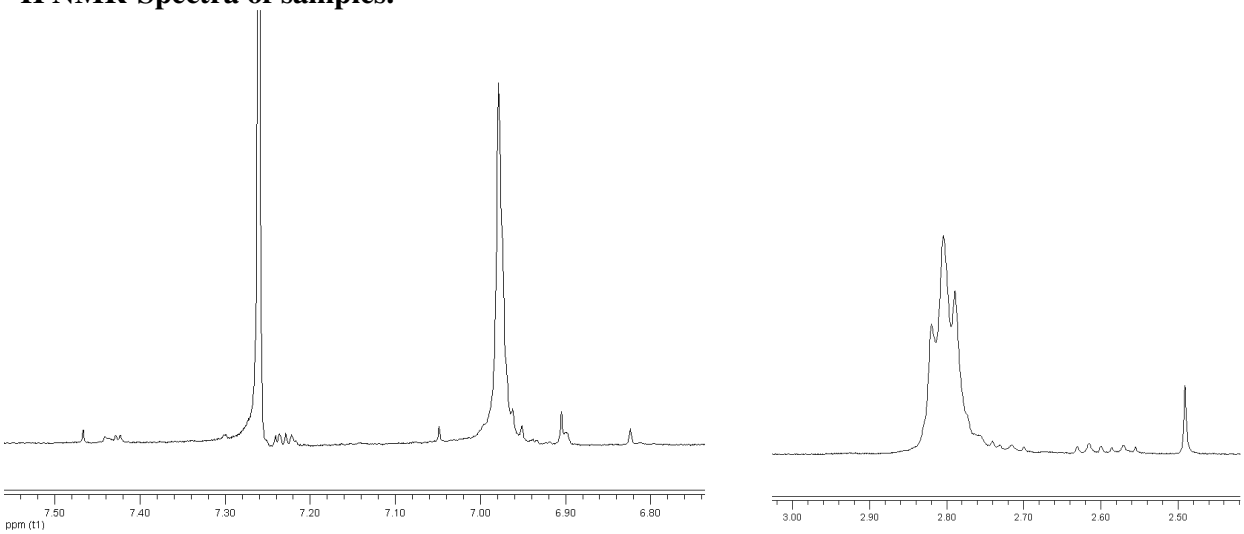

Figure 7. *^{1}H NMR-Spectra of P3HT obtained with $(tpp)_2Ni(o\text{-}Tol)Br$ initiator (MALDI-TOF (Fig. 1)).*

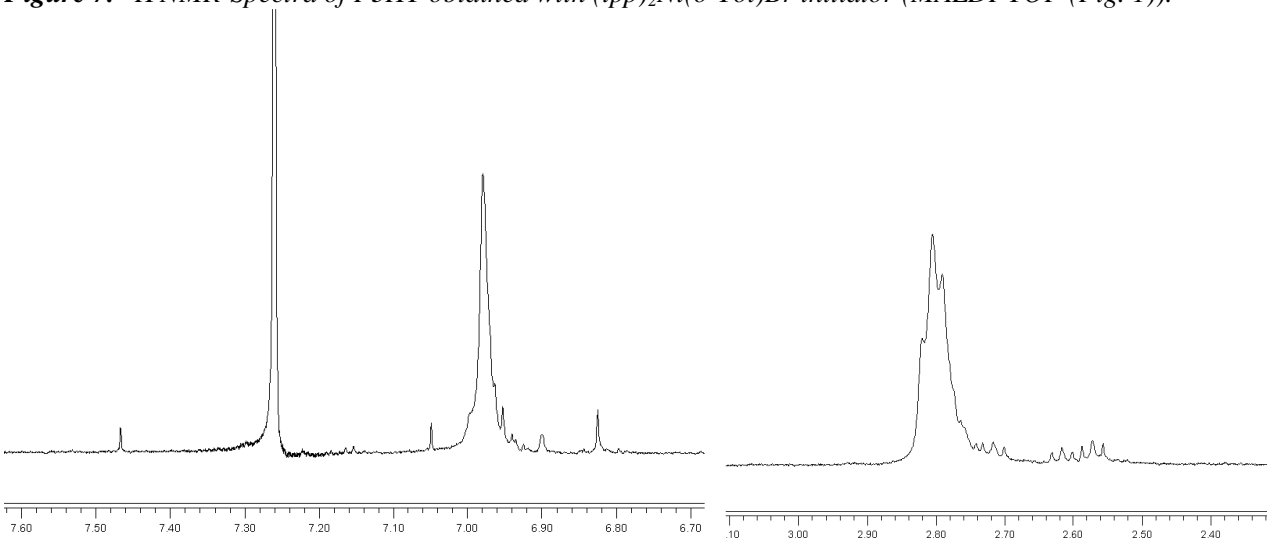

Figure 8. *^{1}H NMR-Spectra of P3HT obtained with $Ni(tpp)_4$ initiator (MALDI-TOF (Fig. 2)).*

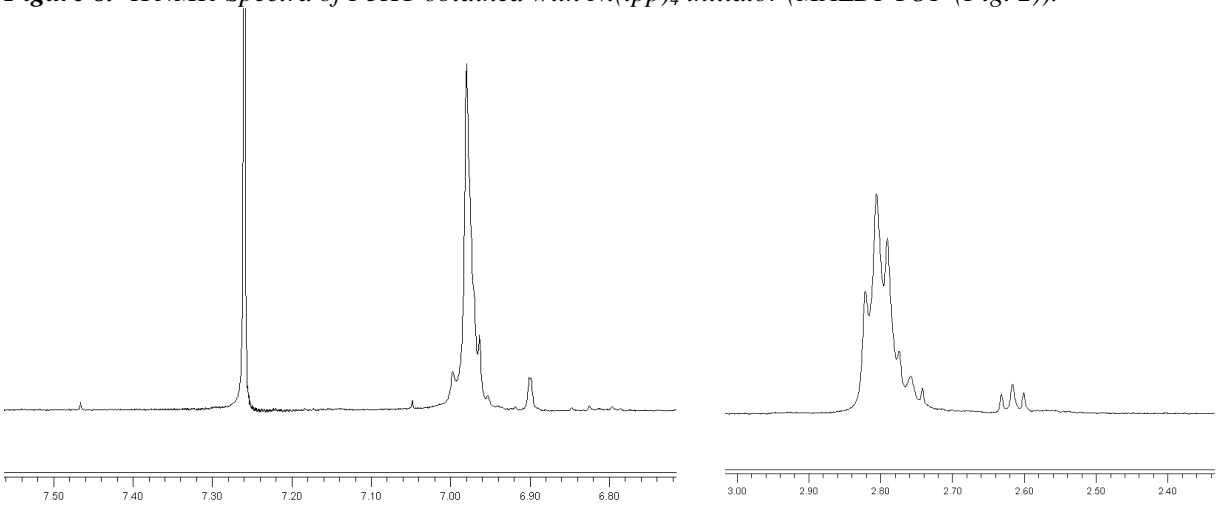

Figure 9. *^{1}H NMR-Spectra of P3HT obtained with $Ni(dppp)CI_2$ initiator (MALDI-TOF (Fig. 3)).*

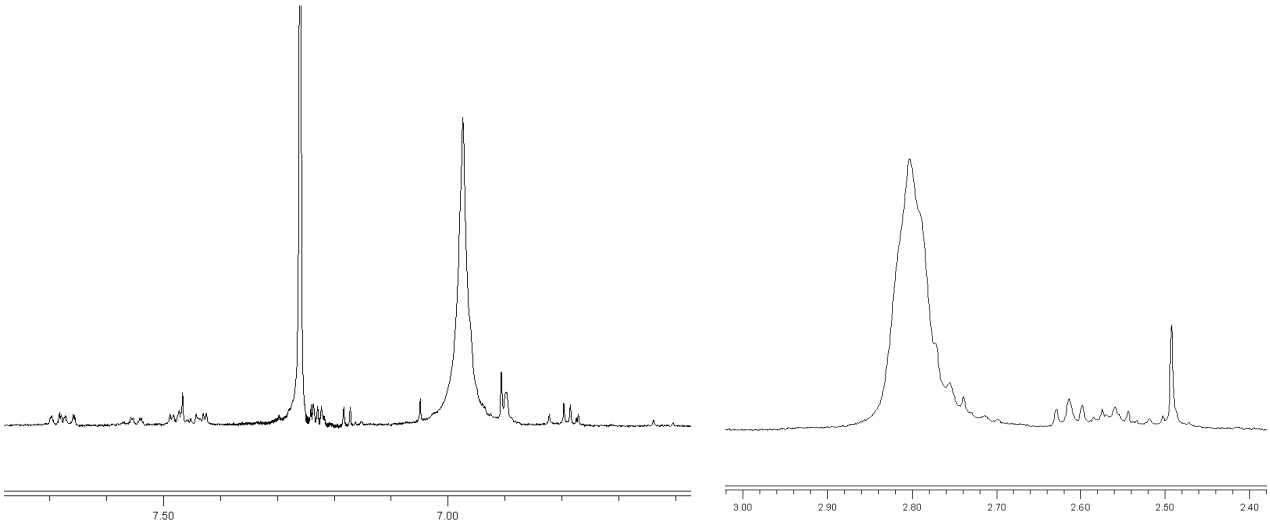

Figure 10. *^{1}H NMR-Spectra of P3OT obtained with $(tpp)_2Ni(o\text{-}Tol)Br$ initiator (MALDI-TOF (Fig. 4)).*

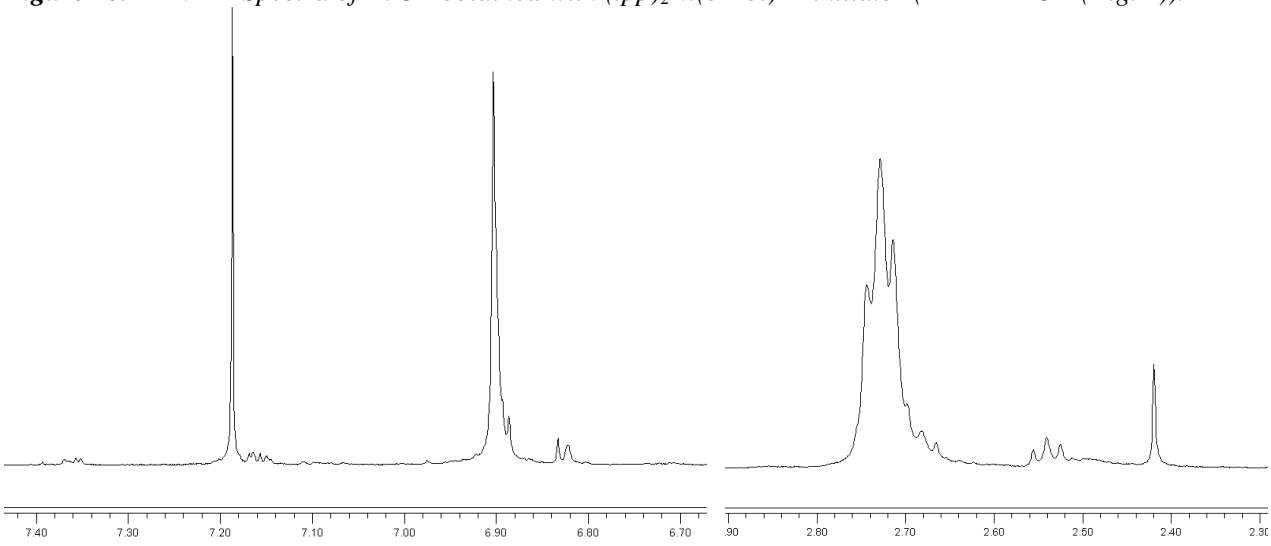

Figure 11. *^{1}H NMR-Spectra of P3DT obtained with $(tpp)_2Ni(o\text{-}Tol)Br$ initiator (MALDI-TOF (Fig. 5)).*

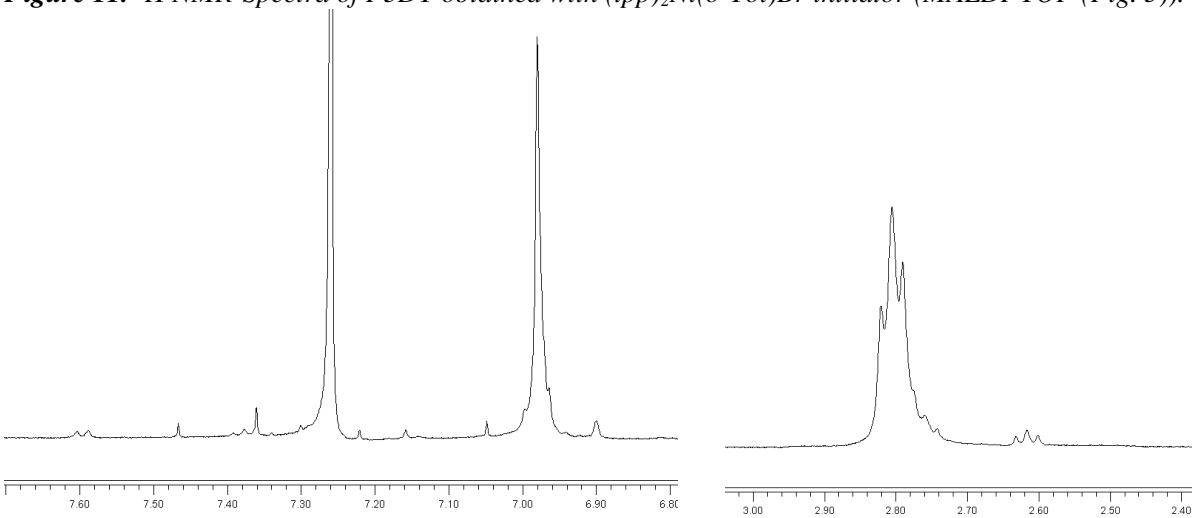

Figure 12. *^{1}H NMR-Spectra of P3HT obtained with $(tpp)_2Ni(Bz)I$ initiator (MALDI-TOF (Fig. 6)).*

Calculation the contact force between the tip and the P3HT brush surface.

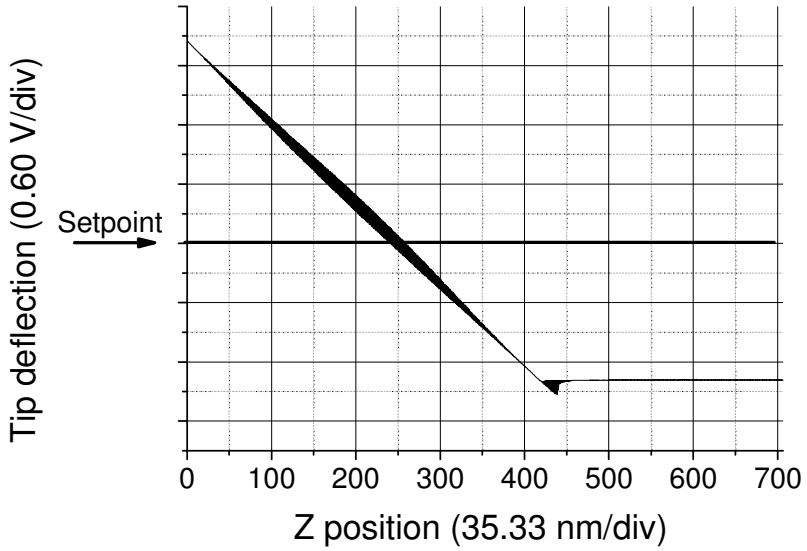

Figure 13. *Force plot of piezo extension versus tip deflection.*

Atomic force microscopy was used to measure the contact force between the tip and the P3HT brush surface. The force curve was determined by measuring the deflection of the cantilever as it approached and retracted from the sample. Multiplying the deflection of the cantilever by its spring constant yielded the force acting on the cantilever (F=k ΔZ).

Recalling that contact force F is equal to k(ΔZ), we can calculate the contact force from the sample plot above. The spring constant of the cantilever for contact mode is k=0.2N/m and calculated ΔZ sensitivity for applied voltages 0.2V is ΔZ=2.3div×35.33nm/div=81.26nm. The contact force for is F=0.2N/m×81.26×10^{-9}m=16.25nN. The force curve plot shows a small adhesion between the tip and grafted P3HT brush surface.

The results of electrical measurement of samples with C-AFM.

The conductivity (σ) of film were calculated using equation:

$$\sigma = \frac{l}{S \cdot R} \quad \text{or} \quad \sigma = \frac{d \times 10^{-7}\, cm}{\pi \cdot r^2 \times 10^{-14}\, cm^2 \cdot R(Ohm)};$$

d – thickness of film; r – radios of tip (35 nm or 35×10^{-7} cm); R – electrical resistance.

1) The 160 nm thick PS-Br-*graft*-P3HT film on the surface of ITO glass. The P3HT brush was grown from 60 nm thick photo-cross-linked PS-Br according to the procedure described in chapter 6.10.

Table 1. *The resistance and conductivity of the pristine PS-Br-graft-P3HT film in contact points (1-7).*

	1	2	3	4	5	6	7
R, Ohm	1.5×10^{10}	2.0×10^{10}	3.2×10^{10}	0.9×10^{10}	2.6×10^{10}	3.0×10^{10}	2.3×10^{10}
σ, S/cm	3×10^{-5}	2×10^{-5}	1.3×10^{-5}	4.6×10^{-5}	1.6×10^{-5}	1.4×10^{-5}	1.8×10^{-5}

Table 2. *The resistance and conductivity of the $FeCl_3$-doped PS-Br-graft-P3HT film in contact points (1-5). The concentration of $FeCl_3$ in ethanol solution is 1M. Doping time is 15 min.*

	1	2	3	4	5
R, Ohm	1.6×10^{6}	2.5×10^{6}	11×10^{6}	2.2×10^{8}	1.6×10^{9}
σ, S/cm	0.26	0.16	0.038	0.19×10^{-2}	0.26×10^{-3}

2) The 200 nm thick HT P3HT film on the ITO glass surface was obtained by spin-coating. The molecular weights of HT P3HT are M_w=7600 and M_n=6000 with a polydispersity (PD) index (M_w/M_n) of 1.26. The concentration of polymer solution is 0.4mg/ml.

Table 3. *The resistance and conductivity of the pristine coated 200 nm HT P3HT film in contact points (1-6).*

	1	2	3	4	5	6
R, Ohm	1.7×10^{10}	2.2×10^{10}	1.0×10^{9}	1.6×10^{10}	26×10^{10}	1.1×10^{9}
σ, S/cm	3.0×10^{-5}	2.3×10^{-5}	5×10^{-5}	3.1×10^{-5}	2.0×10^{-6}	4.7×10^{-4}

Table 4. *The resistance and conductivity of the coated $FeCl_3$-doped-P3HT film in contact points (1-4). The concentration of $FeCl_3$ in ethanol solution is 1M. Doping time is 15 min.*

	1	2	3	4
R, Ohm	1.1×10^{6}	8×10^{5}	4.4×10^{5}	3.8×10^{5}
σ, S/cm	0.47	0.65	1.18	1.36

LIST OF ABBREVIATIONS AND SYMBOLS

AFM	Atomic Force Microscopy
BC	Block copolymer
BPhen	4,7-diphenyl-1,10-phenanthroline (or bathophenanthroline)
CPs	Conjugated (or conductive) polymers
CPBs	Conductive polymer brushes
CV	Cyclic voltammetry
CCD	Charge coupled device
DC	Direct current
DOTT	3,3''-Dioctyl-[2,2';5',2'']terthiophene
DP	Polymerization degree
EQE	External quantum efficiency
IQE	Internal quantum efficiency
ITO	Indium-tin oxide
FETs	Field Effect Transistors
FTIR	Fourier Transform Infrared
GPC	Gel Permission Chromatography
LEDs	Light Emitting Diodes
NMR	Nuclear Magnetic Resonance
HOMO	Highest occupied molecular orbital
KCTP	Kumada catalyst transfer polymerization
LUMO	Lowest unoccupied molecular orbital
MALDI-TOF	Matrix-assisted laser desorption/ionisation-time of flight mass spectrometry
$Ni(tpp)_4$	Tetrakis(triphenylphosphine)nickel(0)
$Ni(dppp)CI_2$	[1,3-bis(diphenylphosphino)propane]dichloronickel (II)
$(tpp)_2Ni(Bz)Br$	bis(triphenylphosphine)benzylbromonickel(II)
$(tpp)_2Ni(Bz)I$	bis(triphenylphosphine)benzyliodonickel(II)
$(tpp)_2Ni(o\text{-}Tol)Br$	bis(triphenylphosphine)ortho-tolylbromonickel(II)
OPV	Organic photovoltaic devices
PCBM	[6-6]- phenyl C_{61}-butyric acid methyl ester
PGMA	Poly(glycidyl methacrylate)
PEDOT:PSS	Poly(3,4-ethylenedioxythiophene) poly(styrenesulfonate)
P3AT	Poly-3-alkylthiophenes
PDI	Polydispersity index
PDOTT	Poly(3,3''-Dioctyl-[2,2';5',2'']terthiophene)
PS-Br	Poly(4-bromostyrene)
PS-I	Poly(4-iodostyrene)
P4VP-*b*-PS-I	Poly(4-vinylpyridine)-*block*-poly(4-iodostyrene)
RE	Reference electrode, e.g. Ag/AgCl
RMS	Root mean square
RBS	Rutherford Backscattering
SAM	Self-assembled monolayer
SCE	Saturated calomel electrode
TAA	Thiophene-3-acetic acid
TBAPF6	Tetra-n-butylammonium hexafluorophosphate
UV-vis.	Ultraviolet-visible spectra
XPS	X-ray Photoelectron Spectroscopy

WE	Working electrode
t_D	Grafting anchor points
λ	Wavelength of light
h	Brush height
$(r^2)^{1/2}$	End-to-end distance
F_{int}	Statistical segments of the chains
F_{el}	Elastic free energy of the chains
N	Segments
R_g	Radius of gyration
E_g	Band gap
R_p and R_s	*p* and *s*-polarized light
F	Faraday constant
D_O	Diffusion coefficient of O
C_O	Concentration of O
x	Distance from the electrode surface
E^0	Equilibrium potential under standard conditions
k	Kinematic factor
I_{SC}	Short-circuit current
V_{OC}	Open-circuit voltage
FF	Fill factor
η	Power conversion efficiency
QE	Quantum efficiency

ACKNOWLEDGEMENTS

First of all, I would like to thank Prof. Dr. Manfred Stamm for giving me the opportunity to carry out this work, and Dr. Anton Kiriy for the scientific supervision. He guided me through my whole PhD time and I am very grateful for the many fruitful discussions we had. I also would like to thank my colleague Dr. Volodymyr Senkovskyy for experimental assistance and for the brilliant cooperation during this time.

I further would like to thanks Dr. Hartmut Komber and Dr. Martin Müller, who measured and helped interpreting the NMR spectra and Infrared (FTIR-ATR). I am grateful to Bettina Pilch and Dr. Ulrich Oertel for the UV-vis. Measurements. Thanks a lot to Mr. Andreas Janke for assisting the AFM measurements. I would like to say many thanks to Christina Harnisch and Petra Treppe for measurements GPC. Also would like to mention Dr. Mirko Nitschke, who helped me to perform the plasma etching experiments

I would express my deepest thanks to Dr. Kinga Haubner for her guidance, which has been a great source of inspiration. Her fruitful suggestions and cooperation have been invaluable. I am very grateful to Dr. Evelin Jähne for a nice collaboration and thank for her self-assemble monolayers (SAMs). Thanks also to Prof. Dr. Dirk Kukling for the MADLI-TOF study.

Thanks a lot to Dr. Moritz Rieke and Dr. Christian Ulrich from group of Prof. Dr. Karl Leo from for good collaboration and a nice photovoltaic measurement of my samples.

I want to thanks to Dr. Rainer Grötzschel for the Rutherford Back Scattering (RBS) measurements at the Forschungszentrum Dresden-Rossendorf.

I am grateful to my colleagues and friends Vera Bocharova, Konstantin Demidenok, Marta Horecha, Dr. Ganna Gorodyska, Dr. Pagra Truman, Dr. Valery Louchnikov, Vyacheslav Gruzdev, Smrati Gupta, Eva Herold, Dr. Jorge Rubio, Dr. Tatyana Beroyzkina, Dr. Nicolay Hubenov, Ksenia Boyko, Prashant Sinha for their help during experiments, stimulating discussions, and for their friendliness during the whole time. And many other my colleagues and friends at IPF.

I also want to acknowledge the Federal Ministry of Education and Research for providing the financial support through the “Deutsche Forschungsgemeinschaft.”

CONTRIBUTION TO ACADEMIC CONFERENCES

Conductive polymer brushes: New photoactive molecular architecture. Khanduyeva, N., Kiriy, A., Stamm, M. Advanced polymer materials (APM-2006), June 11-15, 2006 Bratislava, Slovakia, 20th Bratislava International Conference on Macromolecules

Synthesis and properties of the conductive polymer brushes. N. Khanduyeva, A. Kiriy, M. Stamm EuroNanoForum 2007 ,Nanotechnology in Industrial Applications, June 19-21, 2007, CCD Düsseldorf, Germany

Regioregular Poly(3-alkylthiophene) Brush via Catalyst-Transfer Surface-Initiated Polycondensation. Kiriy, V. Senkovskyy, N. Khanduyeva, M. Stamm. Symposium on Advanced Materials and concepts for Photovoltaics "AMPS", E-MRS 2007 Spring Meeting Strasbourg, France - May 28th to June 1st, 2007

Synthesis and investigation of conductive polymer brushes. Khanduyeva N., Senkovskyy V., Stamm M., Kiriy A. Symposium on functional polymer based materials, Jena, 3-4 April, 2007

Catalyst-transfer surface-initiated polycondensation: toward conductive polymer brushes. N. Khanduyeva, V. Senkovskyy, M. Stamm, A. Kiriy , REACT 2007, 3rd International Symposium on "Reactive Polymers in Inhomogeneous Systems, in Melts, and at Interfaces" Dresden, September 23-26, 2007.

Workshops

N. Khanduyeva, A. Kiriy, "Simple and Versatile Approach for Anchoring of Conductive Polymers" , Workshop SFB-B1, 2.12.2005, Rathen.

N. Khanduyeva, A. Kiriy, M. Stamm, "Conductive Polymer Brushes: New Electro- and Optically Active Molecular Architecture, European Graduate College „Advanced polymer materials", Gliwice, Poland 30.08-01.09.2004.

N. Khanduyeva, A. Kiriy, M. Stamm, "Conductive Polymer Brushes: New Electro- and Optically Active Molecular Architecture", Prag, Czech republic 9-13.04.2005

N. Khanduyeva, A. Kiriy, M. Stamm, "Conductive polymer brushes", Poland, 7-8.02.2007, Meeting.

L E B E N S L A U F

Natalya Khanduyeva 08.09.1979 in Chita Stadt, Russland, ledig

Schulausbildung

School –№ 5 in Gusinoozersk, Respublik Buryatia 1986 – 1996

Hochschulausbildung/Promotion

The Buryat State University in Ulan-Ude, Republic Buryatia, Russia 1996 – 2001
(Diploma at the Buryat Scientific Center of the Siberian Branch of the Russian Academy of Sciences)
Position Student at the chemistry department
Diploma Topic Synthesis of new pyrimidine derivates and polymers on their basis
Supervisors Dr. L. D. Radnaeva, Prof. Dr. D. M. Mognonov

A.N.Nesmeyanov Institute of Organoelement Compounds Russian Academy of Sciences, Moscow, Russia 2001 – 2002
Position Student researcher on a Russian Federation Grant
Topic Chemistry of polyimides and their investigation
Supervisors Prof. Dr. V. A. Vasnev, Dr. L. D. Radnaeva, Prof. Dr. D.M. Mognonov

The Petrochemical Institute of A.V. Topchieva, Moscow, Russia 2002 – 2004
Position PhD student in Chemistry
Topic Copolymerization of butadiene and styrene caoutchouc on metal complex catalysts (Ti-contained, Titan-magnum catalyst TMC)
Supervisors Prof. Dr. E. M. Antipov, Dr. E.A. Mushina

Leibniz Institute of Polymer Research, Dresden, Germany 2004 – present
Position PhD student in Chemistry
Topic Conductive polymer brushes: new electrical and optical applications
Supervisors Dr. A. Kiriy and Prof. Dr. M. Stamm

VERSICHERUNG

Hiermit versichere ich, dass ich die vorliegende Arbeit ohne unzulässige Hilfe Dritter und ohne Benutzung anderer als der angegebenen Hilfsmittel angefertigt habe; die aus fremden Quellen direkt oder indirekt übernommenen Gedanken sind als solche kenntlich gemacht. Die Arbeit wurde bisher weder im Inland noch im Ausland in gleicher oder ähnlicher Form einer anderen Prüfungsbehörde vorgelegt.

Die vorliegende Arbeit wurde unter der wissenschaftlichen Betreuung von Prof. Dr. M. Stamm an dem Leibniz-Institut für Polymerforschung Dresden angefertigt.

Keine frühere erfolglose Promotionsverfahren stattgefunden haben.

Die Promotionsordnung der Technischen Universität Dresden der Fakultät Mathematik und Naturwissenschaft vom 16.04.2003 erkenne ich an.

Natalya Khanduyeva